University of Naples Federico II
Polytechnic and Basic Sciences School

Department of Chemical Sciences

neapōlis

Ph.D. in Chemical Sciences

Natural and bio-inspired phenolic polymers for the design of innovative functional materials: tailoring properties by *ad hoc* synthesis and chemical manipulation

Sara Viggiano

Advisor
Prof. Lucia Panzella

Examiner
Prof. Angelina Lombardi

XXXVII Cycle 2021-2024
Coordinator: Prof. Angelina Lombardi

Index

Abstract

This PhD work was directed to the exploitation of phenolic polymers in the field of materials science. Natural phenolic polymers, such as lignins, tannins and melanin pigments, are the focus of increasing interest for applications in a broad variety of sectors as versatile, stable and multifunctional materials. Lignin and tannins are plant-derived phenolic polymers, particularly abundant also in agri-food wastes and by-products, endowed with potent antioxidant and antimicrobial properties, which have prompted their exploitation in tissue regeneration, stimuli-responsive materials, wound healing, drug delivery, and food packaging. The same applies to eumelanins, the characteristic black-to-brown pigments responsible for the color of skin, hair and eyes in mammals, originating from the oxidation of 5,6-dihydroxyindoles. Particular attention has been devoted also to synthetic, nature-inspired phenolic polymers, displaying in some cases several advantages over the corresponding natural analogues. In this context, this research work has been directed to the recovery or preparation, and when required functionalization, of natural or bio-inspired phenolic polymers for the design of functional materials to be used in the biomedical, cosmetic and food sectors. The main outcomes of this PhD research activity can be summarized as follows:

- The exploration of the oxidation chemistry of 5,6-dihydroxyindole (DHI) under solid-state conditions led to the isolation of hitherto unknown DHI dimers, namely the 4,4'- and 4,7'- biindolyls; moreover, using proteins as the solid matrices, the 4,4'and 4,7' mode of coupling was identified as a potential reaction route occurring in *in vivo* melanogenesis.
- A green procedure combining ball milling with the use of deep eutectic solvents was applied to recover lignin from chestnut shells (CSL), which was exploited as reducing agent toward Ag^+ ions for the

mechanochemical synthesis of silver nanoparticles; AgNPs@CSL were incorporated into poly(lactic acid) electrospun scaffolds providing functional materials to be used for tissue regeneration applications, thanks to the remarkable antioxidant, cytocompatibility and antimicrobial properties.

- An alternative synthetic, biomimetic model of natural lignin was obtained by oxidation of coniferyl alcohol under biomimetic conditions.
- Conventional maceration was identified as the best extraction technique for the recovery of phenolic compounds from dry pine needles; propelargonidin/prodelphinidin tannins were identified as the main phenolic components of the extract, emerging as a valid alternative as a green corrosion inhibitor on aluminum alloy.
- The solubility, photostability, and ability to inhibit photo-induced lipid peroxidation of hydrolysable and condensed tannins were systematically investigated in view of possible dermo-cosmetic applications.
- The access to antioxidant selenoderivatives of condensed tannins was preliminary investigated on catechin as a model compound, by using a protocol involving potassium selenocyanate/cerium(IV) ammonium nitrate.
- A pomegranate peel and seed extract rich in ellagitannins and ellagic acid was efficiently combined with whey proteins to implement antioxidant and antimicrobial coatings for food packaging applications.
- Highly performing adhesive and underwater resistant materials were prepared starting from soy proteins and natural easily accessible phenolic compounds (caffeic, gallic and chlorogenic acid); the addition of agarose led to the formation of hydrogels endowed with cytocompatibility, hemocompatibility, antibacterial activity and, in some cases, also wound healing activity for biomedical applications.

- With the final aim of searching compounds able to inhibit the activity of the enzyme tyrosinase and hence prevent or delay skin hyperpigmentation processes for application in the cosmetic field, or enzymatic browning processes in fruits and vegetables for application in the food sector, extracts from low cost agri-food by-products rich in phenolic compounds were prepared; extracts from chestnut shells, *Morus alba* branches, and pecan nut shells proved to be the most effective inhibitors against tyrosinase, while extracts from strawberry spirit production by-products, fermented pomegranate by-products and again chestnut shells exhibited an evident retarding effect on the enzymatic browning process in apple smoothies.
- Selected gingerol and resorcinol-based cosmetic ingredients were tested for their ability to prevent skin hyperpigmentation, demonstrating to be effective inhibitors of melanin precursor photooxidation and to able to exert a photoprotective role against the damages induced by solar light.

Finally, part of the PhD research activity was performed at the CICECO-Aveiro Institute of Materials of the University of Aveiro (Portugal), under the supervision of Professor Mara G. Freire, and at the European School of Chemistry, Polymers and Materials of the University of Strasburg (France), under the supervision of Professor Vincent Ritleng. The following research activities were developed, respectively:

- The enzyme laccase was investigated as an alternative to the conventional 5,6-dihydroxindol-2-carboxylic acid (DHICA) oxidizing systems. Although still preliminary, the results obtained highlighted the possibility to obtain a pigment with apparently more efficient antioxidant properties with respect to the one obtained using the horseradish peroxidase/hydrogen peroxide oxidizing system.

- Exploiting their ability to interact with several surfaces and compounds, hydrolysable and condensed wood tannins were used for the coating of polyurethane foams and the subsequent functionalization with palladium; the obtained materials acted as heterogeneous and recyclable catalysts in different reactions (phenylacetylene to styrene semi-hydrogenation, nitrobenzene reduction, and Suzuki coupling) over several consecutive cycles.

List of publications

1) **S. Viggiano**, L. Panzella, M. Reichenbach, J. Hans, A. Napolitano "The effect of cosmetic ingredients of phenol type on immediate pigment darkening and their (photo)protective action in association with melanin pigmentation: a model in vitro study", *Cosmetics*, 10 (**2023**), 22; doi: 10.3390/cosmetics10010022
2) R. Argenziano, **S. Viggiano**, R. Esposito, M. Schibeci, R. Gaglione, R. Castaldo, L. Fusaro, F. Boccafoschi, A. Arciello, M. Della Greca, G. Gentile, P. Cerruti, G. D'Errico, L. Panzella, A. Napolitano "All natural mussel-inspired bioadhesives from soy proteins and plant derived polyphenols with marked water-resistance and favourable antibacterial profile for wound treatment applications", J. *Colloid. Interface Sci.*, 652 (**2023**), 1308-1324; doi: 10.1016/j.jcis.2023.08.170
3) M. Salzano de Luna, G. Vetrone, **S. Viggiano**, L. Panzella, A. Marotta, G. Filippone, V. Ambrogi "Pine needles as a biomass resource for phenolic compounds: trade-off between efficiency and sustainability of the extraction methods by life cycle assessment", *ACS Sustain. Chem. Eng.*, 11 (**2023**), 4670−4677; doi: 10.1021/acssuschemeng.2c06698
4) R. Argenziano, **S. Viggiano**, A. Laezza, A. C. Scalia, P. Aprea, B. Bochicchio, A. Pepe, L. Panzella, A. Cochis, L. Rimondini, A. Napolitano "Highly cytocompatible polylactic acid based electrospun microfibers loaded with silver nanoparticles generated onto chestnut shell lignin for targeted antibacterial activity and antioxidant action", *ACS Appl. Mater. Interfaces*, 16 (**2024**), 22; doi: 10.1021/acsami.4c05761
5) **S. Viggiano**, M. L. Alfieri, L. Panzella, O. Crescenzi, A. Napolitano "Disclosing novel pathways toward melanin pigments: unexpected dimers by solid-state oxidation of the biosynthetic precursor 5,6-

dihydroxyindole", *Bioorg Chem.*, 153 (**2024**), 107928; doi: 10.1016/j.bioorg.2024.107928

6) **S. Viggiano**, R. Argenziano, A. Lordi, A. Conte, M. A. Del Nobile, L. Panzella, A. Napolitano "Combining the powerful antioxidant and antimicrobial activities of pomegranate waste extracts with whey protein coating-forming ability for food preservation strategies", *Antioxidants*, 13 (**2024**), 1394; doi: 10.3390/antiox13111394

Manuscript in preparation

1) F. Scherillo, G. Vetrone, **S. Viggiano**, G. Filippone, V. Ambrogi, M. Salzano de Luna, L. Panzella "Polyphenols extracted from waste biomass as green corrosion inhibitors for aluminum alloys", In preparation.

Chapter 1

Introduction

1. Phenolic compounds

Natural phenolic compounds are a huge group of secondary metabolites widely distributed in nature (*e.g.* plants, fruits, vegetables, legumes, cereals, etc.) characterized by a very broad range of structures and properties. As secondary metabolites, they are produced by the plant cells through metabolic pathways derived from the primary metabolism and are involved in the physiological processes occurring in the organism, such as its growth, development, and reproduction. The synthesis of these metabolites depends on the type of species, organs, tissues, cellular functions and cellular developmental stages.[1]

Structurally, natural phenolic compounds are characterized by one or more aromatic rings functionalized with one or more hydroxyl groups, giving rise to a large number of heterogeneous structures ranging from simple phenolic molecules to highly polymerized compounds (*e.g.* melanins, lignins, tannins).[2]

Due to their structural multifunctionality, phenolic compounds exhibit various physical, chemical and biological properties, that have stimulated increasing interest for their possible application in a large variety of fields (*e.g.* functional foods, food packaging, cosmetics, tissue engineering, drug delivery, etc.)

One of the most important and studied property of these compounds is their antioxidant activity.

Oxidation is a chemical reaction in which a substance loses electrons and can be promoted by radical species, such as reactive oxygen species (ROS).[3] In detail, ROS are produced from O_2 reduction as a consequence of the normal

cellular metabolism.[4] The most physiologically significant ROS are the superoxide radical anion ($\bullet O_2^-$), the hydroxyl radical (•OH), and the non-radical hydrogen peroxide (H_2O_2). In particular, under oxidative stress conditions, the ROS present in high concentrations can react with cell components like lipids, proteins, DNA or RNA,[4–6] causing their oxidative modification.[7] As a consequence, this can cause different pathological conditions, including cancer, and neurological and cardio-respiratory disorders.[8,9]

Phenolic compounds are able to protect an oxidizable molecule by delaying or inhibiting its oxidation[10] through several mechanisms: they are able to scavenge radical species, to donate hydrogens/electrons or to chelate transition metal ions involved in the generation of ROS, due to the presence of hydroxyl groups on the aromatic ring.[11,12] Of course, other structural elements can strongly impact on the antioxidant properties of the phenolic compounds.[13–15]

Phenolic compounds also exhibit a large number of other beneficial properties for human health, such as anti-allergenic, anti-inflammatory, anti-thrombotic, cardioprotective and vasodilatory activities.[13] In addition, several studies have demonstrated their beneficial effects against human cancer cell lines as they are able to reduce or inhibit the growth of different tumors (*e.g.* those of mouth, stomach, duodenum, colon, liver, lung, mammary gland or skin)[15–17] and may exert other clinically relevant properties such as chemo-preventive activity against gastric ulcers, long-term diabetes complications, diabetic neuropathy, kidney dysfunction and retinopathy.[18] This is the reason why, for example, vegetables and fruits with high levels of phenolic compounds are so much recommended in the daily diet.

Phenolic compounds also exhibit a marked antibacterial activity against different microorganisms involved in human diseases and deterioration of

foods.[15] On this basis, great attention has been focused on their possible use as natural antioxidant and antimicrobial food preservatives, preferred to the synthetic ones.[19–21] Accordingly, packaging functionalized with natural phenolic compounds is attracting increasing attention.[20,22,23]

Growing interest has been directed also to the exploitation of phenolic compounds in the cosmetic field. Indeed, these compounds are able to prevent skin aging and hyperpigmentation, to provide photoprotective action, and, thanks to their anti-inflammatory activity, to act as support in the treatment of sensitive or sun-stressed skin.[24,25]

Finally, thanks to their plenty and peculiar properties, phenolic compounds have been also used as functional additives for a broad range of other applications, including hydrogels, biocompatible glues, nanostructures for drug delivery, sensors, semiconductors, photo- and thermostabilizing agents, and other devices for biomedicine and organic electronics.[26–29]

1.1.1 Natural phenolic polymers

In recent years, particular attention has been devoted to natural phenolic polymers due to their wide occurrence in sustainable sources, such as agri-food wastes and by-products, and their potential advantage over the corresponding monomers, including *e.g.* greater chemical stability and lower toxicity. The main natural phenolic polymers are lignins, tannins, and melanins.

1.1.1.1 Melanins

Among the broad variety of phenol-type biopolymers found in nature, melanins occupy a prominent position.

Melanins are an important class of phenolic pigments deriving from the oxidative metabolism of tyrosine and they are responsible for the color of skin,

hair and eyes in humans and mammals. These pigments can be classified into two varieties which share a common biosynthetic origin: the dark brown-to-black eumelanins and the lighter, yellowish-to-brown, sulphur containing pheomelanins.[30–32] They are produced in highly specialized cells, namely melanocytes, located between epidermis and derma, able to synthesize the enzyme tyrosinase, that, in turn, leads to the synthesis and the accumulation of the pigments.[33,34] More specifically, the synthesis of melanins begins with the oxidation of L-tyrosine (or L-DOPA) to dopaquinone by tyrosinase (Figure 1.1), followed by different pathways that can occur spontaneously depending on various factors (*i.e.* presence of thiols, pH value, presence of ions such as zinc and copper). In particular, in the presence of cysteine dopaquinone undergoes nucleophilic addition of the -SH group leading to the formation of 1,4-benzothiazine intermediates and then, after further oxidation reactions, to pheomelanins.[35] Instead, in the absence or at low concentrations of cysteine, the intramolecular cyclization of the dopaquinone prevails, with the formation of leucodopachrome. This latter is oxidized in a redox reaction with the dopaquinone leading to the formation of the dopachrome, which can subsequently rearrange, with or without decarboxylation, to generate the 5,6-dihydroxyindole (DHI) and the 5,6-dihydroxyindole-2-carboxylic acid (DHICA). These monomers, in turn, undergo oxidative polymerization to form eumelanins (Figure 1.1).[36] *In vitro* and in absence of enzymatic assistance, decarboxylation of dopachrome is favored whereas *in vivo*, inside melanocytes, the formation of DHICA is favored by the enzymatic action of dopachrome tautomerase (Dct) or tyrosinase-related protein 2 (Tyrp-2) or by the presence of transition metal ions (*e.g.* Cu^{2+} or Zn^{2+}).[37] As a consequence, natural melanins contain over 50% DHICA.[38]

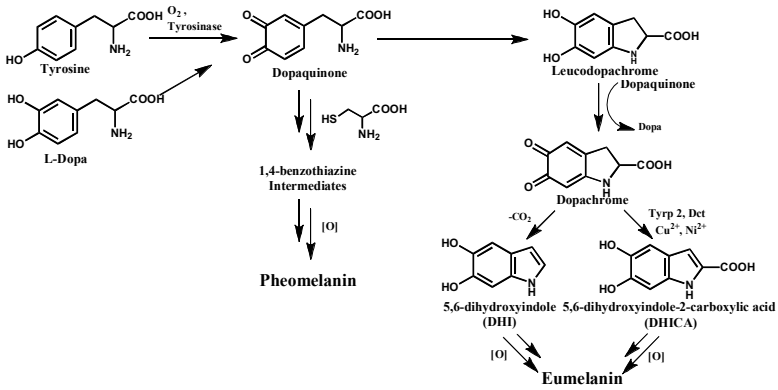

Figure 1.1. Melanin biosynthetic pathway.

Thanks to their peculiar structure and physicochemical properties, over the past decades eumelanins have stimulated a lot of interest as potential biocompatible functional materials to be used for different applications in a variety of fields. For example, eumelanins are characterized by a broadband UV-visible absorption spectrum and excellent antioxidant properties,[39] that can prevent sunburn, DNA damage and skin cancer. Melanin and melanin-like compounds have also been used for electronic and bio-electronic applications, for surfaces functionalization, food packaging applications, drug delivery systems, and a variety of biomedical applications including tissue engineering.[40–42]

1.1.1.2 Lignins

The most abundant class of natural phenolic compounds is represented by lignin, the second most widespread biopolymer on earth after cellulose, accounting for approximately 30% of the organic carbon on the planet. Lignin is an irregular, water-insoluble and high molecular mass phenolic polymer (600-15000 kDa), deriving from the oxidation of three main hydroxycinnamyl alcohol monomers, that are coniferyl, sinapyl and *p*-coumaryl alcohols,

differing in the degree of methoxylation of the phenolic ring (Figure 1.2_a).[43] Different inter-unit bonds can be formed during the radical coupling polymerization of the three monolignols: the most frequent is the β-*O*-4-aryl ether linkage, followed by the β-5-phenylcoumaran, 5,5-biphenil, 4-*O*-5-biphenil ether, β-1-(1,2-diarylpropane), β-β-pinoresinol and α-*O*-4-aryl ether bonds (Figure 1.2_b).[44,45] Depending on the ratio of these different phenolic components, lignin composition is widely varied and mainly depends on the type of plant species, on the stage of cell development as well as on the environmental conditions.[46]

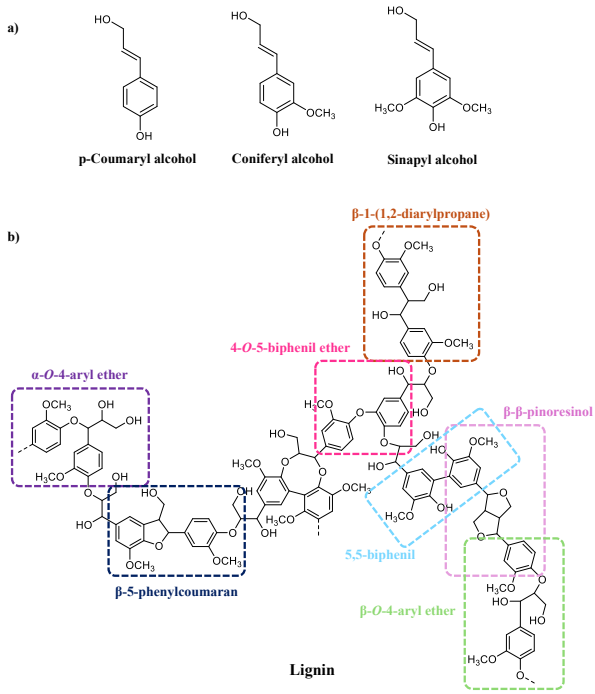

Figure 1.2. Chemical structures of a) lignin monomers and b) lignin scaffold.[47]

Lignin plays important roles in the growth and development of plants. As a complex phenolic polymer, it contributes to plant cell wall rigidity, water and

minerals transport through the vascular bundles, and it represents also an important barrier against pests and pathogens.[48] In addition, it has been reported that lignin has a variety of healthy effects on human health, too, being able to exert antioxidant, antifungal, antibiotic, antitumor and antiviral activities.[49,50] During the last years, also its ability to reduce coronary heart disease, diabetes, obesity and Alzheimer's disease has been reported.[51]

Thanks to its strong absorption capacity in the UV-Vis region, lignin is also able to protect plants or human skin from UV damage. For this reason, together with its strong antimicrobial and antioxidant activities, lignin has been largely applied in dermocosmetic and food packaging applications.[52–55]

In the last years, the growing focus on lignin research has been partially driven by a very huge amount and still not fully exploited lignin produced as by-product by different type of industries. On this basis, lignin has attracted great attention in the production of functional materials. Few examples can be represented by lignin-based carbon fibers and lignin-based porous carbon materials for the development of devices with efficient mechanical properties,[52,55] metal-lignin hybrids prepared as platform for the design of advanced sensing materials or for biomedical applications,[52,54,56] lignin nanoparticles used as drug delivery systems, UV absorbents, and in tissue engineering.[51,52,57]

1.1.1.3 Tannins

Tannins are a class of phenolic polymers widely distributed in many species of plants and mainly classified into condensed and hydrolyzable tannins.[58]

Condensed tannins, also known as non-hydrolyzable tannins or proanthocyanidins, are oligomeric and polymeric flavonoids. Their most common basic units are the flavanols (+)-catechin, (-)-epicatechin, (+)-gallocatechin, and (-)-epigallocatechin (Figure 1.3).[58]

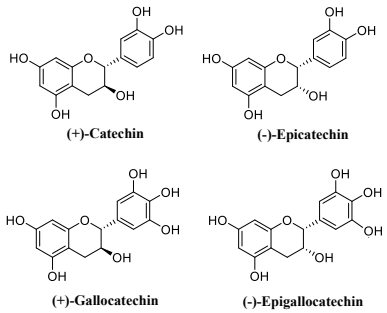

Figure 1.3. Structures of the main monomeric units present in natural condensed tannins.

Due to the possible occurrence of *O*-methylation, C-and *O*-glycosylation, and *O*-galloylation, natural condensed tannins are characterized by a wide structural diversity. Moreover, these species can be further distinguished into procyanidins and profisetinidins.[58] More specifically, procyanidins, predominantly present in grape,[59] can be classified into dimeric B-type and trimeric C-type, characterized by single bond between units (usually between C4-C6 or C4-C8 of the flavanol units), or the A-type, characterized by an additional bond between C2-C7 or C2-5–OH (Figure 1.4). Profisetinidins, predominantly present in some type of wood such as quebracho (*Schinopsis lorentzii*) and mimosa (*Acacia mollissima*),[60] differ from the procyanidins by the absence of a hydroxyl group at C5 position of the A-ring.[58]

Moreover, compared to the hydrolyzable tannins, condensed tannins can contain up to 10 units of monomers with a wide range of molecular weight ranging from 500 to over 20’000.[61]

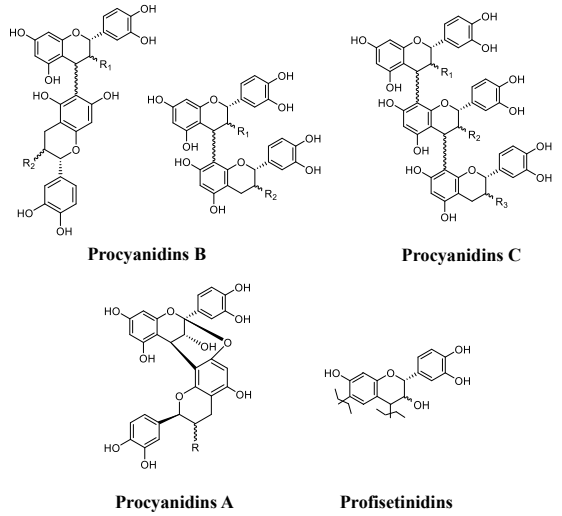

Figure 1.4. General structures of B-type, C-type and A-type procyanidins and profisetinidins.

Hydrolyzable tannins are usually found in plants in lower concentrations than condensed tannins. These types of tannins are abundant in oak wood (*Quercus robur*, *Quercus petraea*, and *Quercus alba*),[62] chestnut wood (*Castanea sativa*),[62–64] and galls (*Quercus infectoria*).

They are composed of a monosaccharide, generally D-glucose, whose hydroxy groups are esterified with phenolic compounds such as ellagic acid or gallic acid to produce ellagitannins and gallotannins, respectively (Figure 1.5).[58] Unlike condensed tannins, the hydrolyzable ones can be hydrolytically broken into their components by acids or some enzymes, such as tannase, resulting in ellagic and gallic acids release.

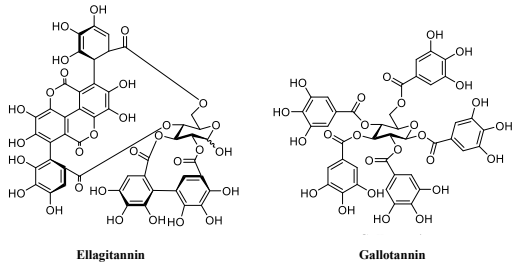

Figure 1.5. Exemplificative structures of natural hydrolyzable tannins.

A minor third class of tannins is represented by phlorotannins, which are polymers of phloroglucinol. They have been isolated from several genera of brown algae,[65] but are not relevant for the human diet.

Among all the natural phenolic compounds with exceptional multifunctional properties, tannins occupy a prominent role.[65–67] For this reason, they are used for several purposes and in several fields. For example, since the ancient society, tannins were used as good substitutes for the toxic chromium in the leather industry, thanks to their ability to strongly interact with protein.[68,69] Considering this aptitude, especially for proline-rich proteins that prevail in gluten, tannins have been also used for a therapeutic approach toward celiac disease.[70]

Tannins antibacterial activity is also widely known. Indeed, thanks to their ability to inhibit the growth of numerous fungi, viruses, bacteria and yeasts, they are extensively used as food additives to extend the shelf life of some foods, but also to improve wine color stability, protect foods against oxidation or to confer astringent taste and flavor.[71]

The antioxidant properties, which are crucial in preventing cellular oxidative damage including lipid peroxidation, may be connected to the tannins' anticarcinogenic and antimutagenic potentials.

In addition, these phenolic compounds have been also found to be able to act as anti-corrosion materials for metals,[71–76] to be used for the production of

almost totally biosourced foams and resins[71] or, in virtue of their capability to interact with a wide variety of different compounds, tannins have been also used in hybrid nanomaterials in catalysis, in functional food packaging, as well as for UV-shielding.[77]

1.2 Agri-food by-products: a sustainable source of phenolic polymers

As mentioned before, natural products, and in particular natural phenolic polymers, are considered attractive value-added compounds to be used in a wide range of application fields, thanks to their peculiar structure and physicochemical properties. In addition, the wide distribution of phenolic polymers in different natural sources, such as fruits, vegetables or lignocellulosic biomasses, has stimulated intense research work aimed at their best exploitation in a variety of fields.

Among the main easily accessible, sustainable and low-cost resource of phenolic polymers, there are agri-food by-products and wastes.[78]

Agri-food industry is responsible for the generation of high volumes of organic biomass (140 billion tons per year), mostly belonging to food waste, composed of leaves, roots, stalks, bark, bagasse, seeds, wood, straw and animal residues.[79] In particular, 1.3 billion tons of global food waste are produced yearly as the result of primary and secondary processes occurring along the supply chain.[80]

Disposal of these by-products represents a cost to the processor and has a negative impact on the environment. As a matter of fact, the decomposition of only one metric ton of organic solid waste results in the release of 50-100 m^3 of CO_2 and 90-140 m^3 of methane into the atmosphere.[81] In addition, organic wastes may be the cause of phytotoxicity events such as water degradation

and deterioration, death of marine organisms, inhibition of seeds germination or digestive disorders in animals.[82]

On this basis, the exploitation and valorization of these materials represent a valuable opportunity,[80] considering that most of the by-products contain equal or greater quantities of phenolic compounds than the initial compound itself.

1.3 Green extraction techniques for the recovery of phenolic polymers from natural sources

In addition to the search for sustainable sources of phenolic polymers for application purposes, very important is also the assessment of the extraction methodologies to be used for the recovery of these compounds. Usually, phenolic compounds are extracted from agri-food by-products by using solid-liquid extraction techniques.[83] Among these, common extraction methods, such as conventional maceration, percolation, and Soxhlet extraction, are very simple to perform. However, these methods are typically expensive and involve long extraction times and very high amounts of organic solvents, characterized by several drawbacks (*e.g.* low boiling points, flammability, toxicity, and non-biodegradability).[84] On this basis and to overcome such disadvantages, several studies have been directed to the implementation of alternative low-cost extraction methodologies in agreement with the green chemistry principles and characterized by minimal environmental impact.

The following is a list of green extraction technique examples.

Microwave-assisted extraction. Microwave-assisted extraction (MAE) is a very fast technique that uses microwaves to interact with the samples. In particular, microwaves can easily penetrate into the sample pores causing the solvent trapped in the pores to heat uniformly and quickly. In this regard, two solvents commonly used in combination or alone are water and ethanol, thanks to their ability to absorb the microwave energy and to solubilize

phenolic compounds.[85] For this reason, MAE is also generally a non-toxic methodology. Since this technique minimizes the extraction time and reduces the consumption of organic solvents, it can be also classified as a green extraction method. Moreover, it allows full control of extraction parameters such as time, power, and temperature.

Ultrasound-assisted extraction. As in the case of MAE, ultrasound-assisted extraction (UAE) is a green extraction technique able to decrease the amount of time and of used solvents for the extraction of phenolic compounds from agri-food wastes.[85] It is based on the acoustic cavitation principle that occurs when ultrasonic waves with a frequency between 20 kHz and 100 MHz travel through the sample in cycles of compression and expansion.[86] In the case of plant extraction, for example, the principle of acoustic cavitation involves the formation, growth, and implosion of bubbles that damage the cell walls of the plant matrix favoring the release, and so the extraction, of phenolic compounds.[87]

Deep eutectic solvent extraction. Deep eutectic solvents (DES)[88,89] have been widely reported as eco-friendly and biocompatible solvents for the extraction of phenolic compounds from agri-food by-products, being biodegradable and less toxic than typical organic solvents. DES are very easily prepared by combining a hydrogen bond acceptor (HBA) and a hydrogen bond donor (HBD) at a proper temperature,[89–91] resulting in a mixture with a lower melting point than its components. Usually, the most used HBA for DES preparation is choline chloride (ChCl), a non-toxic and cheap salt, while compounds like urea, ethylene glycol, glycerol, alcohols, amino acids, carboxylic acids and sugars can be used as HBD.[92,93] The DES components of course influence the physicochemical properties of the final mixture, such as its density, viscosity and polarity.[94] Thanks to the capacity to form hydrogen bonds, DES are considered excellent dissolving solvents toward phenolic polymers in

complex matrix.[95] The possibility to choose the HBD and HBA components and their molar composition allows DES to be properly designed to meet the requirements of the targeted applications.

1.4 Nature-inspired phenolic polymers

In the last years, growing research interest has also been directed to synthetic, nature-inspired phenolic polymers. Compared to the corresponding monomers, they are indeed characterized by several advantages, such as lower volatility, greater chemical stability, lower toxicity, and lower tendency to be released from an incorporating matrix, properties that open important perspectives for various applications.

Although polymerization of phenolic compounds can be carried out using a range of chemical oxidants (*e.g.* ferricyanide, ceric ammonium nitrate, or persulphate), the most convenient oxidation route is nowadays represented by the use under biomimetic conditions of the environmentally compatible tyrosinase or of the system horseradish peroxidase (HRP)/H_2O_2.[96, 97]

Several examples of nature-inspired phenolic polymers exhibiting promising functional properties for application in several fields are available in the literature. One of these is represented by poliCAME (Figure 1.6) obtained by HRP/H_2O_2-catalyzed oxidation of caffeic acid methyl ester (CAME).[98,99] This polymer proved to be very effective in stabilizing linear low-density polyethylene (LLDPE), one of the most used polymers in food packaging, against thermo-oxidation or photo-oxidative degradation.[100–102]

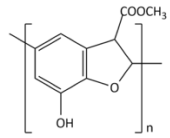

Figure 1.6. Poly(caffeic acid methyl ester) structure.

Another interesting example is the polymer of tyrosol, a phenolic compound known for its numerous properties (*e.g.* antimicrobial, antithrombotic, anti-inflammatory, and antioxidant properties)[103,104] that make it interesting for a range of biological and pharmacological applications.[105,106] Tyrosol was oxidized using the HRP/H_2O_2 system to give a mixture of oligomers (OligoTyr) (Figure 1.7), which proved to be more efficient than tyrosol in several antioxidant assays and, when incorporated into a polylactic acid scaffold, was able to stimulate the alkaline phosphatase activity in cellular systems, showing good potential in osteogenesis promotion for applications in bone tissue engineering.[96]

In addition, a sulphated derivative of OligoTyr (Figure 1.7) simultaneously showed remarkable antioxidant and anticoagulant activity.[107]

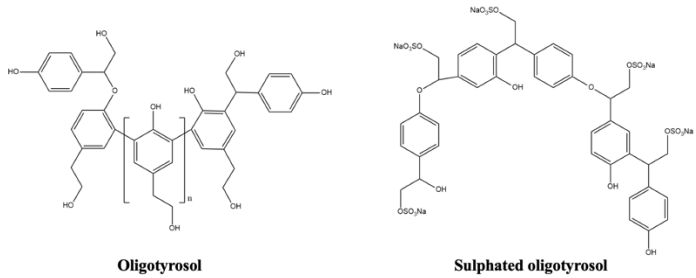

Figure 1.7. Proposed structure for the polymer of tyrosol and its sulphated derivative.

Nature-inspired phenolic polymers occupy a prominent role also in the study of melanin pigments. Indeed, although they are widely distributed in nature, the extraction yields and purity of natural melanins are very low. Additionally, their marked insolubility and chemical heterogeneity make their investigation very challenging.[39,108] On this basis, most studies on this topic have been based on a bottom-up approach, involving the oxidation of the melanin monomeric

precursors (*i.e.* the 5,6-dihydroxyindoles DHI and DHICA) to obtain nature-inspired melanins, which could be more easily characterized and exploited compared to natural eumelanins.[109]

Interestingly, it has been demonstrated that the presence of the carboxylate group in DHICA may significantly affect the structure and properties of DHICA-melanin with respect to DHI-melanin (Figure 1.8). Indeed, the carboxylate group is able to divert the reactivity from the position 2 of the pyrrole moiety to the 4 and 7 benzenoid positions, leading to a twisting of the inter-ring dihedral angles. The thus resulting non-planar structures characterized by weak aggregating interactions lead to a higher accessibility of the indole units to radical species compared to the compact p-stacked DHI-melanin, that is at the basis of the more efficient antioxidant properties commonly attributed to DHICA-melanin compared to DHI-melanin.[110]

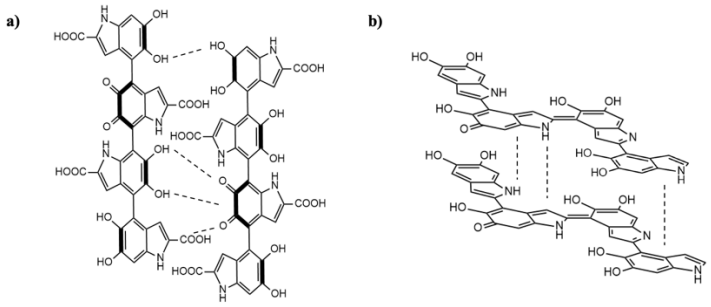

Figure 1.8. Proposed structure for oligomeric constituents of a) DHI and (b) DHICA-melanin.

A more recent study reported that the polymer obtained by oxidation of the methyl ester of DHICA (MeDHICA) is characterized by peculiar antioxidant and photoprotective properties against UV radiation.[110,111] Indeed, MeDHICA-melanin proved to be able to protect skin cells from UVA-induced damage, entering the keratinocytes and activating the cellular antioxidant

system. Therefore, its use has been encouraged in dermo-cosmetic applications.[111]

More recently, another variant of DHICA-melanin has been obtained by aerial oxidation of the carboxybutanamide of DHICA. The pigment exhibited not only a UVA but also a visible absorption more intense than that showed by DHICA-melanin, a noticeable solubility in polar solvents of dermo-cosmetic relevance, and higher antioxidant and photoprotective properties compared to DHICA-melanin.

1.5 Aim of the PhD project

Within the context briefly described in the previous paragraphs, this PhD work was directed to the exploitation of phenolic polymers in the field of material's science. In particular, the general objective of the present project was the recovery and when required functionalization of natural and bio-inspired phenolic polymers for the design of functional materials to be used mainly in the biomedical and food sectors. The investigation was directed at melanins (Chapter 2), lignins (Chapter 3), and tannins (Chapter 4). The possible exploitation of low molecular weight phenolic compounds as functional additives for various applications is also reported (Chapters 5 and 6).

In particular, the following goals were pursued, as described in detail in the following chapters:

a. Examination of the oxidative chemistry of DHI and DHICA under so far underexplored and green conditions for the obtainment of melanin pigments with different structural properties and hence application perspectives;
b. Recovery and functionalization of lignin from selected agri-food by-products to be exploited as functional additives in biocompatible materials for biomedical applications;

c. Examination of the oxidative chemistry of coniferyl alcohol under biomimetic condition (*i.e.* using HRP/H_2O_2) to obtain an alternative synthetic model of natural lignin;
d. Recovery and characterization of tannins form agri-food wastes and by-products to be used as functional additives in food packaging and as corrosion inhibitors;
e. Exploitation of tannins for the preparation of palladium-loaded polyurethane foams to be used as catalysts in organic synthesis;
f. Evaluation of the photostability, solubility, and antioxidant properties of wood tannins to be used in dermocosmetic field;
g. Preliminary evaluation of the efficacy of the potassium selenocyanate/cerium ammonium nitrate reagent system for the synthesis of catechin selenoderivatives exhibiting efficient antioxidant properties;
h. Functionalization of whey and soybean protein isolates with natural phenolic compounds to be used in food preservation and biomedical applications;
i. Evaluation of natural compounds extracted from agri-food by-products as inhibitors of tyrosinase for applications in the dermocosmetic and food sector;
j. Investigation of the effects of selected cosmetic phenolic ingredients on photooxidation of DHI and DHICA in the perspective of their dermocosmetic applications for the prevention of skin hyperpigmentation and damage induced by solar light.

Part of the work performed for the objectives a) and e) were performed during a two-month visit at the CICECO-Aveiro Institute of Materials of the University of Aveiro (Portugal) under the supervision of Professor Mara G. Freire and at the European School of Chemistry, Polymers and Materials of

the University of Strasburg (France) under the supervision of Professor Vincent Ritleng, respectively.

Chapter 2

Exploration of the oxidation chemistry of 5,6-dihydroxindoles under unexplored conditions

2.1 Introduction

As illustrated in the Introduction section, eumelanins are the primary responsible of the brown-to-black color of skin, hair, and eyes in mammals.[112–115] These pigments are characterized by a very wide range of remarkable properties including radical scavenging and radiation protection,[116] that have stimulated their application in *e.g.* the cosmetic, electronic or food field.

However, the marked insolubility and chemical heterogeneity of eumelanins make their structural investigation a most challenging task. Indeed, despite continuing efforts over the past decades, the origin of these biopolymers together with the basic mechanisms of build-up and the features of their supramolecular architecture have remained largely obscure.[116–121]

Nowadays, the study of the oxidative polymerization of 5,6-dihydroxyindoles (DHI and DHICA), the main eumelanin precursors, represents the most promising approach to develop a realistic structural model of natural eumelanins. In addition, this method, commonly known as bottom-up approach, can also lead to the development of polymers with more defined properties compared to the natural ones, a critical requisite for their full exploitation as technologically advanced materials.[119]

Previous studies carried out over the past two decades have highlighted the species formed during the early stages of DHI or DHICA oxidation under different conditions.

In particular, DHI oxidation carried out under biomimetic conditions, that is by use of enzymatic oxidants like HRP/H_2O_2 or tyrosinase in aqueous buffer at neutral pH, led to the formation of dimers and trimers characterized by a predominant 2,4'- and 2,7'-mode of coupling.[122,123] Besides a high oxidizability, the *o*-diphenol moiety imparts metal-chelating properties to the 5,6-dihydroxyindole. In fact, the presence of transition metal cations (*e.g.* Zn^{2+} and Ni^{2+}) critically affect the regiochemistry of the oxidation reaction leading to the 2,2'-dimer as the main product (Figure 2.1_a).[124]

Concerning DHICA, the carboxylic acid group at the 2-position decreases the nucleophilicity of the pyrrole moiety through its electron-withdrawing nature. As a consequence, the main isolated dimers formed during the initial phase of DHICA oxidation at neutral pH are characterized by a 4,4'-, 4,7'- and 7,7'-mode of coupling (Figure 2.1_b).[123,125]

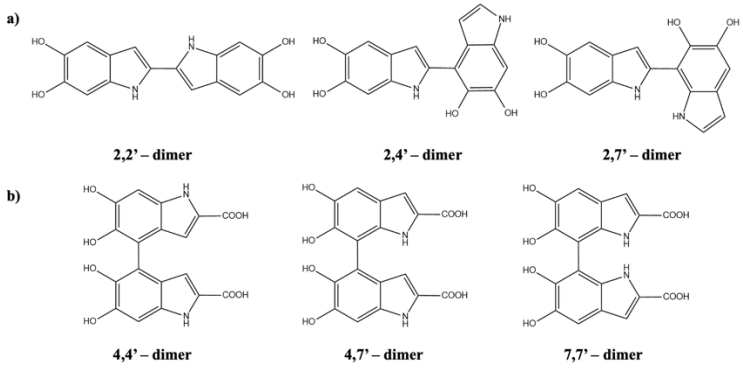

Figure 2.1. Structures of the main oligomers formed in the initial stages of the oxidation of a) DHI and b) DHICA.

In this context the research work described herein focused onto the examination of 5,6-dihydroxyindoles oxidation chemistry under conditions so

far poorly investigated, in the perspective of getting access to new melanin-related materials endowed with hitherto unknown functional properties.
In particular, this Chapter will be focused on:

- the exploration of the oxidative chemistry of DHI under solid-state conditions;
- the exploration of the oxidative chemistry of DHICA in the presence of the enzyme laccase as a green oxidizing agent.

2.1.1 Solid state oxidation of DHI

2.1.1.1 Exploration of DHI oxidation by mechanochemistry

Recently, solid-state reactions have been recognized as cleaner and faster alternative to conventional synthetic protocols involving the use of solvents. Mechanochemistry[126] in particular, *i.e.* chemical synthesis enabled or sustained by mechanical force, is emerging as a solvent-free technique for organic synthesis,[127–129] since it offers many potential advantages including simple work-up procedures, shorter reaction times and elimination of potentially toxic organic solvents, despite temperature is not a parameter easily controlled.[127,130,131] Furthermore, this approach allows to bypass solubility issues in the reaction medium or bypass problems due to reactions in which the solvent can interfere.[132]

On this basis, DHI reactivity under solid-state conditions was investigated, with the aim also of mimicking conditions that can be found in melanosomes where melanin growth can take place on a solid proteinaceous matrix.

In a first series of experiments the DHI solid-state oxidation was carried out using a small-scale laboratory ball mill (50 oscillations/s, room temperature) in the presence of different additives, mostly endowed with basic properties considering that no significant DHI consumption was observed under neutral conditions.

The reaction was initially performed in the presence of two molar equivalents (eqs) of sodium or potassium carbonate, monitoring the course of the oxidation by HPLC analysis at different reaction time (30-90 min). To overcome the marked air sensitivity of 5,6-dihydroxyindole compounds, a work-up procedure of the reaction mixture was adopted. Specifically, the mixture was taken up in water with the addition of a reducing agent to halt the reaction, then repeatedly extracted with ethyl acetate and, finally, the

combined organic phases were acetylated with acetic anhydride and pyridine after being dried with the aid of a rotary evaporator.

As shown in Figure 2.2, the HPLC analysis of the acetylated mixture at 90 min reaction time revealed the presence of two main products eluted at ca. 19 and 21 min, herein indicated as **1** and **2**, respectively, together with small amounts of other species more retained, along with unreacted DHI (eluted as the acetylated derivative at ca. 15 min).

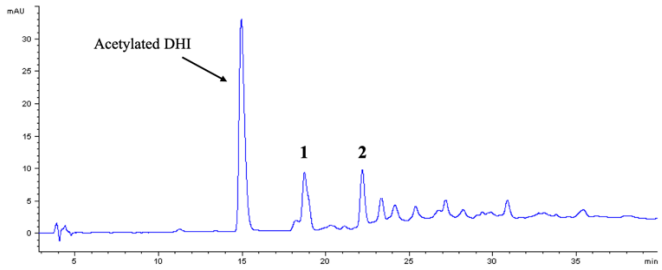

Figure 2.2. HPLC profile of the acetylated reaction mixture obtained by solid-state oxidation of DHI in the presence of 2 molar eqs of potassium carbonate after 90 min.

To obtain more information on the identity of the reaction products, the mixture was analyzed by MALDI-MS. DHI oligomers up to the tetramer stage were identified from a well-detectable cluster of peaks in the mass range up to *m/z* 1280. As shown, the main signals corresponded to the dimers' peaks.

In agreement with this observation, LC-MS analysis of the mixture indicated for the main DHI oxidation products pseudomolecular ion peaks ($[M+H]^+$ at *m/z* 465, $[M+Na]^+$ at *m/z* 487 and $[M+K]^+$ at *m/z* 503) compatible with acetylated biindolyl dimers.

Interestingly, none of these compounds corresponded to the commonly known 2,4'-, 2,7'-, and 2,2'-DHI dimers obtained in previous studies,[122,124] as evident from a comparison of their elutographic mobility with that of authentic standards available in the laboratory.

Subsequent experiments were then aimed at optimizing the reaction conditions in order to increase DHI consumption and the accumulation of the new products.

The best result was obtained running the reaction for 30 min in the presence of 10 molar eqs of potassium carbonate. Indeed, the HPLC profile showed a higher consumption of DHI together with the formation of higher amounts of **1** and **2** dimers (Figure 2.3). Unfortunately, it was not possible to increase DHI consumption by prolonging the reaction time, since concurrent oxidation of the products led to poorly chromatographable oligomeric species.

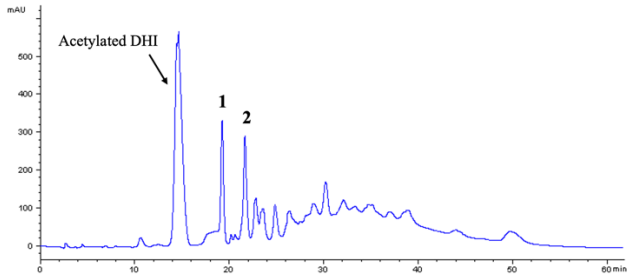

Figure 2.3. HPLC profile of the acetylated reaction mixture obtained by solid-state oxidation of DHI for 30 min in the presence of 10 molar eqs of potassium carbonate.

The reaction pattern obtained carrying out the DHI oxidation in the presence of carbonate was not observed when other non-alkaline or less alkaline salts *e.g.* sodium dihydrogen phosphate, sodium acetate or sodium chloride, were used.

Further experiments were directed to the evaluation of the efficacy of other oxidants. In particular, oxidizing agents commonly used in chemical synthesis (*e.g.* potassium ferricyanide and sodium periodate) or metal ions (*e.g.* Ni^{2+}, Cu^{2+}, Zn^{2+}) were tested in the presence or absence of potassium carbonate. The HPLC profile of the mixture obtained in the presence of periodate and

analyzed after the work-up protocol described above didn't show the presence of any product or starting material, due to a complete conversion of DHI to melanin. On the contrary, a more complex pattern of products was observed in the presence of potassium ferricyanide or metal ions. However, these products were identified, by comparison with authentic standards, as isomeric hexahydroxydiindolocarbazoles (triazatruxene derivatives, TAT), whose formation typically occurs under strongly acidic condition (Figure 2.4).[133]

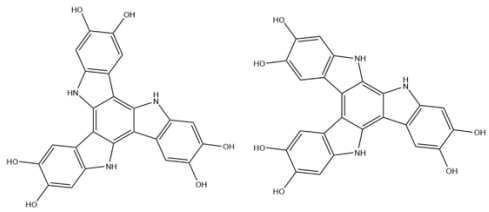

Figure 2.4. Structures of the main reaction products of DHI (TAT) under acidic conditions.

2.1.1.2 Structural characterization of DHI - dimers

To get more information about the structure of the new dimers, the solid-state DHI reaction was repeated on a larger scale and the products were isolated in pure form (about 20% w/w yield) by preparative TLC. The compounds thus obtained were identified as 5,5',6,6'-tetraacetoxy-4,4'-biindolyl (**1**) and 5,5',6,6'-tetraacetoxy-4,7'-biindolyl (**2**) (Figure 2.5), respectively, by a complete NMR characterization.

The ^{1}H NMR spectrum of compound **1** (Figure 2.6) was consistent with a symmetric acetylated dimer in which only the resonances of the H-2, H-3 and H-7 protons were present in the aromatic region, together with the signals of the four acetyl groups at δ 1.94 and δ 2.25. On the basis of chemical shifts and coupling constants[134], the signals at δ 5.99 and δ 7.37 were attributed to the H-3 and H-7 protons, respectively. This result was also confirmed by the

^{1}H,^{1}H COSY spectrum (Figure 2.7) which showed a correlation between the signals of the H-3 proton and the H-2 and NH proton at δ 7.30 and δ 10.44, respectively. Finally, the 4,4'-bonding was further confirmed by the ^{13}C spectrum (Figure 2.8) exhibiting a signal at δ 121.41 due to a substituted C-4 indole carbon.

The mode of linking of the indole units in dimer **2** was likewise apparent from the ^{1}H NMR spectrum (Figure 2.9), in which the resonances of one H-4 and one H-7 proton were clearly missing. Support to the proposed structure was also provided by the correlation of the signal of the H-3 proton at δ 5.89 with those of the vicinal H-2 (δ 7.32) and NH (δ 10.51) protons, and of the signal of the H-3 proton at δ 6.54 with those of the vicinal H-2 (δ 7.29) and NH protons (δ 9.62) showed by the ^{1}H,^{1}H COSY spectrum (Figure 2.10). Finally, the presence of two singlets at δ 118.75 and δ 113.98 ppm in the ^{13}C NMR spectrum (Figure 2.11), typical of substituted C-4 and C-7 indole carbons, respectively, further confirmed the hypothesized structure.

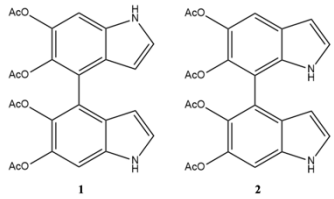

Figure 2.5. Structures of the main solid-state oxidation products of DHI isolated as acetyl derivatives: 5,5',6,6'-tetraacetoxy-4,4'-biindolyl (**1**) and 5,5',6,6'-tetraacetoxy-4,7'-biindolyl (**2**).

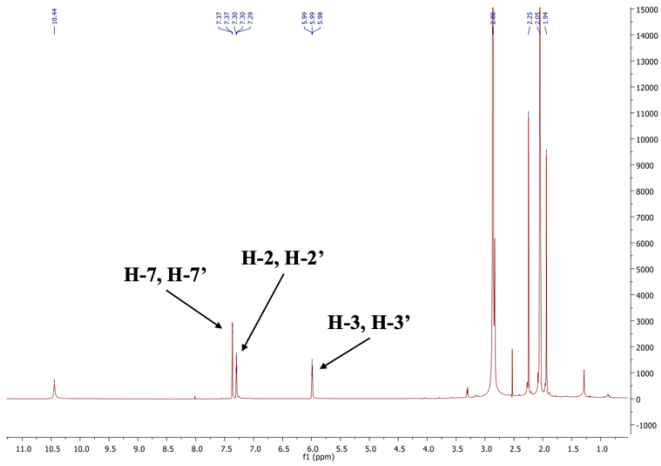

Figure 2.6. ^{1}H NMR spectrum of **1** in acetone-d_6.

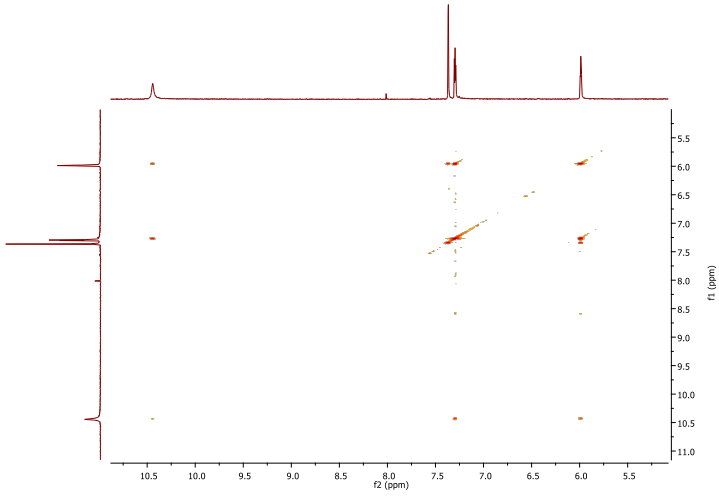

Figure 2.7. ^{1}H,^{1}H COSY NMR spectrum of **1** in acetone-d_6.

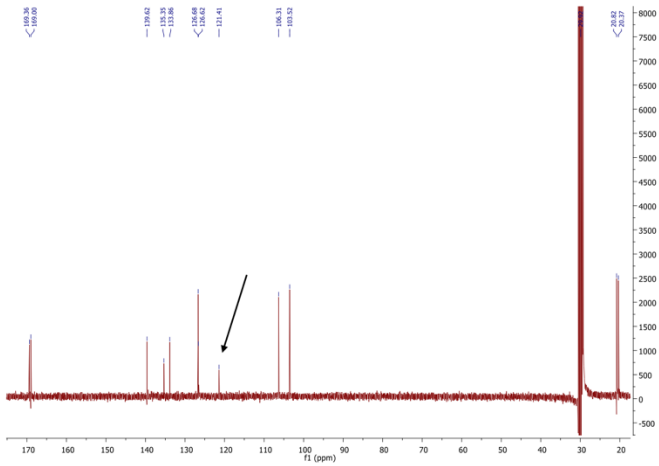

Figure 2.8. ^{13}C NMR spectrum of **1** in acetone-d_6.

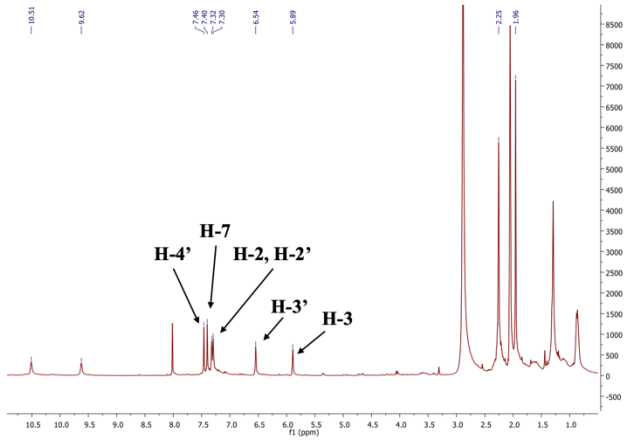

Figure 2.9. ^{1}H NMR spectrum of **2** in acetone-d_6.

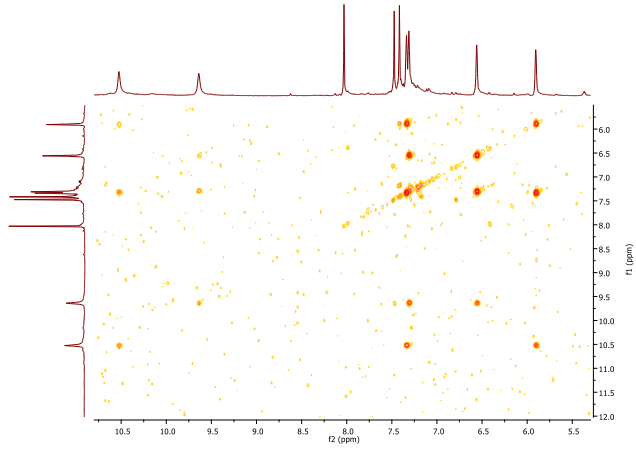

Figure 2.10. $^{1}H,^{1}H$ COSY NMR spectrum of **2** in acetone-d_6.

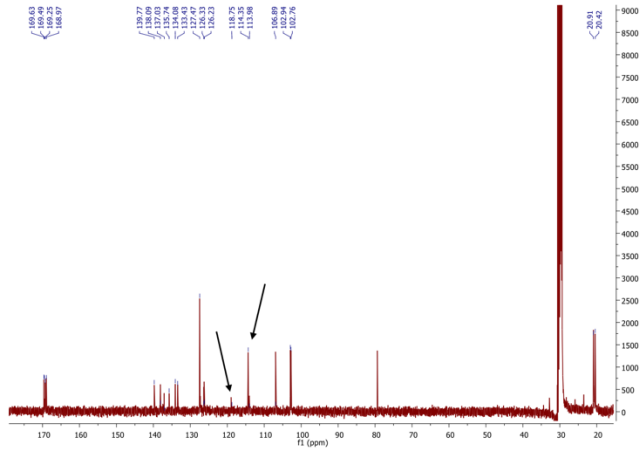

Figure 2.11. ^{13}C NMR spectrum of **2** in acetone-d_6.

2.1.1.3 Mechanism assessment of the DHI solid-state oxidation

As mentioned in the Introduction, the main products of the DHI oxidation reaction carried out under biomimetic conditions are the 2,4'- and 2,7'- DHI dimers. This selective mode of coupling is likely attributable to the attack of the nucleophilic 2-position of one indole to the electrophilic 4- or 7-position

of a transient 5,6-indolequinone intermediate originating, in turn, from the initially formed DHI radical disproportionation.[122,123,135]

The results reported herein highlighted for the first time an unexpected tendency of DHI to polymerize through a radical and not ionic mechanism, involving oxidative coupling at 4 and 7 positions. To better understand this interesting issue, a series of experiments directed to the study of the mechanism of DHI solid-state oxidation were carried out.

First experiments were directed to the re-examination of DHI oxidation in solution using different oxidizing agents. In particular, sodium periodate in aqueous buffer at pH 7 or *p*-chloranil in aprotic solvents of different polarity, such as acetonitrile and dichloromethane, were investigated as oxidizing agents. These reaction conditions led to the formation of the 2,4'- and 2,7'-dimers only. Interestingly, the same result was obtained using a strongly alkaline medium (phosphate buffer at pH 12 in the presence of potassium ferricyanide under an argon atmosphere), suggesting that the altered regiochemistry of DHI dimerization observed under the solid-state conditions can't be attributable only to the strong alkalinity of potassium carbonate.

On the other hand, the formation of dimers **1** and **2**, together with the 2,4'- and 2,7'-dimers, was observed carrying out the oxidation of DHI with *p*-chloranil or sodium periodate in a ball mill.

So, on this basis, it is clear that the solid-state is fundamental to obtain the 4,4'- and 4,7'-dimers from DHI oxidation, result likely attributable to the capacity of this condition to sufficiently stabilize the radical intermediates, although, even under solid-state conditions, depending on the particular oxidizing system used, the formation of also the usual 2,4'- and 2,7'-dimers was observed.

To obtain additional information on this issue, in other experiments the solid-state reaction was carried out using a different procedure. In particular, a drop-

casting deposition of a thin film of DHI on a glass slide was performed, which was then exposed to gaseous ammonia. Further analysis indicated the formation of 4,4'-, 4,7'-, 2,4'- and 2,7'-dimers, confirming that the specific space constraints associated with the solid-state conditions is fundamental for the formation of **1** and **2**.

Subsequently, other experiments were carried out involving the 2,2-diphenyl-1-picrylhydrazyl (DPPH) radical. When DPPH was added to a DHI solution in acetonitrile or when the solid-state reaction was performed using DPPH as the oxidizing agent, the formation of the 2,4'-dimer as the main product, together with the other three dimers, was observed. On the other hand, when DPPH was added drop-by-drop in the DHI solution in acetonitrile, 2,4'- and 4,4'-dimers formed in equal amount.

So, on this basis, it may be concluded that the 2,4'- and 2,7'- dimers are formed as main compounds when the oxidation reaction proceeds fast, as in the presence of HRP/H_2O_2 or chloranil or periodate in solution, while 4,4'- and 4,7'- dimers can only form when the reaction proceeds slowly, in organic solvent or under solid-state conditions. Moreover, some studies reported in literature discussed about the possible formation of radicals during the mechanical impact event of milling.[136]

In conclusion, all these findings support a radical-radical coupling mechanism involvement in the formation of the 4,4'- and 4,7'- dimers. Of course, formation of these products is favored by the use of potassium carbonate which, thanks to its basic nature, would allow a slow radical generation (Figure 2.12).

Actually, based on the proposed mechanism, the reaction should have led also to the formation of 7,7'-dimer. Indeed LC-MS analysis indicated the presence of another unknown compound characterized by a pseudomolecular ion peak $[M+H]^+$ at *m/z* 465 that, however, was not possible to purify and characterize.

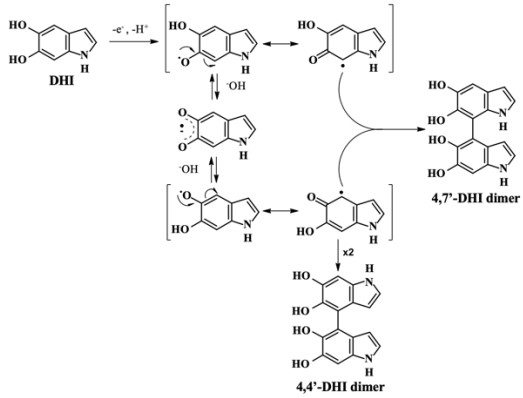

Figure 2.12. Proposed mechanism accounting for the formation of the 4,4'- and 4,7'-dimers.

2.1.1.4 Evaluation of the impact of solid-state reaction conditions on DHI-melanin structure and melanogenesis

Further experiments were directed at investigating how the structure of the final melanin pigment can be influenced by the indole mode of coupling observed under solid-state conditions. With this aim, the DHI solid-state oxidation reaction in the presence of potassium carbonate was carried out for a longer time. After 3 h, LC-MS analysis of the black powder obtained, showed a complete consumption of the monomer and all of the chromatographable oligomeric species.

The powder was then treated with alkaline hydrogen peroxide and the resulting mixture was analyzed by LC-MS analysis to identify and quantify the three diagnostic markers of eumelanin pigments, *i.e.* pyrrole-2,3-dicarboxylic acid (PDCA), pyrrole-2,3,5-tricarboxylic acid (PTCA) and pyrrole-2,3,4,5-tetracarboxylic acid (PTeCA). In detail, the oxidative fission of DHI units linked through the 2-position and the 2- and 3-positions leads to the formation of PTCA e PTeCA, respectively, while PDCA is obtained from indole units unsubstituted at the 2-position (Figure 2.13).[115,137–140]

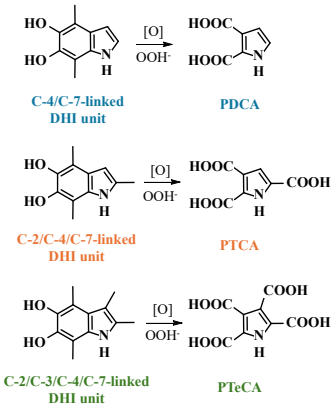

Figure 2.13. Proposed origin of PDCA, PTCA and PTeCA by alkaline hydrogen peroxide degradation of melanin pigments.

The 2-unsubstituted *versus* the 2-linked units were therefore quantified by means of the PDCA/PTCA and PDCA/PTeCA ratios, and the results were compared to the ones obtained with a standard DHI-melanin prepared using the HRP/H_2O_2 system commonly adopted in previous studies.[140] Based on the results reported in Table 2.1, the DHI-melanin prepared under solid-state conditions showed higher PDCA/PTCA and PDCA/PTeCA ratios than the standard melanin ones. It's important to specify that this result cannot be attributed to the presence of residual DHI. Indeed, as mentioned above, the complete consumption of the monomer was confirmed by LC-MS analysis of the melanin powder after acetylation.

Table 2.1. PDCA/PTCA and PDCA/PTeCA ratios for DHI-melanin obtained under solid-state condition *versus* DHI-melanin obtained using the enzymatic system HRP/H_2O_2.

Sample	PDCA/PTCA	PDCA/PTeCA
DHI melanin (solid-state reaction)	3.08	6.03
DHI melanin (HRP/H_2O_2 system)	0.42	0.34

Another experiment was aimed at the demonstration of the fundamental role of the solid-state condition to obtain a radical-radical coupling mechanism even in the advanced stages of melanogenesis. In particular, DHI oxidation was carried out under air in potassium carbonate buffer at pH 10 at the same DHI/salt ratio (1:10 w/w) used for solid-state oxidation. The collected precipitate was then subjected to the same chemical degradation treatment, and PDCA/PTCA and PDCA/PTeCA ratios were calculated. The obtained values, equal to 1.46 and 0.17, respectively, were very different from those obtained for solid-state melanin, confirming the specific role of the solid-state conditions in inducing a radical-radical coupling mechanism.

Finally, considering that the natural process of melanogenesis (*i.e.* the synthesis of melanin) occurs within the protein matrix of melanosome organelles, further experiments were aimed at evaluating whether the coupling mode of indole units during *in vivo* DHI polymerization was influenced by this solid matrix. Previous studies reported that DHI spontaneously oxidizes in egg albumen forming a stable purple chromophoric phase (melanochrome), transient in the solution reaction, indicating that the formation of stable species confined in the solid matrix during DHI oxidation may affect the reaction evolution.[141]

In this framework, to mimic the melanogenesis process, common proteins such as albumin, whey proteins isolate, or soy proteins isolate were used in the DHI solid-state oxidation mixture. These reactions led to the formation of

1 and **2**, together with the 2,4'- and 2,7'-dimers, as evidenced by LC-MS analysis.

The obtained results proved that the regiochemistry of DHI oxidative coupling can be significantly (though not completely) deviated by a solid matrix of great biological relevance like a protein. On this basis, it can be concluded that the reaction pathways, followed by melanogenesis occurring *in vivo* on melanosomal proteins, could be different from that so far pictured.

2.1.1.5 Assessment of the chromophoric properties of the 4,4'- and 4,7'- DHI dimers

Another part of the present work was directed to the oxidation of **1** and **2** under various conditions and to the study of the chromophores of the generated species.

The dimers, stored as the acetyl derivatives to avoid their oxidation, were firstly deprotected *in situ* using a procedure reported in literature that involves the use of sodium *tert*-butoxide in methanol under an argon atmosphere, and then immediately oxidized.[142] In particular, the oxidation was performed:

i) in the presence of the HRP/H_2O_2 system;
ii) in air at neutral pH;
iii) in the presence of potassium ferricyanide.

Under condition i), dimers **1** and **2** exhibited analogous chromophoric changes and evolution kinetics (Figure 2.14). As shown by UV-Vis analysis, after the first minute the absorption maxima of the dimers **1** and **2** at 320 nm (t_0) underwent a bathochromic shift, accompanied by the formation of a broad visible chromophore centered at around 580 nm. Subsequently, melanins slowly accumulated over time, whereas the absorption bands decreased and broadened.

Carrying out the reaction under the conditions ii) and iii), comparable but less defined chromophoric changes were observed.

On the other hand, the chromophores observed from oxidation of the 2,4'- and 2,7'-biindolyls showed less defined absorption maxima in the visible region at around 550 nm,[143] attributable to quinone methide species extended over the two indole units[135] that broadened over time.

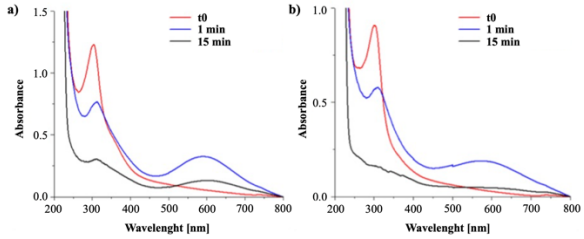

Figure 2.14. UV-Vis spectra of the HRP/H_2O_2 oxidation mixtures of deacetylated dimers a) **1** and b) **2**.

DFT method was then applied to formulate a structural hypothesis regarding the chromophores observed from dimers **1** and **2**. This activity was performed by Professor O. Crescenzi at University of Naples Federico II.

As reported in literature, the most stable quinonoid forms of 2,4'- and 2,7'-dimers are characterized by approximately planar geometries. So, in this case, the quinonoid system is able to extend on both indole rings.[135,143]

On the contrary, the 4,4'- and 4,7'-dimers didn't exhibit a coplanarity of the indole rings due to the presence of a hindered biphenyl-type interring connectivity. Indeed, the most stable quinonoid forms were found to be those localized on a single indole ring (Figure 2.15 and 2.16).

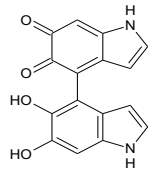

Figure 2.15. Structures of the most significant quinonoid forms of deacetylated dimer **1** in water.

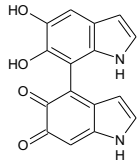

Figure 2.16. Structures of the most significant quinonoid forms of deacetylated dimer **2** in water.

2.1.1.6 Conclusions

The study of the 5,6-dihydroxyindoles oxidation pathway is an interesting approach to better understand the structure features of the final pigment and the associated functional properties.

In this framework, the DHI oxidation under solid-state conditions was explored, leading to the formation of hitherto unknown 4,4'- and 4,7'-biindolyls. Mechanistic experiments allowed to propose coupling of radicals stabilized by confinement inside a solid matrix as the predominant mechanistic route. The potential relevance of this reaction route to *in vivo* melanogenesis was suggested by prevalence of the 4,4'- and 4,7'- mode of coupling when the reaction was run using model proteins as the solid matrices.

2.1.1.7 Experimental section

Materials and Methods. Potassium carbonate, horseradish peroxidase (HRP, EC 1.11.1.7), hydrogen peroxide (30% v/v), sodium dithionite, albumin from bovine serum, *p*-chloranil, sodium periodate, potassium ferricyanide, 2,2-diphenyl-1-picrylhydrazyl (DPPH), 25% ammonium hydroxide solution, acetic anhydride, pyridine, anhydrous sodium sulphate, and sodium *tert*-butoxide were purchased from Sigma-Aldrich. Whey and soy proteins isolate were purchased from a local shop. DHI was synthetized using a previously developed protocol.[122]

UV-Vis spectra were recorded on a Jasco V-730 spectrophotometer.

HPLC analysis were performed on an instrument equipped with an SPD-10AV VP UV-Vis detector, using a Phenomenex Sphereclone C18 column (250 × 4.60 mm, 5 μm) at a flow rate of 0.7 mL/min; the gradient elution was as follows: 0.1% formic acid (solvent A)/ acetonitrile (solvent B), 30% B, 0-5 min; from 30 to 70% B, 5-45 min; the detection wavelength was set at 254 nm.

LC-MS analysis were run on an Agilent LC-MS ESI-TOF 1260/6230DA instrument operating in positive ionization mode in the following conditions: nebulizer pressure 35 psig; drying gas (nitrogen) 5 L/min, 325°C; capillary voltage 3500 V; fragmentor voltage 175 V. A Eclipse Plus C18 column (150 × 4.6 mm, 5 μm) at a flow rate of 0.4 mL/min was used, using the same eluant as above. For the chemical degradation mixtures, analyses were run in negative ion mode using the following gradient elution condition: 0.1% formic acid (solvent A)/ acetonitrile (solvent B), from 5% to 95% B, 0-50 min.

MALDI mass spectra were recorded on a 4800 MALDI TOF/TOF (Sciex) instrument operating in positive ion mode using a 2,5-dihydroxybenzoic acid water solution (1% w/v) as a matrix. 1 μL of a sample solution (1 mg/mL in

chloroform) was mixed with 1 μL of matrix solution and then loaded on the plate. The analysis was carried out after sample air-dried.

NMR spectra were recorded on a Bruker spectrometer at 400 MHz and the samples were dissolved in acetone-d_6. Chemical shifts are given in ppm.

Analytical and preparative TLC were carried out on silica gel plates (0.25 and 0.50 mm, respectively) from Merck using chloroform/methanol 96:4 v/v as eluent.

Computational investigations were performed with the Gaussian package of programs. Geometry optimizations were carried out at the DFT level with a reasonably large basis set, 6-31+G(d,p). UV-vis spectra of the main species were computed in vacuo or in solution using the time dependent-density functional theory (TD-DFT) approach,[144,145] with the 6-311++G(2d,2p) basis set and three different density functionals, PBE0, wB97X-D[146] and CAM-B3LYP.[147] This activity was performed by Professor O. Crescenzi at University of Naples Federico II.

Solid-state oxidation of DHI in the presence of carbonate salt. DHI (10 mg) was reacted with 2-10 molar eqs of sodium or potassium carbonate (19-93 mg, respectively) using a small-scale laboratory ball mill Fritsch Pulverisette 23 at 50 oscillations/s (stainless steel grinding jar with two 2 mm-diameter stainless steel grinding balls). After an appropriate amount of time (30-90 min) the obtained powder was treated with a saturated solution of sodium dithionite in water (15 mL), and the obtained mixture was extracted with ethyl acetate (15 mL × 3). The combined organic phases were dried over sodium sulphate and taken to dryness with the aid of a rotary evaporator. The residue thus obtained was acetylated with acetic anhydride-pyridine 95:5 v/v at room temperature. After 24 h the solution was washed with methanol and then analyzed by TLC, HPLC, LC-MS and MALDI-MS.

For preparative purposes 50 mg of DHI and 465 mg of potassium carbonate (10 molar eqs) were reacted in the ball mill for 30 min. The grey powder obtained was treated as described above and fractionated by preparative TLC to give acetylated 5,5',6,6'-tetrahydroxy-4,4'-biindolyl (**1**) (R_f = 0.39, 40 mg, 20% w/w yield) and acetylated 5,5',6,6'-tetrahydroxy-4,7'-biindolyl (**2**) (R_f = 0.45, 46 mg, 23% w/w yield) in pure form.

To collect enough material for **1** and **2** isolation and characterization, the reaction was repeated due to the limited capacity of the grinding cavity (maximum ca. 0.6 g of reactants).

Acetylated 5,5',6,6'-tetrahydroxy-4,4'-biindolyl (**1**):

ESI$^+$/MS: *m/z* 465 $[M+H]^+$, 487 $[M+Na]^+$, 503 $[M+K]^+$.

UV-Vis: λ_{max} 295 nm; ε= 8489 $M^{-1}cm^{-1}$

^{1}H NMR δ: 1.94 (3H × 2, s, $COCH_3$), 2.25 (3H × 2, s, $COCH_3$), 5.99 (1H × 2, m, H-3, H-3'), 7.30 (1H × 2, m, H-2, H-2'), 7.37 (1H × 2, bs, H-7, H-7'), 10.44 (1H × 2, bs, NH, N'H).

^{13}C NMR δ: 20.4 ($OCOCH_3$, C-5), 20.8 ($OCOCH_3$, C-6), 103.5 (C-3,C-3'), 106.3 (C-7,C-7'), 121.4 (C-4, C-4'), 126.6 (C-9,C-9'), 126.7 (C-2,C-2'), 133.9 (C-8, C-8'), 135.4 (C-5,C-5'), 139.6 (C-6, C-6'), 169.0 ($COCH_3$), 169.4 ($COCH_3$).

Acetylated 5,5',6,6'-tetrahydroxy-4,7'-biindolyl (**2**):

ESI$^+$/MS: *m/z* 465 $[M+H]^+$, 487 $[M+Na]^+$, 503 $[M+K]^+$.

UV-Vis: λ_{max} 295 nm; ε= 9575 $M^{-1}cm^{-1}$

^{1}H NMR δ: 1.96 (3H × 2, s, $COCH_3$), 2.25 (3H × 2, s, $COCH_3$), 5.89 (1H, m, H-3), 6.54 (1H, m, H-3'), 7.30 (1H, m, H-2'), 7.32 (1H, m, H-2), 7.40 (1H, bs, H-7), 7.46 (1H, s, H-4'), 9.62 (1H, bs, N'H), 10.51 (1H, bs, NH).

^{13}C NMR δ: 20.4 ($OCOCH_3$), 20.9 ($OCOCH_3$), 102.8 (C-3'), 102.9 (C-3), 106.9 (C-7), 114.0 (C-7'), 114.4 (C-4'), 118.8 (C-4), 126.2 (C-9'), 126.3 (C-9), 127.5 (C-2, C-2'), 133.4 (C-8'), 134.1 (C-8), 135.7 (C-5), 137.0 (C-6'),

138.1 (C-5'), 139.7 (C-6), 169.0 (COCH3), 169.2 (COCH3), 169.5 ($COCH_3$), 169.6 ($COCH_3$).

Solid-state oxidation of DHI in the presence of other reagents. DHI (10 mg) was reacted with 0.5 molar eqs of *p*-chloranil (17 mg), 0.25 molar eqs of sodium periodate (3.5 mg) or 0.5 molar eqs of DPPH (13 mg) in a ball mill at 50 oscillations/s. After an appropriate amount of time (3-30 min) the obtained powder was worked-up as described above and analyzed by LC-MS. In control experiments the reaction was run in the absence of additives for 30 min.

In other experiments, DHI (10 mg) was dissolved in 100 μL of ethyl acetate, air-dried on a 2 cm^2 glass slide and exposed to ammonia vapor for 20 min. The resulting coated glass slide was washed with acetic anhydride and pyridine. After 24 h the obtained solution was taken to dryness and the residue dissolved in methanol and analyzed by LC-MS.

Solid-state oxidation of DHI in the presence of protein matrices. DHI (10 mg) was reacted with bovine serum albumin, whey proteins isolate or soy proteins isolate (100 mg) in a ball mill at 50 oscillations/s. After 30 min, the obtained powder was worked-up as described above, and finally analyzed by LC-MS.

DHI oxidation in solution. DHI (10 mg) was reacted with HRP (72 U/mL) and H_2O_2 (2 molar eqs) in 0.1 M phosphate buffer at pH 7 (4.2 mL). After 19 s, the mixture was diluted in a saturated aqueous solution of sodium dithionite (15 mL) and rapidly extracted with ethyl acetate (15 mL × 3). The collected organic phases were dried using a rotary evaporator, acetylated as described above and analyzed by LC-MS.

In other experiments the oxidation reaction was performed in the presence of:

i) 1 molar equivalent (eq) of sodium periodate (14 mg) in 0.1 M phosphate buffer at pH 7 (4.2 mL), for 19 s;

ii) 0.5 molar eqs of *p*-chloranil (17 mg) in dichloromethane or acetonitrile (4.2 mL), for 20 s;
iii) 1 molar eq of potassium ferricyanide (22 mg) in 0.1 M phosphate buffer at pH 12 (4.2 mL) under argon atmosphere, for 20 s;
iv) 0.5 molar eqs of DPPH (13 mg pre-dissolved in 250 µL of acetonitrile) in acetonitrile (4.2 mL), for 20 s;
v) 0.5 molar eqs of DPPH (13 mg pre-dissolved in 250 µL of acetonitrile) added drop-by-drop every 5 s to DHI solution in acetonitrile (3.95 mL).

Preparation and chemical degradation of melanins in solid-state or solution conditions. DHI (30 mg) was reacted with 10 molar eqs of potassium carbonate (300 mg) in a ball mill at 50 oscillations/s. After 3 h, melanin was recovered as dark powder.

In parallel, DHI (30 mg dissolved in the minimal amount of methanol) was reacted with 10 molar eqs of potassium carbonate (300 mg) in 12.5 mL of water (final concentration of DHI = 16 mM). The mixture was left under vigorous stirring for 24 h and the pigment was then recovered by centrifugation and lyophilization.

50 mg of melanin obtained in the solid-state or 5 mg of melanin prepared in solution was suspended in 1 mL of 1 M NaOH and treated with 1.5% H_2O_2 (final concentration) at room temperature under vigorous stirring. The mixture thus obtained after 24 h was treated with a $Na_2S_2O_5$ solution at 5% w/v (200 µL), taken to pH 4 with 85% H_3PO_4, filtered through a nylon membrane (13 mm, 0.45 µm), and analyzed by LC-MS.

In order to check the DHI consumption, an aliquot of melanin samples was acetylated with acetic anhydride-pyridine 95:5 v/v at room temperature for 24 h and analyzed by LC-MS after washing with methanol.

Spectrophotometric monitoring of dimer oxidation. 3 mg of acetylated dimers **1** or **2** were dissolved in methanol to reach a final concentration of 3.6 mM. To remove protective groups, a procedure already reported in literature was followed,[142] involving treatment of 1.8 mL of the dimer solution with 8 molar eqs of sodium *tert*-butoxide under an argon atmosphere. After 5 min, the pH of the mixture was taken to 2 by addition of 4 M HCl. Then, the resulting mixture was added to 0.1 M phosphate buffer at pH 7.4 (6.5 mL) to reach a final concentration of 1 mM, and the oxidation was performed:

i) in the presence of HRP (2 U/mL) and H_2O_2 (1 molar eq);
ii) in air at neutral pH;
iii) in the presence of potassium ferricyanide (1 molar eq).

The reaction mixtures were periodically analyzed by UV-vis spectrophotometry.

2.1.2 Oxidation of DHICA with the enzyme laccase

2.1.2.1 Exploration of DHICA oxidation with laccase

The herein reported preliminary work was in part carried out during a two-month research period abroad at the University of Aveiro (Portugal). This work was focused on the exploration of the potential use of laccase as an alternative oxidative system for the eumelanin precursor DHICA. Contrary to the commonly employed HRP, which needs the use of H_2O_2 to work, laccase does not require a cofactor for its catalytic activity.[148–150] It is a low-cost multi-copper oxidase, widely spread in bacteria, insects and, especially in fungi, which catalyzes the oxidation of various phenolic and non-phenolic compounds using oxygen as electron acceptor and generating water as by-product (Figure 2.17).[151,152]

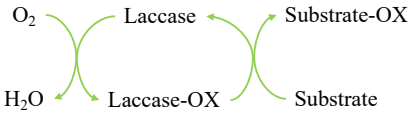

Figure 2.17. Laccase reaction mechanism.[153]

The low substrate specificity and high catalytic efficiency make this enzyme interesting for various applications in different fields.[154–157]

In this framework, a first series of experiments was directed to a systematic investigation of the experimental conditions for the oxidation of DHICA with laccase from *Trametes versicolor* in terms of pH of the reaction mixture, monitoring the reaction course through UV-Vis spectroscopy.

The laccase's origin can influence the optimal pH of the enzyme activity for the phenolic substrate.[158] In the specific case of fungal laccases (*e.g.* from *T. versicolor*) the optimum pH for phenolic substrates varies between 3 and 5.5, becoming stable at around 7 and essentially inactive at alkaline pHs.[159,160]

On this basis, and considering previous reported conditions and solubility issues, DHICA (3.6 mM) and laccase (28 U/mL) were reacted at room temperature in 0.1 M sodium phosphate buffer exploring a large range of pHs (3-7).[161] After comparing the UV-Vis spectra of the reaction mixtures, the buffer at pH 5 was chosen to run the oxidation of DHICA with the enzyme. Indeed, in this case, the peculiar absorption maximum of DHICA at 320 nm slowly decreased over time compared to the other pH conditions explored, and a bathochromic shift to 340 nm was observed, together with the appearance of an absorption maximum at 530 nm (Figure 2.18_a), likely due to the formation of oxidized compounds. Indeed, running the same experiment in the absence of laccase (CTRL), the UV-Vis absorption profile showed just a slight decrease of the DHICA absorption at 320 nm over time (Figure 2.18_b), likely due to a progressive precipitation of the indole from the acidic buffer solution.

The HPLC profile of the reaction mixture analyzed after 5 min showed a slight consumption (ca. 30%) of DHICA eluted at ca. 21 min, together with the formation of two main products eluted at ca. 22 and 24 min (Figure 2.19), identified as DHICA dimers by LC-MS analysis ($[M+H]^+$ at *m/z* 385). These latter corresponded to the previously reported 4,4'- and 4,7'-DHICA dimers obtained in previous studies,[123,125] as evident from the comparison of their elutographic mobility with that of authentic standards available in the laboratory.

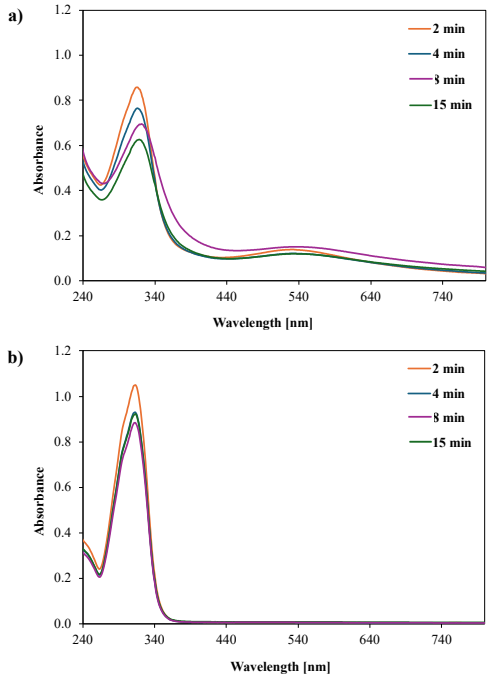

Figure 2.18. UV-Vis spectra of DHICA (3.6 mM) reaction mixture over time in 0.1 M phosphate buffer 0.1 M at pH 5 a) in the presence or b) absence (CTRL) of laccase (28 U/mL).

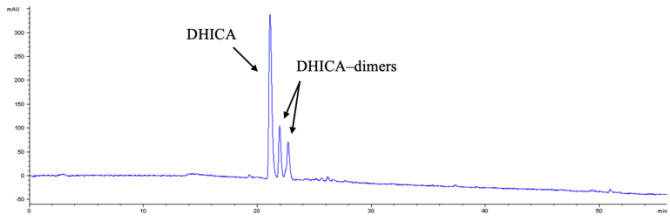

Figure 2.19. HPLC profile of the DHICA (3.6 mM) oxidation reaction in the presence of laccase (28 U/mL), in phosphate buffer 0.1 M at pH 5, after 5 min.

After having selected the best working pH, further experiments were devoted to the optimization of the experimental conditions for the DHICA dimers formation in terms of DHICA/laccase concentration and reaction time.

Initially, the mixtures were analyzed by HPLC analysis after 15 min using the following DHICA/laccase concentrations:

i) 3.6 mM DHICA + 28 U/mL laccase;
ii) 0.5 mM DHICA + 14 U/mL laccase;
iii) 10 mM DHICA + 14 U/mL laccase.

Reaction i) led to an almost complete consumption of DHICA after 15 min, whereas in the case of reaction iii) only a 50% of DHICA consumption was observed after the same amount of time. On the other hand, reaction ii) was too slow, showing no consumption of the monomer after 15 min. On this basis, reactions i) and iii) were chosen to be followed more accurately over time (0-15 min) by HPLC analysis.

In both cases the formation of the two main products cited above was observed after 5 min. However, neither condition showed a gradual accumulation of the products, but only their degradation over time, together with the consumption of DHICA.

On this basis, conditions iii) was chosen for further analysis, involving the use of a lower amount of laccase.

Subsequent experiments were then directed to the use of ionic liquids (ILs) as reaction medium. Indeed, previous studies have reported that the laccase-catalyzed reactions might be strongly influenced by the solvent system considering that, compared to others, its active site isn't located deeply inside the enzyme.[162,163] Interesting results in this direction have been obtained in particular with ILs, which are currently widely exploited as reaction media thanks to their low volatility, low toxicity and unique solubilization properties for organic and inorganic materials.[164]

More specifically, cholinium-based ILs have been reported in literature as the most promising candidates to improve laccase activity.[165] On this basis, the optimized oxidation reaction between DHICA and laccase was also run in the

presence of different percentages (1-0% w/w) of choline dihydrogen phosphate (ChDHP) or choline dihydrogen citrate (ChCit).
Unfortunately, no significant differences were observed by HPLC analysis with the reaction performed using phosphate buffer only as the reaction medium.

2.1.2.2 Exploration of laccase as an oxidizing system for DHICA melanin formation

Further experiments were focused on the assessment of laccase as an oxidizing system for extensive DHICA polymerization to melanin. With this aim, the DHICA oxidation reaction in the presence of the enzyme was carried out for a longer time, using the previously described optimized condition. In particular, DHICA (10 mM) and laccase (14 U/mL) were reacted in 0.1 M sodium phosphate buffer at pH 5, and after 2 h, melanin **I** was recovered as a black powder, washed and finally lyophilized. Notably, the melanin recovery yield was found to be higher than 100% w/w. This result could be attributable to the occurrence of strong interactions between melanin and laccase inducing precipitation of the enzyme together with the pigment, resulting in a such high yield (as also mentioned in the following 2.1.2.3 paragraph).
For comparison, a standard DHICA-melanin (**II**) obtained using the HRP/H_2O_2 system was also prepared, following a procedure reported in literature (ca. 20% w/w yield).[166]
The thus prepared melanins were analyzed by UV-Vis spectroscopy proving to have very similar profiles characterized by an absorption maximum at 320 nm and a broadband absorption spanning the entire visible range with a monotonic wavelength dependence, typical of eumelanins (Figure 2.20).[39,113,143] However, although the two spectra were recorded at the same concentration (0.05 mg/mL), the profile of melanin **I** was less intense than

that of melanin **II**, as expected based on the contribution of laccase to the weight of the recovered melanin.

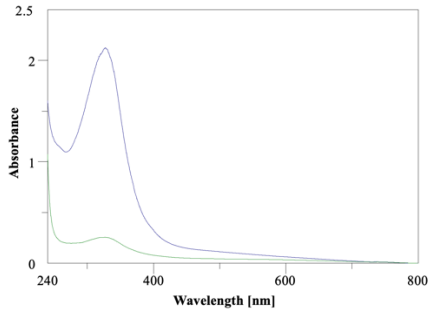

Figure 2.20. UV-Vis spectra of melanin **I** (blue) and melanin **II** (green) at 50 mg/mL in methanol.

Subsequentially, the alkaline hydrogen peroxide degradation was performed on both melanins, and the resulting mixtures were analyzed by LC-MS analysis. The profiles for both melanins showed the presence of pyrrole-2,3,5-tricarboxylic acid (PTCA) as the specific marker arising from DHICA-derived structures, although in a lower content for melanin **I**, as expected.[115]

Finally, further experiments were devoted to the evaluation of the antioxidant properties of melanins **I** and **II** using two conventional chemical assays, *i.e.* the 2,2-diphenyl-1-picrylhydrazyl (DPPH) and the ferric reducing antioxidant power (FRAP) assays (Table 2.2). Notably, similar antioxidant properties were exhibited in both assays, although the real melanin content in sample **II** should be lower with respect to melanin **I**. Laccase is of course a redox system, but its activity should be an oxidizing activity rather than a reducing activity, so a role of laccase in the really efficient antioxidant properties exhibited my melanin **II** could be ruled out. In any case, this aspect will be the subject of furthermore detailed studies.

Table 2.2. Results of DPPH and FRAP assays expressed as EC_{50} values and Trolox eqs (mg Trolox/mg sample), respectively, calculated for melanin **I** and **II** obtained from the DHICA oxidation reaction in the presence of laccase or HRP/H_2O_2, respectively. Mean values ± SD from at least three experiments are reported.

Sample	EC_{50} (mg/mL)	mg of Trolox/ mg (sample)
Melanin **I**	0.01565 ± 0.00001	1.4 ± 0.1
Melanin **II**	0.01310± 0.00001	1.9 ± 0.1

2.1.2.3 Evaluation of aqueous biphasic system as a promising method for laccase recovery and reuse in DHICA oxidation

Despite the very great catalytic properties of laccase, the use of this enzyme has some limitations such as its recovery from the reaction medium and reusability, which of course lead to an increase of the process costs.[167,168] To overcome such limitations, in previous studies aqueous biphasic system (ABS) has been recognized as an excellent and promising alternative to conventional liquid-liquid extraction for separation and purification of biomolecules, since it provides a suitable and friendly environment for the maintenance of the enzymatic activity and its reuse.[165,167,169,170] ABS is composed of water and at least two water-soluble components (*e.g.* polymers and salts) which, when are present above a certain quantity[171], form two phases allowing the separation of the products of interest from the enzyme.[172] For example, the possibility to recover and reuse the laccase in the reaction with 2,2′-azino-bis(3-ethylbenzothiazoline-6-sulphonic acid) (ABTS) for at least five consecutive cycles with no losses in the enzymatic activity has been recently demonstrated.[169]

On this basis, the oxidation reaction of DHICA with laccase described above was performed using an ABS already reported in literature for similar systems[173] composed of polypropylene glycol (PPG) 400 (33% w/w) and KH_2PO_4 (6.4% w/w) as polymer and salt, respectively, in water. DHICA (10 mM) and laccase (14 U/mL) were reacted under vigorous stirring (heterogeneous medium) for 5 min. The mixture was then centrifuged to separately recover the two phases which were analyzed by HPLC. The upper polymer-phase (UP) contained the same two DHICA-dimers obtained under the standard reaction conditions. Interestingly, in the lower salt-phase (LP) no compound was detected.

To evaluate in which phase the enzyme was confined and to understand if its catalytic activity decreased after the first cycle, laccase activity was measured using ABTS as substrate, following a procedure reported in literature.[173] The activity was expressed as U/L, where 1 unit (U) of laccase activity corresponds to the amount of enzyme necessary for the oxidation of 1 μmol of the substrate ($\varepsilon = 36.000\ M^{-1}\ cm^{-1}$) per min. A control sample obtained in the absence of DHICA was also analyzed.

Noteworthy, LP showed a very great activity (331 ± 3 U/L) comparable to the CTRL sample (330 ± 5 U/L), indicating preservation of the enzyme activity. On the contrary, no activity was observed in the UP, suggesting that an efficient separation between the reaction compounds and the enzyme occurred.

Then, similarly to the previous experiments, the reaction was repeated following it over time (0-15 min). However, even in this case no gradual accumulation of the products was observed, but only their degradation over time, together with a progressive consumption of DHICA.

In other experiments, the laccase-catalyzed DHICA-melanin formation was investigated in the ABS. After 2 h of reaction under vigorous stirring, the two

phases were separated by centrifugation, which also allowed recovery of the precipitated melanin. The ABTS assay confirmed the presence of laccase activity only in the LP. However, the laccase activity of LP was lower than the one calculated for the control sample (in the absence of DHICA) (Table 2.3). In any case, the DHICA polymerization reaction was repeated using the previously collected LP in a second cycle, whereas the DHICA-enriched UP was removed and substituted with the same volume of a solution containing DHICA and the UP constituents.[169] However, ABTS assay indicated a gradual decrease of enzyme efficiency (Table 2.3), as evident also from the decrease in melanin formation. This result, although preliminary, could be attributed to the formation of intermediate species during the polymerization process which can interact with laccase, inhibiting it, as previously reported *e.g.* for intermediates originated from laccase-catalyzed lignin degradation.[174]

Table 2.3. Results of the laccase activity in the LP measured with ABTS assay and expressed as U/L. Mean values ± SD from at least three experiments are reported.

Cycle	U/L
0	366 ± 8
1	70 ± 1
2	16 ± 3

2.1.2.4 Conclusions

Although the obtained results are still preliminary and several aspects have to be improved, concerning in particular the lack of accumulation of DHICA dimers, this study demonstrated that laccase could be a valid alternative to the conventional DHICA polymerization method. Indeed, laccase led to the formation of a melanin apparently endowed with more potent antioxidant

properties compared to the one obtained using the HRP/H_2O_2 oxidizing system. In addition, the ABS system containing PPG and KH_2PO_4, proved to be able to separate the reaction products from laccase, opening interesting perspectives toward the possible reusability of the enzyme.

2.1.2.5 Experimental section

Materials and methods. 5,6-dihydroxyindole-2-carboxylic acid has been synthetized using a procedure reported in literature.[115] Commercial laccase from *Trametes versicolor* (EC 1.10.3.2, 1.4 U/mg), horseradish peroxidase (HRP, EC 1.11.1.7), hydrogen peroxide (30% v/v), 2,2-diphenyl-1-picrylhydrazyl (DPPH), iron (III) chloride (97%), 2,4,6-tris(2-pyridyl)-s-triazine (TPTZ) (≥ 98%), (±)-6-hydroxy-2,5,7,8-tetramethylchromane-2-carboxylic acid (Trolox) (97%), dipotassium hydrogen phosphate trihydrate, and polypropylene glycol with a molecular weight of 400 g/mol (PPG 400) were acquired from Sigma-Aldrich.

HPLC analysis were performed on an instrument equipped with an SPD-10AV VP UV-Vis detector, using a Phenomenex Sphereclone C18 column (250 × 4.60 mm, 5 μm) at a flow rate of 1.0 mL/min; the gradient elution was as follows: 0.1% formic acid (solvent A)/ methanol (solvent B)): 5% B, 0-10 min; from 5 to 80% B, 10-47.5 min; the detection wavelength was set at 254 nm.

LC-MS analysis were run on an Agilent LC-MS ESI-TOF 1260/6230DA instrument operating in positive ionization mode in the following conditions: nebulizer pressure 35 psig; drying gas (nitrogen) 5 L/min, 325°C; capillary voltage 3500 V; fragmentor voltage 175 V. A Eclipse Plus C18 column (150 × 4.6 mm, 5 μm) at a flow rate of 0.4 mL/min was used, using the same eluant as above.

DHICA oxidation in the presence of laccase. The reaction of DHICA with laccase was optimized in terms of pH, DHICA/enzyme concentrations, and time. In particular, DHICA (10 mg, pre-dissolved in 100 mL of DMSO) was reacted with laccase in air in 0.1 M sodium phosphate buffer at different pH (3-7). Fixed the pH at 5, optimal DHICA and laccase concentrations were investigated:

i) 3.6 mM DHICA + 28 U/mL laccase;
ii) 0.5 mM DHICA + 14 U/mL laccase;
iii) 10 mM DHICA + 14 U/mL laccase.

All the reaction mixtures were analyzed over time (0-15 min) by UV-Vis, HPLC and LC-MS. As a comparison, a control mixture prepared without the enzyme was also analyzed.

DHICA oxidation in the presence of laccase and ionic liquids solvent. DHICA (10 mM) and laccase (14 U/mL) were reacted under the optimized conditions in 0.1 M sodium phosphate buffer at pH 5 containing choline dihydrogen phosphate or choline dihydrogen citrate at 1%, 5%, 10%, 20% w/w with respect to the total system weight.

The mixtures were analyzed by HPLC.

Preparation and chemical degradation of melanins. ***Melanin I:*** DHICA (50 mg) was reacted with 14 U/mL of laccase (254 mg) in 26 mL of 0.1 M sodium phosphate buffer at pH 5, in air and at room temperature. After 2 h, the reaction mixture was centrifuged, and the precipitate washed 3 times with 0.01 M HCl and one time with H_2O, and finally lyophilized. ***Melanin II:*** DHICA (50 mg) was reacted with HRP (15 U/mL) and H_2O_2 (1.2 eqs) in 25 mL of 0.1 M phosphate buffer at pH 7, following a procedure reported in literature slightly modified.[166] After 2 h, the reaction mixture was first acidified to pH 5 with 6 M HCl, then centrifuged. Finally, the precipitate was

washed 3 times with 0.01 M HCl and one time with H_2O, and finally lyophilized as above.

For chemical degradation, 5 mg of melanin **I** or **II** was suspended in 1 mL of 0.1 M NaOH 1 M and treated with 1.5% H_2O_2 (final concentration) at room temperature under vigorous stirring. After 24 h the mixture was treated with a $Na_2S_2O_5$ solution at 5% w/v (200 μL), taken to pH 4 with 85% H_3PO_4, filtered through a nylon membrane (13 mm, 0.45 μm), and analyzed by LC-MS.

DPPH assay.[175,176] Various volumes of melanin **I** or melanin **II** solution (10 mg/mL in DMSO) were added to a 200 μM ethanolic solution of DPPH (7.6-50 mg/mL final dose). After 10 min under stirring at room temperature, the absorbance of each solution at 515 nm was measured. The antioxidant power was expressed as EC_{50}, that is the sample concentration capable of reducing the initial absorbance of the DPPH solution by 50%. Experiments were run in triplicate.

FRAP assay.[177] FRAP solution was prepared by mixing 36 mL of 0.3 M acetate buffer (pH 3.6), 3.6 mL of an aqueous 20 mM $FeCl_3$ solution (1.7 mM final concentration) and 3.6 mL of a 10 mM TPTZ solution prepared in 40 mM HCl (0.83 mM final concentration). Various volumes of melanin **I** or melanin **II** solution (10 mg/mL in DMSO) were added to the FRAP solution (0.7-4 mg/mL final dose) and after 10 min under stirring at room temperature the absorbance of each solution at 593 nm was measured. Trolox was used as a reference antioxidant and the results were expressed as Trolox eqs (mg Trolox/mg sample). Experiments were run in triplicate.

DHICA oxidation in the presence of laccase and ABS. The laccase-catalyzed DHICA oxidation was carried out in an aqueous biphasic system (ABS)[173] composed of PPG 400 (33% w/w), KH_2PO_4 (6.4% w/w) and H_2O (59.4% w/w), to which DHICA (10 mM) and laccase (14 U/mL) were added (percentage are referred to the total system weight). At different times, the

reaction mixture was centrifuged (3500 rpm, 30 min, 25°C) and the two obtained phases were separated and analyzed by HPLC. A control sample was also prepared without the use of DHICA. Two consecutive cycles of DHICA polymerization (2 h) were performed. After the first cycle, the DHICA-enriched top phase was removed and substituted with the same volume of the polymer-rich solution containing 64.2% w/w PPG, 0.37% KH_2PO_4, 34.23% w/w H_2O and 10 mM DHICA (percentage are referred to the new top phase weight). After each cycle the laccase activity was determined by the ABTS assay (see below).

Laccase activity assay. The laccase activity was measured following a procedure reported in literature.[173] In particular, the sample (50 μL) was added to a mixing composed of 1.7 mM ABTS aqueous solution (250 μL) and citrate phosphate buffer at pH 4.5 (700 μL). The citrate phosphate buffer was prepared combining 3.43 g of citric acid and 5.07 g disodium hydrogen phosphate with 250 mL of water.

The absorbance per min of the resulting mixture was then measured at 420 nm by UV-Vis analysis and expressed in U/L using the following expression:

$$\frac{U}{L} = \frac{\Delta Abs \times 60 \times f_{dil} \times 10^6}{\varepsilon}$$

where ΔAbs is the difference between the absorbance at 30 s and the absorbance at 0 s; 60 corresponds to the conversion of seconds to minutes; f_{dil} is the sample dilution factor; 10^6 corresponds to the conversion of μL to mL; e is ABTS molar extinction coefficient (36.000 M^{-1} cm^{-1}). Experiments were run in triplicate.

Chapter 3

Exploitation of natural and bio-inspired lignins as antioxidant compounds for different applications

3.1 Recovery and functionalization of lignin from chestnut shell to be exploited as a functional additive in biocompatible materials for biomedical applications

3.1.1 Introduction

As mentioned in the Introduction, lignin is one of the main phenolic compounds widely distributed in nature. Among all the available sources, a lot of interest has been recently directed to agri-food by-products, representing a sustainable and easily accessible resource of value-added compounds including lignin.[22,178,179] Thanks to their antioxidant, antimicrobial, and filler properties, lignin is finding increasing applications in a variety of sectors. In particular, increasing attention has been directed to the use of lignin as active compound in hybrid systems for application in the biomedical field. In this framework, another interesting additive are silver nanoparticles (AgNPs), due to their remarkable bactericidal, antifungal and antitumor properties,[180] together with their easy preparation and incorporation into biomaterials.[181,182] However, the preparation procedure of AgNPs may be very critical considering the toxicity of the often-used reducing and stabilizing agents. In this perspective, the use of alternative, low-cost and green compounds endowed with marked reducing ability, such as lignin, has been recently implemented.

On this basis, the subsequent 3.1 paragraphs will be focused on the:

- recovery of lignin from chestnut shells (CS), using a green procedure based on DES-extraction combined with a mechanical pre-treatment;
- use of CS lignin (CSL) as reducing agent for mechanochemical synthesis of AgNPs;
- incorporation of CSL or Ag(0) nanoparticles in poly(D,L-lactic acid).

3.1.2 Extraction of lignin from chestnut shells

Based on a previous reported study focused on the extraction of lignin from nut shells[183], the work herein reported was focused on the extraction of lignin from chestnut shells by using a slightly modified previously developed green protocol.[184] In particular, in order to achieve a more efficient extraction, a mechanical pre-treatment in a ball mill was performed. This step should induce not only an increase of the surface area but also a cleavage of glycosidic linkages and β-O-4' bonds in lignin components, leading to improved extraction yields[185–188] and, likely, to the release of phenolic hydroxyl groups with a subsequent enhancement of the antioxidant capabilities.

Then, the minced shells were extracted using deep eutectic solvents (DES), that recently have become increasingly popular as efficient as well as eco-friendly solvents for the recovery of phenolic compounds from agri-food by-products.[189–193] In particular, a DES composed of choline chloride and lactic acid at 1:2 mol/mol ratio was used, and the extraction was performed for 24 h at 120 °C. After the addition of 0.01 M HCl, lignin was simply recovered as a brown powder by simple precipitation followed by centrifugation, extensive washings with water, and lyophilization. The extraction and recovery yields calculated with respect to the amount of starting material or dissolved in the DES resulted equal to 19% and 27% w/w, respectively.[194]

3.1.2.1 Assessment of antioxidant properties of CSL

The antioxidant properties of CSL were evaluated using two conventional chemical assays, that is the 2,2-diphenyl-1-picrylhydrazyl (DPPH) assay, measuring the hydrogen- and/or electron-donor ability of a given species, and the ferric reducing antioxidant power (FRAP) assay, measuring the iron (III) reducing power through electron donation.

CSL was very active in the DPPH assay, showing an EC_{50} value, that is the sample concentration capable of reducing the initial absorbance of the DPPH solution by 50%, equal to 30 ± 1 mg/mL.

In the FRAP assay CSL exhibited not excellent reducing properties expressed as Trolox equivalents (eqs) and equal to 0.076 ± 0.003, likely attributable to the lower solubility of the powder in the FRAP medium assay.

A total phenolic content (TPC) of 0.32 ± 0.01 gallic acid eqs was determined by the Folin-Ciocalteu assay.

3.1.3 Synthesis of silver nanoparticles using CSL as reducing agent

Thanks to its antioxidant properties, CSL could act as an efficient reducing agent toward Ag^+ ions for the synthesis of silver nanoparticles. With this purpose, an eco-friendly mechanochemical procedure previously reported and slightly modified was used to prepare AgNPs. Mechanochemical reactions are chemical transformations induced by the direct absorption of mechanical energy and are currently widely used for the synthesis of organic and inorganic materials, thanks to the many advantages including short reaction times, simple work-up procedures, and lack of use of potentially toxic organic solvents.[127,195–199]

In particular, CSL and $AgNO_3$ were reacted by using a ball mill, investigating different CSL/$AgNO_3$ ratios (55:45, 70:20, 85:15 w/w), reaction times (30-210 min), and frequencies of the milling process (30-50 Hz). X-ray diffraction (XRD) analysis for determining Ag(0) content was then used to identify the best reaction conditions. This activity was performed in collaboration with the researchers at the Department of Chemical, Materials and Industrial Production Engineering of University of Naples Federico II.

The best result in terms of Ag(0) content was obtained by reacting CSL and $AgNO_3$ at 85:15 w/w ratio for 180 min at 50 Hz. Indeed, the powder thus obtained was characterized by an amount of Ag(0) equal to 8 ± 1% w/w, corresponding to ca. 85% of the calculated theoretical value (9.4%). This sample was named AgNPs@CSL.[200]

3.1.4 Incorporation of AgNPs@CSL into poly(D,L-lactic acid) electrospun fibers

With the aim of preparing functional hybrid materials with antioxidant and antibacterial activity for tissue engineering applications, the AgNPs@CSL or the CSL alone for comparison were incorporated in poly(D,L-lactic acid) (PDLLA) e-spun scaffolds at two doses (0.7 and 2.1% w/w). The best composition was selected from previous and numerous experiments to create defect-free and smooth microfibrous scaffolds. This activity was performed by researchers at Department of Science of University of Basilicata, Potenza. Despite PDLLA forms homogeneous e-spun scaffolds, the major drawback that limits biological applications is its hydrophobicity. So, to overcome this limitation, hydrophilic natural polymers, polysaccharidic in nature, *i.e.* cellulose nanocrystals (CNCs) and chitosan (CHT), were used as additives, being also reported in literature to be able to establish efficient interactions with lignin *via* hydrogen bonds between OH groups or, in the specific case of

CHT, electrostatic interactions of the $-NH_3^+$ ions with phenoxide anions of lignin.[201,202]

Table 3.1 shows the composition of the different scaffold prepared.

Table 3.1. Composition of the prepared e-spun scaffolds. Control samples are in red.

Scaffold	PDLLA (% w/v)	CSL (% w/v)	AgNPs@CSL (% w/v)	CNCs (% w/v)	CHT (% w/v)
A	14	0.7			
B	14	2.1			
C	14		0.7		
D	14		2.1		
E	14				
F	13	0.7		3	
G	13	2.1		3	
H	13		0.7	3	
I	13		2.1	3	
J	13			3	
K	12	0.7			1
L	12	2.1			1
M	12		0.7		1
N	12		2.1		1
O	12				1

The morphological features of each scaffold were characterized by scanning (SEM) and transmission (TEM) electron microscopy.

As a representative example, Figure 3.1 shows the SEM images of the e-spun fibers containing PDLLA-CNCs with CSL (H, I) or AgNPs@CSL (F, G) at low and high concentration. All the samples showed small agglomerates compared to the control (J), probably caused by the presence of lignin.

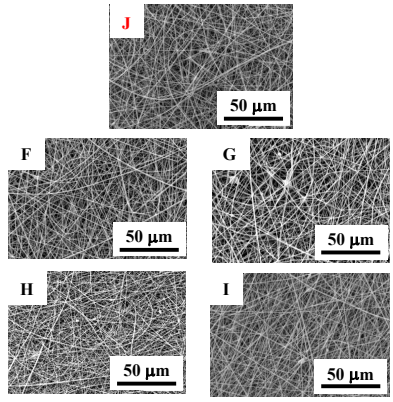

Figure 3.1. SEM images of samples: e-spun PDLLA-CNC scaffold (J); e-spun PDLLA-CNCs-*l*-CSL (F); PDLLA-CNCs-*h*-CSL (G); PDLLA-CNCs-*l*-AgNP@CSL (H); PDLLA-CNCs-*h*-AgNP@CSL (I).

TEM images visibly exhibited silver nanoparticles in lignin agglomerates (Figure 3.2_a), even after their incorporation into e-spun fibers (Figure 3.2_d).

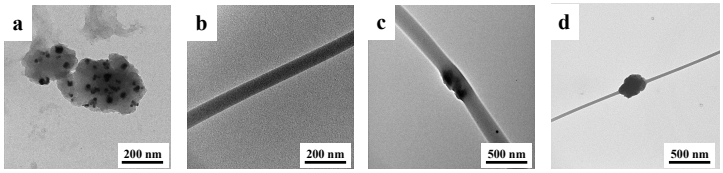

Figure 3.2. TEM images of: (a) AgNPs incorporated in CSL matrix; (b) e-spun PDLLA scaffold (E); (c) e-spun PDLLA-*h*-CSL (B); (d) e-spun PDLLA-*h*-AgNPs@CSL (D).

SEM and TEM images were used to estimate the AgNPs@CSL average size, equal to ca. 30 nm (29.4 ± 9.8 nm (n = 30) from statistical analyses of TEM images), while the fibers exhibited dimeters of around 100-500 nm.

3.1.4.1 Evaluation of the swelling capacity of PDLLA electrospun fibers

Further experiments were directed to swelling tests carried out on the electrospun fibers containing CSL or AgNPs@CSL at the highest concentration, with the aim of assessing the influence on water absorption of CNCs and CHT used as polysaccharide additives of PDLLA. In particular, the samples were immersed in water and shaken at 60 rpm at room temperature for 60 min. The average swelling of the scaffold, *i.e.* the absorbed water, was then calculated following the equation:

$$\text{Swelling (\%)} = \frac{m_w - m_d}{md} \times 100$$

where m_w and m_d are the masses (g) of wet and dry scaffolds, respectively.

As expected considering the hydrophilic nature of CNCs or CHT, the sample J and O exhibited an increase of swelling (25 ± 8%, 29 ± 11%, respectively), compared to the control sample E (12 ± 7%). Also the presence of CSL (B) or AgNPs@CSL (D) led to a significant rise of wettability (28 ± 8%, 23 ± 7%, respectively). The combination of CNCs and CSL (G) or AgNPs@CSL (I) let to values of 35 ± 15% and 28 ± 7%, not so different from the lignin-free control J. On the other hand, the e-spun containing CHT and CSL (L) turned out to be more hydrophilic (44 ± 6%) compared to the one containing AgNPs@CSL (N) (23 ± 5%) or the control (O).

3.1.4.2 Evaluation of the antioxidant properties of PDLLA electrospun fibers

Subsequent experiments were directed to the assessment of the antioxidant properties of the PDLLA e-spun fibers.[183]

Firstly, the antioxidant power of the AgNPs@CSL were evaluated by use of the DPPH assay. To allow for a proper comparison, the DPPH reducing ability

of CSL subjected to the same mechanochemical treatment used to produce the silver nanoparticles was measured. Indeed, as stated also above, mechanical energy could induce the breaking of the peculiar β-O-4' bonds of lignin moieties and an increase of the surface area, resulting in highest antioxidant properties of the grinded powder. However, comparing the antioxidant power of CSL before (reported in 3.1.2.1) and after the treatment, no significant differences were observed.

As expected, AgNPs@CSL resulted to be less active (EC_{50} = 0.058 ± 0.003 mg/mL) than CSL alone (EC_{50} = 0.024 ± 0.002 mg/mL), as a consequence of the efficient reduction Ag^+ ions by lignin. However, the material still exhibited absolutely good antioxidant properties.

Subsequently, the DPPH assay was used to evaluate the antioxidant properties of the e-spun fibers incorporating the highest content of CSL (B, G, L) or AgNPs@CSL (D, I, N). Each material was first cut into pieces of 1 cm^2 and dipped in 2, 4, or 6 mL of a DPPH ethanolic solution (200 μM). Then, the DPPH consumption was periodically monitored by UV-Vis analysis at 515 nm over 120 min. As observed in Table 3.3, all the functionalized fibers showed better antioxidant properties compared to the control samples (E, J, O). Confirming the previous data, the scaffolds containing AgNPs@CSL showed approximately doubled EC_{50} values with respect to the CSL-containing ones. A clear dose-dependent response was observed for all the samples (Figure 3.3).

Table 3.3. EC_{50} values of the PDDLA samples determined in the DPPH assays at 120 min. Mean values ± SD from three different experiments are reported. Control samples are in red.

Name	Composition	EC_{50} (mg/mL)
B	PDLLA-*h*-CSL	1.56 ± 0.09
D	PDLLA-*h*-AgNPs@CSL	3.5 ± 0.3
E	PDLLA	10 ± 2
G	PDLLA-CNCs-*h*-CSL	1.6 ± 0.1
I	PDLLA-CNCs-*h*-AgNPs@CSL	3.0 ± 0.3
J	PDLLA-CNCs	7 ± 1
L	PDLLA-CHT-*h*-CSL	1.99 ± 0.08
N	PDLLA-CHT-*h*-AgNPs@CSL	3.0 ± 0.3
O	PDLLA-CHT	5.8 ± 0.2

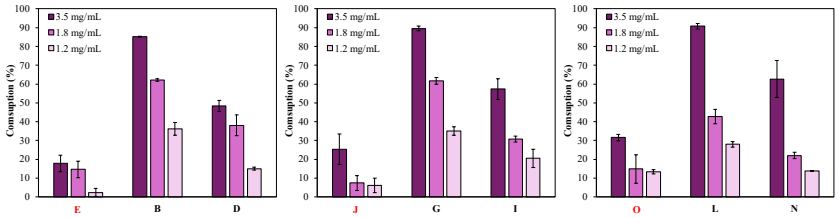

Figure 3.3. Results of the DPPH assay for samples PDLLA (E), PDLLA-*h*-CSL (B), PDLLA-*h*-AgNPs@CSL (D), PDLLA-CNCs (J), PDLLA-CNCs-*h*-CSL (G), PDLLA-CNCs-*h*-AgNPs@CSL (I), PDLLA-CHT (O), PDLLA-CHT-*h*-CSL (L), PDLLA-CHT-*h*-AgNPs@CSL (N) at different doses (3.5, 1.5, 1.2 mg/mL), expressed as DPPH consumption (%) at 120 min reaction time. Mean values ± SD from three different experiments are reported.

To assess the antioxidant potential of the samples in a more physiologically relevant environment, that is at neutral pH, the cupric ion reducing antioxidant capacity (CUPRAC) assay, monitoring the capacity of a sample to reduce

Cu(II) to Cu(I), was also performed using the same protocol described for the DPPH assay. The absorbance increases at 450 nm, due to the formation of the copper(I)-neocuproine complex, was periodically monitored by UV-Vis analysis over 120 min. The results were expressed as Trolox eqs.

As shown in Figure 3.4, all the samples showed a clear dose-dependent response also in this case. Interestingly, the samples containing CNCs (G, I) or CHT (L, N) besides the active component, showed better reducing properties with respect to the material containing only CLS (B) or AgNPs@CSL (D), which in turn resulted similar. The latter result is in line with the similar outcome obtained for CSL and AgNPs@CSL powder (0.48 ± 0.02 and 0.51 ± 0.02 Trolox eqs, respectively) in the same assay.

On this basis, and as expected considering that CUPRAC medium is an aqueous buffer, it can be concluded that the hydrophilicity of CNCs/CHT-containing samples clearly affected the performance in this assay.

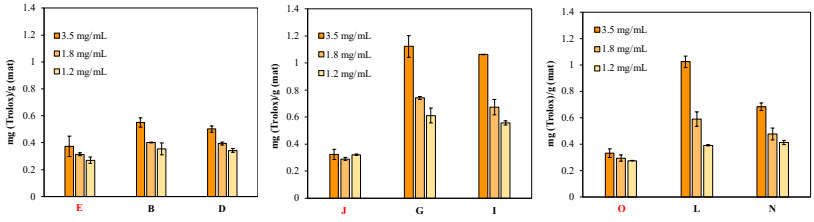

Figure 3.4. Results of the CUPRAC assay for samples PDLLA (E), PDLLA-*h*-CSL (B), and PDLLA-*h*-AgNPs@CSL (D), PDLLA-CNCs (J), PDLLA-CNCs-*h*-CSL (G), and PDLLA-CNCs-*h*-AgNPs@CSL (I), PDLLA-CHT (O), PDLLA-CHT-*h*-CSL (L), and PDLLA-CHT-*h*-AgNPs@CSL (N) at different doses (3.5, 1.8, 1.2 mg/mL), expressed as mg Trolox/g of material evaluated at 120 min reaction time. Mean values ± SD from three different experiments is reported.

Finally, FRAP assay was performed on both powders and e-spun scaffolds. Notably, the reducing power of the CSL powder after mechanochemical

treatment improved significantly, result likely attributable to the increase of the surface area in contact with the FRAP assay medium. However, no significant differences were observed between CSL and AgNPs@CSL powders (1.8 ± 0.1 and 1.6 ± 0.1 Trolox eqs, respectively), and no significant dose-dependent response was observed for all the analyzed scaffolds. As an example, Figure 3.5 shows the results for the E, B and D samples at 3.5 and 1.8 mg/mL.

The different outcomes obtained from FRAP and CUPRAC assays could be associated to the acidic conditions required by the first one, hindering an efficient interaction between the lignin and the medium due to the very low solubility of lignin at acidic pHs.

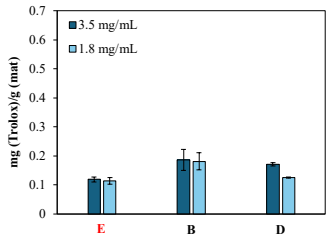

Figure 3.5. Results of the FRAP assay for samples PDLLA (E), PDLLA-*h*-CSL (B), and PDLLA-*h*-AgNPs@CSL (D) at different doses (3.5, 1.8 mg/mL), expressed as mg Trolox/g of material evaluated at 120 min reaction time. Mean values ± SD from three different experiments is reported.

3.1.4.3 Evaluation of the e-spun scaffolds cytocompatibility

The use of silver as antibacterial agent makes the balance between cytocompatibility of the materials and their ability to prevent infection very important. Therefore, the cytocompatibility of the e-spun scaffolds was evaluated by researchers at Department of Health Sciences, Center for Translational Research on Autoimmune and Allergic Diseases-CAAD, of the

University of Piemonte Orientale (Novara) using human mesenchymal stem cells (hMSCs). These latter represent an *in vitro* model frequently used to assess the capacity of implantable biomedical materials to assist the recruitment and colonization of progenitor cells migrating toward the wounded region, in order to avoid making the material toxic.[203]

The samples not containing CSL or AgNPs@CSL were used as control.

As shown in Figure 3.6, no significant variation ($p > 0.05$) of metabolic activity of cells cultivated on the control material surfaces (E, J, O) compared to those grown on the functionalized ones (A, D, F, I, K, N) was observed over time.

As reported in Figure 3.6_a(iv), 3.6_b(iv), 3.6_c(iv), cell growth reached a plateau at days 1 and 2, likely due to the adhesion and spread of the cells on the surface, which proved to be cytocompatibile even after functionalization. From days 2 to 5, instead, a marked increase was observed. This result is consistent with a greater metabolic activity resulting from an increased number of cells, associated to the cell's ability to proliferate.

This hypothesis was supported by fluorescence images (Figure 3.7) which confirmed the correct fibroblastic shape (cytoskeleton marked in red by phalloidin) of the hMSC cells.

Finally, the hypothesis of adaptation and colonization of the surface was confirmed by SEM analysis (Figure 3.8). Indeed, cells were seen to be able to cover more than 90% of the available area with fibers still visible beneath them (Figure 3.8, panels E, B and D, indicated by the red arrows).

According to the results, all the analyzed samples were found to be cytocompatible.

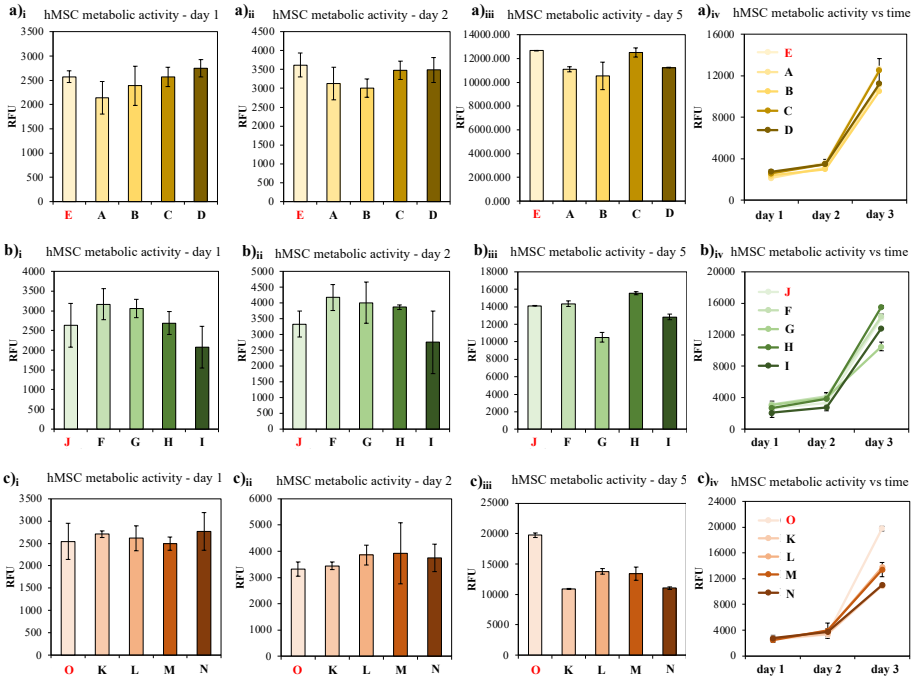

Figure 3.6. Metabolic activity of cells cultivated on control samples (E, J, O) or functionalized ones (A-D, F-I, and K-N) at different times (1-5 days), expressed in relative fluorescence units (RFUs). Bars represent mean values ± SD of n = 3 replicates.

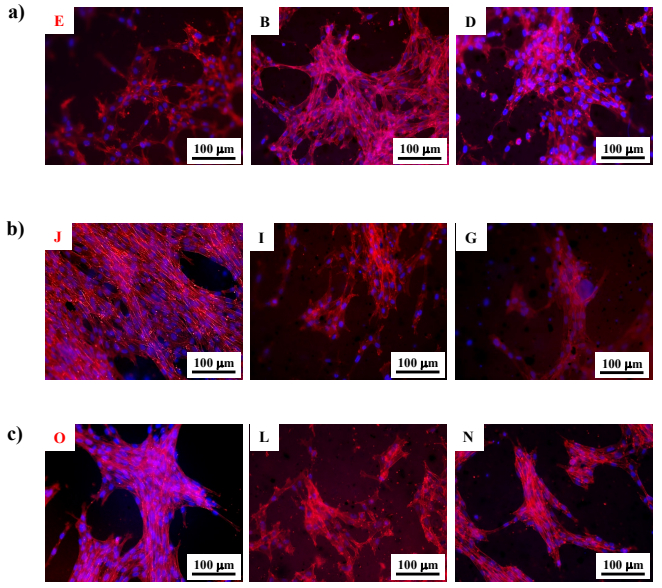

Figure 3.7. Fluorescence analysis of cells cultivated on control samples (E, J, O) or on functionalized samples (A-D, F-I, and K-N) after 5 days.

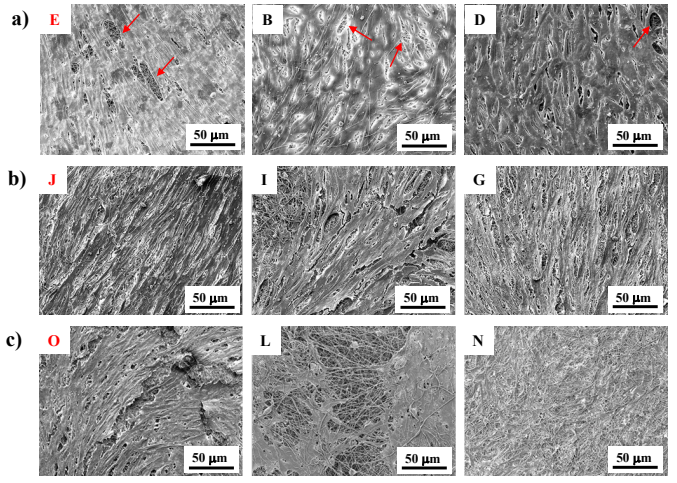

Figure 3.8. SEM analysis of cells cultivated on control samples (E, J, O) or functionalized ones (A-D, F-I, and K-N) after 5 days.

3.1.4.4 Evaluation of the e-spun scaffolds antibacterial efficacy

The antibacterial activity of the e-spun scaffolds was subsequently tested.

In particular, the antibacterial activity of the e-spun scaffolds was tested against *Staphylococcus epidermidis* (Gram +),[204] *Escherichia coli* (Gram −),[205] and *Pseudomonas aeruginosa* (Gram −),[206] three pathogens usually found in dental or orthopedic implant infections. Similarly to cytocompatibility studies, the bacteria were directly placed on the material surface (1 cm^2) with the purpose of mimic the colonization process of resident bacteria at the contaminated spot, and a great number of pathogens (1×10^5 cells/piece) was used in order to simulate the real infection that can lead to the implant disposal.[207]

Figure 3.9 reports the antibacterial activity results for AgNPs@CSL-doped e-spun scaffolds (C, D, H, I, M, N) with respect to the controls (E, J, O). The samples resulted very effective against *E. coli* (Figure 3.9_a_i, 3.9_a_{ii}, 3.9_a_{iii}) compared to the controls ($p < 0.05$ indicated by #), reducing by 1-1.5 log the number of viable colonizing bacteria. In fact, in the SEM images of the controls (E, J, O) the number of bacteria was higher with respect to the highest-doped samples (D, I, N) (Figure 3.10_a_i, 3.10_a_{ii}, 3.10_a_{iii}).

A 1 log reduction in treated samples compared to controls ($p < 0.05$, indicated by § and *, respectively) was also observed with *S. epidermidis* (Figure 3.9_b_i, 3.9_b_{ii}, 3.9_b_{iii}) and *P. aeruginosa* (Figure 3.9_c_i, 3.9_c_{ii}, 3.9_c_{iii}). Similarly, SEM images (Figure 3.10_b_{ii}, 3.10_b_{iii}, 3.10_c_{ii}, 3.10_c_{iii}) confirmed this trend, in particular in the case of I and N scaffolds.

Interestingly, all the data reported in Figure 3.9 showed no relevant differences between the samples with highest (D, I, N) and lowest (C, H, M) silver loading.

However, it is important to specify that the definition of antibacterial activity refers to materials/treatments that lead to a 3 logs reduction compared to the

controls. Therefore, despite the promising results herein obtained by mimicking an intense infection scenario, future studies will be focused to increase the antibacterial efficacy of the developed material.

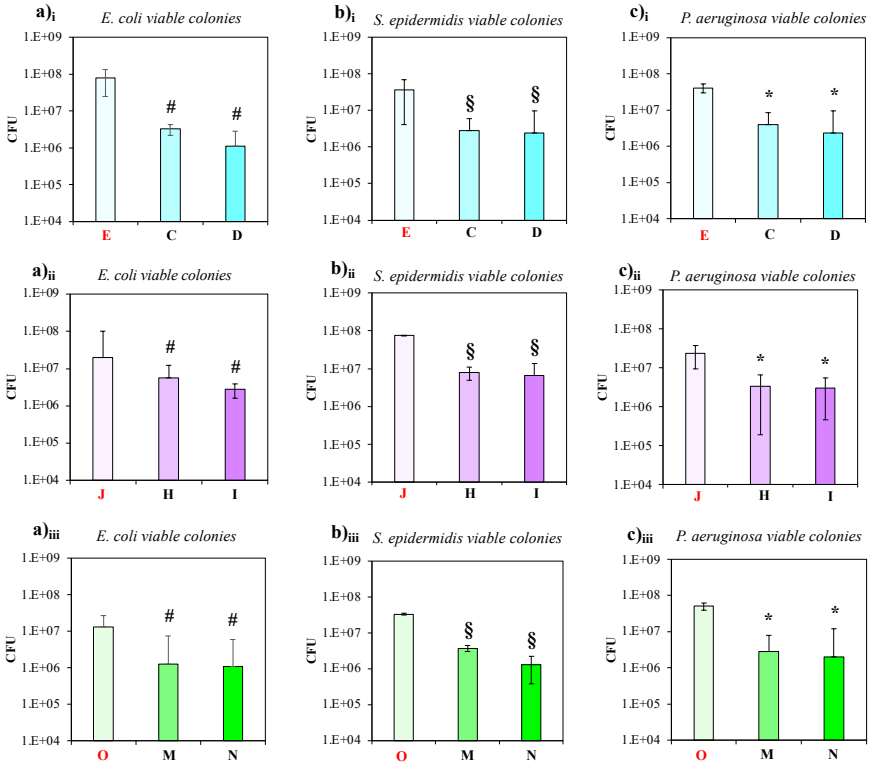

Figure 3.9. Antibacterial activity of the e-spun scaffolds tested using: (a_i, a_{ii}, a_{iii}) *E. coli*, (b_i, b_{ii}, b_{iii}) *S. epidermidis*, and (c_i, c_{ii}, c_{iii}), *P. aeruginosa* on control samples (E, J, O) or functionalized ones (C, D, H, I, M, N). Bars represent means ± SD of n = 3 replicates. ($p < 0.05$ indicated by #, §, *).

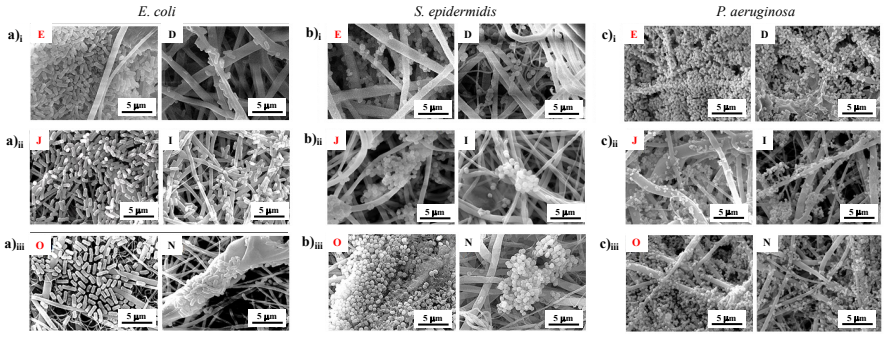

Figure 3.10. SEM images of control samples (E, J, O) or functionalized ones (D, I, N) in the presence of (a_i, b_i, c_i) *E. coli*, (a_{ii}, b_{ii}, c_{ii}) *S. epidermidis*, and (a_{iii}, b_{iii}, c_{iii}) *P. aeruginosa*.

3.1.4.5 Evaluation of the e-spun scaffolds targeting effectiveness

In further studies, a bacteria-cell coculture assay was used, in an environment where hMSCs and *E. coli* were competitors, to assess if the antibacterial activity showed by the samples was directed towards pathogens while preserving cells' viability. Indeed, as previously demonstrated,[208,209] in a real clinical scenario the cells and the pathogens are not separated, rather, they compete to adhere and colonize the same surface.[210]

E. coli, selected because it is the most common pathogen involved in the systemic infections, and hMSCs were seeded on the material surface loaded with the highest Ag(0) concentration (D, I, N). For comparison, the control materials (E, J, O) were also tested, together with polystyrene (considered the gold standard as a substrate for adherent hMSCs). After 24 h, the colony-forming unit (CFU) count was applied to quantify viable bacteria after detachment, while SEM was used to visually check the cells able to adhere and spread.

Pathogens were able to adhere and colonize the material surfaces in the absence of the antibacterial agent, as demonstrated by the CFUs' number ($p >$

0.05) observed with polystyrene (poly) and control samples (Figure 3.11). On the other hand, the number of viable bacteria in the Ag(0)-loaded samples was lower compared to the control ($p < 0.05$, indicated by #, §, *), suggesting that silver has a targeted effect on bacterial viability while protecting cells (Figure 3.11).

These results were confirmed by SEM images (Figure 3.12). Indeed, in the absence of Ag(0) (E, J and O samples) a high concentration of bacteria attached to cells[211], damaged them irreversibly (white boxes). On the contrary, in the case of Ag(0)-loaded samples, cells presented a physiological morphology while the number of bacteria was significantly reduced, especially in I and N samples, that demonstrated the best antibacterial activity confirming the previous results.

This outcome can of course be attributable to the Ag(0) antibacterial activity. However, by producing indoleamine-pyrrole 2,3-dioxygenase (IDO), which depletes tryptophan in cell culture, and by releasing antimicrobial peptides like cathelicidin, which permanently damage bacterial membranes, also hMSCs are known to possess antibacterial activity.[212] So, the protection of cells from pathogens can be attributable to a synergistic effect between Ag(0) contained in the sample and the metabolism of viable stem cells.

Interestingly, the best results were obtained for the N sample, containing CHT. In literature CHT is reported to be characterized by antibacterial power, ascribable to its strong electrostatic interactions with bacterial membranes, which disintegrates them irreversibly.[213] Thus, in addition to intrinsic hMSCs and Ag(0) activity, a third potential synergistic effect could be attributable to the presence of CHT.

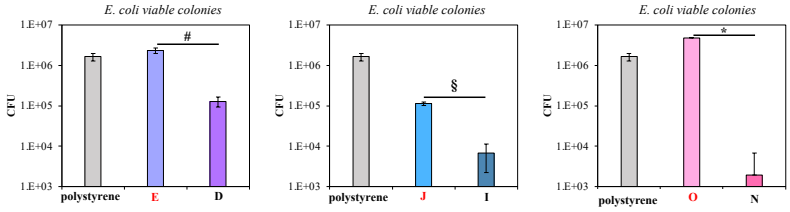

Figure 3.11. Results of bacteria-cell coculture experiments performed on control samples (E, J, O), functionalized samples (D, I, N), and polystyrene (standard), using *E. coli* and hMSCs. Bars represent means ± SD values of n = 3 replicates. ($p < 0.05$, indicated by #, §, *).

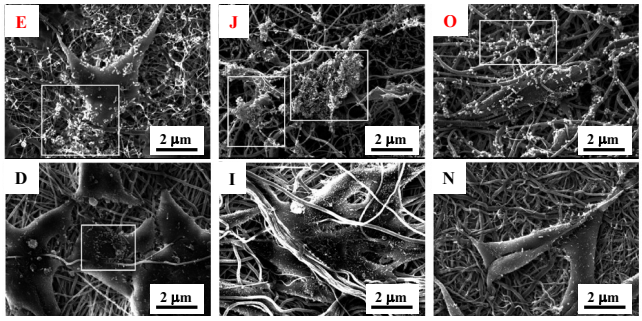

Figure 3.12. SEM images of control samples (E, J, O) and functionalized ones (D, I, N) in the presence of *E. coli* and hMSCs, as cells.

3.1.5 Conclusions

In conclusion, the designed PDLLA-based e-spun scaffolds showed promising properties stimulating interest in tissue healing applications, where osseointegration of implants is required.

In detail, the incorporation of lignin extracted from CS using an eco-friendly methodology confers to the final material efficient antioxidant properties. The same result was obtained, although to a lower extent, for the materials containing silver nanoparticles generated by exploiting the reducing activity of lignin.

All the fibers exhibited high cytocompatibility towards human mesenchymal stem cells, even those containing AgNPs, capable of conferring antibacterial properties to the samples. Among all, particularly interesting is the e-spun scaffold containing chitosan and AgNPs@CSL, able to prevent bacterial infection from *E. coli* while protecting hMSCs.

In conclusion the herein highly versatile produced fibers combined multifunctional biological properties and green chemistry tools.

3.1.6 Experimental section

Materials and Methods. 2,2-diphenyl-1-picrylhydrazyl (DPPH), iron(III) chloride, 2,4,6-tris(2-pyridyl)-*s*-triazine (TPTZ), Folin-Ciocalteu reagent, (±)-6-hydroxy-2,5,7,8-tetramethylchromane-2-carboxylic acid (Trolox), gallic acid and silver nitrate were purchased from Sigma-Aldrich**.** Chestnut shells were obtained from the Malerba chestnut agricultural company (Montella, AV, Italy) and ground to a fine powder using a ball mill Fritsch Pulverisette 23.

UV-Vis spectra were recorded using a Jasco V-730 spectrophotometer.

XRD analysis of AgNPs@CSL were performed using a X'Pert Pro diffractometer, equipped with Empyrean Cu HR X-ray generator under CuKα radiation, a high-resolution parallel beam X-ray mirror (BBHD) on the incident beam path, and a PIXCel 1D detector on the diffracted beam path. Powder spectra were collected under ambient conditions in the range 23−120° 2θ, with a step size of 0.013 °2θ and counting time of 28 seconds per step. The PANalytical High-Score package, equipped with the ICDD PDF 5+ database, was used to identify the crystalline phases in the samples and retrieve their structural information. Besides the deliberately added Al_2O_3 (PDF 5+ ref code no. 01-088-4954), the other two phases detected were Ag (PDF 5+ ref code no. 04-014-0266) and AgCl (PDF 5+ ref code no. 04-002-8237). The amount of AgNPs@CSL in the samples was evaluated by the RIR/Rietveld method[214]:

a weighted amount (10% w/w) of corundum (NIST Standard Reference Material 676a) was added to each sample, the mixture was carefully homogenized, and the diffraction spectrum was acquired. Then, the relative mass percentage was calculated by a quantitative analysis carried out using the GSAS-II software.[215] The results were rescaled accounting for the actual amount of corundum, obtaining the absolute weight percentage of each phase as the mean value from three different samples, together with the indirect estimation of the amorphous content.

SEM images were acquired with a voltage of 20 kV and different magnifications after gold sputter-coating on a Philips FEI ESEM XL30 instrument. SEM-EDS JEOL JSM-IT 500 was used to appreciate fibers' guidance toward cells.

The ImageJ software supplied with the DiameterJ plug-in was used to evaluate the diameter of the fibers.

TEM images were obtained using Fei Tecnai G2 20 Twin transmission electron microscopes at a 100 kV beam intensity.

Electrospinning was performed on a Linari Engineering Gamma-High-Voltage generator electrospinning system. In a 10 mL glass syringe with an 18 G stainless-steel needle the polymer mixtures were loaded and then electrospun (19 kV, flow rate of 1.0 mL/h of the pump). A round copper plate (90 mm diameter) coated with aluminum foils was used as target, while 19 cm was set as distance between the collector and the needle.

Fluorescence signals were evaluated with a spectrophotometer (Spark, Tecan Trading AG, CH) by an excitation wavelength of 570 nm and a fluorescence emission reading of 590 nm.

A confocal microscope Leica SP8 confocal platform, Leica Microsystems, Germany was used to visualize cells' morphology.

Biological results were analyzed by using the SPSS software (v25, IBM, New York City, NY, USA) by the oneway ANOVA followed by Tukey's test as post hoc analysis. Biological evaluations were performed using technical triplicates. The significance level was set at $p < 0.05$.

Swelling test statistical analysis was analyzed using the student's test. The significance level was set at $p \leq 0.01$.

Extraction of lignin from CS. A previously reported procedure was followed with slight modifications.[183] For DES preparation, 43.8 g of choline chloride and 56.3 g of lactic acid (1:2 mol/mol ratio) were heated at 50°C and stirred until a homogeneous solution was obtained, which was then stored in the dark at room temperature. No crystal precipitation was observed over the period of use. 10 g of chestnut shells, previously grinded by the use of a ball mill for 15 min at 50 oscillations/s, were added to 100 g of the prepared DES containing 20% w/w water. The mixture was taken under stirring in a pyrex glass bottle at 120°C for 24 h, cooled at room temperature and centrifuged (7000 rpm, 4°C, 10 min). The solid residue was washed three times with 50 mL of ethanol (7000 rpm, 4°C, 10 min), and the washings were collected and dried using a rotary evaporator. Then they were poured together with the previously obtained supernatant into 1 L of 0.01 M HCl and kept at 4°C. CSL was then obtained as a dark brown precipitate, recovered by centrifugation (7000 rpm, 4°C, 10 min), washed twice with 0.01 M HCl and once with distilled water, and finally lyophilized (20% w/w yield).

Preparation of AgNPs@CSL. 140 mg of CSL was treated with 25 mg of $AgNO_3$ (15% w/w) into the ball mill at 50 oscillations/s for 180 min. The obtained powder was washed three times with 50 mL of water (7000 rpm, 4°C, 10 min) and then lyophilized (9% w/w yield).

Electrospinning. This activity was performed by researchers at Department of Science, University of Basilicata, Potenza. The protocol performed for the

electrospinning of solutions/suspensions required the addition of 2 mg of CSL or 6 mg of AgNPs@CSL to 2 mL of HFP. The solution was then sonicated for 10 min and then stirred at room temperature for 2 h. At this point 8.2 mg of CNCs or 2.4 mg of CHT, if needed, were added and the solution was stirred for 2 h. Finally, PDLLA was introduced and stirred overnight at 310 K. In particular, 280 mg of PDLLA were used for scaffolds from A to E, and 260 mg for scaffolds from F to O.

Swelling test analysis. This activity was performed by researchers at Department of Science, University of Basilicata, Potenza. Each scaffold was divided into four pieces; each piece was immersed in 10 mL of milli-Q water and shaken at 60 rpm on an orbital shaker. The excess of water was then removed on a filter paper and the materials were weighted. The absorbed water was calculated following the equation:

$$\text{Swelling (\%)} = \frac{m_w - m_d}{md} \times 100$$

where m_w and m_d are the masses (g) of wet and dry scaffolds, respectively.

TEM analysis. This activity was performed by researchers at Department of Science, University of Basilicata, Potenza. TEM images were acquired after depositing the e-spun fibers onto carbon-coated copper grids (400 mesh) for 35 s to ensure the deposition of only a few fibers onto the grids. AgNPs embedded in the CSL matrix, e-spun PDLLA scaffold (sample E), e-spun PDLLA-*h*-CSL (sample B), and e-spun PDLLA-*h*-AgNPs@CSL (sample D) were analyzed as previously reported.[216]

Folin-Ciocalteu assay. CSL powder was added to a solution consisting of Folin-Ciocalteu reagent, 75 g/L Na_2CO_3, and water in a 1:3:14 v/v/v ratio (0.0125-0.4 mg/mL final dose). After 30 min incubation at 40°C, the absorbance at 765 nm was measured. Gallic acid was used as reference and the results were expressed as gallic eqs (mg gallic acid/mg sample). Experiments were run in triplicate.[217]

DPPH assay. [175] CSL powder or AgNPs@CSL powder were added to a 200 μM ethanolic solution of DPPH (0.025-0.067 mg/mL and 0.03-0.2 mg/mL final dose, respectively). After 10 min under stirring at room temperature, the absorbance of each solution at 515 nm was measured. Similarly, electrospun fibers sections of ca. 1 cm^2 total surface area (corresponding to 7 mg of material) were immersed in 2 ,4 or 6 mL of a 200 μM ethanolic solution of DPPH. Control samples without the films were also prepared. The absorbance of each solution at 515 nm was periodically (10, 30, 60, and 120 min) measured. The antioxidant power was expressed as EC_{50}, that is the sample concentration capable of reducing the initial absorbance of the DPPH solution by 50%. Experiments were run in triplicate.

FRAP assay.[177] FRAP solution was prepared by mixing 36 mL of 0.3 M acetate buffer (pH 3.6), 3.6 mL of a 20 mM aqueous $FeCl_3$ solution (1.7 mM final concentration), and 3.6 mL of a 10 mM TPTZ solution prepared using 40 mM HCl (0.83 mM final concentration). CSL or AgNPs@CSL powder was added to FRAP solution (0.002-0.015 and 0.0003-0.015 mg/mL final dose, respectively), and after 10 min under stirring at room temperature, the absorbance of each solution at 593 nm was measured. Electrospun fibers sections of ca. 1 cm^2 total surface area (corresponding to 7 mg of material) were immersed in 2,4 or 6 mL of FRAP solution. Control samples without the films were also prepared. The absorbance of each solution at 593 nm was periodically (10, 30, 60, and 120 min) measured. Trolox was used as a reference antioxidant and the results were expressed as Trolox eqs for the powders (mg Trolox/mg sample) or as Trolox eqs per gram of material for the scaffolds (mg Trolox/g mat). Experiments were run in triplicate.

CUPRAC assay. CUPRAC solution was prepared by mixing $CuCl_2$ (10 mM), neocuproine (7.5 mM), acetate ammonium buffer (1 M at pH 7.0), and water in ratio 1:1:1:0.9 v/v, in that order.[218] Electrospun fibers sections of ca. 1 cm^2

total surface area (corresponding to 7 mg of material) were immersed in 2,4 or 6 mL of CUPRAC solution and the absorbance of each solution at 450 nm was periodically analyzed (10, 30, 60, and 120 min). Trolox was used as a reference antioxidant and the results were expressed as Trolox eqs for the powders (mg Trolox/mg sample) or as Trolox eqs per gram of material for the scaffolds (mg Trolox/g mat). Experiments were run in triplicate.

Cytocompatibility assessment. This activity was performed by researchers at Department of Health Sciences, Center for Translational Research on Autoimmune and Allergic Diseases-CAAD, University of Piemonte Orientale (Novara). To perform cytocompatibility tests, human bone marrow-derived mesenchymal stem cells (hMSCs) were cultivated in low-glucose Dulbecco's Modified Eagle Medium (DMEM), supplemented with 15% fetal bovine serum (FBD) and 1% antibiotics (penicillin/streptomycin) at 37°C and 5% CO_2 atmosphere, and were grown until 80-90% confluence. Then, cells were enzymatically detached by trypsin ethylenediaminetetraacetic acid (EDTA) solution (0.25% in PBS), harvested, and used for the experiments.

E-spun pieces of ca. 1 cm^2 were sterilized by direct UV-light exposure (30 min) and then the cytocompatibility was evaluated by their direct contact with hMSCs (2.5×10^4 cells/scaffold piece), cultivated for 1-2 days. At the selected time point, the viability of the cells was evaluated by means of their metabolic activity using the Alamar Blue colorimetric assay. Fluorescence signals were evaluated by an excitation wavelength of 570 nm and a fluorescence emission reading of 590 nm, and results were expressed in relative fluorescence units (RFUs). In order to visually check cells' morphology, after 2 days the scaffolds were washed with PBS, fixed with 4% w/v paraformaldehyde for 20 min at room temperature, permeabilized with 0.5% w/v Triton in PBS (20 min). Finally, to visualize F-actin cytoskeleton filaments and nuclei, the scaffolds were stained with Texas Red-X Phalloidin and DAPI, respectively.

Then, scaffolds were fixed with 2.5% w/v glutaraldehyde, dehydrated by the alcohol scale (50, 70, 90, and 100%, 2 h each), treated with hexamethyldisilazane, and finally mounted onto aluminum stubs, surface metalized with gold to acquire SEM images to better appreciate fibers' guidance toward cells.

Antibacterial activity evaluation. This activity was performed by researchers at Department of Health Sciences, Center for Translational Research on Autoimmune and Allergic Diseases-CAAD, University of Piemonte Orientale (Novara). Firstly, the bacteria (*S. epidermidis/E. coli/P. aeruginosa*) suspensions were prepared following the manufacturer's instructions, whereas fresh broth cultures were prepared prior to the experiment by adjusting bacterial concentration to 1×10^5 bacteria/mL by optical density (0.001 at 600 nm). Scaffolds' infection was performed following the ISO 22196 standard: 100 µL of the bacterial suspensions was directly seeded on scaffold's pieces and incubated at 37°C for 24 h. Then, the samples were washed three times with PBS to remove non-adherent bacteria, and the colony-forming unit (CFU) count was applied to quantify viable bacteria.[219] Finally, SEM was used to visualize the biofilm-like 3D structures formed onto the samples' surface.

Targeted activity evaluation. This activity was performed by researchers at Department of Health Sciences, Center for Translational Research on Autoimmune and Allergic Diseases-CAAD, University of Piemonte Orientale (Novara). 2.5×10^4 cells/material hMSC were seeded onto the scaffolds' surface and allowed to adhere and spread for 24 h. The thus prepared samples were infected with 1 mL of antibiotics-free DMEM containing 1×10^3 *E. coli* colonies. The number of viable bacteria colonizing after 48 h of the infection was ranked by CFU count after detachment, whereas the cell morphology was visually verified by SEM as described above.

3.2 Examination of the oxidative chemistry of coniferyl alcohol under biomimetic condition to obtain a synthetic model of natural lignin

3.2.1 Introduction

As mentioned before, increasing research interest has been directed in the last year to the development of nature-inspired phenolic polymers, usually obtained by oxidation of the corresponding monomers under biomimetic conditions, endowed with several advantages with respect to the natural counterparts, *e.g*. a higher structural homogeneity and more defined chemical and physical properties.

In the specific case of lignin, for instance, its structural heterogeneity and tight connection with cellulose and hemicellulose through both covalent and non-covalent interactions[220] make its recovery at high purity degree very challenging, sometimes hindering a full exploitation of this material for application purposes. In this framework, synthetic phenolic polymers "inspired" to lignin have been recently investigated for applicative purpose.[221–223]

On this basis, the subsequent 3.2 paragraphs will be focused on the:

- exploration of the oxidative chemistry of coniferyl alcohol, one of the main lignin precursors, using biomimetic condition to obtain information about the polymerization pathway;
- preliminary evaluation of the effect of a mechanochemical treatment, usually performed for lignin recovery from natural sources, on the antioxidant properties of the obtained polymer.

3.2.2 Isolation and characterization of the main product of coniferyl alcohol oxidation

Coniferyl alcohol (1 mM) was oxidized using horseradish peroxidase (HRP) (2.5 U/mL) and H_2O_2 (1.2 molar eqs) and after 1 h the mixture was analyzed by HPLC (Figure 3.13). Interestingly, a significant consumption of the starting monomer eluted at ca. 28 min was observed, together with the formation of a main product eluted at ca. 34 min.

Subsequently, with the aim of isolating the observed product to obtain information about its structure, the oxidation reaction was run on 100 mg of coniferyl alcohol and after extraction in with ethyl acetate different purification procedures were tested. Whereas column chromatography on silica didn't show a good separation of the reaction products, good results were obtained using preparative HPLC allowing the separation of the main product in pure form, identified as a coniferyl alcohol dimer by LC-MS analysis ($[M+H]^+$ at *m/z* 359).

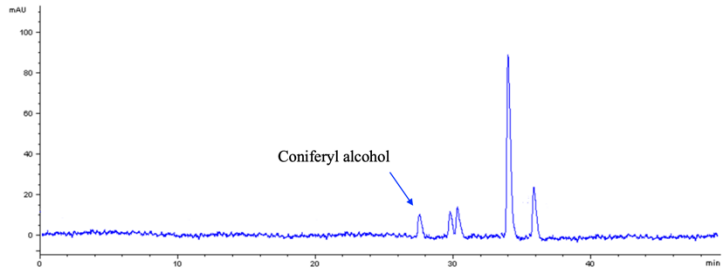

Figure 3.13. Elutographic profile of the reaction mixture of coniferyl alcohol in the presence of HRP/H_2O_2 after 1 h.

The UV-Vis spectrum of the isolated coniferyl alcohol dimer showed a defined absorption maximum at 278 nm and two broad maxima at ca. 315 and 350 nm (Figure 3.14).

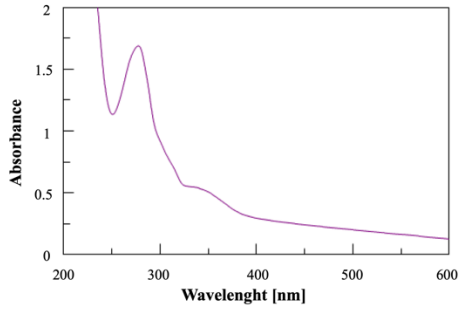

Figure 3.14. UV-Vis spectrum of the isolated coniferyl alcohol dimer (25 μg/mL in methanol).

The ^{1}H NMR spectrum (Figure 3.15) showed a complex pattern of signals in the aromatic proton region (6.7-6.9 ppm), together with the expected signals of the propenoic chain protons in a, b and g position, *i.e.* one doublet integrating for a proton at 6.54 ppm (J = 15.6 Hz), a double triplet integrating for a proton at 6.23 ppm (J = 15.6 and 6.0 Hz) and a doublet integrating for two protons at 4.20 ppm (J = 6.0 Hz). Furthermore, a doublet (J = 6.4 Hz) integrating for a proton at 5.52 ppm was evident, which in the ^{1}H,^{1}H COSY spectrum (Figure 3.16) showed correlations with a multiplet integrating for a proton at 3.48 ppm. The latter correlated in turn with a signal at 3.83 ppm, partially covered by the signals relating to the two methoxy groups at 3.81 and 3.86 ppm.

According to the ^{1}H,^{13}C HSQC-DEPT (Figure 3.17). ^{1}H,^{13}C HMBC (Figure 3.18) and ^{13}C NMR (Figure 3.19) spectra and to data reported in literature,[224] the isolated product was identified as the β-5' dehydrodimer (Figure 3.20), likely formed through the mechanism reported in Figure 3.21. [225]

This result provided information about the main polymerization route of coniferyl alcohol under biomimetic conditions.

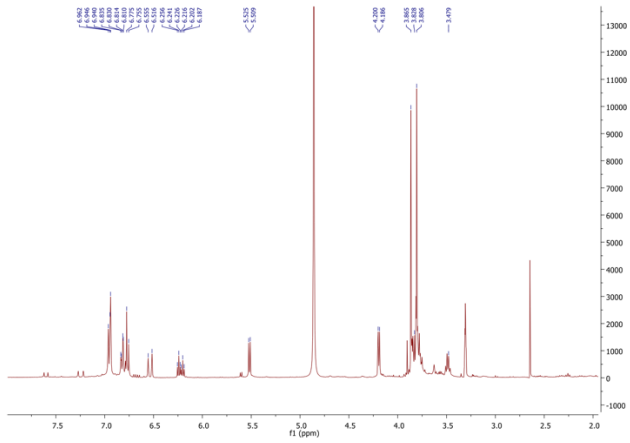

Figure 3.15. ^{1}H NMR spectrum of the isolated coniferyl alcohol dimer in CD_3OD.

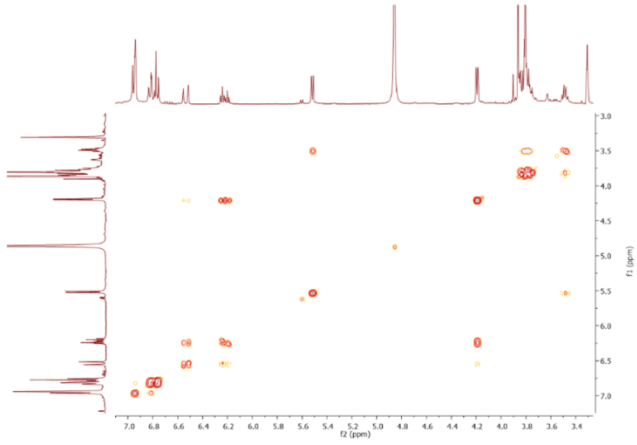

Figure 3.16. ^{1}H, ^{1}H COSY spectrum of the isolated coniferyl alcohol dimer in CD_3OD.

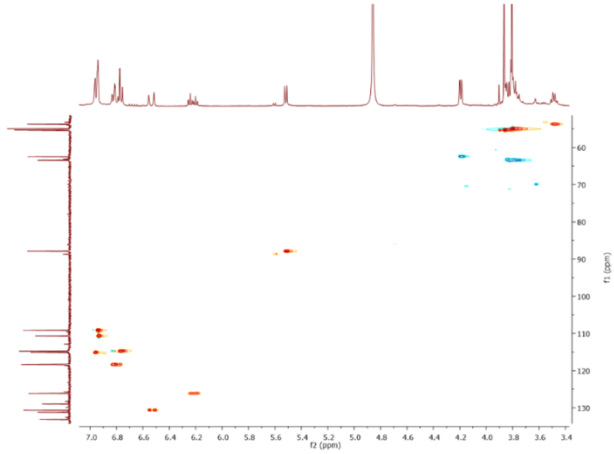

Figure 3.17. $^{1}H,^{13}C$ HSQC-DEPT spectrum of the isolated coniferyl alcohol dimer in CD_3OD.

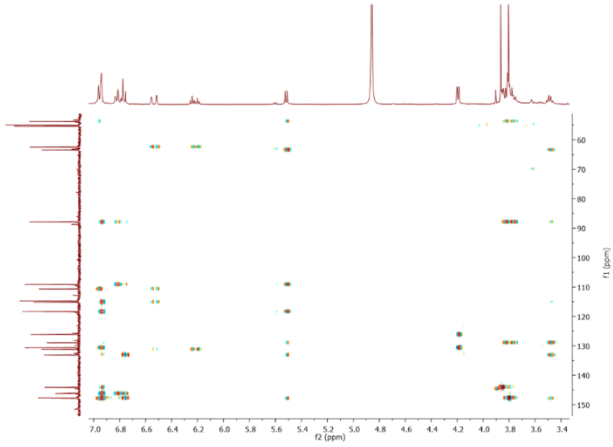

Figure 3.18. $^{1}H,^{13}C$ HMBC spectrum of the isolated coniferyl alcohol dimer in CD_3OD.

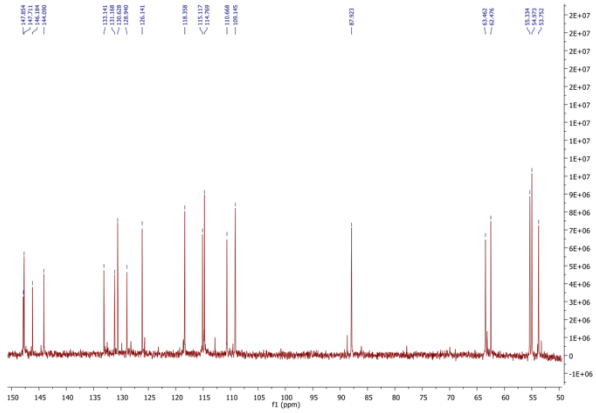

Figure 3.19. ^{13}C NMR spectrum of the isolated coniferyl alcohol dimer in CD_3OD.

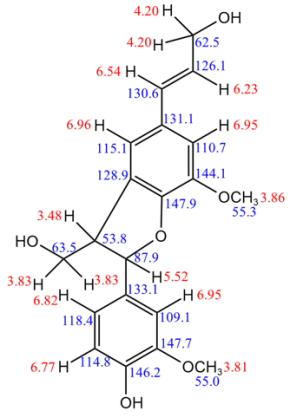

Figure 3.20. Structure and proton (red) and carbon (blue) resonances of the isolated coniferyl alcohol dimer.

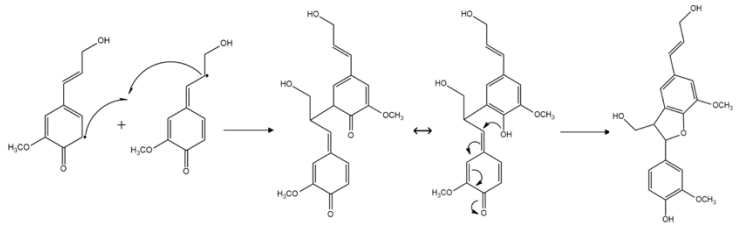

Figure 3.21. Formation mechanism of coniferyl alcohol β-5' dehydrodimer.

3.2.3 Preparation of a synthetic lignin by oxidation of coniferyl alcohol

To obtain a polymer, in other experiments the oxidation of the coniferyl alcohol was carried out using a higher amount of HRP. In detail, the monomer was oxidized in phosphate buffer at pH 6.8 using HRP (10 U/mL) and H_2O_2 (1.2 molar eqs) for 24 h. A yellow precipitate was obtained with was collected by centrifugation and lyophilization with a recovery yield of 55% w/w. The polymer was subsequently analyzed by UV-Vis spectroscopy in comparison with the monomer (Figure 3.22). As expected, the polymer (in blue) was characterized by a significant broadening of the absorption bands compared to the monomer, at higher extent with respect to the dimer (Figure 3.14), indicating a significant degree of polymerization of the starting phenolic monomer.

The extensive polymerization of coniferyl alcohol was also confirmed by the absence of any chromatographable species in the HPLC profile.

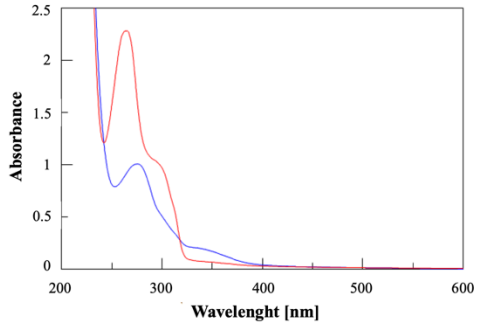

Figure 3.22. UV-Vis spectra of coniferyl alcohol (red) and coniferyl alcohol polymer (blue) at 25 µg/mL in methanol.

Subsequently, the polymer was analyzed by ^{1}H NMR (Figure 3.23_a) in comparison again with coniferyl alcohol (Figure 3.23_b). As expected, the polymer spectrum was much more complex than that of the monomer,

confirming the polymeric nature of the sample. In particular, Figure 3.23_b shows signals in the 4.5-5.5 ppm range which were absent in the spectrum of the starting coniferyl alcohol, suggesting a significant involvement of the monomer side chain in the polymerization.

On the other hand, the phenolic OH group involvement in the polymerization process was also evident from the significantly lower intensity of the signal at ca. 9 ppm in the polymer spectrum compared to the monomer.

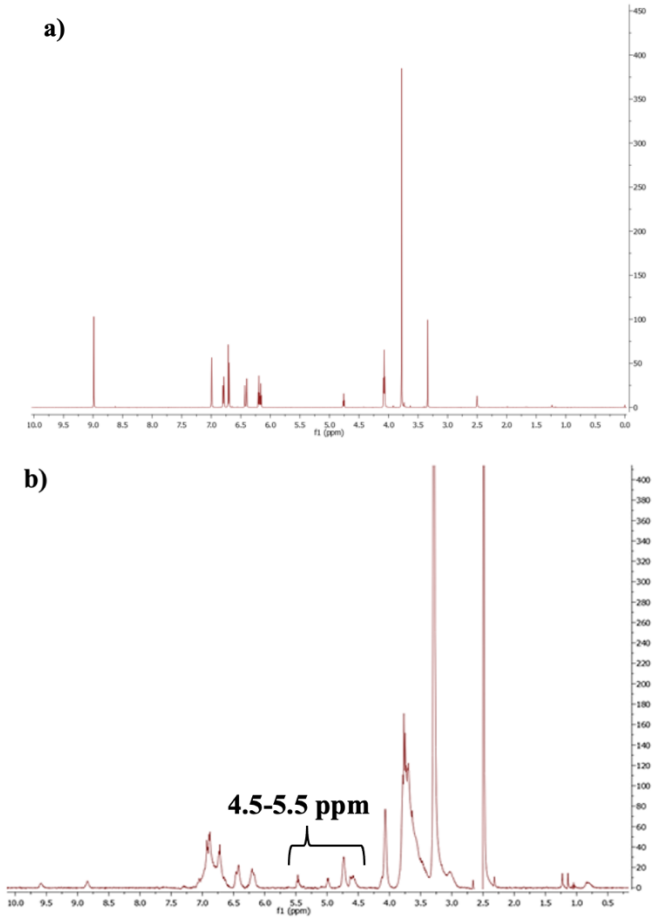

Figure 3.23. ^{1}H NMR spectra of a) coniferyl alcohol and b) coniferyl alcohol polymer in DMSO-d_6.

3.2.4 Assessment of the antioxidant properties of the coniferyl alcohol polymer before and after a mechanochemical treatment

As mentioned before, besides its important use for the synthesis of organic and inorganic compounds, mechanochemical methodologies have been largely employed also as a fundamental step in the lignin extraction process from natural sources. Indeed, it has been reported that ball milling is able to induce the cleavage of glycosidic and β-O-4' bonds,[187,226] which in turn cause the release of phenolic -OH groups leading to an increase in the antioxidant properties of the treated sample.

On this basis, further experiments were directed to the evaluation of effects of a mechanochemical treatment on the antioxidant properties of the coniferyl alcohol polymer, as a "pure" lignin-like model not linked to cellulose or hemicellulose

The antioxidant properties of the sample, before and after the ball milling treatment, were evaluated by the DPPH assay. However, as shown by the EC_{50} values determined to be 0.114 ± 0.06 and 0.094 ± 0.05 mg/mL for the starting and treated polymer, respectively, the mechanochemical treatment didn't lead to particularly significant variations in the antioxidant properties. This result would suggest that the variation of the antioxidant properties mentioned above in the case of natural lignins is mostly attributable to the cleavage of glycosidic bonds between lignin and hemicellulose/cellulose, rather than to structural variations induced on the phenolic component.

It is also true that, based on the structure of the isolated dimer, the polymerization of the coniferyl alcohol under the examined conditions would proceed mainly through the formation of β-5' bonds, while the mechanochemical treatment has been reported to break the β-*O*-4' bonds.

3.2.5 Conclusions

In conclusion, in order to obtain a synthetic model of lignin, coniferyl alcohol, one of the main components of this phenolic polymer, was oxidized under biomimetic conditions using the HRP/H_2O_2 system.

The reaction led to the formation of a dimer identified as the β-5' dehydrodimer, providing information on the polymerization route of coniferyl alcohol under the oxidative conditions used.

Subsequently, further experiments were directed to the preparation of the coniferyl alcohol polymer, which was subjected to a mechanochemical treatment typically used for the recovery of lignins from lignocellulosic biomass, which has been reported to lead to the cleavage of the β-O-4' bonds present in the natural polymer leading to an increased antioxidant power. However, the obtained results, would suggest that in the case of natural lignins the variation in the antioxidant power is mainly due to the breaking of the lignin-cellulose/hemicellulose bonds, although care should be taken in drawing this conclusion, since under the adopted conditions the main polymerization pathway seemed to proceed through formation of a the β-5'-bond.

Although still preliminary, these outcomes open interesting perspectives for the use of bioinspired phenolic polymers not only as an alternative, for applicative purposes, to the more complex natural phenolic polymers, but also as a structural model for the study of chemical transformations that may affect such polymers during the isolation and purification processes from natural sources.

3.2.6 Experimental section

Materials and Methods. Coniferyl alcohol, horseradish peroxidase (HRP) (234 U/mg), hydrogen peroxide (30% v/v) and 2,2-diphenyl-1-picrylhydrazyl (DPPH) were purchased by Sigma-Aldrich.

UV-Vis spectra were recorded using a Jasco V-730 spectrophotometer.

NMR spectra were recorded in DMSO-d_6 or CD_3OD at 400 MHz on a Bruker instrument.

HPLC analysis were performed on an instrument equipped with an Agilent G1314A UV-Vis detector, using a Phenomenex Sphereclone C18 column (250 × 4.60 mm, 5 μm) at a flow rate of 1.0 mL/min; the gradient elution was as follows: 0.1% formic acid (solvent A)/methanol (solvent B), 5% B, 0-10 min; from 5 to 80% B, 10-47.5 min; the detection wavelength was set at 254 nm.

Preparative HPLC was performed on an instrument equipped with an Agilent 1200 UV-Vis detector. The purification was performed on a Grace Econosphere C18 (250 × 22 mm) column with 10 mm-diameter particles. The isocratic elution was performed with 0.1% formic acid/methanol at 65:35 v/v ratio, at a flow rate of 40 mL/min; the detection wavelength was set at 254 nm.

LC-MS analysis were run on an Agilent LC-MS ESI-TOF 1260/6230DA instrument operating in positive ionization mode in the following conditions: nebulizer pressure 35 psig; drying gas (nitrogen) 5 L/min, 325°C; capillary voltage 3500 V; fragmentor voltage 175 V. A Eclipse Plus C18 column (150 × 4.6 mm, 5 μm) at a flow rate of 0.4 mL/min was used, using the same eluant adopted for HPLC analysis.

Isolation of the main coniferyl alcohol dimer. 100 mg of coniferyl alcohol, solubilized in 1 mL of methanol, were added to phosphate buffer 50 mM at pH 6.8 (555 mL) to reach a final concentration of 1 mM. 2.5 U/mL of HRP and 1.2 molar eqs of H_2O_2 were then added. After 1 h under stirring at room

temperature, the mixture was extracted with ethyl acetate (150 mL × 3) and the combined organic phases were dried over sodium sulphate and taken to dryness using a rotary evaporator. The final residue was solubilized in methanol, purified by preparative HPLC (36% w/w yield) and analyzed by UV-Vis, LC-MS and NMR analysis.

ESI^+/MS: $[M+H]^+$ at *m/z* 359;

UV-VIS: λ_{max} (CH_3OH) 278, 315, 350 nm;

^1H NMR (CD_3OD) δ (ppm): 3.48 (1H, m), 3.81 (3H, s), 3.83 (2H, m), 3.86 (3H, s), 4.20 (2H, d, 6.0 Hz), 5.52 (1H, d, 6.4 Hz), 6.23 (1H, dt, 15.6, 6.0 Hz), 6.54 (1H, d, 15.6 Hz), 6.77 (1H, d, 8.0 Hz), 6.82 (1H, dd, 8.0, 2.0 Hz), 6.95 (2H, m), 6.96 (1H, br s);

^{13}C NMR (CD_3OD) δ (ppm): 53.8, 55.0, 55.3, 62.5, 63.5, 87.9, 109.1, 110.7, 114.8, 115.1, 118.4, 126.1, 128.9, 130.6, 131.1, 133.1, 144.1, 146.2, 147.7, 147.9.

Preparation of the coniferyl alcohol polymer. 100 mg of coniferyl alcohol, solubilized in 1 mL of methanol, were added to 50 mM phosphate buffer at pH 6.8 (555 mL), to reach a final concentration of 1 mM. 2.5 U/mL of HRP and 0.3 molar eqs of H_2O_2 were then added 4 times every hour. After 24 h under stirring at room temperature, the mixture was centrifuged (5000 rpm, 4°C, 15 min) and the solid residue (55 mg) was washed with water (3 times) and finally lyophilized.

30 mg of the polymer were then subjected to a mechanochemical treatment (50 oscillations/min for 60 min) by using a laboratory ball mill (Fritsch-Pulverisette 23).

DPPH assay. Several volumes (5-140 μL) of a coniferyl alcohol polymer solution (5.4 mg/mL in DMSO), before or after the mechanochemical treatment, were added to a 200 μM ethanolic solution of DPPH. After 10 min under stirring at room temperature, the absorbance of each solution at 515 nm

was measured.[175] The antioxidant power was expressed as EC_{50}, that is the sample concentration capable of reducing the initial absorbance of the DPPH solution by 50%. Experiments were run in triplicate.

Chapter 4

Exploitation of tannins as precious resource for several applications

4.1 Pine needles as a sustainable source of natural phenolic compounds to be used as green corrosion inhibitors for aluminium alloys

4.1.1 Introduction

Pine needles (PN) represent a largely available and still not fully exploited source of phenolic compounds, including kaempferol, rhamnetin, isorhamnetin, myricetin, laricitrin, syringetin, taxifolin, luteolin, naringenin and quercetin, together with condensed tannins (Figure 4.1).

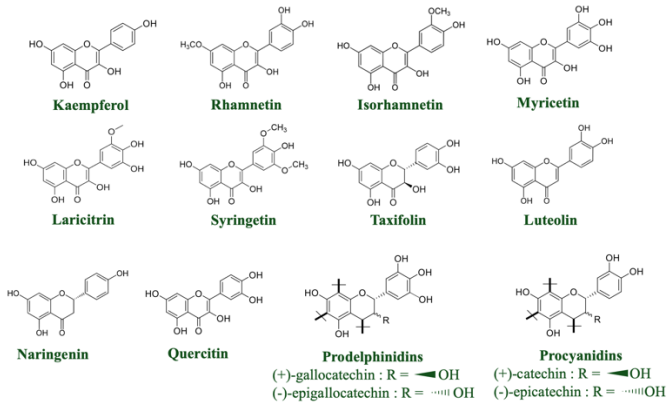

Figure 4.1. Main phenolic components of PN.

Every year, million tons of dry pine needles accumulate on forest floors, limiting flora's growth and, even worse, causing uncontrollable forest

fires.[227,228] In this context, in order to valorize this waste biomass, the research work described herein was focused on the extraction and characterization of phenolic compounds from PN of Pīnŭs pīnea, one of the most widespread Mediterranean pine species along the Italian coast.[229]

Generally speaking, it's important to underline that the choice of the vegetable source as well as of the extraction technique can influence the yield, purity and composition of a phenolic extract.[230,231] Conventional extraction techniques, such as maceration, percolation and reflux/Soxhlet extraction, are very simple procedures to perform. However, their main drawbacks are the long processing times and the use of large amounts of solvents.[232,233] Nowadays, these disadvantages have been overcome by the introduction of other techniques considered greener and more sustainable, such as pressurized liquid, supercritical fluid, ultrasound-assisted and microwave-assisted extraction.[234] However, despite the numerous advantages introduced with these alternative extraction methods, the sustainability of the process and/or of the resulting products is not guaranteed. So, the choice and optimization of the proper extraction method have to take into account its actual impact on the human health and on the environment, determined by the life cycle assessment (LCA), besides the efficiency of the process in terms of product properties and yield.[235]

On this basis, the subsequent 4.1 paragraphs will be focused on the is focused on the:

- comparison of three extraction techniques applied on a laboratory scale of phenolic compounds from PN, in terms of efficiency and sustainability of the process;
- structural characterization of the extracted PN phenolic compounds;
- evaluation of a the PN extract as a sustainable alternative to traditional corrosion inhibitors of aluminum alloys.

4.1.2 Comparison between selected extraction techniques

4.1.2.1 Assessment of the extraction techniques efficiency in terms of yield, total phenolic and condensed tannins contents

First experiments were directed to the comparison of three different extraction methods, namely conventional maceration (CM), ultrasound-assisted extraction (UAE) and microwave-assisted extraction (MAE), in terms of extraction yields. This activity was performed by researchers at Department of Chemical, Materials, and Production Engineering of University of Naples Federico II.

In particular, using a procedure already reported in literature,[236] dry pine needles were extracted at 1:10 w/v solid-to-liquid ratio using an acetone/water mixture (70:30 v/v) as medium. Then, in the case of conventional maceration (CM), the mixture was kept in a 40°C bath under stirring. The ultrasound-assisted extraction (UAE) was carried out using a probe directly immersed in the extraction mixture, while microwave-assisted extraction (MAE) was performed using a domestic oven. Finally, the extracts were collected as powder and the extraction yields were calculated at selected times as reported in Figure 4.2. The most effective method was UAE, in accordance with literature[237] data, which have highlighted the excellent capability of this technique in extracting bioactive substances from pine seeds. On the other hand, MAE yield was very low with respect to CM and UAE ones. Actually, MAE is known to be effective when performed at relatively high temperature,[237,238] that however was in this case controlled to reach a maximum of 40°C to prevent phenol degradation.

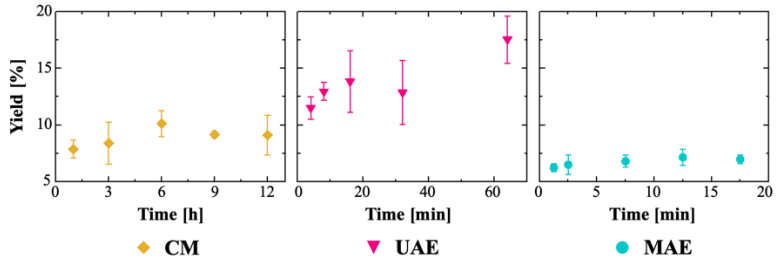

Figure 4.2. Time evolution (h or min) of the extraction yield (%) for CM, UAE and MAE. Mean values ± SD from at least three separate samples are reported.

However, as mentioned in the 4.1.1 paragraph, the extraction yield is only partially related to the efficiency of the method. A more complete picture can be obtained evaluating the quality of the extract, in terms of the active compounds present. On this basis, Folin-Ciocalteu and vanillin-HCl assays were performed on the extracts to quantify the total phenolic and the condensed tannins contents (TPC and CTC), respectively, being condensed tannins already reported as the main phenolic components of pine needles.[239] The results are reported in Figure 4.3 as a function of the extraction time.

In particular, CM seemed to be more efficient than UAE in terms of recovery of phenolic compounds, probably due to the use of less aggressive conditions. Indeed, data reported in literature have highlighted the formation of radical species during UAE process, likely responsible for a partial degradation of the phenolics contained in the extract.[240]

Also MAE provided extracts exhibiting good TPC and CTC values.

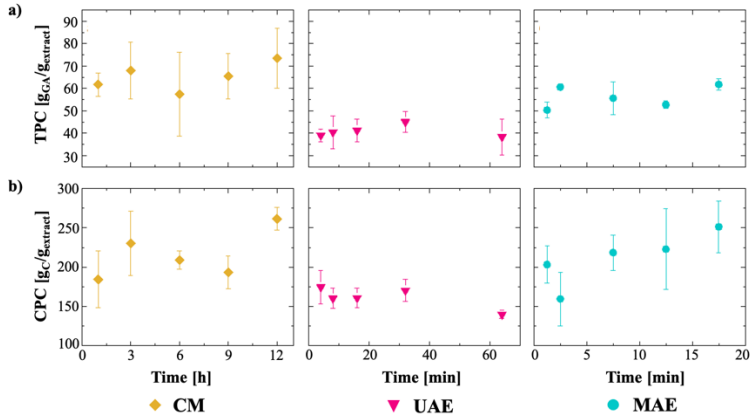

Figure 4.3. a) TPC and b) CTC per gram of dry PN fibers reported as a function of the extraction time for: CM, UAE and MAE. TPC is expressed as g of gallic acid/g of extracts, whereas CTC is expressed as g of catechin/g of extract. Mean values ± SD from at least three separate samples are reported.

4.1.2.2 Assessment of the process sustainability

Subsequently, an LCA study was applied to evaluate the sustainability of the three extraction methods. This activity was performed by researchers at Department of Chemical, Materials, and Production Engineering University of Naples Federico II.

Firstly, the optimal process duration of each method was evaluated, considering that higher extraction times mean higher spent energy. The optimal process duration characterized by the lowest values of the investigated impact categories, were identified as 1 h, 4 min and 1.5 min for CM, UAE and MAE, in that order.

Then, the three extraction processes were compared in terms of sustainability at the best identified operation times. CM and UAE proved to be less impactive than MAE, as shown in Figure 4.4 reporting this result as single score indicator, *i.e.* a parameter able to give a total picture of several impact

categories based on a set of variables that are used to normalize and weight the impact values.

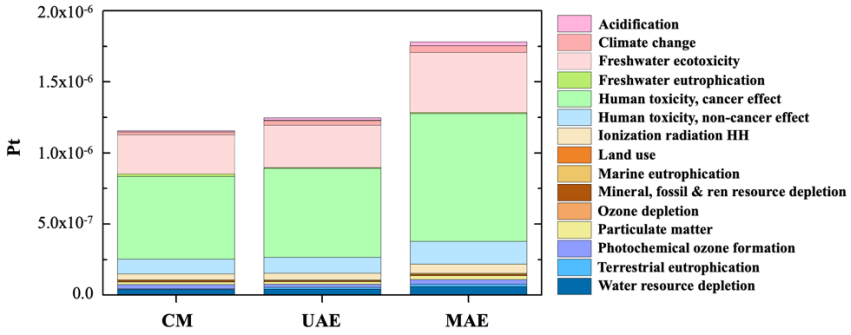

Figure 4.4. Single score results of CM at 1h, UAE at 4 min and MAE at 1.5 min.

Since the environmental impact showed by CM and UAE was very similar and considering that the latter is well-known to be "greener" with respect to CM thanks to the lower extraction time, the best choice could have been the use of UAE method. However, the use of a so energy-consuming extraction technique is actually convenient from an environmental perspective only if it leads to very high extraction yields in a short time, which was not the case with the present study.

Therefore, considering all the collected results, the optimal balance between extraction efficiency, particularly in terms of phenolic/condensed tannins content, and sustainability of the process was provided by CM method.

4.1.3 Structural characterization of the main phenolic components of CM PN extract

The selected PN extract obtained by CM was subjected to a complete structural characterization.

The UV-Vis spectrum of the sample (Figure 4.5_a) showed an absorption maximum at 275 nm accompanied by a broadened absorption band between 300 and 400 nm, typical of phenolic polymers such as condensed tannins. In agreement with is observation, HPLC analysis did not reveal the presence of any chromatographable compound.

^{1}H nuclear magnetic resonance (NMR) spectrum of the sample (Figure 4.5_b) was characterized by the presence of signals typical of condensed tannins, *i.e.* broad signals in the 6.0-7.2 ppm and 3.4-5.4 ppm chemical shift regions.[241,242] The presence of these compounds was also confirmed by electron paramagnetic resonance (EPR) spectroscopy, a technique commonly used to identify and characterize phenolic polymers.[183,184,243,244] In particular, in agreement with the data reported in the literature[245], the EPR signal of the extract (Figure 4.5_c) was characterized by a g value typical of carbon-centered radicals (2.0034 $\pm$ 0.0002), and by a relatively high DB value (6.5 $\pm$ 0.2 G) and low spin density (8.1 $\pm$ 0.5 $\times 10^{14}$ spin/g), typical of phenolic polymers characterized by a low extent of p-electron delocalization.[244] In agreement with these observations, the normalized power saturation profile (Figure 4.5_d), characterized by a monotonously increase of the intensity followed by a slope change, indicated a high extent of molecular heterogeneity of the PNs paramagnetic centers.[245,246]

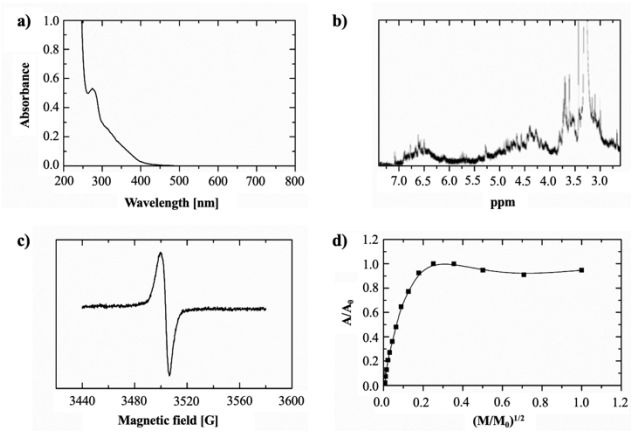

Figure 4.5. a) UV-vis spectrum (0.1 mg/mL in methanol), b) ^{1}H NMR spectrum (DMSO-d_6), c) EPR spectrum, and d) EPR power saturation profile of PN extract obtained using CM.

Subsequently, the extract was subjected to chemical degradation experiments, and the resulting mixtures were analyzed by HPLC and LC-MS analysis to get information about the main flavanol constituents of the condensed tannins contained in the sample. The main constituent units were identified analyzing the mixture obtained by phloroglucinolysis. In particular, afzelechin and epi-afzelechin were identified as the main terminal units, while gallocatechin/epigallocatechin as the main internal units, together with very small amounts of catechin/epicatechin (Figure 4.6). On this basis, mixed propelargonidin/prodelphinidin tannins were identified as the main phenolic constituents of the PN extract, in agreement with the data reported in the literature in the case of *Pinus sylvestris* L. and *Pinus densiflora* L.[247,248]

This observation was supported by the identification of 4-hydroxybenzoic acid as one of the main products present in the alkaline hydrogen peroxide and alkali fusion degradation mixtures, together with a very small amount of gallic acid. Indeed, these products can likely be obtained by the oxidative degradation of (epi)afzelechin and (epi)gallocatechin subunits, respectively.

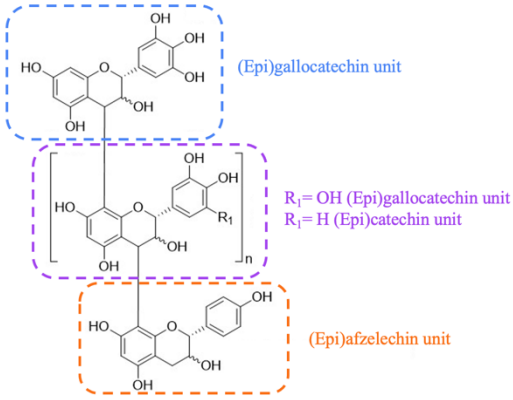

Figure 4.6. Mixed propelargonidin/prodelphinidin tannins as the proposed main condensed tannins contained in the CM PN extract.

4.1.4 Assessment of the corrosion inhibition ability of CM PN extract

Previous studies reported in literature have highlighted the good metal protection ability against corrosion of synthetic phenolic antioxidants.[249] On this basis, PN extract was finally investigated as a sustainable alternative to traditional corrosion inhibitors of aluminum alloys, using an aluminum bar immersed in a NaCl solution as model. This activity was performed by researchers at Department of Chemical, Materials, and Production Engineering University of Naples Federico II.

In this model, a cathodic and an anodic corrosion process can be distinguished, corresponding to the reduction of dissolved oxygen and the dissolution of aluminum into the solution, respectively. Their combination lead to the formation of aluminum hydroxide ($Al(OH)_3$), which subsequently precipitates on the metal surface and gradually transforms into aluminum oxide (Al_2O_3) able to form a protective passive layer on the metal surface.[250,251] However, chloride ions present in the solution can easily penetrate the formed coating,

breaking it and damaging the alloy forming few nanometers cracks (process well-known as pitting corrosion) (Figure 4.7).[252]

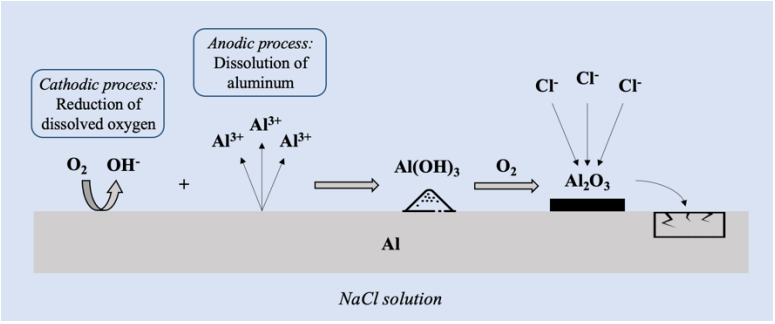

Figure 4.7. Schematic representation of the corrosion process of an aluminum bar in a NaCl solution.

Therefore, to evaluate how the PN extract can impact on the aluminum corrosion process, potentiodynamic polarization measurements were carried out. Aluminum samples dipped in the NaCl solution in the absence (CTRL) or presence of PN extract at different concentration (from 0.01 up to 10 g/L) were analyzed. Based on the obtained results (data not shown),[250,253,254] the PN extract was identified as a mixed type or adsorption inhibitor, capable of hindering both cathodic and anodic processes. The optimal corrosion inhibition activity for both cathodic and anodic processes was gained using PN extract at 0.1 g/L. This result, indicating the good anticorrosive property of the PN extract at relatively low concentration, can be attributable to the presence of condensed tannins in the sample which are capable not only to act as scavengers of oxidative species but also to form a protective layer by absorbing at the alloy/water interface reducing the interaction of the aluminum surface with the corrosive environment. At the end of the potentiodynamic polarization analyses, the metal surfaces were analyzed by the optical microscopy. As shown in Figure 4.8_A, the control sample showed

a rather high number of large pits with a dimension of hundreds of microns. The pit size didn't change in the presence 0.1 g/L of PN extract, but the number of pits was significantly reduced (Figure 4.8_B).

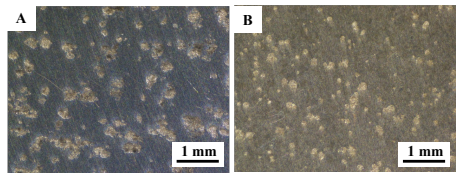

Figure 4.8. Stereomicroscopy images of aluminum bar after potentiodynamic tests in a 1 M NaCl solution in the (A) absence (CTRL) or presence (B) of 0.1 g/L of PN extract.

4.1.5 Conclusions

In conclusion, CM was identified as the best extraction technique of PN thanks to the optimal balance obtained between extraction yield, extract composition and process sustainability. PN extract showed promising properties as a green corrosion inhibitor on aluminum alloy even at relatively low concentration (0.1 g/L). This result is likely due to its phenolic composition, characterized by the presence of mixed propelargonidin/prodelphinidin tannins, able to create a protective layer on the metal surface, protecting it from the corrosion environment.

4.1.6 Experimental section

Materials and methods. Dry pine needles (PN) from Pi̅n̆s pi̅nea were hand harvested in an area close to the Vesuvius National Park (Ercolano, Italy). Folin-Ciocalteu reagent, gallic acid, catechin, vanillin, phloroglucinol, ascorbic acid, hydrogen peroxide (30% v/v) sodium metabisulphite and sodium dithionite were purchased from Sigma-Aldrich.

LCA and anticorrosion efficacy tests were carried out by researchers at Department of Chemical, Materials, and Production Engineering of the University of Naples Federico II.

^{1}H NMR spectrum was recorded in DMSO-d_6 at 400 MHz.

UV-vis spectra were recorded using a Jasco V-730 spectrophotometer.

EPR measurements were performed using X-band (9 GHz) spectrometer endowed which a superhigh sensitivity probe head. The weighed amounts of the samples were transferred to flame-sealed glass capillaries, which in turn were coaxially inserted in a standard 4 mm quartz sample tube. Spectra were performed at room temperature with a sweep width of 140 G, a 1024-point resolution and a scan time of 20.97 s. The amplitude of the field modulation (1.0 G) and the microwave power were preventively checked to avoid detectable signal overmodulation and to avoid microwave saturation, respectively. 16 scans were accumulated to improve the signal-to-noise ratio. For power saturation experiments, the microwave power was gradually incremented from 0.02 to 164 mW. The g value and the spin density were evaluated by means of an internal standard, Mn^{2+}-doped MgO, prepared by a synthesis protocol reported in the literature.[255]

HPLC analysis were performed on an instrument equipped with an Agilent G1314A UV-Vis detector, using a Phenomenex Sphereclone ODS column (250 × 4.60 mm, 5 μm) at a flow rate of 1.0 mL/min; the gradient elution was as follows: 0.1% formic acid (solvent A)/methanol (solvent B), 5% B, 0-10 min; from 5 to 80% B, 10-47.5 min; from 80 to 5% B, 47.5-57.5 min; the detection wavelength was set at 280 nm.

LC-MS analysis were run on an Agilent LC-MS ESI-TOF 1260/6230DA instrument operating in positive and negative ionization mode in the following conditions: nebulizer pressure 35 psig; drying gas (nitrogen) 5 L/min, 325°C; capillary voltage 3500 V; fragmentor voltage 175 V. A Eclipse Plus C18

column (150 × 4.6 mm, 5 μm) at a flow rate of 0.4 mL/min was used, using the same eluant as above.

Electrochemical measurements were carried out by researchers at Department of Chemical, Materials, and Production Engineering University of Naples Federico II.

Extraction procedure. PN were washed with tap water, oven-dried at 45°C for 3 h, and ground in a cutting mill to a fine powder. The obtained fibers were extracted using CM, UAE, and MAE. The extraction conditions were selected from the literature.[236] In particular, 1.5 g of PN were added to 15 mL of acetone/water 70:30 v/v. In the case of CM, a thermal bath at 40°C under magnetic stirring (250 rpm) was used carrying out the extraction in the time range 1-12 h. In the case of UAE, an ultrasound probe was directly immersed in the extraction mixture, and 30 s of irradiation – 30 s of rest time cycles were applied for 64 min. In the case of MAE, the mixture was exposed to radiation using a household microwave oven and 20 s of irradiation – 30 s of rest time cycles were applied for 17.5 min. The mixture extracted using UAE or MAE were placed in a cooling bath in order to maintain the temperature at a maximum of 40°C. After the extraction process, the mixture was filtered to remove the residual solid while the acetone was evaporated using a rotatory evaporator. The obtained aqueous solution was lyophilized obtaining a brown powder. The extraction yields were calculated from the weight ratio between the obtained powder and the initial quantity of PNs. Each experiment was run in triplicate.

Folin-Ciocalteu assay. [217] Different volumes (2-40 μL) of 2 mg/mL DMSO solutions of extract or gallic acid were mixed with a solution consisting of Folin-Ciocalteu reagent, 75 g/L Na_2CO_3, and water in a 1:3:14 v/v/v ratio. After 30 min incubation at 40°C under stirring, the absorbance at 765 nm was

measured. Gallic acid was used as reference and the results were expressed as gallic eqs (mg gallic acid/mg sample). Experiments were run in triplicate.

Vanillin-HCl assay.[256] Different volumes (20-200 μL) of DMSO solutions of extracts (20 mg/mL) or catechin (10 mg/mL) were mixed with 1 mL of methanolic vanillin solution (1% w/v). Then 1 mL of 9 M HCl was added, and the final mixture was taken under stirring at 30°C. After 10 min, the absorbance at 505 nm was measured. Catechin was used as reference compound and the results were expressed as catechin eqs (mg catechin/mg sample). Experiments were run in triplicate.

Phloroglucinolysis.[23,245] Following a procedure reported in literature, sample powder (2 mg) was treated with a solution (400 μL) containing 50 mg/mL of phloroglucinol and 10 mg/mL of ascorbic acid in methanolic 0.1M HCl, under stirring at 50°C. After 20 min the mixture was treated with 40 mM aqueous sodium acetate (2 mL) and filtered on a 0.20 μm PVDF filter. The obtained solution was analyzed by HPLC and LC-MS analysis.

Alkaline hydrogen peroxide degradation.[257–259] Following a procedure reported in literature, sample powder (5 mg) was treated with 1 M NaOH (1 mL) and H_2O_2 (30% v/v) (50 μL). After 24 h under stirring the mixture was treated with sodium metabisulphite aqueous solution (5% w/w) (200 μL), acidified with 6 M HCl (200 μL) and filtered on a 0.20 μm PVDF filter. The obtained solution was analyzed by HPLC and LC-MS analysis.

Alkali fusion.[258,260] Following a procedure reported in literature, sample powder (20 mg) was added to a mixture previous prepared melting in an oven 100 mg of KOH, 100 mg of NaOH and 2 mg of sodium dithionite at 240°C. After 10 min at 240 °C, the mixture was treated with 10 mL of a sodium dithionite water solution (1% w/v), acidified to pH 3 with 6 M HCl and then extracted with ethyl acetate (15 mL × 3). The organic phases were anhydrified on dry sodium sulphate and taken to dryness with a rotary evaporator. The oily

residue was analyzed by HPLC and LC-MS after dissolution in methanol (2 mL).

4.2 Exploitation of tannins for the preparation of palladium-based recyclable catalysts

4.2.1 Introduction

Thanks to their peculiar chemical structure, tannins are capable to interact with various surfaces or compounds through both strong covalent and non-covalent interactions. On this basis, they have been widely used for adhesive and coating applications.[71]

In this framework, and starting from a previous study performed using polydopamine (PDA),[261] the present research work was focused on the investigation of hydrolysable and condensed wood tannins to be used as coating systems of open-cell polyurethane foams (PUF) to obtain, after functionalization with palladium, eco-friendly and reusable heterogeneous catalysts.

In particular, the open-cell PUF represents a commercially available, inexpensive and mechanically flexible valid alternative to the common structured catalytic supports (SCSs), whose preparation has several drawbacks including the use of high quantity of energy and materials.[262] However, unlike SCSs, PUF are lacking in microporosity, a critical requisite that permits the deposition of the active phase (catalyst). So, the use of compounds able to interact with PUF surface and, at the same time, to strong anchor the catalyst, represents a valid solution to overcome this issue.

On this basis, the subsequent 4.2 paragraphs will be focused on the:

- use of hydrolysable and condensed wood tannins for the preparation of palladium-functionalized PUF to be used as heterogeneous and recyclable catalysts;
- evaluation of the catalytic activity and recyclability of the prepared foams over several number of different reactions, *e.g.*

phenylacetylene to styrene hydrogenation, nitrobenzene reduction and Suzuki coupling.

4.2.2 Preparation of Pd-functionalized hydrolysable and condensed tannin-coated PUF

The herein reported preliminary work was in part carried out during a two-month research period abroad at the University of Strasbourg (France). Thanks to the easily engineered preparation of commercial open cell PUF it's possible to properly choose their size and shape. So, the form of the catalysts can easily fit any reactor's dimension and shape, facilitating also the scale-up of the process for an industrial application.

In this work, the new heterogeneous catalysts were prepared by following a two-step dipping procedure. Firstly, PUF of ca. 8 cm^3 were coated with hydrolyzable (HT) or condensed (CT) tannins by immersion in a 0.1 mg/mL tannin solution for 2 h under stirring. In particular, HT from chestnut (*Castanea sativa*) wood mainly composed of ellagitannins (*e.g.* castalagin and its isomer vescalagin) and CT from quebracho (*Schinopsis lorentzii*) wood, mainly constituted by linear profisetinidins, were exploited (Figure 4.9).

After the coating procedure, the foams were repeatedly washed with ethanol and the washings were analyzed spectrophotometrically until no detectable absorption was observed, to avoid any future leaching in the reaction medium. Then, the $^{0.1}$HT/CT@PUFs were functionalized with Pd following a procedure already reported in literature[261] involving the immersion of the foam into a well stirred hydroalcoholic solution (water/ethanol 1:5 v/v) of $[Pd(NH_3)_4Cl_2]\times H_2O$ at room temperature for 19 h (Figure 4.10). Finally, the foams were washed with water and ethanol and air-dried.

The PUF thus prepared were then tested as catalysts in model reactions aimed to evaluate their efficacy and stability over several cycles.

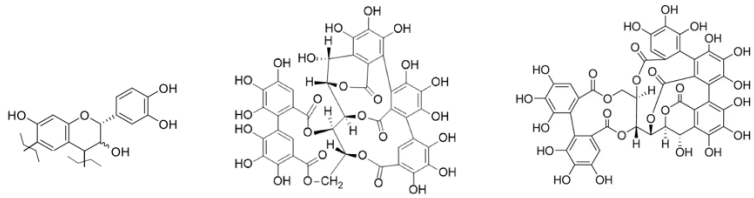

Figure 4.9. Profisetinidins, castalagin and vescalagin structures.

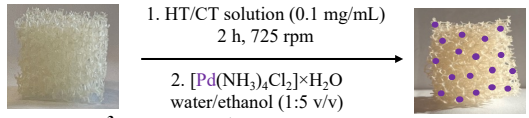

Figure 4.10. Coating and functionalization of PUF (8 cm^3) by a simple two-step procedure involving: 1) dipping of the PUF in the $^{0.1}$HT/CT solution for 2 h under stirring; 2) dipping of the $^{0.1}$HT/CT@PUF into a well stirred hydroalcoholic solution of $[Pd(NH_3)_4Cl_2]\times H_2O$ at room temperature for 19 h to obtain the final Pd@$^{0.1}$HT/CT@PUF.

4.2.3 Catalytic activity and reusability assessment of Pd-functionalized $^{0.1}$HT/CT-coated PUF

4.2.3.1 Application of Pd@$^{0.1}$HT@PUF in hydrogenation reactions

The Pd@$^{0.1}$HT@PUF was investigated as catalyst in the semi-hydrogenation reaction of phenylacetylene (PA) to styrene (ST), using a procedure optimized in a previous study where a polydopamine-coated PUF was used.[261] This particular reaction was chosen for the importance of removing PA during polystyrene production to avoid the deactivation and poisoning of the polymerization catalysts.[263]

In particular, the foam was insert in a Schlenk tube and immersed in ethanol at room temperature. Through a needle, that reach the bottom of the flask without compressing or causing structural deformation of the foam, a constant flow rate (13 mL/min) of H_2 into the solution was insufflated to maintain its concentration constant during the whole duration of the catalytic process. Then, PA (3 mmol) was added in one portion by syringe to the stirred solution and the reaction was kinetically monitored by GC analysis over time.

Interestingly, after only 1 h, 87% of PA conversion and 95% of ST selectivity were observed (Figure 4.11), similarly to the result obtained carrying out the reaction with conventional catalyst, *i.e.* Pd/C (91 and 95%, respectively).[261]

Notably, ethylbenzene (EB) started to be produced in appreciable quantity only after the full conversion of PA into ST. This result can be ascribed to the high PA adsorption properties on Pd@$^{0.1}$HT@PUF, which would prevent ST to be adsorbed before all PA was consumed.

On the other hand, the EB formation course seemed very similar to that of ST, indicating that the consecutive hydrogenation reactions are initiated on similar active sites.

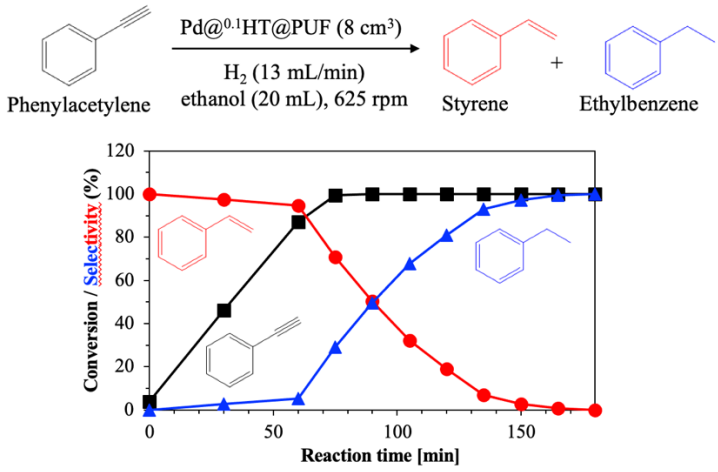

Figure 4.11. Hydrogenation of PA with Pd@$^{0.1}$HT@PUF (8 cm^3); black squares: PA conversion; red circles: ST selectivity; blue triangles: EB selectivity.

Next, the catalytic activity of the spent Pd@$^{0.1}$HT@PUF was investigated in another reaction, usually difficult to perform by hydrogenation with heterogeneous catalysts: *i.e.* the reduction of nitrobenzene to aniline.[264,265] Similarly to the semi-hydrogenation, the reaction was carried out in ethanol, at room temperature, using a constant 13 mL/min H_2 flow rate and 3 mmol nitrobenzene. Monitoring it over time by GC analysis, substrate conversion proved to be slower with respect to that observed for PA hydrogenation. However, an almost complete consumption (95%) of nitrobenzene was observed after 8 h (Figure 4.12).

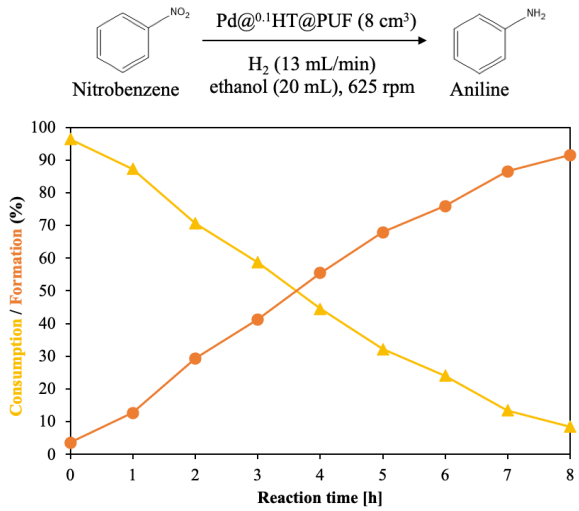

Figure 4.12. Reduction of nitrobenzene with Pd@$^{0.1}$HT@PUF (8 cm^3); yellow triangles: nitrobenzene consumption; orange circles: aniline formation.

4.2.3.1.1 Assessment of Pd@$^{0.1}$HT@PUF leaching in the reaction medium

In order to evaluate whether palladium leaching from the foam in the reaction medium occurred with the Pd@$^{0.1}$HT@PUF, the "stop-&-go" reaction protocol[261] was performed in the nitrobenzene reduction. In particular, the reaction was started dipping the foam into the reaction solution. Then, after 2 h, the Pd@$^{0.1}$HT@PUF was removed from the reaction medium for 2 h, reintroduced in the reacting vessel for 1.5 h and finally removed again for 1.5 h. During the whole process, H_2 was constantly fed into the solution to maintain its concentration constant, and the reaction course was monitored by GC.

As shown in Figure 4.13, the nitrobenzene reduction to aniline does not progress in the absence of the functionalized foam in the solution (between the 2nd-4th and 5.5th-7th hours), indicating that no significant leaching of the catalyst into the solution occurred.

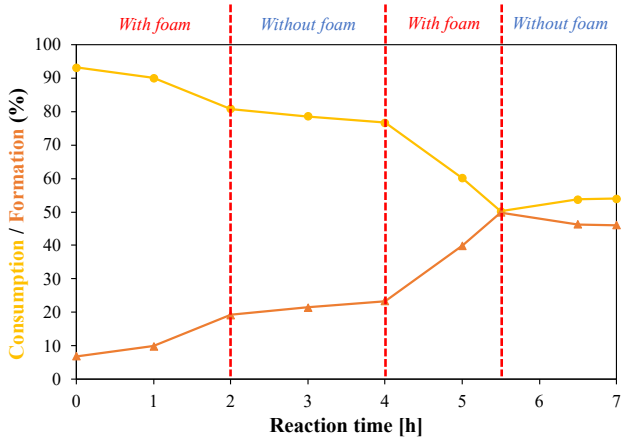

Figure 4.13. "Stop-&-go" experiment for the reduction of nitrobenzene with Pd@$^{0.1}$HT@PUF (8 cm^3) up to 7 hours; yellow triangles: nitrobenzene consumption; orange circles: aniline formation.

4.2.3.2 Application of Pd@$^{0.1}$CT@PUF

Basing on the previous results, the application of the Pd@$^{0.1}$CT@PUF was then investigated.

In particular, preliminary experiments were directed at testing the foam catalytic activity in the nitrobenzene reduction following the reaction course by GC analysis (Figure 4.14). Interestingly, Pd@$^{0.1}$CT@PUF proved to be able to convert almost all nitrobenzene (92%) with high selectivity (> 99%) after 7 h, proving to have even slightly higher efficiency than Pd@$^{0.1}$HT@PUF.

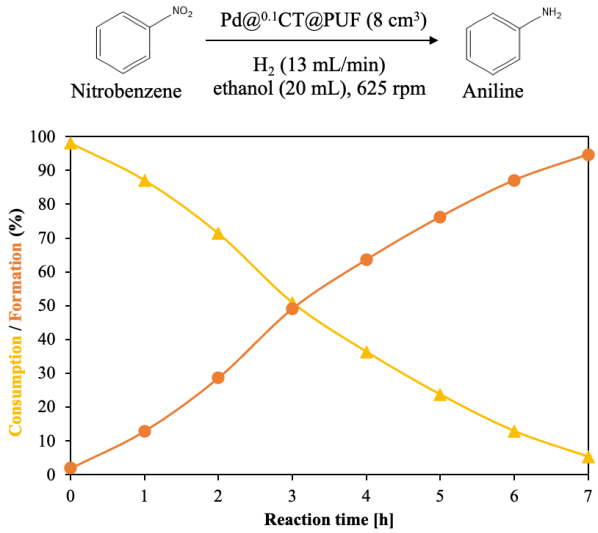

Figure 4.14. Reduction of nitrobenzene with Pd@$^{0.1}$CT@PUF (8 cm^3); yellow triangles, nitrobenzene consumption; orange circles, aniline formation.

4.2.3.3 Reusability evaluation of Pd@$^{0.1}$HT/CT@PUF in Suzuki reaction

Finally, in further experiments the recyclability of the HT and CT foams was tested in the Suzuki coupling reaction, typically used for the production of biaryl compounds,[266] and largely exploited in the synthesis of natural products or pharmaceuticals, and in the preparation of organic electronics. In particular, 4-bromotoluene and phenylboronic acid were used as starting materials applying a procedure already reported in literature.[261]

In particular, the reaction was run by immersion of the Pd@$^{0.1}$HT/CT@PUF in a hydroalcoholic solution at 65°C, using K_2CO_3 as base, and the reaction course was followed by HPLC analysis.

Interestingly, both HT and CT foams proved to be highly efficient without any pre-activation procedure, as shown in Figure 4.15 and 4.16. Moreover, the catalytic efficiency remained unchanged over the first 5/6 runs showing a

complete conversion (>99%) of the reagents, after only 10 min, in the expected biaryl, *i.e.* 4-phenyltoluene, identified by LC-MS analysis.

After the first 5/6 runs, the conversion extent gradually decreased. However, with both HT and CT-based catalysts, a complete conversion could be reached at longer reaction times.

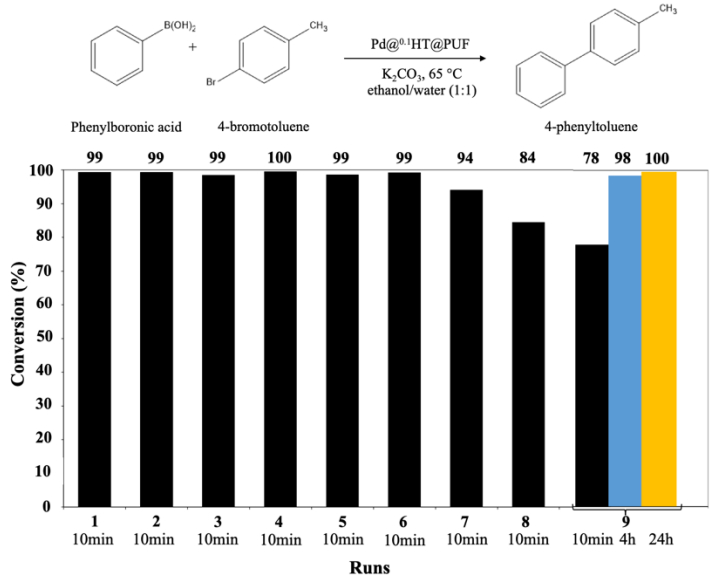

Figure 4.15. Conversion (%) measured over 9 successive runs of Suzuki coupling, using 4-bromotoluene and phenylboronic acid as starting materials, catalyzed by Pd@$^{0.1}$HT@PUF.

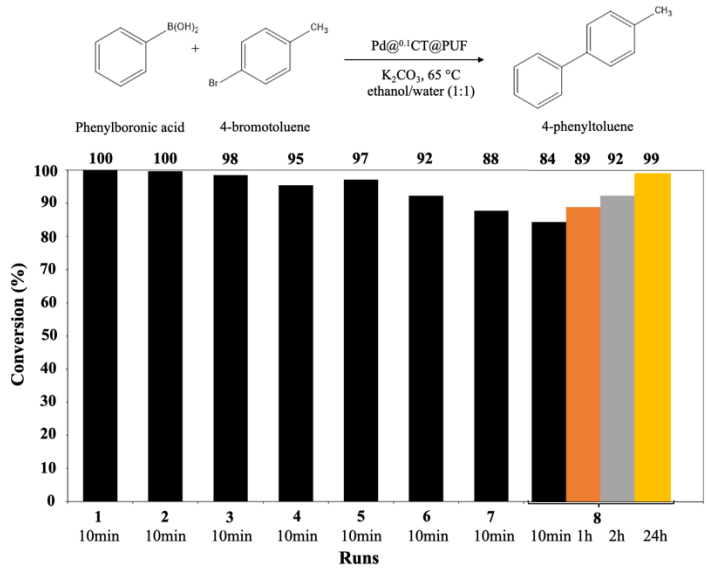

Figure 4.16. Conversion (%) measured over 9 successive runs of Suzuki coupling, using 4-bromotoluene and phenylboronic acid as starting materials, catalyzed by Pd@$^{0.1}$CT@PUF.

4.2.3.3.1 Evaluation of the reaction scope in Suzuki coupling reaction

Last experiments were directed to the preliminary evaluation of the scope of the Suzuki reaction. In particular, it was briefly tested using as aryl compound the sterically hindered methyl 2-bromobenzoate.

A conversion higher than 70% was observed after only 2 h, reaching 90% over 24 h. However, the conversion rate resulted lower in comparison with the one observed for the reaction carried out using 4-bromotoluene (Figure 4.17).

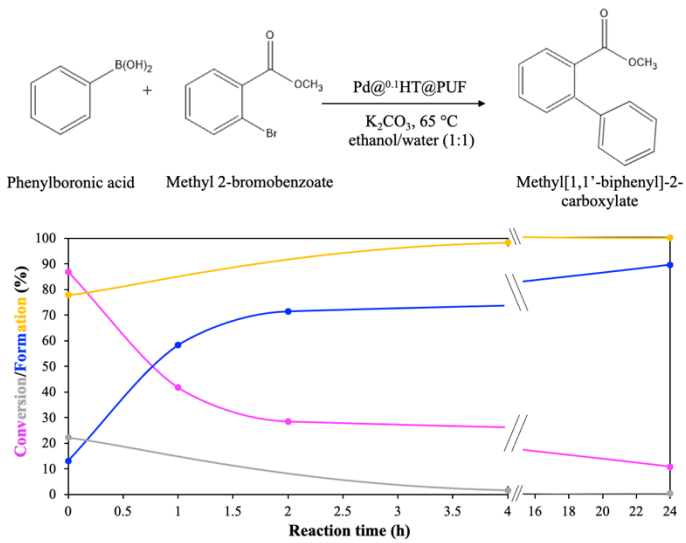

Figure 4.17. Suzuki coupling performed with Pd@$^{0.1}$HT@PUF (8 cm^3) followed over time, reacting phenylboronic acid with 4-bromotoluene or methyl 2-bromobenzoate; pink line: phenylboronic acid conversion in the presence of methyl 2-bromobenzoate; grey line: phenylboronic acid conversion in the presence of 4-bromotoluene; blue line: methyl[1,1'-biphenyl]-2-carboxylate formation; yellow line: 4-phenyltoluene formation.

4.2.4 Conclusions

In summary, HT and CT were used for the coating of PUF subsequently functionalized with palladium to obtain heterogeneous and recyclable catalysts.

Preliminary experiments demonstrated the catalytic activity of the prepared foams in different reactions. Interestingly, both HT and CT foams proved to be highly efficient without any pre-activation procedure, maintaining the catalytic activity over several cycles of reactions. Indeed, no activity decay was observed after at least 9 consecutive reactions. Moreover, the easily

recyclability of the catalyst, which only needed to be washed before being reused, was demonstrated.

In order to obtain more information about the tested Pd@$^{0.1}$HT/CT@PUFs, ICP-MS and XPS analysis are undergoing.

4.2.5 Experimental section

Materials and methods. Chestnut and quebracho tannins were provided by Silvateam (S. Michele Mondovi (CN)-Italia). Polyurethane open-cell foams (20 pores per inch, TCL 40100 soft white reticulated) were provided by FoamPartner. 4-bromotoluene (98%) and $[Pd(NH_3)_4Cl_2]\times H_2O$ (≥99.9%) were purchased from Sigma-Aldrich. Phenylacetylene (98%), phenylboronic acid (98%), methyl 2-bromobenzoate (99%) and nitrobenzene (99%) were purchased from Alfa Aesar.

HPLC analysis was performed on an instrument equipped with an Agilent G1314A UV-Vis detector, using a Phenomenex Sphereclone ODS column (250 × 4.60 mm, 5 μm) at a flow rate of 1.0 mL/min; the gradient elution was as follows: 0.1% formic acid (solvent A)/methanol (solvent B), 50% B, 0-10 min; from 50 to 80% B, 10-30 min; 80% B, 30-40 min; from 80 to 50% B, 40-45 min; 50% B, 45-47.5 min; the detection wavelength was set at 280 nm. Gas chromatographic (GC) analyses were performed on a GC Agilent instrument with a FID detector using an Agilent HP1 column (30 m, 0.35 mm, 0.25 μm), with hydrogen as the gas carrier and with tetradecane as the internal standard. The retention times and GC responses in terms of area *vs* concentration of the reagents and products were calibrated using pure components diluted in an acetone solution at various concentrations.

Coating of open-cell PUF with HT and CT. A 0.1 mg/mL water solution of HT or CT was prepared. A cubic PUF (ca. 8 cm^3) was coated by immersion for 2 h under stirring in the previously prepared tannin solution. The resulting

tannin-coated foam ($^{0.1}$HT/CT@PUF) was then taken out of the solution, washed in vigorously stirred ethanol (100 mL × 3, 1 h) and air-dried. The washings were analyzed by UV-Vis spectroscopy.

Functionalization of $^{0.1}$HT/CT@PUF with palladium. The previously prepared tannin-coated foams were functionalized with $[Pd(NH_3)_4Cl_2]\times H_2O$ according to a procedure reported in literature.[261] In particular, the foam was immersed in 120 mL of a hydroalcoholic (water/ethanol 1:5 v/v) solution of $[Pd(NH_3)_4Cl_2]\times H_2O$ (20 mg, 0.076 mmol) at room temperature, and was taken under vigorous stirring for 19 h. The resulting Pd-functionalized foam (Pd@$^{0.1}$HT/CT@PUF) was removed from the reaction medium, washed in vigorously stirred water (100 mL × 3) and ethanol (100 mL × 3), and then air-dried.

General procedure for the catalytic phenylacetylene-to-styrene hydrogenation using Pd@$^{0.1}$HT@PUF. The Pd@$^{0.1}$HT@PUF (ca. 8 cm^3) was introduced in a Schlenk tube. 20 mL of ethanol was then added to totally cover the foam, and H_2 was bubbled through the solution using a needle, at room temperature under a constant flow rate (13 mL/min). After 30 min, phenylacetylene (3 mmol) was added in one portion by syringe to the stirred solution (625 rpm) (t_0). The reaction was kinetically monitored by GC analysis, sampling regularly the reaction medium starting from t_0 (the 50 µL aliquots were diluted in 3 mL of acetone). After each run, the foam was washed in ethanol (20 mL × 3) for 10 min and dried under vacuum.

General procedure for the catalytic nitrobenzene reduction using Pd@$^{0.1}$HT/CT@PUF. The Pd@$^{0.1}$HT/CT@PUF (ca. 8 cm^3) was introduced in a Schlenk tube. 20 mL of ethanol was then added to totally cover the foam, and H_2 was bubbled through the solution using a needle, at room temperature under a constant flow rate (13 mL/min). After 30 min, nitrobenzene (3 mmol) was added in one portion by syringe to the stirred solution (625 rpm) (t_0). The

reaction was kinetically monitored by GC analysis, sampling regularly the reaction medium starting from t_0 (the 50 μL aliquots were diluted in 3 mL of acetone). After each run, the foam was washed in ethanol (20 mL × 3) for 10 min and dried under vacuum.

"Stop-and-go" experiment for the catalytic nitrobenzene reduction using Pd@$^{0.1}$HT@PUF. The above-described catalytic nitrobenzene reduction was performed using Pd@$^{0.1}$HT@PUF. After 2 h of reaction, the foam was removed from the reaction medium for 2 h, to be reintroduced in the reacting vessel for 1.5 h, and finally removed definitively. During the whole process, H_2 was constantly fed into the medium to maintain its concentration constant. The course of the reaction was monitored by sampling the reaction medium and analyzing the removed aliquots (50 μL) by GC after dilution in acetone (3 mL).

General procedure for the Suzuki cross-coupling of aryl bromides and phenylboronic acid using Pd@$^{0.1}$HT/CT@PUF. In a tube similar to the one used in the hydrogenation experiments, phenylboronic acid (0.17 mmol), K_2CO_3 (0.21 mmol) and 4-bromotoluene/methyl 2-bromobenzoate (0.14 mmol) were added in 2.25 mL of ethanol/water (1:1 v/v). In the resulting mixture the Pd@$^{0.1}$HT/CT@PUF (ca. 8 cm^3) was immersed, and the solution was taken under stirring (625 rpm) and heated in an oil bath at 65°C. The course of the reaction was monitored by sampling the reaction medium and analyzing the removed aliquots (20 μL) by HPLC and LC-MS as such or after 1:10 dilution with methanol.

4.3 Examination of the properties of hydrolysable and condensed tannins from wood to be used in dermo-cosmetic applications

4.3.1 Introduction

The remarkable antioxidant power of tannins already mentioned in the Introduction, made their use very interesting also in the dermo-cosmetic field. Indeed, thanks to this property, they can counteract cellular aging. In addition, based on their UV absorption properties, they may protect human skin from solar UV radiations.

In this framework, this Chapter will be focused on the systematic examination of properties of selected wood tannin samples (from chestnut, quebracho, tara and gall) for their possible application in the dermo-cosmetic field. In particular, the photostability and solubility of these samples in different solvents were evaluated, as well as their effect on photo-induced lipid peroxidation.

4.3.2 Solubility assessment of the selected samples

Chestnut, quebracho, tara and gall wood extracts are well-known to be rich in tannins. In detail, chestnut, tara and gall woods extract are a source of hydrolysable tannins, whereas quebracho wood extract is constituted mainly by condensed tannins, and in particular by linear profisetinidins.[22,60,178]

First experiments were directed to the evaluation of the solubility of the samples, available in a powder form, using five different solvents:

i) 100 % water
ii) 100 % DMSO
iii) 100 % ethanol
iv) 5% ethanol in 0.1 M phosphate buffer (PB) 0.1 M at neutral pH

v) acetone/olive oil in a 4:1 v/v ratio

In particular, after 30 minutes under stirring each sample was analyzed by UV-Vis spectroscopy before or after centrifugation, in order to confirm the concentration at which the powder appeared visibly dissolved.

As reported in Table 4.1, tara (TAN/T) and gall (TAN/G) tannins showed marked solubility at high concentration in every solvent, while chestnut (TAN/C) and quebracho (TAN/Q) were effectively dissolved only in DMSO.

Table 4.1. Maximum solubility (mg/mL) of tannin samples in different solvents.

Sample	100 % water	100 % DMSO	100 % ethanol	5% ethanol in 0.1M PB	Acetone/Olive oil 4:1 v/v
TAN/C	~ 60 mg/mL	> 200 mg/mL	< 10 mg/mL	~ 37 mg/mL	< 10 mg/mL
TAN/Q	~ 75 mg/mL	> 200 mg/mL	< 10 mg/mL	< 10 mg/mL	< 10 mg/mL
TAN/G	> 200 mg/mL	> 200 mg/mL	> 200 mg/mL	> 200 mg/mL	> 200 mg/mL
TAN/T	> 200 mg/mL	> 200 mg/mL	> 200 mg/mL	> 200 mg/mL	> 200 mg/mL

4.3.3 Partition coefficients calculation

After the solubility evaluation, in order to assess the concentration in which the analyzed tannins are distributed between two immiscible organic and aqueous phases at equilibrium, the partition coefficients[267] were calculated according to the follow equation:

$$P_{ow} = \frac{[\text{tannin}]_o}{[\text{tannin}]_w}$$

where *o* and *w* correspond to the organic and aqueous solvents, respectively. Through this value, it is possible to identify the level of hydrophilicity ($P_{ow} < 1$) or hydrophobicity ($P_{ow} > 1$) of the analyzed samples.

In detail, octanol and water in 1:1 v/v ratio were selected as solvents and the mixture formed by adding the tannin powder at a final concentration of 0.1 mg/mL was stirred for 3 h. After separation, the two phases were analyzed by UV-Vis spectrophotometry at 280 nm. Using calibration curves previously built for each sample, the tannin concentrations in the organic and aqueous phases and then the partition coefficients were calculated. As shown in Table 4.2, TAN/C and TAN/Q were found to be more hydrophilic ($P_{ow} < 1$) than TAN/T and TAN/G, instead characterized by hydrophobic character ($P_{ow} > 1$).

Table 4.2. Partition coefficients calculated for the tannin samples. Mean values ± SD from at least three separate samples are reported.

Sample	P_{ow}
TAN/C	0.475 ± 0.001
TAN/Q	0.92 ± 0.05
TAN/G	2.013 ± 0.001
TAN/T	1.750 ± 0.001

4.3.4 Evaluation of the photostability properties

Further experiments were directed to the evaluation of tannin photostability, intended as the sample ability to remain unaltered after irradiation. All the samples were tested at 15 mg/mL using water as solvent, which was previously demonstrated to ensure a good solubilization of the samples. The mixtures were then exposed to a solar simulator and periodically analyzed by UV-vis spectroscopy.

As an example, in Figure 4.18 is reported the UV-Vis spectrum of TAN/G in water, showing a profile almost unchanged over the time indicating a good photostability. Similar results were obtained with the other samples.

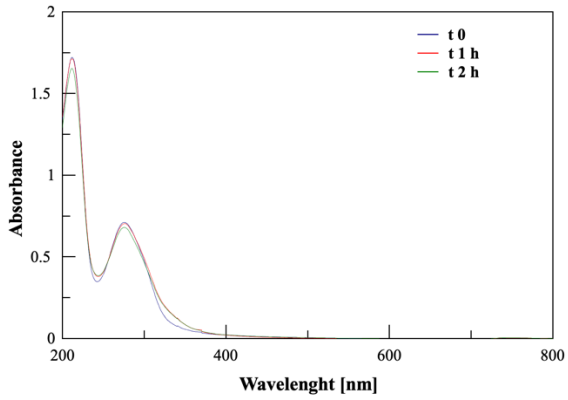

Figure 4.18. UV-Vis spectrum of TAN/G in water at 0, 1 and 2 h irradiation time.

4.3.5 Assessment of the inhibition effect of tannins on the photo-induced lipid peroxidation of linoleic acid

Deeply studied in the dermo-cosmetic field is lipid peroxidation. This is a radical chain oxidation process of polyunsaturated lipids constituting cell membranes, which can be induced by skin exposure to reactive oxygen species and UVA and visible light. The first formed products are lipid hydroperoxides (LOOH), which can further react to produce toxic species leading to the onset of pathological conditions such as skin phototoxicity and carcinogenesis.

The ability of tannins to inhibit the lipid peroxidation induced by light exposure was explored using a method already reported in literature which involve linoleic acid and riboflavin.[268]

In detail, linoleic acid, an unsaturated fatty acid (18:2) and an important structural component of cell membranes, was used as a model substrate. When

subjected to lipid peroxidation, it forms conjugated dienes detectable by UV spectroscopy (λ_{max} = 234 nm). Riboflavin was instead chosen because when excited by light, it reacts with oxygen bringing it to its singlet oxygen state, with a consequent acceleration of the lipid peroxidation.[269]

Solutions containing linoleic acid, riboflavin, sodium dodecyl sulphate (SDS) and tannins at different concentrations (1.25, 2.5 and 4 µg/mL) were prepared in sodium phosphate buffer. Each solution was then exposed to the solar simulator and periodically analyzed by UV spectroscopy at 234 nm.

The most effective inhibition was observed using 2.5 µg/mL as final tannins' concentration. So, comparing the responses obtained for all the samples at this concentration (Figure 4.19), TAN/G showed the greater lipid peroxidation inhibition properties, while TAN/C was found to be even pro-oxidant compared to the control sample (prepared without the use of tannins).

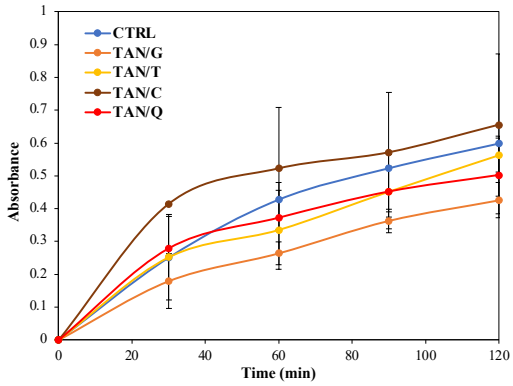

Figure 4.19. UV-Vis spectra of solutions containing linoleic acid, riboflavin, SDS in sodium phosphate buffer in the absence (CTRL) or presence of tannins (2.5 mg/mL), analyzed after exposure to a solar simulator. Mean values ± SD from at least three separate samples are reported.

In line with the obtained results, TAN/G exhibited great antioxidant properties in the 2,2-diphenyl-1-picrylhydrazyl (DPPH) assay (Table 4.3).[175]
Comparable antioxidant power was showed by TAN/Q and TAN/T while TAN/C proved to be the less active.

Table 4.3. EC_{50} values (mg/mL) determined for the tannin sample in the DPPH assay. Mean values ± SD from at least three separate experiments are reported.

Sample	EC_{50} (mg/mL)
TAN/C	0.0126 ± 0.0005
TAN/Q	0.0048 ± 0.0001
TAN/G	0.0045 ± 0.0004
TAN/T	0.57 ± 0.0002

4.3.6 Conclusions

Thanks to their interesting properties and to the increasing request of natural products, nowadays tannins have stimulated a lot of interest for their possible application in the dermo-cosmetic field. On this basis, a systematic examination of selected hydrolysable and condensed tannins properties (solubility, photostability, ability to inhibit photo-induced lipid peroxidation and antioxidant power) was performed, highlighting the particular efficacy of gallotannins.

4.3.7 Experimental section

Materials and methods. Chestnut, quebracho, tara and gall tannins were provided by Silvateam (S. Michele Mondovi (CN)-Italia). 2,2-Diphenyl-1-picrylhydrazyl (DPPH), linoleic acid, riboflavin, and sodium dodecyl sulphate (SDS) were purchased by Sigma-Aldrich. Olive oil was bought in a local supermarket.

UV-Vis spectra were recorded using a Jasco V-730 spectrophotometer.

Photo-induced lipid peroxidation of linoleic acid was performed with a Thermo-Oriel solar simulator.

Solubility test. A solution of each sample at 300 mg/mL as final concentration was prepared using: 100% water, 100% DMSO, 100% ethanol, 5% ethanol in 0.1 M phosphate buffer at neutral pH, or acetone/olive oil in a 4:1 v/v ratio. The obtained mixture was taken under stirring for 30 min and subsequently analyzed by UV-Vis spectroscopy before and after centrifugation (7000 rpm, 4 °C, 3 min). Each experiment was run in triplicate.

Partition coefficient evaluation. Tannin's powder was added at a 0.1 mg/mL final concentration in a water/octanol solution at 1:1 v/v ratio. After 3 h under stirring, the two immiscible phases were left to separate by stopping the stirring and analyzed by UV-Vis spectroscopy at 280 nm. Each experiment was run in triplicate.

Photostability assessment. A solution of TAN/G or TAN/T at 15 mg/mL in water was prepared, exposed to the solar simulator and periodically analyzed by UV-Vis spectroscopy over time (0-2 h). Each experiment was run in triplicate.

Photo-induced lipid peroxidation of linoleic acid. A solution was prepared combining: 100 mL of an acetonitrile linoleic acid solution (2.5 mM); 1.8 mL of 0.1 M sodium phosphate buffer at pH 7.0 containing 50 mM SDS; 100 mL of an aqueous riboflavin solution (20 mM). Each tannin sample was then added to the prepared mixture at 1.25, 2.5 or 4 μg/mL final concentration. The obtained solution was exposed to the solar simulator and analyzed by UV-Vis spectroscopy at 234 nm every 30 min for 2 h. As control, the solution without the tannins was also analyzed. Each experiment was run in triplicate.

DPPH assay. Several volumes of an aqueous tannin solution (0.5 mg/mL) were added to a 200 μM ethanolic solution of DPPH (2.5-20 mg/mL final

dose). After 10 min under stirring at room temperature, the absorbance at 515 nm was measured.[175] The antioxidant power was expressed as EC_{50}, that is the sample concentration capable of reducing the initial absorbance of the DPPH solution by 50%. Experiments were run in triplicate.

4.4 Preliminary experiments on the functionalization of catechin with selenium: a model study toward the enhancement of the antioxidant properties of condensed tannins

4.4.1 Introduction

As mentioned in paragraphs 1.4 and 3.2.1, growing interest has been recently directed to the study of bio-inspired phenolic polymers characterized by interesting and improved properties compared to the natural ones or to the corresponding monomers. In this framework, increasing attention has been devoted to the enhancement of their antioxidant activity by chemical manipulation.

Among all the possible methodologies, the already mentioned biomimetic phenol polymerization represents an effective route. For instance, besides OligoTyr obtained by polymerization with HRP/H_2O_2 system, which resulted to have higher antioxidant power compared to tyrosol,[107] a remarkable example is represented by catechin polymer, a more efficient superoxide ion scavenger than the starting catechin.[270]

Another fascinating and well documented manipulation involves the use of chalcogen atoms, especially sulphur and selenium, which are able to enhance the H-atom donating, metal chelating, and reducing power of phenolic systems.[271] Indeed, the introduction of organochalcogens residues ((S, Se,Te)-R) in the *ortho*-position of a phenolic compound lowers its O-H bond dissociation enthalpy (BDE),[272] hence improving its antioxidant and hydroperoxide-scavenging powers.[273] In this context, an example is represented by the benzoselenophene derivative obtained by the selenylation

of resveratrol, which showed higher antioxidant activity with respect to the starting phenol. In this framework, it could be interesting to investigate the possibility of preparing selenoderivatives of catechin as a model of condensed tannins. On this basis, these 4.3 paragraphs will report an evaluation of the efficacy of using the potassium selenocyanate (KSeCN) and cerium(IV) ammonium nitrate ($(NH_4)_2Ce(NO_3)_6$, CAN)[274] system for the preparation of catechin selenocyanoderivatives and of the possibility to convert the selenocyanoderivatives into catechin selenides and diselenides.

4.4.2 Exploration of the reactivity of catechin with the potassium selenocyanate/cerium ammonium nitrate system

Preliminary experiments were directed to the preparation of catechin selenocyanoderivatives using a procedure reported in the literature for the selenocyanation of electron-rich organic compounds such as styrenes and indoles, based on the use of KSeCN/CAN.[274] The latter is a common oxidizing agent whose role would be that to oxidize the selenocyanate anion to the corresponding radical (with concomitant reduction of Ce(IV) to Ce(III)), thus generating the electrophilic species which can in turn take part to an electrophilic aromatic substitution reaction.

Catechin (50 mM) was reacted with 2 molar equivalents (eqs) of KSeCN and CAN (added in 4 aliquots every 30 min), and the reaction course was followed by HPLC analysis. As shown in Figure 4.20, after 2.5 h the formation of a main product eluted at 29 min was observed, with a catechin (eluted at 23 min) consumption of about 70%.

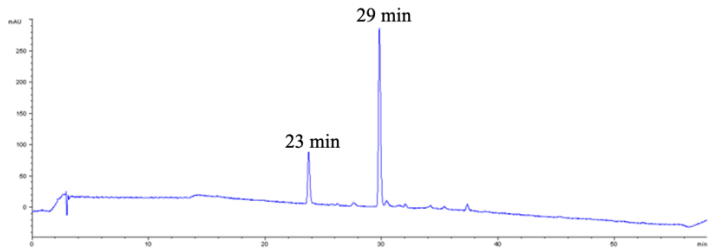

Figure 4.20. HPLC profile of the reaction mixture of catechin (50 mM) with KSeCN and CAN (2 total molar equivalents each) after 2.5 h.

LC-MS analysis of the reaction mixture indicated pseudomolecular ion peak $[M+H]^+$ at *m/z* 396 for the product eluted at 29 min, suggestive of a selenocyanoderivative of catechin.

Unfortunately, all the attempts to isolate the reaction product failed, due to its high instability.

Interestingly, LC-MS analysis of the reaction mixture after evaporation of the solvent and re-dissolution in methanol indicated formation of two new products identified as a catechin selenide and di-selenide, which could be interesting as catechin derivatives thanks to their potential powerful antioxidant properties as well as other properties of biological interest. For example, diselenides are known to mimic the enzyme glutathione peroxidase for hydrogen peroxide scavenging.[275]

On this basis, further experiments were directed to the optimization of the reaction conditions to efficiently convert the selenocyanoderivative in the selenide and diselenide.

Firstly, a procedure reported in literature involving the use of $NaBH_4$ to obtain diselenides from selenocyanoderivatives was used.[276,277] Noteworthy, HPLC analysis of the reaction mixture of catechin with KSeCN/CAN treated for 2 h with the reducing agent showed a partial conversion of the selenocyanoderivative (t_R 29 min) to the diselenide (t_R 32 min) (Figure 4.21).

A conversion of the selenocyanoderivative into the selenide was instead observed (t_R 34 min) following air drying of the reaction mixture (Figure 4.22).

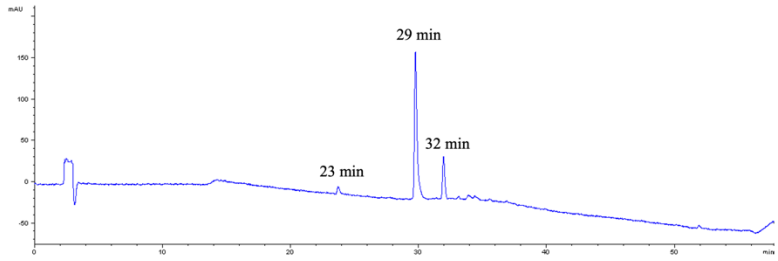

Figure 4.21 HPLC profile of the reaction mixture of catechin (50 mM) with KSeCN and CAN (2 total molar equivalents each) after 2 h of $NaBH_4$ treatment.

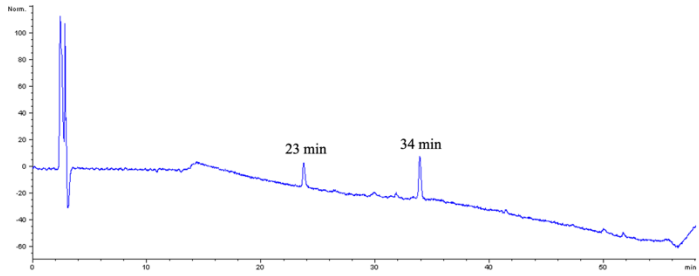

Figure 4.22. HPLC profile of the reaction mixture of catechin (50 mM) with KSeCN and CAN (2 total molar equivalents each) after 2 h of air-drying treatment.

Unfortunately, all the preliminary attempts to purify the selenide and the diselenide failed, likely due, as before, to their instability.

4.4.3 Conclusions

Based on the recent interest in phenolic compounds functionalized with heavy chalcogens in view of their strong antioxidant properties, a preliminary exploration of the possibility to access to selenoderivatives of a catechin, as a model of condensed tannins, was carried out. Protocols were developed to prepare the selenocyanoderivatives of catechin by reaction with KSeCN/CAN system and to convert it into a catechin diselenide or selenide. Although preliminary attempts of isolation of the selenoderivatives invariably failed, the results achieved maybe of interest as a starting point for the preparation of selenoderivatives of condensed tannins endowed with interesting antioxidant and biological properties to be exploited for example in the prevention of pathologies associated with oxidative stress conditions.

4.4.4 Experimental section

Materials and methods. Catechin, cerium(IV) ammonium nitrate (CAN) and sodium borohydride were purchased by Sigma-Aldrich. Potassium selenocyanate (KSeCN) was purchased by Acros Organics.

HPLC analysis were performed on an instrument equipped with an Agilent 1100 UV-Vis detector, using a Phenomenex Sphereclone ODS column (250 × 4.60 mm, 5 μm) at a flow rate of 1.0 mL/min and the detection wavelength was set at 254 nm. The gradient elution was as follows: 0.1% formic acid (solvent A)/methanol (solvent B), 5% B, 0-10 min; from 5 to 80% B, 10-47.5 min; from 80 to 5% B, 47.5-57.5 min.

LC-MS analysis were run on an Agilent LC-MS ESI-TOF 1260/6230DA instrument operating in positive and negative ionization mode in the following conditions: nebulizer pressure 35 psig; drying gas (nitrogen) 5 L/min, 325 ◦C; capillary voltage 3500 V; fragmentor voltage 175 V. A Eclipse Plus C18

column (150 × 4.6 mm, 5 μm) at a flow rate of 0.4 mL/min was used, using the same eluant as above.

Reaction between catechin and KSeCN/CAN. 10 mg of catechin dissolved in 690 μL of methanol (50 mM final concentration) were reacted with 10 of KSeCN and 38 mg of CAN (2 total molar eqs of each reagent) added in four aliquots at 30 min intervals. The mixture was kept under magnetic stirring at room temperature in a closed vial and analyzed periodically by HPLC and LC-MS. After 2.5 h it was centrifuged (7000 rpm, 4°C, 10 min) and subjected to different treatments:

- evaporation using a rotary evaporator;
- addition of 1 molar eq of $NaBH_4$ for 2 h under stirring at room temperature;
- air-drying.

The reaction mixtures were analyzed by HPLC and LC-MS analysis.

Chapter 5

Phenolic compounds as functional additives for the preparation of protein-based materials for various applications

5.1 Combination of tannins from pomegranate wastes and whey protein properties for food preservation strategies

5.1.1 Introduction

As widely mentioned in the previous chapters, agri-food wastes and by-products have received considerable attention as sustainable sources of value-added compounds, including phenolic compounds. Among these waste biomasses, a noteworthy example is the one derived from pomegranate juice processing. Indeed, for every ton of pomegranate juice, 4.2 tons of by-products (peels and seeds) are produced, which have a 10-fold higher phenolic content than the pulp, making this waste material one of the most intriguing industrial by-products.[278] In particular, besides anthocyanins and flavonoids, the main phenolic compounds present in the pomegranate peels and seeds (PPS) are punicalagin and punicalin (ellagitannins),[14,22,234,278] together with ellagic acid, compounds well-known for their health beneficial properties (Figure 5.1).[14,22,234,278–280]

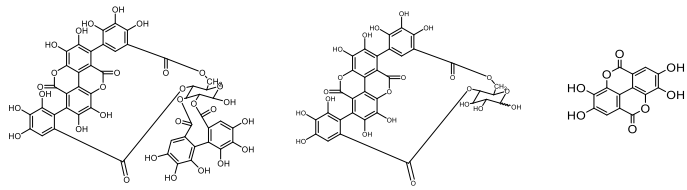

Figure 5.1. Main phenolic components of pomegranate by-products.

Thanks to the high phenol content,[281] and to the antioxidant[281] and antimicrobial[282,283] activities, PPS extracts have been exploited also as additives for cosmetic or, in particular, food applications.[284,285] In this specific framework, the use of natural and safe compounds for food packaging and food-preserving applications has been encouraged, including also proteins and carbohydrates-based biopolymers to be used as an alternative to the commonly employed synthetic polymers (*e.g.* polyethylene, polypropylene or polystyrene).[286,287] In particular, the combination between the functional properties of biopolymer-based materials and phenol-rich extracts has been considered a valuable alternative to develop new materials endowed with improved characteristics. For instance, in previous studies PPS extracts and chitosan were combined to form films which proved to have enhanced mechanical properties and resistance to microbial growth.[288]

On this basis, herein will be reported the:

- extraction and characterization of phenolic compounds from PPS;
- exploration of the combination between PPS extract and whey proteins isolate (WPI) to be used in food packaging applications.

5.1.2 Extraction and characterization of phenolic compounds from PPS

5.1.2.1 Extraction of phenolic compounds

First experiments were directed to the extraction of phenolic compounds from PPS. In particular, after lyophilization and grinding by using a kitchen blender, PPS (100 mg/mL) were taken under stirring for 1 h in three different solvents: water, ethanol or water/ethanol (4:6 v/v). The thus obtained PPS extracts were then recovered by centrifugation. Considering the high sugar content of the extracts which hindered their complete lyophilization, the extraction yields were calculated quantifying the dried solid residues (Table 5.1). The highest extraction yield was obtained using the hydroalcoholic solvent.

Table 5.1. Extraction yields from PPS using water, ethanol or water/ethanol (4:6 v/v). Mean values ± SD from at least three experiments are reported. Different letters denote significant differences ($p < 0.1$).

Solvent	Extraction yield (% w/w)
water	43 ± 5^{ab}
ethanol	36 ± 3^{b}
water/ethanol	52 ± 2^{a}

5.1.2.2 Assessment of total phenol content and antioxidant properties of PPS extracts

The antioxidant properties of PPS extracts were evaluated using two conventional chemical assays, *i.e.* the 2,2-diphenyl-1-picrylhydrazyl (DPPH) and the ferric reducing antioxidant power (FRAP) assays. In both cases, the hydroalcoholic and water PPS extracts proved to have better antioxidant properties with respect to the ethanolic one.

The total phenol content (TPC) was instead calculated by the Folin-Ciocalteu assay. In this case the hydroalcoholic extract showed the highest TPC, followed by the water and the alcoholic one.

The results are reported in Table 5.2.

Table 5.2. Results of DPPH, FRAP and Folin-Ciocalteu assays expressed as EC_{50} values, Trolox equivalents (eqs) (mg Trolox/mg sample) and gallic acid eqs (mg gallic acid/mg sample), in that order, for PPS extracts. Mean values ± SD from at least three experiments are reported. Different letters denote significant differences ($p < 0.05$ for DPPH and FRAP assay, $p < 0.1$ for TPC assay).

Solvent	EC_{50} (mg/mL)	mg Trolox/ mg sample	mg gallic acid/ mg sample
water	0.022 ± 0.001^{a}	0.35 ± 0.01^{a}	0.16 ± 0.01^{a}
ethanol	0.049 ± 0.001^{a}	0.26 ± 0.02^{a}	0.09 ± 0.02^{b}
water/ethanol	0.020 ± 0.001^{b}	0.33 ± 0.02^{b}	0.24 ± 0.04^{b}

5.1.2.3 Assessment of antimicrobial activity

Subsequently, the antimicrobial activity of PPS extracts was tested by researchers at University of Foggia at 5% w/v against typical food spoilage microorganisms, *e.g. Pseudomonas spp.* and yeasts. As shown in Figure 5.2,

the hydroalcoholic and ethanol extracts proved to be more effective against both species with respect to the aqueous one.

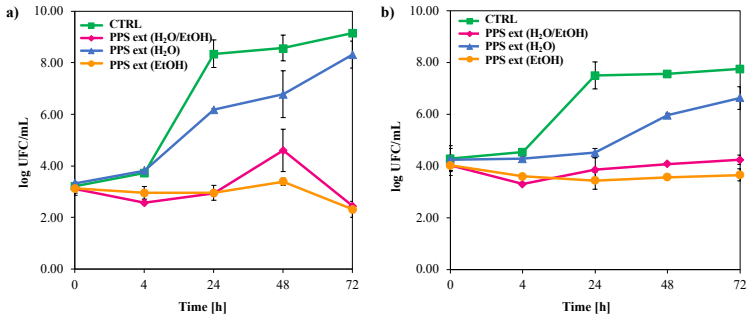

Figure 5.2. a) *Pseudomonas spp.* and b) yeasts evolution in the presence or absence (CTRL) of water, ethanol or water/ethanol (4:6 v/v) PPS extracts. Means values ± SD are reported.

5.1.3 Characterization of the hydroalcoholic PPS extract properties and evaluation of its properties

5.1.3.1 Characterization of the main phenolic compounds in hydroalcoholic PPS extract

Based on all the previous results, the hydroalcoholic PPS extract was selected for further characterization. The UV-Vis spectrum showed two absorption maxima at 260 and 375 nm, typical of ellagic acid and ellagitannins (Figure 5.3_a). Accordingly, HPLC analysis (Figure 5.3_b) showed three main products eluted at ca. 19, 21 and 36 min, identified as punicalagin isomers and ellagic acid by LC-MS analysis.

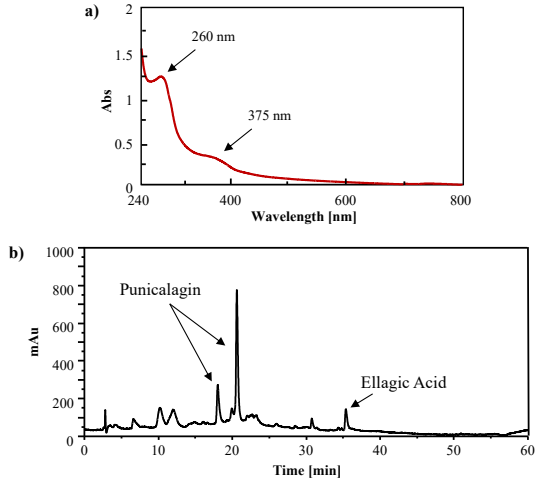

Figure 5.3. a) UV-Vis spectrum and b) HPLC profile of the hydroalcoholic PPS extract.

The ellagic acid and punicalagin isomer content was estimated to be 5% w/w, using ellagic acid as standard. Then, to evaluate the presence of non-chromatographable species contributing to the total weight of the extract, an acid degradation treatment of the sample was performed,[289] which indicated a hydrolysable tannin content expressed as ellagic acid equivalent of 16% w/w.

5.1.3.2 Assessment of the properties of the hydroalcoholic PPS extract for food applications

To assess the possible use of the PPS hydroalcoholic extract in the food sector, its antimicrobial activity was tested *in vitro* at different concentrations against *Alicyclobacillus acidoterrestris*, a common bacterium that typically causes juice spoiling. This activity was performed in collaboration with researchers of the University of Foggia.

As shown in Figure 5.4, the presence of the PPS extract at various concentrations (1, 1.5 and 2% w/v) completely inhibited *A. acidoterrestris* growth.

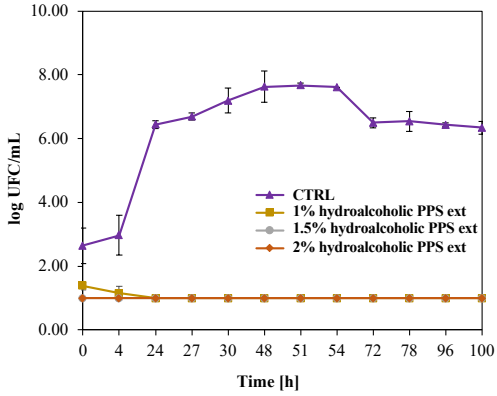

Figure 5.4. *A. acidoterrestris* growth in the presence or absence (CTRL) of the hydroalcoholic PPS extract at different concentration (1, 1.5 and 2% w/v). Means values ± SD are reported.

It's important to underline that previous studies already demonstrated the efficacy of PPS extracts against several bacteria. For instance, similarly to the present study, pomegranate peel extracts produced using different solvents proved to be very efficient against different pathogens, like *Staphylococcus aureus*, *Enterobacter aerogenes*, *Salmonella typhi* and *Klebsiella pneumoniae*.[290] Other studies have also demonstrated the efficiency of PPS extracts against microbes responsible for food spoilage.[291]

However, considering that the antimicrobial activity of PPS extracts has never been tested against *A. acidoterrestris*, the obtained results proved to be very interesting integrating also the scientific literature on the PPS extract properties.

On the basis of the promising *in vitro* test results, the hydroalcoholic PPS extract was subsequently tested in apple juice inoculated with *A. acidoterrestris*. In order to assess the efficacy of the extract under real working conditions, the microbiological and sensorial quality were monitored during a three-week storage period. Figure 5.5 shows the growth of the *A. acidoterrestris* over time in the analyzed samples. In particular, in the control sample (CTRL), prepared without the addition of the PPS extract, *A. acidoterrestris* grew over time, while in the sample containing only apple juice (blank), no bacteria growth was observed. On the other hand, the extract proved to be effective against *A. acidoterrestris* at all the tested concentrations leading to a complete microbial growth inhibition.

When the sensory quality of the apple juice during storage was tested, the blank sample showed an overall quality higher than 3 weeks, not having underwent any substantial variation in odor or color in this period of time. After inoculation the sample with *A. acidoterrestris* (CTRL), intolerable odor generation occurred after 12 days.[292] On the other hand, the addition of the PPS extract extended the life of the sample (17-20 days), demonstrating that the bacterial growth inhibition efficacy was reflected in a better sensory quality (Table 5.3).[292]

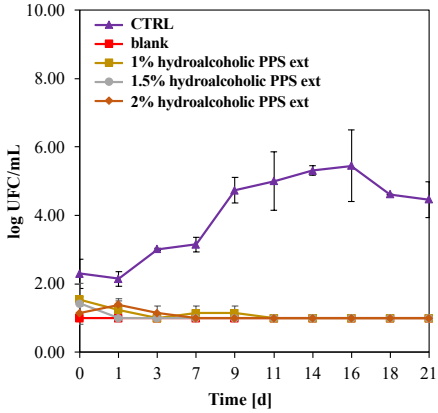

Figure 5.5. Evolution of *A. acidoterrestris* inoculated in apple juice in the absence (CTRL) or in the presence of the hydroalcoholic PPS extract at different concentrations (1, 1.5 and 2% w/v). Blank sample is apple juice not inoculated with *A. acidoterrestris.* Means values ± SD are reported.

Table 5.3. Results of sensory shelf life of apple juice (blank) and *A. acidoterrestris* inoculated apple juice in the absence (CTRL) or in the presence of the hydroalcoholic PPS extract at different concentration (1, 1.5, 2% w/v) calculated by the fitting procedure. Different letters denote statistically significant differences ($p < 0.05$).

Sample	**Overall quality fitting parameter (day)**
Blank	> 25
CTRL	11.26 ± 0.93^{c}
1 % w/v PPS hydroalcoholic extract	20.02 ± 1.21^{a}
1.5 % w/v PPS hydroalcoholic extract	17.77 ± 0.92^{b}
2 % w/v PPS hydroalcoholic extract	17.14 ± 0.64^{b}

Finally, in a last series of experiments the PPS hydroalcoholic extract was tested as inhibitor of the enzymatic browning process in apple smoothies. A colorimeter was used to periodically analyze the color change of the mixtures obtained by grinding the apples with a common kitchen blender in the absence (CTRL) or presence of PPS extract at 0.1% w/v. More specifically, a colorimeter is a tool that quantify colors according to international standards, whereas the color changing over time is indicating by the browning index (BI). This latter, in particular, depends on three different factors of the CIELAB space (L*a*b*), corresponding to one of the most popular color spaces. Indeed, BI is equal to:

$$BI = \frac{100(x-0.31)}{0.17}$$

$$x = \frac{a^{*}+1.75L^{*}}{5.645L^{*}+a^{*}-3.012b^{*}}$$

where L* indicates brightness and a* and b* are chromaticity coordinates. In particular +a* is the red direction, -a* is the green direction, +b* is the yellow direction, and -b * is the direction of blue.

The inhibition effect of the PPS extract was clear comparing the two samples after 30 min (Figure 5.6_a, 5.6_b). This result was also confirmed by the browning index (Figure 5.6_c) calculated with respect to the initial value (t_0). Indeed, after 30 min, the smoothy containing the extract reached a value of 27.5 ± 1.5%, with respect to the 45.5 ± 0.3% value showed by the CTRL.

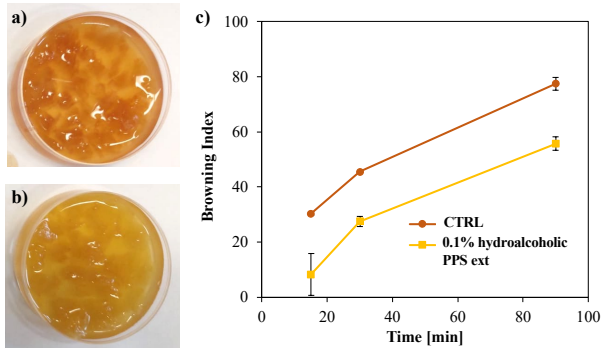

Figure 5.6. Apple smoothies a) in the presence or b) absence (CTRL) of 0.1% w/v hydroalcoholic PPS extract at 30 min. c) Browning index for apple smoothies in the absence (CTRL) or presence of 0.1 % w/v hydroalcoholic PPS extract calculated over time with respect to the initial value (t_0). Mean ± SD values of three different experiments are reported (three different measurements were taken during each experiment).

5.1.4 Evaluation of the combination of the hydroalcoholic PPS extract and WPI for food packaging applications

Based on the promising antioxidant properties, the efficient microbial growth inhibition power in apple juice and the ability to delay enzymatic browning in apple smoothies, the possible application of the hydroalcoholic PPS extract in food packaging was then investigated.

In particular, the combination with WPI, widely available as a dairy industry waste, was evaluated. Indeed, thanks to its β-lactoglobulin (3.03 g/L) and α-lactalbumin (1.02 g/L) content,[293,294] WPI is well-known for its ability to form highly performing biodegradable and biocompatible edible films to be used in food packaging applications,[295] without the needing of glycerol and/or other plasticizers.

Firstly, denaturation of WPI was carried out taking a WPI suspension in water at 10% w/w to pH 12 under stirring over 30 min. Subsequently, the

hydroalcoholic PPS extract was added to the denaturated WPI suspension at 5% w/w final concentration with respect to WPI to give PPS@WPI. It's important to specify that ethanol was preliminarily removed by using a rotary evaporator before the incorporation. Then, in order to evaluate if the extract maintains its antioxidant properties in the PPS@WPI final material, DPPH and FRAP assays were performed. However, no activity was observed in either assay. This result can be attributable to the alkaline pH conditions used for WPI denaturation causing a significant oxidation of the phenolic compounds.

On this basis, in further experiments the denaturated WPI suspension was acidified to pH 7 before the incorporation of the extract, leading to a PPS@WPI final material endowed with antioxidant properties as demonstrated by DPPH and FRAP assays. Indeed, the EC_{50} value of PPS@WPI was 5-fold lower than the one exhibited by WPI alone. This result was also confirmed by FRAP assay, in which no reducing activity was observed for WPI alone, differently from what observed for PPS@WPI (Table 5.4). Moreover, considering that the extract was added at 5% w/w with respect to WPI, the EC_{50} value and Trolox eqs for PPS@WPI should have been equal to 0.0165 and 0.4, respectively. These values are of the same order of magnitude of those experimentally determined, demonstrating that the phenolic components are able to confer their antioxidant power to the final material.

Table 5.4. Results of DPPH and FRAP assays expressed as EC_{50} values and Trolox eqs (mg Trolox/mg sample), respectively, for the denaturated WPI suspension and PPS@WPI samples. Mean values ± SD from three different experiments are reported.

Sample	EC_{50} (mg/mL)	mg of Trolox/ mg of sample
PPS@WPI	0.7 ± 0.1	0.0185 ± 0.0008
WPI	3.9 ± 0.6	≤ 0.0005

5.1.4.1 Assessment of PPS@WPI properties in food applications

PPS@WPI was then tested as an active coating material for food matrices, *i.e.* cheese and apple samples. In particular, apples were cut and dipped in the PPS@WPI solution or in the denaturated WPI solution for comparison, while, as control, an uncoated sample was tested (CTRL). The samples were air-dried for 24 h (Figure 5.7_a) after that an easily removable film on the apple surface was observed. As reported in Table 5.5, after the removal of the coating no significant differences were observed comparing the mass loss values of the treated samples, which however resulted lower with respect to what determined for the CTRL, indicating that the WPI barrier properties were not negatively affected by the extract.

Then, the enzymatic browning of the same samples was evaluated after removal of the coating and compared to the CTRL (Figure 5.7_b). Interestingly, a delay of the browning process was observed in the treated samples, showing a browning index equal to 41.6 ± 0.9% and 47 ± 3% in the case of coating with PPS@WPI or WPI alone, against a value of 60 ± 3% determined for the CTRL. This result confirmed the enzymatic browning inhibition power of the extract, contributing to the oxygen and water vapor barrier properties exhibited by the WPI coating.

Table 5.5. Mass loss (%) evaluation of the apple samples uncoated (CTRL) or coated with WPI or PPS@WPI solutions after the coating removal. Mean values ± SD from three different experiments are reported. Different letters denote statistically significant differences ($p < 0.05$)

Apple sample	Mass loss (%)
CTRL	75 ± 4^{a}
WPI	58 ± 3^{b}
PPS@WPI	64 ± 6^{b}

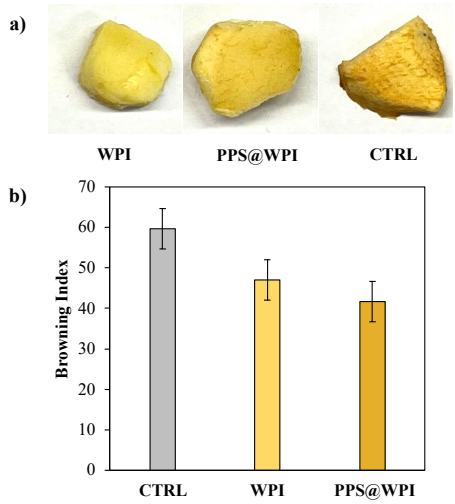

Figure 5.7. a) Pictures of apple cuts uncoated (CTRL) or coated with WPI or PPS@WPI, after 24 h drying; b) browning index for apple cuts uncoated (CTRL) or coated with WPI or PPS@WPI after 24 h drying and film removal. Mean ± SD values of three experiments are reported (three different measurements were taken during each experiment).

Further experiments were directed to the assessment of PPS@WPI coating to preserve Gouda cheese from accelerated lipid peroxidation. In particular, cheese samples were cut and dipped in the PPS@WPI or denaturated WPI solution and heated in an oven at 50°C. As a comparison the same procedure was repeated for an uncoated sample (CTRL). After 12 days, the film formed on the treated cheese samples was observed and removed, and all the samples were subjected to the thiobarbituric acid reactive substances (TBARS) assay following a procedure reported in literature.[296,297] The results are reported in Figure 5.8 as the lipid peroxidation inhibition (%) calculated with respect to the CTRL. Both PPS@WPI and WPI proved to be able to delay the process, with a higher efficiency observed for the PPS@WPI coating, confirming that the PPS extract was able to efficiently impart its antioxidant power to WPI.

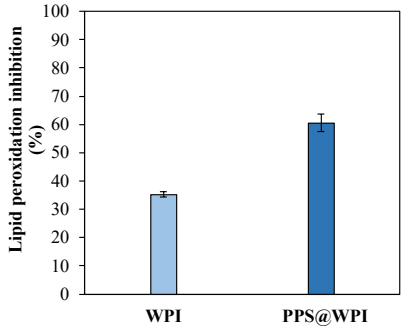

Figure 5.8. Inhibition of lipid peroxidation (%) in Gouda cheese samples coated with WPI or PPS@WPI. The results are expressed with respect to the CTRL. Mean ± SD values of three experiments are reported (three different measurements were taken during each experiment).

5.1.4.2 Conclusions

Thanks to its well-known antioxidant and antimicrobial power, an hydroalcoholic PPS extract rich in punicalagin isomers and ellagic acid was investigated as a functional additive for food packaging applications. In particular, the high antimicrobial efficiency that the extract exhibited against *A. acidoterrestris,* a common contamination bacterium of apple juice, represents a valuable contribution to the antimicrobial studies on pomegranate extracts already reported in the literature. Indeed, it proved to completely inhibit this bacterium growth inoculated in the apple juice even at low concentration (1% w/w), preserving its organoleptic properties.

Further experiments were then directed to the evaluation of the combination between the great properties showed by the hydroalcoholic PPS extract and the film forming ability of WPI to implement a material for edible food packaging application, not requiring the use of glycerol or other plasticizers. Interestingly, PPS@WPI exhibited an efficient gas barrier action due to WPI together with an efficient antioxidant power and enzymatic browning inhibition activity due to the presence of the hydroalcoholic PPS extract.

The results herein presented provide fresh insights into food preservation techniques while also demonstrating the excellent qualities of the hydroalcoholic PPS extract, which can be used to create value-added and sustainable WPI-based functional packaging.

5.1.5 Experimental section

Materials and methods. Pomegranates, apples (Red Delicious), cheese (Gouda) were purchased at a local supermarket. Whey proteins isolate (WPI) were obtained from a commercial source (MyProtein) and used without further purification. 2,2-diphenyl-1-picrylhydrazyl (DPPH), iron (III) chloride (97%), 2,4,6-tris(2-pyridyl)-s-triazine (TPTZ) (≥ 98 %), (±)-6-

hydroxy-2,5,7,8-tetramethylchromane-2-carboxylic acid (Trolox) (97 %), Folin-Ciocalteu reagent, gallic acid (≥ 97.5 %), ellagic acid (≥ 95 %), gallic acid, trichloroacetic acid, thiobarbituric acid and ammonium iron (II) sulphate ($(NH)_4Fe(SO_4)_26H_2O$, ≥ 98 %) were obtained from Sigma-Aldrich.

UV-Vis spectra were recorded using a Jasco V-730 spectrophotometer.

HPLC analyses were performed on an instrument equipped with an Agilent G1314A UV-Vis detector, using a Phenomenex Sphereclone C18 column (250 × 4.60 mm, 5 μm) at a flow rate of 1.0 mL/min; the gradient elution was as follows: 0.1% formic acid (solvent A)/methanol (solvent B), 5% B, 0-10 min; from 5 to 80% B, 10-47.5 min; the detection wavelength was set at 254 nm.

LC-MS analysis were run on an Agilent LC-MS ESI-TOF 1260/6230DA instrument operating in positive and negative ionization mode in the following conditions: nebulizer pressure 35 psig; drying gas (nitrogen) 5 L/min, 325 ◦C; capillary voltage 3500 V; fragmentor voltage 175 V. A Eclipse Plus C18 column (150 × 4.6 mm, 5 μm) at a flow rate of 0.4 mL/min was used, using the same eluant as above.

A Chroma Meter CR-400/410 (Konica Minolta) colorimeter was used to analyze changes in color.

Extraction of phenolic compounds from PPS. PPS were lyophilized and grinded with a kitchen blender. Then, 1 g of dry PPS was added to 10 mL of water, ethanol or water/ethanol (4:6 v/v) and taken under stirring for 1 h at room temperature. The mixture thus obtained was centrifuged (7000 rpm, 4°C, 10 min). The solid residues were lyophilized to calculate the extraction yields while the supernatants were stored at -25°C. The ethanol was always removed by using a rotary evaporator.

Denaturation of WPI. An aqueous WPI mixture (100 mg/mL) was taken to pH 12 by addition of 6 M NaOH. After 30 min under stirring at room temperature, the pH was adjusted to 7 by addition of 6 M HCl.

Preparation of PPS@WPI. The hydroalcoholic PPS extract was added at 5% w/w with respect to WPI to the denaturated WPI suspension prepared as above.

DPPH assay.[175] Various volumes of the PPS extracts were added to a 200 μM ethanolic solution of DPPH (10-62 μg/mL final dose). After 10 min under stirring at room temperature, the absorbance of each solution at 515 nm was measured. The same assay was performed on the denaturated WPI suspension (final dose 0.2-0.7 mg/mL) and on the PPS@WPI suspension (final dose 0.2-1.4 mg/mL). The antioxidant power was expressed as EC_{50}, corresponding to the sample concentration capable of reducing the initial absorbance of the DPPH solution by 50%. Experiments were run in triplicate.

FRAP assay.[177] FRAP solution was prepared mixing 36 mL of 0.3 M acetate buffer (pH 3.6), 3.6 mL of an aqueous 20 mM $FeCl_3$ solution (1.7 mM final concentration) and 3.6 mL of a 10 mM TPTZ solution prepared in 40 mM HCl (0.83 mM final concentration). Various volumes of the PPS extracts were added to the FRAP solution (2.7-12.5 μg/mL final dose) and, after 10 min under stirring at room temperature, the absorbance of each solution at 593 nm was measured. The same assay was performed on the denaturated WPI suspension (final dose 1.5-5 mg/mL) and on the PPS@WPI suspension (final dose 0.07-0.28 mg/mL). Trolox was used as a reference antioxidant and the results were expressed as Trolox eqs (mg Trolox/mg sample). Experiments were run in triplicate.

Folin-Ciocalteu assay.[217] Various volumes of the PPS extract solutions were added to a solution consisting of Folin-Ciocalteu reagent, 75 g/L Na_2CO_3, and water in a 1:3:14 v/v/v ratio (2.5-100 μg/mL final dose), and the final mixture was incubated at 40°C for 30 min. Then, the absorbance at 765 nm was measured. Gallic acid was used as reference compound and the results were

expressed as gallic acid eqs (mg gallic acid/mg sample). Experiments were run in triplicate.

Test of antimicrobial activity of PPS extracts. This activity was performed by researchers at Department of Foggia. *In vitro* tests were performed to evaluate the antimicrobial activity of the PPS extracts against common food spoilage bacteria (*i.e. P. putida* and *P. fluorescens* isolated from spoiled mozzarella) and fungi (*i.e. yeasts* isolated from red pomace). The efficacy of each extract was tested at 5% w/v evaluating the microbial and fungal growth at different incubation time up to 72 h. Hydroalcoholic PPS extract (1-5% w/v) was tested also against *A. acidoterrestris* as typical juice spoilage bacterium at 44°C for 48 h. The hydroalcoholic PPS extract efficacy against *A. acidoterrestris* was determined in apple juice, too, at 1, 1.5, 2% w/v. Blank (only juice) and control juice (CTRL) inoculated with the bacterium in the absence of PPS extract were also prepared. All the samples were stored at 37°C for two weeks and periodically analyzed.

Sensory evaluation. During the storage period, the apple juice samples tested for the antimicrobial activity were also subjected to sensory evaluation (color, odor, overall quality) by seven trained panelists, researchers at the Food Department of Foggia University (female, age between 28 and 48 years).

Acid degradation of hydroalcoholic PPS extract. 5 mL of 4 M HCl were added to 50 mg of hydroalcoholic PPS extract previously lyophilized in a Pyrex tube and incubated in an oven at 90°C, after 1 min vortexing.[289] Then, after 24 h, the mixture was cooled at room temperature and pH 2.5 was reached adding 6 M NaOH. After centrifugation (7000 rpm, 4°C, 10 min), the supernatant was recovered and taken to 10 mL by addition of water. The thus obtained mixture was filtered on a 0.45 μm PVDF filter and analyzed by HPLC. The solid residue obtained from centrifugation was analyzed by HPLC after being dissolved in 10 mL of DMSO/methanol 1:1 v/v.

Apple smoothie browning inhibition assay. 5 g of peeled apple (Red Delicious variety) were finely blended using a kitchen mixer in the absence (CTRL) or in the presence of 0.1% w/v hydroalcoholic PPS extract water solution. The final mixture was then transferred on a watch glass. The color variations over time were periodically analyzed to measure the browning index by using a colorimeter.[298] Three different experiments were performed and for each one three different measurements were taken.

Apple cut browning inhibition assay. 500 mg of peeled apple cuts (Red Delicious variety) were dipped in the PPS@WPI or denatured WPI solutions prepared as previously described, and air-dried. After 24 h the film formed on the surfaces was removed, and the color variation was evaluated using a colorimeter.[298] The same experiment was performed on an uncoated peeled apple cut as reference (CTRL). Three different experiments were performed and for each one three different measurements were taken.

Determination of apple cuts mass loss. 500 mg of peeled apple cuts (Red Delicious variety) were dipped in the PPS@WPI or denatured WPI solutions prepared as previously described, and air-dried. After 24 h the film formed on the surfaces was removed, and the mass loss was determined by weighing the samples. The same experiment was performed on an uncoated peeled apple cut as reference (CTRL). Experiments were run in triplicate.

Lipid peroxidation assay on cheese. Following a procedure reported in literature,[296,297,299] gouda cheese samples (surface area of about 4 cm^2) were dipped in the PPS@WPI or denatured WPI solutions. After 12 days in an oven at 50°C, the film formed on the surfaces was removed, and the sample was minced in 60 mL of chloroform/methanol mixture (2:1) using a kitchen blender. The mixture was filtered under vacuum using Whatman No. 1 filter paper and the filtrated was dried with the aid of a rotary evaporator. 200 mg of the obtained residue were homogenized in 25 mL of butanolic

trichloroacetic acid at 7.5% w/w, and 5 mL of the resulting mixture were added to 5 mL of a 0.02 M thiobarbituric acid solution in butanol. After 2 h at 95°C, the mixture was cooled at room temperature and the absorbance at 539 nm was measured. The same experiment was performed on an uncoated cheese piece as reference (CTRL). Experiments were run in triplicate.

5.2 Combination of plant derived phenolic compounds and soy proteins properties for biomedical applications

5.2.1 Introduction

In the last years phenolic compounds have found application also in field of bioadhesives for soft tissue healing, thanks to their biocompatibility and antibacterial activity, critical requisites for wound healing applications. Nowadays, the design of efficient adhesives endowed with great mechanical characteristics under physiologically relevant conditions as well as underwater resistance is still difficult. In this framework, a very inspiring example is the adhesion mechanism of some marine organisms,[300] such as mussels. The exceptional wet adhesion capabilities of mussel byssus foot proteins are due to the formation of excellent underwater-resistant cross-linked networks by the strong interaction between the 3,4-dihydoxyphenylalanine (DOPA) catechol systems and the lysine amino groups. So, on this basis, numerous studies have been directed to the development of synthetic mussel-inspired materials endowed with cohesion properties and water-resistant adhesion. In particular, to achieve this goal, biopolymers and natural macromolecules systems were modified with DOPA or its analogue dopamine combining the catechol and amino functionality.[301–303] An example is represented by hydrogels obtained by the cross-linking between Al^{3+}-coordinated alginate-dopamine chains with acrylamide-acrylic acid polymers, which showed high mechanical characteristics and strong fibroblast cell adhesion.[304] Solid adhesiveness to various type of layers and great hemostatic properties were exhibited also by a material obtained from dopamine conjugated to poly(-glutamic acid).

Despite the very interesting advantage related to the dopamine-use in the mussel-inspired strategy, a main drawback is its potential neurological effects.

On this basis, the use of alternative phenolic compounds has been recently evaluated. Some examples can be represented by a low-cost water-resistant plant-inspired bioadhesive obtained by the oxidative coupling between tannic acid and animal gelatine nucleophilic residues,[305] or by a lignin-based glue obtained by the radical polymerization of acrylic acid followed by the formation of a pectin-polyacrylic acid hydrogel network.[306,307]

An interesting low-cost and environmentally friendly alternative to polysaccharides and synthetic polymers to be exploited in biomedical devices are proteins,[308] deriving from agri-food wastes and by-products such as soy proteins isolate (SPI),[309,310] characterized by a high amino groups content. However, the main drawbacks of SPI are its very poor water resistance and mechanical properties, which however can be overcome by cross-linking modifications using either synthetic or natural compounds capable of covalently link to the protein scaffold.[311–316] In this framework, the use of phenolic compounds *e.g.* tannic acid,[317] tannins,[318] lignins,[319] or other phenolic polymers,[317] which can give rise to high performance materials have been investigated.

On this basis, the following 5.2 paragraphs will report the preparation of hydrogels starting from SPI combined with plant derived phenolic compounds to implement new, green and sustainable interesting materials to be used for tissue healing.

5.2.2 Preparation of hydrogels by combination of soy proteins and phenolic compounds

A first series of experiments was directed to the optimization of the SPI/phenol hydrogels preparation procedure. A fundamental step for the preparation of efficient adhesive material is SPI denaturation, to allow its interaction with phenols or their oxidation products through the exposed aminoacidic residues,

i.e. lysine amino groups. Indeed, previous studies have demonstrated that the use of denaturing agent at alkaline pH (*e.g.* urea or guanidine) led to final materials endowed with increasing mechanical characteristics.[320] In the current investigation, the use of harsh alkaline conditions to denature SPI was avoided, in order to prevent the decomposition of the phenolic compounds and their oxidation products and to prepare materials compatible with tissue healing application, therefore thermal denaturation conditions were investigated.

Caffeic acid (CA), chlorogenic acid (CGA), and gallic acid (GA) were chosen as available and broadly distributed in plant sources phenolic compounds.

Thermal denaturation was performed preparing a mixture of SPI in water at 10% w/w, and stirring it for 1 h at 85°C. Then, the phenol component was added at various concentrations (10-30 mM) to the denaturated SPI mixture, and the mixture was stirred for 2 h at 50°C and pH 9, reached by addition of 0.1 M NaOH. The best result in terms of phenolic compound consumption was obtained using 28 mM as phenol final concentration. Indeed, after centrifugation, the formation of a hydrogel was observed, characterized by a higher consistency than the one obtained using only the denaturated SPI, result likely attributable to the conjugation of the nucleophilic amino acid residues of SPI with the phenolic compound oxidation products generated at the slight alkaline pH conditions adopted. The almost total consumption of the starting phenolic compounds obtained was confirmed by spectrophotometric analysis of the supernatants recovered after centrifugation.

In the specific case of CGA, a green chromophore was observed in the hydrogel, which invariably proved the occurrence of SPI-phenol covalent interactions. Indeed, previous works demonstrated the formation of a green benzacridine pigment from the oxidative coupling of caffeic acid esters, such as CGA, and amines and/or amino groups of proteins (Figure 5.9).[321]

In the CA and GA cases, the obtained hydrogels were yellowish-brown in color.

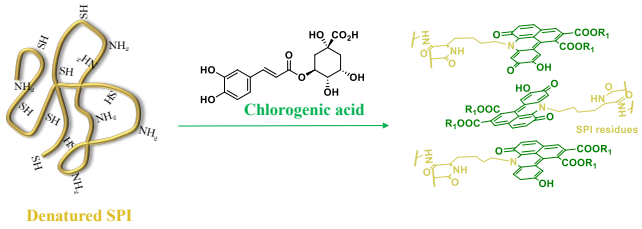

Figure 5.9. Proposed interaction mode between denatured SPI and CGA.

5.2.3 Evaluation of the adhesive properties and underwater resistance of SPI/phenol hydrogel

Subsequently, adhesive properties and underwater resistance of the prepared SPI/phenol hydrogels were evaluated with respect to only denaturated SPI (CTRL) sample. In particular, the materials were applied between two wood specimens, which were subsequently dipped in water after being clamped together for 24 h. The samples thus obtained were periodically checked until the separation of the two wood specimens. As shown in Table 5.6, all the phenol-containing hydrogels, and in particular the SPI/CGA one, proved to be more resistant (22 days) than the CTRL (24 h).

In the perspective of using these materials in tissue healing, the underwater resistance of the hydrogels was also tested by using defatted and washed chicken skin. However, the discouraging results (underwater resistance < 30 min) led to the assessment of different experimental conditions, aiming at the possible use of these materials as surgical glues. On this basis, SPI/phenols hydrogels were firstly subjected to a 6 h curing treatment (in air), and then applied between two slices of chicken breast muscle, which were subsequently immersed into 1× saline phosphate buffer solution (PBS) after

being clamped together over night. As shown in Table 5.6, SPI/GA showed the best resistance results, followed by SPI/CGA.

Table 5.6. Underwater resistance (days) of wood specimens and chicken breast muscle slices glued with SPI or SPI/phenol hydrogels. Mean values from three different experiments are shown (SD = ± 1).

Sample	SPI	SPI/CA	SPI/CGA	SPI/GA
Wood specimens	1	9	22	5
Chicken breast muscle slices	1	2	7	15

5.2.4 Evaluation of the SPI/phenols hydrogel structural and morphological properties

To obtain more information about the interaction established between SPI and the phenolic compounds in the hydrogels, the -SH and -NH_2 groups content of SPI after reaction with the phenols was quantified. In particular, the Ellman's reagent and the *o*-phtalaldehyde reaction were used,[322] followed by spectrophotometric measurement. The contribution of the sample absorption at the detection wavelength was appropriately considered.

Using a calibration curve with glutathione as thiol group reference or with alpha *N*-BOC lysine as amino group reference, the -SH and -NH_2 groups content into the denaturated SPI resulted equal to 1.8% and 3% w/w. Data reported in Figure 5.10, expressed with respect to the denaturated SPI (CTRL), indicated an efficient interaction between both amino and sulphydryl groups of SPI and phenols, showing a very low content of unreacted -SH

groups in all the hydrogels samples, while the reacted amino groups value was higher in SPI/GA than in SPI/CA and SPI/CGA.

These results are supported by previous MALDI-MS analysis which reported the covalent binding formation between tannins and SPI amino groups.[323]

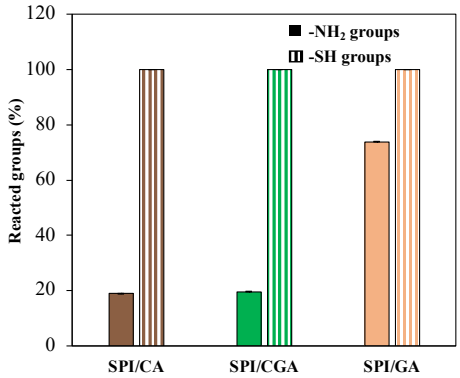

Figure 5.10. Reacted protein -NH_2 and -SH groups (%) in SPI/phenol hydrogels calculated with respect to denatured SPI. Mean ± SD values of three experiments are reported.

The SPI/phenol hydrogels were also analyzed by electron paramagnetic resonance (EPR), a common technique used to identify radicals obtained by the quinone/catechol disproportionation. During a preliminary investigation of denatured SPI (Figure 5.11, black line), in agreement with data reported in literature,[324,325] an asymmetrical free-radical signal was found, ascribable to carbon-centered radicals generated and trapped in the dry protein after exposition to the oxygen. For comparison, the oxidized phenolic compounds procured under the same conditions, *i.e.* in air, at pH 9 and 50°C, were also analyzed (Figure 5.11, dotted lines).

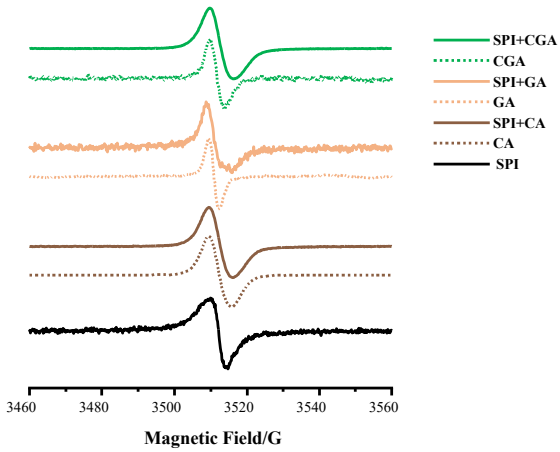

Figure 5.11. EPR spectra of denatured SPI (black line), SPI/phenol hydrogels (green, pink, brown lines), and oxidized phenols (dotted lines).

CA and SPI/CA showed a symmetric and wide signal characterized by a higher spin density than SPI (Table 5.7). Comparing the CA and SPI/CA spin density, the decreasing of 2 order of magnitude of the latter indicated a content of approximately 1% of CA-derived components in the final material. Moreover, the radical centers were found to be polydisperse as indicated by the predominate Gaussian line form denoting no effect caused by the protein presence.

On the contrary, the radical dispersity was relatively small in the case of GA, which was characterized by a Lorentzian lineshape and a narrow symmetric line. Moreover, it's a low spin density was observed, resulting in the same order of magnitude of SPI/GA and SPI. The higher signal broadness can be explained by the superposition of the signals of protein and GA, as demonstrated by the asymmetric line seen in the SPI/GA.

The SPI/CGA and the CGA signals were nearly symmetrical. Notably, the CGA spin density remains the same in the SPI/CGA hydrogel. A significant increase in broadness passing from CGA to SPI/CGA was observed (DB

changed from 3.9 to 5.4 G). However, this result cannot be attributable only to the superposition of the signals of the protein and of CGA, suggesting the formation of species with a strong radical character when CGA oxidation products interact with protein.

In general, the change in the EPR spectroscopic parameters of the phenolic compounds with respect to the SPI/phenol materials indicated the occurrence of different interactions between SPI and the phenol oxidation products.

Table 5.7. EPR spectral parameters of SPI, SPI/phenol hydrogels, and oxidized phenols.

Sample	Spin density/g^{-1}	DB/G (± 0.2)	Gaussian contribution	g-factor (± 0.0003)
SPI/CGA	2.1×10^{17}	5.4	0.74	2.0040
CGA	2.7×10^{17}	3.9	0.72	2.0040
SPI/GA	9.8×10^{15}	6.7	0.35	2.0046
GA	1.9×10^{15}	3.0	0.49	2.0045
SPI/CA	3.1×10^{16}	6.2	0.72	2.0039
CA	1.0×10^{18}	6.1	0.64	2.0049
SPI	3.4×10^{15}	5.5	-	2.0027

Finally, scanning electron microscopy (SEM) analysis was performed on air-dried hydrogel samples. Firstly, the presence of poor connection between protein and phenols in the SPI hydrogel material was indicated by the presence of a loose structure and microporosity (20-150 micron) typical of SPI (Figure 5.12_a). This was the case of SPI/CGA and SPI/GA samples (Figure 5.12_b, 5.12_c). On the contrary, the SPI/CA hydrogel showed a unique microstructure (Figure 5.12_d), exhibiting a denser morphology with fewer macropores on the surface. This would indicate that CA is able to interact with SPI leading to the formation of a more homogeneous and compact structure.

This characteristic is also in agreement with its great adhesive behavior described in the Paragraph 5.2.3.

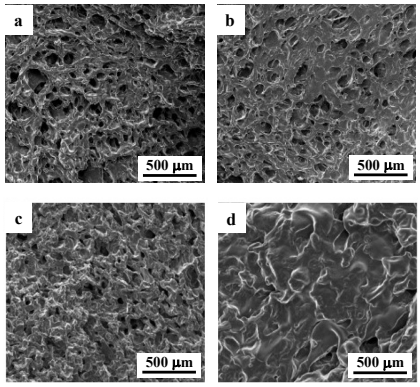

Figure 5.12. SEM images of (a) SPI, (b) SPI/CGA, (c) SPI/GA and (d) SPI/CA.

5.2.5 Preparation of SPI/agarose/phenol hydrogels and evaluation of their physical and adhesion properties

The prepared SPI/phenol hydrogels proved to be very interesting to be used in wound healing application. On this basis, the formation of more flexible, stretchable and robust materials by addition of additives or using different preparation conditions was investigated in collaboration with the researchers of the Institute for Polymers, Composites and Biomaterials.

In this framework, an improved procedure was applied, involving addition of agarose as a component of the SPI/phenol hydrogels. An SPI/agarose gel was prepared by addition of the thermally denatured SPI to an aqueous agarose solution at 70°C. The obtained material was first cooled down and then immersed in a previously prepared aqueous solution of the phenolic compounds (10 mM) at pH 9, for 2 h. The ability of the phenols to interact with proteins penetrating into the SPI/agarose gel was demonstrated by the

formation of a material green in color (benzacridine system) in the case of CGA.

Subsequently, the physical properties of the obtained SPI/agarose/phenol materials were evaluated. However, the hydrogel used as such or after drying proved to be very weak and difficult to handle. On this basis, they were first air-dried and then rehydrated, in order to obtain more tough and stretchable materials.

As shown in Figure 5.13 for the SPI/agarose/CGA hydrogel as a representative example, the material resulted semi-transparent and was able to maintain the same shape of the container. Moreover, when subjected to compression, the hydrogel was able to restore its initial shape. Finally, the same hydrogel was tested after treatments at various temperature (-5°C, 25°C, 37°C, 50°C) for 1 h, keeping its properties unchanged. Thanks to its remarkable stretchability and compressive performance, it was also possible to apply the dried hydrogel on a human joint bending it, without causing any discomfort to those who volunteered for these studies. Interestingly, any skin irritation was observed, and its removal didn't leave any residue, maintaining its good adhesion properties even after 25 repeated peeling/adhering cycles. The material proved to be able to adhere to different types of hydrophilic and hydrophobic surfaces, such as glass, steel, polypropylene, and polycarbonate, besides human skin, showing very good adhesiveness even underwater (Figure 5.14).

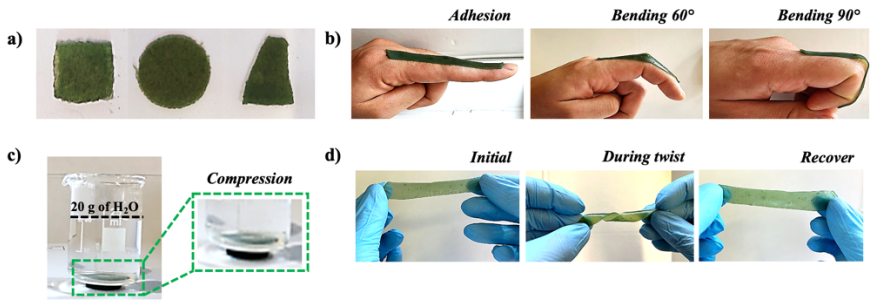

Figure 5.13. Macroscopic demonstration of the physical properties of the SPI/agarose/CGA hydrogel: a) plasticity and shapeability of the hydrogel; b) adhesion to a human finger at various bending angle; c) compression with 20 g of water; d) bending and crossover stretching.

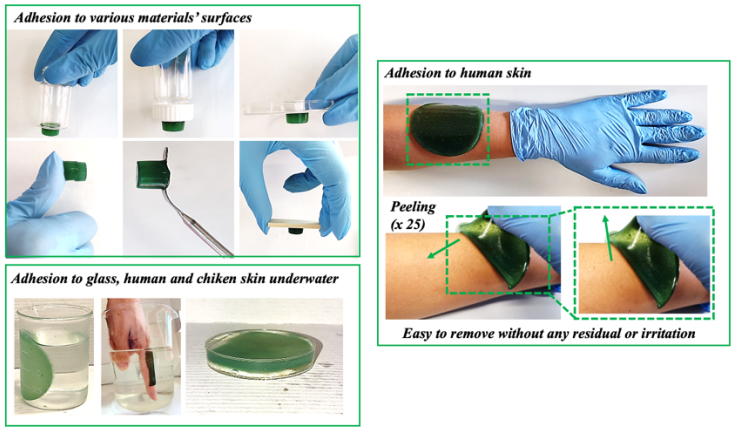

Figure 5.14. Adhesion of the SPI/agarose/CGA hydrogel to various materials, even underwater.

Finally, the water vapor permeability (WVP) of the air-dried SPI/agarose/phenol hydrogels was investigated, in the prospective of using these materials as wound dressing devices (Table 5.8). As expected, the addition of the phenols into the polymer hydrogel changed its properties leading to a WVP increase (1 order of magnitude), result likely attributable to

the formation of phenol aggregates which cause a discontinuous structure in the hydrogels.

Table 5.8. Water vapor permeability (WPV) measurement results for the SPI/agarose and SPI/agarose/phenols hydrogels.

Sample	WVP (g/m·Pa·s)
SPI/agarose	$5.13 \pm 0.27 \times 10^{-12}$
SPI/agarose/CA	$4.64 \pm 0.22 \times 10^{-11}$
SPI/agarose/GA	$3.88 \pm 0.18 \times 10^{-11}$
SPI/agarose/CGA	$4.99 \pm 0.22 \times 10^{-11}$

Finally, the tensile properties were evaluated. In particular, the SPI/agarose system was characterized by a low strain at break value. On the other hand, the SPI/agarose/phenol hydrogels showed a higher degree of deformability due to the ability of phenols to act as "plasticizers" for SPI.

5.2.6 Evaluation of cytocompatibility and wound healing properties of SPI/agarose/phenol hydrogels

Before evaluating the healing properties of the SPI/agarose/phenol hydrogels, their cytotoxic effects against human keratinocytes (HaCaT cells) and human dermal fibroblasts (HDF cells) were evaluated by researchers at University of Piemonte Orientale. Low and not statistically significant cytotoxicity was demonstrated by the Trypan blue exclusion test (Figure 5.15). Indeed, the quantity of dead blue cells after the treatment with SPI/agarose/phenol hydrogels, was found to be comparable to that of the cell control samples.

Then, further experiments were directed to the investigation of the SPI/agarose/phenols hydrogel ability to induce wound re-epithelialization by HaCaT cell line in an *in vitro* wound healing test. In particular, a HaCaT cell

monolayer was wounded by using a pipette tip, and then incubated with various SPI/agarose or SPI/agarose/phenol hydrogel component mixture. The same experiment was also performed without the use of the SPI/phenol systems as a control (CTRL).

Better result in terms of wound healing activity was observed in the case of SPI/agarose/CGA hydrogel, which proved to be capable of significantly reduce the wounded area compared to CTRL and SPI/agarose hydrogel (Figure 5.16).

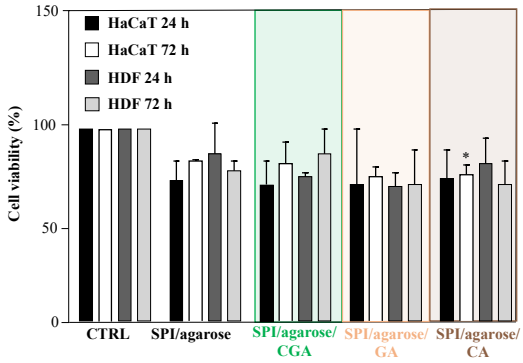

Figure 5.15. Cytotoxic effects of SPI/agarose/phenol hydrogels in HaCaT cells and HDF cells after 24 h and 72 h of incubation. Cell viability (%) was assessed by MTT assay and expressed as the percentage of viable cells with respect to untreated cells (CTRL). Mean ± SD values of three experiments are reported (each experiment was carried out with triplicate determinations).

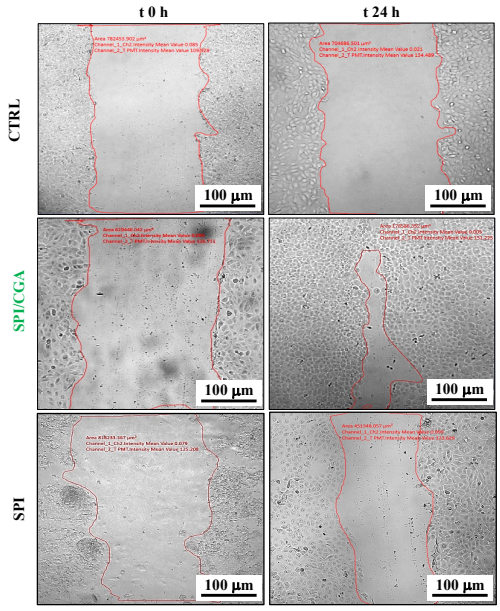

Figure 5.16. Wound healing activity of SPI/agarose and SPI/agarose/CGA hydrogels in HaCaT cells monolayer at t_0 and after 24 h of incubation with respect to CTRL. Cells were wounded prior to treatment.

5.2.7 Evaluation of hemocompatibility of SPI/agarose/phenol hydrogels

Hemocompatibility experiments were also performed by using tromboelastogram (TEG) analysis to assess how the SPI/agarose/phenol hydrogels in contact with blood can influence its behavior. The same experiment was also performed without the use of the hydrogel as control (CTRL). This activity was performed by researchers at Ospedale Maggiore della Carità's transfusional center, in Novara.

In particular, TEG analysis measures:

- the reaction time (R), corresponding to the time between the beginning of the test of the coagulation process; it is physiologically included between 3.8 and 9.8 min;

- the coagulation time (K), corresponding to the length of the coagulation process; it is physiologically included between 0.7 and 3.4 min;
- the alpha angle time, corresponding to the coagulation velocity; it is physiologically included between 47.8° and 77.7°;
- the maximum amplitude (MA), corresponding to the clot strength; it is physiologically included between 49.7 and 72.7 mm.

The results obtained for the hydrogels fell all in the ranges listed above, demonstrating that the physiological healthy blood behavior didn't change when in contact with the samples (Figure 5.17). The obtained results were also confirmed by the blood clot formation assay which evaluates the natural blood behavior. Indeed, no significant differences were observed comparing the CTRL and hydrogel data, indicating that the blood natural behavior was not affected by the interaction with the hydrogels.

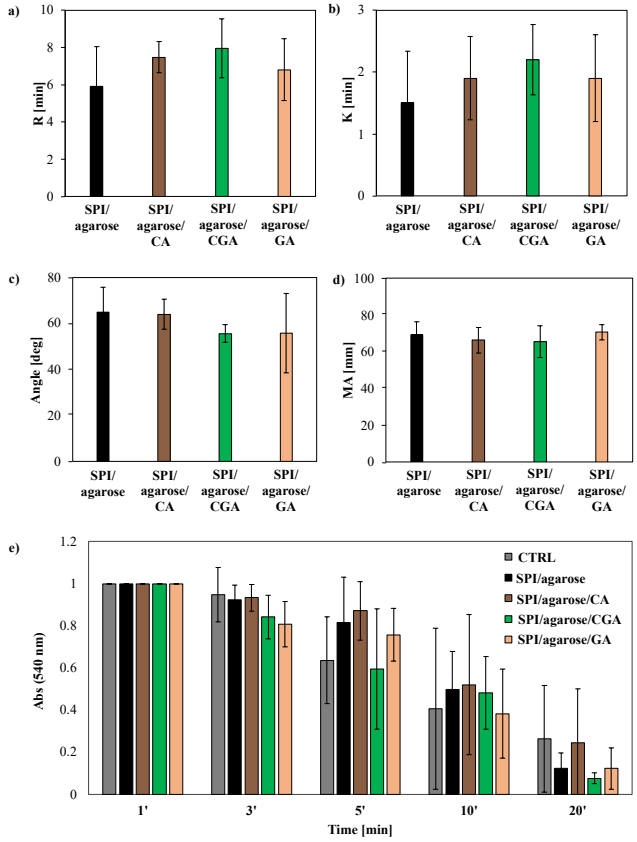

Figure 5.17. TEG analysis coagulation parameters: a) reaction time (R); b) coagulation time (K); c) coagulation velocity (alpha angle); d) clot strength (MA); e) clotting time of CTRL, SPI/agarose and SPI/agarose/phenol hydrogels.

5.2.8 Evaluation of SPI/agarose/phenol hydrogels antibacterial activity

Subsequently, the antibacterial activity of the air-dried SPI/agarose/phenol hydrogels against various common pathogenic bacteria (*e.g. Staphylococcus*, *Acinetobacter*, and *Pseudomonas* species) was evaluated through the appearance of the inhibition halo on inoculated plates. This activity was performed by researchers at University of Piemonte Orientale. All the tested

hydrogels proved to be effective against Gram(+) *Staphylococcus* species such as *S. aureus* ATCC 12600 and *S. epidermidis* ATCC 35984, or clinically isolated *MRSA* WKZ-2 strain, causing their death (Figure 5.18), whereas the SPI/agarose/CA hydrogel was also able to induce the death also of the Gram(–) *A. baumannii* ATCC 9606 strain.

Then, the percentage of bacterial growth in liquid media was assessed. Noteworthy, all the hydrogels resulted effective against *P. aeruginosa* cells, with a ca. 50% of growth inhibition in the case of SPI/agarose/GA and SPI/agarose/CGA hydrogels, whereas all the hydrogels proved to be very effective against all the other strains, completely inhibiting their growth.

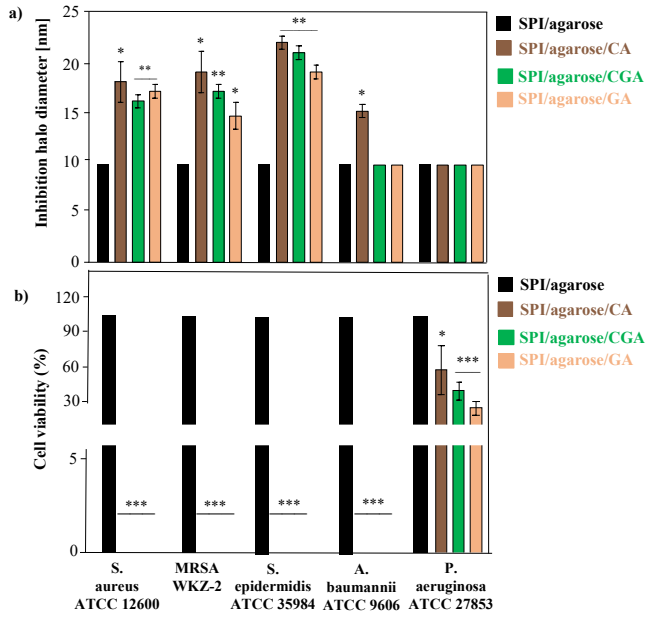

Figure 5.18. Antimicrobial activity of SPI/agarose-based hydrogels: a) inhibition halo diameter evaluated by agar diffusion assay; b) ability of samples to inhibit bacterial growth in liquid medium expressed as cell viability (%). Each graph refers to at least a biological duplicate and statistical analyses were performed by using Student's *t*-test. Significant differences were indicated as *P < 0.05, **P < 0.01 or ***P < 0.001.

5.2.9 Proposed interaction mode between SPI and the phenolic compounds

Lastly, based on all the obtained results and combining the chemical, spectroscopic and microscopic approaches, the interaction mode between denatured SPI and the investigated phenols was hypothesizes. The SPI thiol groups were completely involved in the covalent interactions with the electrophilic units obtained by phenol oxidation, generating a strong SPI-phenol crosslink. On the contrary, the amino groups were involved in different extent depending on the phenol (a higher number of bonds was observed with GA).

Considering GA, previous studies have demonstrated that the condensation reaction of the GA quinone with the amino compounds is favored with respect to Michael type addition.[326]

Considering CA, in agreement with the data reported in literature using comparable oxidation conditions,[327] it reacts with amino groups by addition on the quinone units, leading of its oxidation products. This reaction justified the very dense hydrogel's shape as well as the great performance of SPI/CA glues.

Finally, the SPI/CGA hydrogels exceptional underwater resistance could be attributable to the hydrophobic nature of the benzacridine units obtained from the interaction between the amino groups and the oxidized dimeric CGA. Moreover, the compact structure of the hydrogel could be attributable to the dynamic pi-stacking interactions between these units, as well as to redox interactions, as indicated by EPR analysis. Indeed, it highlighted the presence of a range of species at various redox states that can produce stable carbon-centred radicals.

5.2.10 Conclusions

In these paragraphs, hydrogels were prepared starting from natural easily accessible components, including SPI and plant-derived phenolic acids (CA, GA and CGA). Interestingly, all the prepared hydrogels showed extraordinary adhesiveness and remarkable underwater resistance.

Additionally, the incorporation of agarose in the hydrogels provided materials endowed with good mechanical properties and long-lasting adhesiveness, besides biocompatibility, hemocompatibility, antibacterial activity and, in some cases, also wound healing activity.

5.2.11 Experimental section

Materials and methods. Soy proteins isolate (SPI) (99%) was purchased from a commercial source (MyProtein) and used without further purification. Caffeic acid (CA), chlorogenic acid (CGA), gallic acid (GA), agarose (analytical nucleic acid electrophoresis grade), urea, vinyl alcohol, 5,5′-dithio-bis(2-nitrobenzoic acid) (DTNB), tris(hydroxymethyl)aminomethane (Tris), glycine, ethylenediaminetetraacetic acid (EDTA), *o*-phthalaldehyde, glutathione, *N*-BOC lysine, sodium dodecyl sulphate (SDS), and b-mercaptoethanol were acquired from Sigma-Aldrich. All experiments were conducted using deionized water. A carpentry shop provided the pine wood specimens. Fresh chicken tissues (skin and muscle) were acquired from a local butcher and kept at 4°C until usage, which was usually within 1-2 days.

Uv-Vis spectra were recorded using a Jasco V-730 spectrophotometer.

EPR measurements were performed using a X-band spectrometer (Bruker, Rheinstetten, Germany). Flame-sealed glass capillaries containing the samples were coaxially inserted in a standard 4 mm quartz sample tube. Spectra were acquired at room temperature. The instrumental settings were as follows: sweep width: 100 G; time constant: 10.24 ms; conversion time: 20.48

ms; modulation frequency: 100.00 kHz; modulation amplitude: 1.0 G; receiver gain: 60 dB. Power saturation experiments were preliminarily performed, with the microwave power gradually increasing from 0.001 to 128 mW. Single spectra were then acquired at a microwave power optimized for each sample to avoid microwave saturation of resonance absorption curve. Several scans, typically 128, were accumulated to improve the signal-to-noise ratio. The g value and the spin density were evaluated by means of an internal standard, Mn^{2+}-doped MgO. The broadness of each spectrum was evaluated as distance, in G, between the maximum and the minimum of the observed signal (ΔB).

Preparation of the SPI/phenol hydrogels. 1 g of SPI was added to 10 mL of water and taken under stirring at 85°C. After 1 h, the phenol (GA, CA or CGA) was added at 28 mM final concentration. The resulting mixture was brought to pH 9 with 0.1 M NaOH and stirred in air at 50°C. After 2 h, the solid material was collected by centrifugation (7000 rpm, 4°C, 10 minutes) and, when required, lyophilized.

Preparation of the SPI/agarose/phenol hydrogels. The denatured SPI suspension (10% w/w) was added to solution of agarose at 2% w/w in water (pre-dissolved at 70°C) at 2:1 v/v ratio and heated at 70°C for 15 min. The resulting mixture was then poured into a Petri dish and left to cool at room temperature for 1 h. The hydrogel thus obtained was dipped in a 10 mM phenol solution in 0.05 M phosphate buffer at pH 9. After 2 h, the material was finally washed with water (10 mL × 3) and, when required, air dried before being rehydrated with water.

Determination of the -SH content in SPI/phenol hydrogels by use of Ellman's reagent.[322] To prepare Ellman's reagent, 4 mg of DTNB were dissolved in 1 mL of Tris-glycine buffer, obtained by mixing 0.086 M Tris, 0.09 M glycine, and 4 mM EDTA at pH 8.0. After lyophilization, the hydrogel

powder (15 mg) was first dissolved in 5 mL of Tris-glycine buffer (3 mg/mL final concentration) and then added with 50 mL of Ellman's reagent. The solution was stirred at room temperature and after 1 h the absorbance at 412 nm was analyzed by UV-Vis. The obtained value was adjusted for the contribution of each material at the same concentration (determined in the absence of Ellman's reagent). As reference, the same assay was performed on denatured SPI, to quantify the initial -SH group content. This latter was determined through a calibration curve obtained using a glutathione solution (0.002-0.01 mg/mL) as reference. The data were expressed as a percentage of reacted -SH groups in SPI/phenol material compared to pure SPI.

Determination of the -NH_2 content in SPI/phenol hydrogels.[322] A slightly modified version of the *o*-phthalaldehyde (OPA) technique for soy proteins was used to determine the free amino group content of the samples. 40 mg of OPA were dissolved in a solution composed by 1 mL of methanol, 2.5 mL of a 20% w/v SDS solution, 25 mL of a 0.1 M borax solution and 100 mL of b-mercaptoethanol. Distilled water was then added until the total volume reached 50 mL. The samples were added to the OPA reagent solution at 0.18 mg/mL as final concentration. After 2 min under stirring at 35°C, the absorbance was measured at 340 nm. The obtained value was adjusted for the contribution of each material at the same concentration (determined in the absence of OPA reagent). As reference, the same assay was performed on denatured SPI, in order to quantify the initial -NH_2 group content. This latter was determined through a calibration curve built using a-BOC-L-lysine (3-9 μg/mL). The data were expressed as percentage of reacted -NH_2 groups in SPI/phenol material compared to pure SPI.

Evaluation of adhesive properties and underwater resistance of SPI/phenol hydrogel. SPI or SPI/phenol hydrogels prepared as previously described were applied between two 2 cm^2 soft wood (pine) specimens (30 ×

20 × 50 mm thickness, breadth, and length) (protein concentration on about 1.80 mg/cm^2). The pieces were pressed together for 24 h and then the wood specimens were immersed in deionized water at room temperature and periodically observed in order to evaluate the water resistance.

In further experiments, a protocol previously described was adopted to perform the tests on chicken skin.[328] In particular, the skin was first defatted using a scalpel. Pieces of approx. 15 × 20 mm were cut, gently washed with hand soap once, rinsed with tap water, immersed in ethanol for 2 min and again rinsed with water, and finally immersed into 10 mM HEPES buffer at pH 7.5 for 30 min before their use for the adhesion tests. SPI or SPI/phenol hydrogels prepared as previously described were applied between two 2 cm^2 skin pieces before being clamped together for 24 h and immersed in water.

In the case of chicken breast, slices of approximately 5 × 3 mm were cut with a knife and then immersed in HEPES buffer as above, to remove the lipid layer. Then, they were rinsed with water, gently wiped onto a tissue paper to blot the excess liquid and finally, hydrogels were applied between two slices before they were squeezed together. After 10 h, the samples were immersed in PBS at room temperature and periodically checked to assess the water resistance.

Water vapor permeability (WVP) tests. WVP measurements were performed by researchers of the Institute for Polymers, Composites and Biomaterials applying ASTM E96 standard method, plotting the hydrogel's weight loss against time.

Evaluation of SPI/phenol hydrogels cytocompatibility. The cytocompatibility of the hydrogels was evaluated through MTT and Trypan blue exclusion tests assays[329] in immortalized HaCaT and HDF cells, cultivated at 37°C and incubated for 24 and 72 hours in the presence of: agarose (0.625 mg/mL); agarose (0.625 mg/mL) + 0.875 mg/ml SPI; agarose

(0.625 mg/mL) + 0.875 mg/ml SPI + 0.0875 mg/ml CGA or 0.005 mg/ml CA or 0.005 mg/ml GA. The cells viability (%) was expressed as ratio between the number of live cells compared to the initial total number. Experiments were performed in duplicate with triplicate determinations.

Evaluation of SPI/phenol hydrogels hemocompatibility. The hemocompatibility of the hydrogels was tested performing blood clot formation test and TEG analysis using blood samples (four healthy human donors) supplied by Ospedale Maggiore della Carità's transfusional center (Novara). The blood clot formation test was performed spectrophotometrically (450 nm) analyzing the samples obtained by mixing of SPI/phenols hydrogels with 50 mL of human blood. TEG analysis was performed evaluating starting time, coagulation time, coagulation speed, and clot strength of samples obtained by pouring 1 mL of human blood onto air dried hydrogels at 37°C, accelerating the process, after 30 min, by addition of Kaolin and $CaCl_2$. Experiments were run in triplicate.

Wound healing evaluation - scratch test. The SPI/phenol hydrogels wound healing efficacy was evaluated by *in vitro* analysis[330] using HaCaT keratinocytes. After 24 h incubation at 37°C, the HaCaT cell monolayers were scratched using a pipette tip and, after removing the culture medium, the cells were washed twice with PBS. Subsequently they were treated with new different culture media containing: agarose (0.625 mg/mL); agarose (0.625 mg/mL) + 0.875 mg/ml SPI; agarose (0.625 mg/mL) + 0.875 mg/ml SPI + 0.0875 mg/ml CGA or 0.005 mg/ml CA or 0.005 mg/ml GA. Then, wound closure was evaluated at t_0 or after 24 h of incubation, using an inverted microscope (Zeiss LMS 700, Carl Zeiss, Germany). Experiments were run in triplicate.

Antibacterial activity assessment. To examine the antibacterial activity of air-dried SPI/agarose/phenol hydrogels, different bacterial strains were used,

including *Staphylococcus aureus* ATCC 12600, Methicillin Resistant *Staphylococcus aureus* (MRSA) WKZ-2, *Staphylococcus epidermidis* ATCC 35984, *Acinetobacter baumannii* ATCC 9606, and *Pseudomonas aeruginosa* ATCC 27853.

To assess the inhibition halo of air-dried SPI/agarose/polyphenols hydrogels, 1 cm^2 of air-dried hydrogel was put in contact with cells and incubated at 37°C for 24 h. The bacterial growth around the hydrogels was then evaluated.

Finally, in order to evaluate the percentage of cell viability, 1 cm^2 of air-dried hydrogel was put in contact with bacterial culture and incubated at 37°C. After 24 h the colony counting was performed.

Chapter 6

Use of phenolic compounds in dermocosmetic and food applications

6.1 Evaluation of tyrosinase inhibition activity of extracts from agri-food wastes for cosmetic and food applications

6.1.1 Introduction

As largely discussed before, thanks to their peculiar properties phenolic compounds has been widely applied in various fields, including the cosmetic and food sectors. One of the main problems that these two sectors have in common is the control of the activity of tyrosinase. This enzyme belongs to the polyphenol oxidases (PPO) class having phenolic compounds as substrates. In particular it catalyzes two types of reactions[331] (Figure 6.1):

- the hydroxylation of monophenols to *o*-diphenols (tyrosine hydroxylase, monophenolase or cresolase activity);
- the oxidation of *o*-diphenols to *o*-quinone (dopa oxidase, diphenolase or catecholase activity).[332,333]

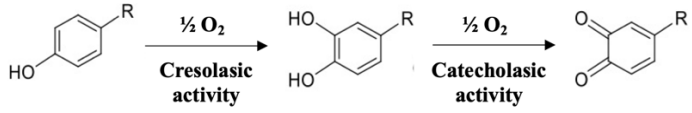

Figure 6.1. Reactions catalyzed by tyrosinase.

Tyrosinase is the main enzyme involved in the biosynthesis of melanin pigments, and in particular in the hydroxylation of the monophenol L-tyrosine

to the corresponding *o*-diphenol (L-3,4-dihydroxyphenylalanine or L-DOPA) and in the oxidation of L-DOPA to the corresponding *o*-quinone (dopaquinone).[334] L-tyrosine and L-DOPA have the same binding site, and the process involves an electron exchange with copper atoms coordinated by histidine residues inside the active site of the enzyme.[334,335] This process can be influenced by many physiological and external events, causing the onset of hyperpigmentation or hypopigmentation phenomena. For example, skin disorders such as acne, atopic dermatitis or *Lichen planus* can be accompanied by localized post-inflammatory hyperpigmentation.[336] Another example is albinism, which includes a group of hereditary diseases characterized by little or no production of melanin by the body.[337] Instead, an example of a common environmental stimulus is sunlight, which can have consequences on epidermal pigmentation (such as the appearance of sunspots or freckles). [338]

Tyrosinase is involved also in undesirable phenomena of interests for food industries, occurring mainly in fruit and vegetables during harvesting, transportation, storage and processing.[339] Indeed, mechanical actions such as peeling, cutting, slicing and mincing of fruits and vegetables during processing or storage can cause physical damage to the tissues, following which the PPO and phenolic compounds typically present in these food items are released and exposed to oxygen, giving rise to oxidation reactions that transform the phenolic compounds into the corresponding quinones, highly reactive species that can undergo polymerization reactions leading to the formation of dark pigments. This phenomenon can determine an alteration of the organoleptic properties of the product resulting in the loss of commercial and nutritional value.[339]

So, the use of non-toxic, stable, and low-cost compounds available on a large scale and capable of inhibiting the activity of tyrosinase thus controlling the production of melanin or the enzymatic browning process, has been largely

investigated.[25,340] Recently, many effective tyrosinase inhibitors have been extracted from various natural sources including agri-food by-products, such as hydroquinones, flavonoids, stilbenes, or coumarins.

Within this context the research activity described in the 6.1 paragraphs will be focused on the exploration of agrifood by-product extracts as inhibitors of tyrosinase, for their possible application in the cosmetic or food field.

6.1.2 Preparation of the extracts from selected agri-food by-products

Agri-food by-products were selected based on their phenolic composition, giving priority to those containing compounds with potential inhibitory activity towards tyrosinase (Table 6.1).

Table 6.1. Selected sources and their main phenolic compounds with potential inhibitory activity against tyrosinase.

Natural source	Phenolic compounds
Chestnut shells	Gallic acid and ellagic acid ester derivatives
Walnut shells	Ellagic acid, catechin and epicatechin
Pecan nut shells	Condensed tannins
Morus alba branches	Resveratrol, moracin, flavonoids
By-product of apples spirit production	Flavonoids and phenolic acids
By-product of strawberry spirit production	Flavonoids and phenolic acids
By-product of fig spirit production	Flavonoids and phenolic acids

By-product of peach spirit production	Flavonoids and gallic, ferulic, and chlorogenic acid
Fermented pomegranate by-products	Ellagitannins, ellagic acid

The selected agri-food by-products were then roughly grinded with a kitchen blender and homogeneously pulverized by using a ball mill (50 oscillations/s, 15 min) to decrease the particles size, increase the surface area and thus make the extraction process more efficient and reproducible. In the specific case of *Morus alba* branches, a first lyophilization phase was necessary to make the sample more easily pulverized.

Subsequently, the obtained powders were treated at 100 mg/mL w/v for 90 min at room temperature with eco-friendly solvents (water, ethanol, water/ethanol at 4:6 v/v ratio or DMSO). After centrifugation, the supernatants were recovered, while the residual solids were lyophilized to calculate the extraction yield with respect to the dry weight of the starting materials (Table 6.2). The fruit distillate production by-products showed the highest extraction yields together with the fermented pomegranate by-products, ranging from 26% to 74% by weight. On the contrary, the lowest values were obtained in the case of nut shells.

Table 6.2. Extraction yields (% w/w) obtained from the selected agri-food by-products in each solvent (water, ethanol, water/ethanol at 4:6 v/v ratio or DMSO). Mean SD ± values are reported from at least three separate experiments.

Source	water	ethanol	water/ ethanol	DMSO
Chestnut shells	3%	10%	9%	46%
Walnut shells	19%	9%	19%	2%
Pecan nut shells	5%	5%	8%	28%
Morus alba branches	39%	14%	25%	13%
By-product of apples spirit production	53%	59%	51%	34%
By-product of strawberry spirit production	27%	26%	29%	36%
By-product of fig spirit production	54%	35%	55%	51%
By-product of peach spirit production	58%	38%	51%	74%
Fermented pomegranate by-products	43%	48%	54%	56%

6.1.3 Evaluation of the tyrosinase inhibition activity of the agri-food by-product extracts

The tyrosinase inhibitory activity of all the prepared extracts was then investigated. Given the difficulties of obtaining mammalian tyrosinase, the experiments were carried out using a commercially available fungal (mushroom) tyrosinase, commonly used as a model of human tyrosinase.[341] To evaluate the inhibition activity, a spectrophotometric assay was performed using L-DOPA as the substrate.

In particular, each extract was incubated in phosphate buffer (pH 6.8) in the presence of mushroom tyrosinase. After 10 min, L-DOPA was added and the concentration of dopachrome, obtained by cyclization of dopaquinone produced in turn by the oxidation of the substrate induced by tyrosinase, was spectrophotometrically determined at 475 nm after 10 min (Figure 6.2).

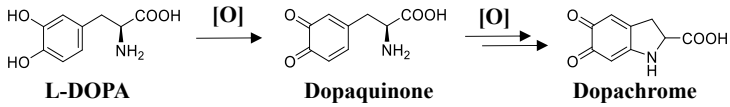

L-DOPA **Dopaquinone** **Dopachrome**

Figure 6.2. Simplified scheme of the reactions involved in the mushroom tyrosinase inhibition assay.

In Table 6.3 the inhibitory capacity of each analyzed sample is reported, expressed as IC_{50}, that is the concentration of the sample capable of inhibit the enzyme activity by 50%. Kojic acid was used as positive control, exhibiting an IC_{50} value equals to 0.0050 ± 0.0004 mg/mL. Indeed, kojic acid is able to chelate the copper ions present in the active site of the enzyme acting as an inhibitor of its activity.

Promising results were obtained in the case the hydroalcoholic extract of chestnut shells, which showed an IC_{50} value equals to 0.0006 ± 0.0004 mg/mL, that is one order of magnitude lower than that of kojic acid. A good inhibitory capacity was shown also by the ethanolic extract of chestnut shells and *Morus alba* branches, showing an IC_{50} value comparable to that obtained for the reference compound. Among the other samples only the hydroalcoholic and water extracts from pecan nut shells exhibited remarkable inhibition properties, while less encouraging were the results obtained for the remaining extracts. For some samples it was not even possible to determine the IC_{50} due to their poor activity.

In Figure 6.3, the IC_{50} values of the most promising extracts are reported for a more immediate comparison, with respect to kojic acid.

Table 6.3. IC_{50} values (mg/mL) of the selected agri-food by-product extracts determined in the mushroom tyrosinase inhibition assay using L-DOPA as substrate. Mean SD ± values are reported from at least three separate experiments.

Natural source	**water**	**ethanol**	**water/ ethanol**	**DMSO**
Chestnut shells	/	0.0060 ± 0.0005	0.0006 ± 0.0004	/
Walnut shells	2.28 ± 0.03	1.404 ± 0.006	1.69 ± 0.03	1.404 ± 0.006
Pecan nut shells	0.068 ± 0.002	/	0.054 ± 0.002	/
Morus alba branches	/	0.0090 ± 0.0003	/	/
By-product of apples spirit production	/	0.557 ± 0.005	0.937 ± 0.001	2.56 ± 0.05
By-product of strawberry spirit production	/	0.711 ± 0.007	0.4800 ± 0.0005	/
By-product of fig spirit production	/	/	1.404 ± 0.006	/
By-product of peach spirit production	/	1.09 ± 0.01	1.07 ± 0.03	/
Fermented pomegranate by-products	0.620 ± 0.002	0.475 ± 0.003	0.511 ± 0.002	0.5410 ± 0.0006

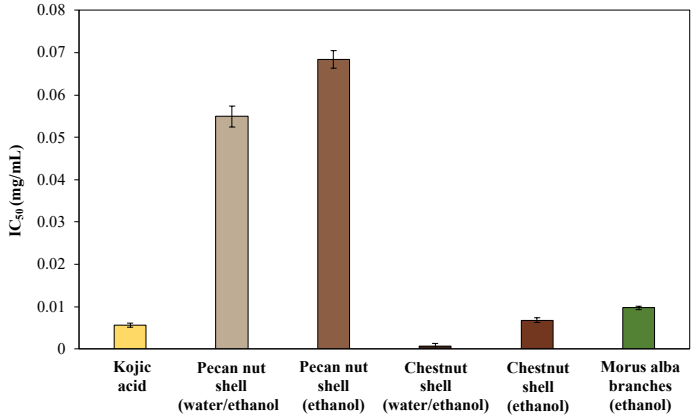

Figure 6.3. IC_{50} values (mg/mL) of the most promising extracts determined in the mushroom tyrosinase inhibition assay using L-DOPA as substrate. Mean SD ± values are reported from at least three separate experiments.

In a second series of experiments, the inhibitory capacity of the most promising extracts was also evaluated against the monophenolase (or cresolase) activity of mushroom tyrosinase, using L-tyrosine as a substrate instead of L-DOPA. As reported in Table 6.4 and Figure 6.4, the best inhibitory activity was shown by the ethanolic chestnut shell extract, followed by the hydroalcoholic chestnut shell extracts, the ethanolic *Morus alba* branches extract and the hydroalcoholic pecan nut shell extract. All the other samples were significantly less active than kojic acid.

Table 6.4. IC_{50} values (mg/mL) of the selected agri-food by-products extracts determined in the mushroom tyrosinase inhibition assay using L-tyrosine substrate. Mean SD ± values are reported from at least three separate experiments.

Natural source	**water**	**ethanol**	**water/ ethanol**	**DMSO**
Chestnut shells	/	0.0070 ± 0.0005	0.012 ± 0.001	/
Pecan nut shells	0.36 ± 0.03	/	0.028 ± 0.009	/
Morus alba branches	/	0.0110 ± 0.0001	/	/
By-product of apples spirit production	/	1.21 ± 0.03	1.14 ± 0.05	/
By-product of strawberry spirit production	/	0.591 ± 0.003	0.351 ± 0.004	/
By-product of peach spirit production	/	1.77 ± 0.05	/	/
Fermented pomegranate by-products	1.5 ± 0.3	1.34 ± 0.06	0.838 ± 0.004	1.22 ± 0.08

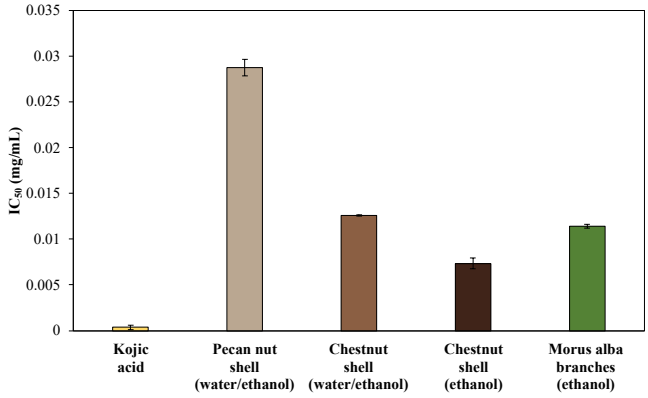

Figure 6.4. IC_{50} values (mg/mL) of the most promising extracts determined in the mushroom tyrosinase inhibition assay using L-tyrosine as substrate. Mean SD ± values are reported from at least three separate experiments.

6.1.4 Evaluation of the enzymatic browning inhibition activity of the agri-food by-product extracts in apple smoothies

As already mentioned in 6.1.1 paragraph, when fruits or vegetables are subjected to cuts or injuries, cytosolic tyrosinase and phenolic compounds confined in vacuoles come in contact and, if exposed to oxygen, oxidation reactions and formation of dark pigments occur. On this basis, a final series of experiments was directed to the evaluation of the ability of selected extracts to inhibit or at least delay enzymatic browning processes exhibited by previously obtained extracts. Apple smoothies were used as a model system, considering their high rate of browning.

In particular, apples (Red Delicious variety) were rapidly peeled and finely ground using a kitchen blender in the absence (CTRL) or presence of the previously prepared agri-food by-product extracts at 0.1% w/w in water. Same experiments were also performed using kojic acid and ascorbic acid as

positive controls which were able to inhibit the browning process over the first 24 h and 4 h, respectively, with a progressively disappearing of the inhibitory effect (Figure 6.5). Indeed, while kojic acid is able to act as an inhibitor of the enzyme, ascorbic acid, typically used to delay the enzymatic browning processes in the food industry, is able to act as a reducing agent towards the quinone species generated by the oxidation of the phenolic compounds in the food matrix, as well as an acid, causing a lowering of the pH of the food matrix (polyphenol oxidases exert their action at a pH value between 6 and 7).

Most of the samples did not show any inhibitory effect. The best results were obtained using the extracts from fermented pomegranate by-products in DMSO, chestnut shells in water/ethanol (4:6 v/v) and strawberry spirit production by-products in water/ethanol (4:6 v/v) (Figure 6.6), although the delay effect on the browning process was clearly apparent only in the first minutes.

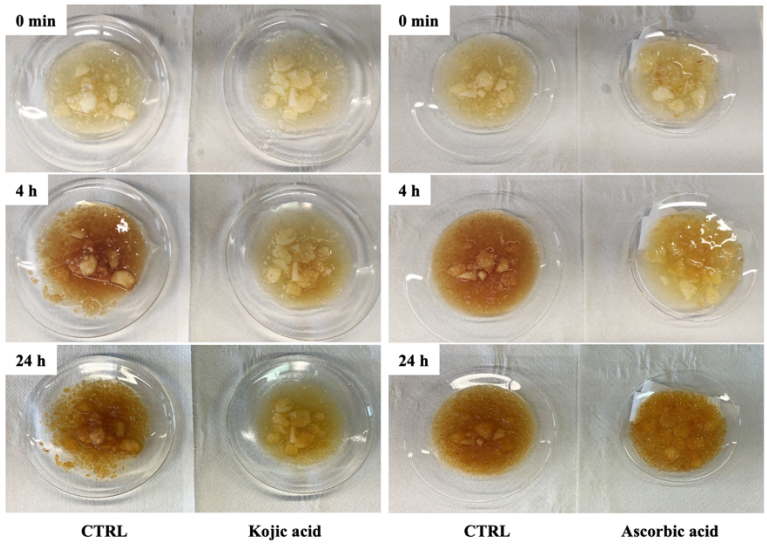

Figure 6.5. Effect of kojic acid and ascorbic acid on the enzymatic browning of apple smoothies at different times.

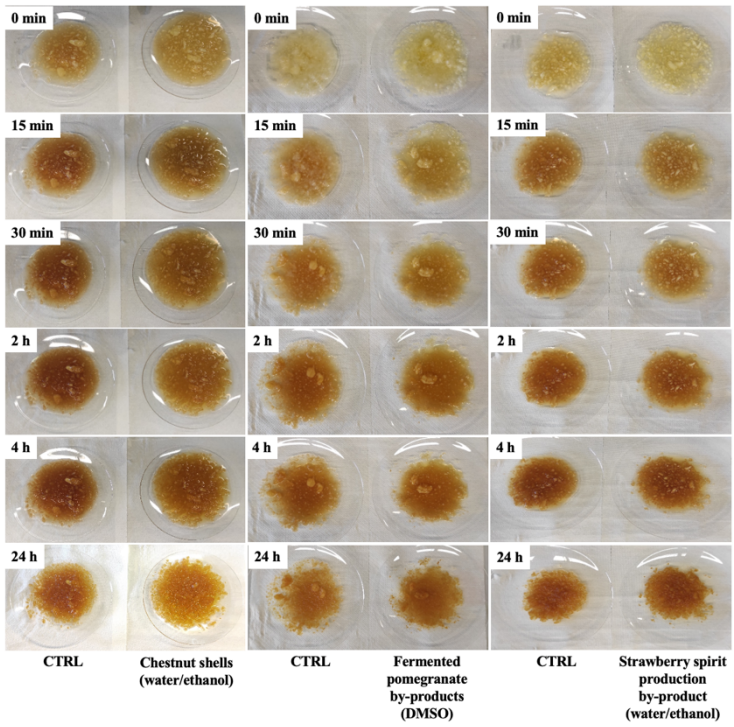

Figure 6.6. Effect of chestnut shell extract in water/ethanol (4:6 v/v), fermented pomegranate by-product extract in DMSO and strawberry spirit production by-products extract in water/ethanol (4:6 v/v) on the enzymatic browning of apple smoothies at different times.

Then, a colorimetric analysis was performed every 30 min up to 3 hours by using a colorimeter (see paragraph 5.1.3.2), and the results are reported in Table 6.5 confirming the visually observed enzymatic browning process delay. Indeed, the strawberry extract showed in the first 30 min an encouraging result, comparable to that observed for kojic or ascorbic acid. However, this effect immediately disappeared at later times.

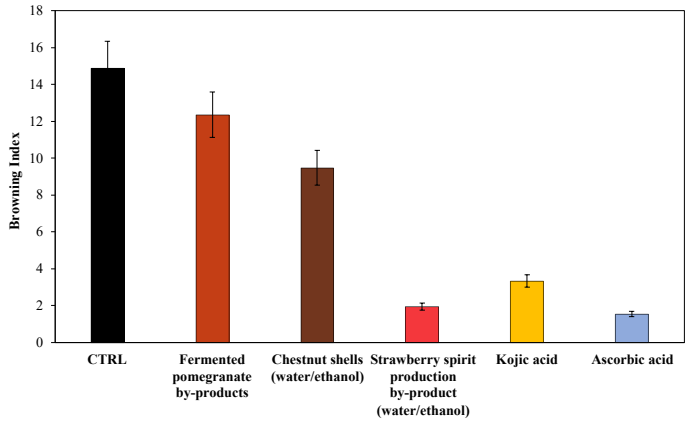

Figure 6.7. Browning index values calculated for apple smoothies treated with selected extracts, kojic acid, or ascorbic acid, and a plain apple smoothie (CTRL) after 30 min. Mean values ± (SD ≤ 10) from at least three separate experiments are reported.

6.1.5 Conclusions

Recently, increasing attention has been directed to the search of compounds capable of acting as tyrosinase inhibitors, and hence of preventing or delaying skin hyperpigmentation processes in the cosmetic field, or enzymatic browning processes of fruits or vegetables in the food sector. On this basis, the present work was aimed at the preparation of extracts from low cost agri-food by-products rich in phenolic compounds and to the evaluation of their mushroom tyrosinase inhibition activity.

In particular, among all the tested extracts, those from chestnut shells, *Morus alba* branches and pecan nut shells showed IC_{50} values against tyrosinase higher or comparable with respect to the value determined for kojic acid (positive reference compound). On the other hand, extracts from strawberry spirit production by-products, fermented pomegranate by-products and again

chestnut shells exhibited an evident retarding effect on enzymatic browning process of apples smoothies.

These results, although still preliminary, open new perspectives for the use of these sustainable materials in the cosmetic and food industries.

6.1.6 Experimental section

Materials and methods. By-products from fruit spirit production were provided from the agrifood company Berolà (Portico di Caserta, Caserta, Italy), fermented pomegranate by-products were obtained from Cuatro Ciénegas, Coahuila, México. Chestnut shells were provided from the agrifood industry Malerba (Montella, Avellino, Italy). Walnut and pecan nut shells were obtained from samples purchased at a local supermarket. Morus Alba branches were obtained from a local garden. Apples (Red Delicious variety) were purchased from a local supermarket. Mushroom tyrosinase (EC 1.14.18.1), L-3,4-dihydroxyphenylalanine (L-DOPA), L-tyrosine, kojic acid and ascorbic acid were purchased from Sigma-Aldrich.

UV-Vis spectra were recorded on V-730 UV-visible spectrophotometer.

A Chroma Meter CR-400/410 (Konica Minolta) colorimeter was used to analyze changes in color.

Preparation of extracts from the selected agri-food by-products. Chestnut, walnut and pecan nut shells were roughly ground using a kitchen blender, and then pulverized using a ball mill (Fritsch Pulverisette 23) at 50 oscillations/min for 15 min. In the case of Morus Alba branches a lyophilization step was necessary before the mechanochemical treatment. The fruit spirit production by-products (already crushed) were only pulverized using the ball mill (50 oscillations/s, 15 min).

300 mg of each agri-food by-product were added to 3 mL of water, ethanol, water/ethanol (4:6 v/v) or DMSO, and the suspension was taken under stirring

at room temperature. After 90 min, the mixture was centrifuged (5000, 20°C, 10 min). The supernatants were recovered, while the residual solids were lyophilized to calculate the extraction yields. In the specific case of DMSO, the residual solid was washed two times with water before lyophilization.

Tyrosinase inhibition assay.[342] Different solutions were prepared: mushroom tyrosinase was dissolved in 50 mM phosphate buffer (pH 6.8) (4000 U/mL); L-DOPA was dissolved in 0.6 M HCl (100 mM); L-tyrosine was dissolved in 0.6 M HCl (100 mM).

10 mL of tyrosinase solution were incubated in 2 mL of 50 mM phosphate buffer (pH 6.8) (final concentration 20 U/mL) at room temperature in the absence (CTRL) or in the presence of the extracts (0.0003-1.5 mg/mL final dose) or of kojic acid used as positive control (2.5-17 μg/mL final dose). After 10 min, 20 μL of the L-DOPA or L-tyrosine solution (final concentration 1 mM) were added, and the reaction mixture was again stirred for 10 minutes. Finally, the absorbance at 475 nm was measured. The inhibition activity was expressed as IC_{50}, corresponding to the sample concentration capable of inhibiting the enzyme activity by 50%.

Apple smoothie browning inhibition assay. 50 g of peeled apple (Red Delicious variety) were finely blended using a kitchen mixer in the absence (CTRL) or in the presence of 0.1% w/v extract water solution. The final mixture was then transferred on a watch glass. The color variations over time were periodically analyzed by using a colorimeter[298] and was evaluated calculating the browning index (BI) as follows:

$$BI = \frac{100(x-0.31)}{0.17}$$

$$x = \frac{a^{*}+1.75L^{*}}{5.645L^{*}+a^{*}-3.012b^{*}}$$

where L* indicates brightness and a* and b* are chromaticity coordinates. In particular +a* is the red direction, -a* is the green direction, +b* is the yellow direction, and -b * is the direction of blue.

Three different experiments were performed and for each one three different measurements were taken. Kojic and ascorbic acid were used as positive controls.

6.2 Synergic effect of phenolic cosmetic ingredients and melanin pigments on immediate pigment darkening

6.2.1 Introduction

Nowadays, the role of melanins in photo-exposed skin is still controversial. Indeed, as mentioned before, melanin is produced by mammals to protect the skin against ultraviolet light injury, but, at the same time, it has been reported that the overproduction and accumulation of melanin can cause several skin disorders, including melasma, freckles, age spots and other hyperpigmentation events.[343] In fact, over the years, several *in vivo*[344] and *in vitro*[345] studies had challenged the traditional view of melanins as efficient photoprotective agents against the damage of fundamental cellular constituents (*e.g.* DNA and membrane lipids). Thanks to their significant absorption in the UV-Vis region, these pigments may actually act as photosensitizers favouring the production of injuring species such as reactive oxygen species (ROS) (*e.g.* superoxide anion, singlet oxygen, hydroxyl radical and hydrogen peroxide), that are capable of damaging cellular structures like DNA.[346,347] On the other hand, other studies based on electron paramagnetic resonance (EPR) techniques highlighted the capacity of synthetic melanins to scavenge the ROS they themselves generated on irradiation.[348]

In this framework, nowadays the research for efficacious sunscreen formulations acting as inhibitors of melanogenesis have been widely investigated for their application in skin care products for the treatment or prevention of abnormal hyperpigmentation.[349] The attention has been focused not only on the use of UVA/B filters to reduce the effects of carcinogenic and photodamaging solar UV radiation, but also on the development of additional ingredients that may scavenge the ROS.[350] The accumulation of ROS, in fact,

may activate tyrosinase in the epidermis with the subsequent production of melanin in the melanocytes.

Many natural phenolic compounds have been previously investigated for their ability to inhibit the tyrosinase activity. On this basis, the present 6.2 paragraphs will be focused on the:

- exploration of the effects of selected phenolic cosmetic ingredients (CIs) on skin hyperpigmentation;
- evaluation of the photoprotective role of the CIs against the damages induced by solar light using model systems of lipid peroxidation and DNA damage;
- evaluation of the effects of melanin pigments on CIs behavior.

6.2.2 Evaluation of the effect of CIs on photoinduced oxidation of melanogenic dihydroxyindoles

First experiments were directed to the evaluation of the effects of selected CIs on the photooxidation of the 5,6-dihydroxyindoles melanin precursors (DHI and DHICA), taken as *in vitro* model of the immediate pigment darkening (IPD) process. More specifically, IPD corresponds to the first phase of the pigmentary response of human skin to UVA radiation (320-400 nm)[351] exposure, characterized by the oxidation of the melanogenic dihydroxyindoles available in epidermal melanocytes leading to the production of the dark eumelanin pigments, and followed by persistent pigment darkening (PPD) and delayed tanning (DT).[352]

In particular, the selected evaluated CIs are gingerol-based CIs, namely paradol-6, and a ginger extract containing [6]-gingerol as the main component, together with phenylethyl resorcinol (Figure 6.8). Gingerols are well-known for a variety of biological activities including antioxidant, antimicrobial, anticancer, anti-allergic and anti-inflammatory properties.[353]

On the other hand, resorcinol derivatives are well-known to be effective in trapping the tyrosinase generated dopaquinone,[341] or in affecting the signaling pathway that leads to tyrosinase production,[354,355] inhibiting the initial stages of the melanin pigmentation pathway.

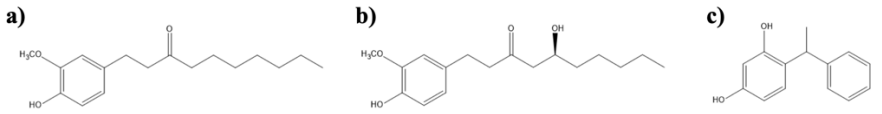

Figure 6.8. Structure of: a) paradol-6; b) main component of the ginger extract, and c) phenylethyl resorcinol.

Initially, DHI and DHICA oxidation was carried out in phosphate buffer at pH 7 using a solar simulator. However, no substantial changes in the UV-Vis absorption spectra of the indole solutions were observed over the first 30 min. On this basis, the use of two photosensitizers (PS), natural or mimicking those occurring in the skin, that is riboflavin (RF) and protoporphyrin IX (pPIX), was considered. In particular, RF is classified as a type I/II photosensitizer since it is capable of generating either superoxide/hydrogen peroxide or singlet oxygen, while protoporphyrin IX is a type II photosensitizer, producing only singlet oxygen.[356]

In the presence of both PS (1 mM), the conversion of the indoles to melanin was observed over 30 min, and the scattering of the insoluble pigment generated an increase of the absorbance in the visible region of the UV-Vis spectrum of the solution (Figure 6.9).

Based on this result, the indoles concentration and the reaction time were optimized with the aim of obtaining more reproducible results. Optimal outcomes were obtained performing the reaction for 1 h, with the indole at 50 mM concentration (Figure 6.9).

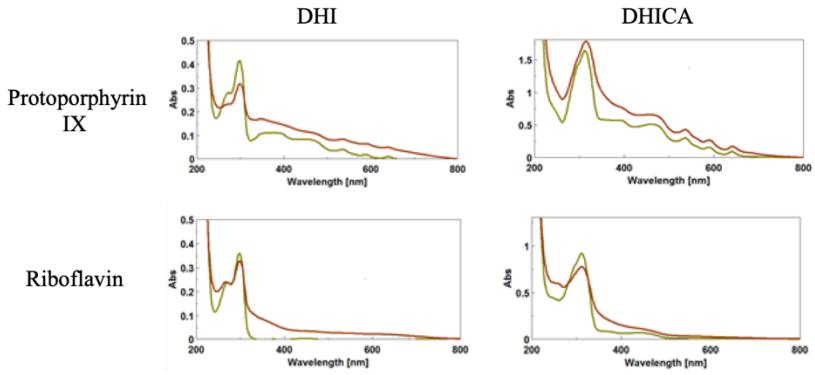

Figure 6.9. UV-Vis spectra of irradiated DHI and DHICA (50 mM) in the presence of RF or pPIX (1 mM) at time 0 (green) and 30 min (brown).

The contribution of PS and of the solar simulator in the DHI/DHICA oxidation was demonstrated through control experiments. Indeed, both PS didn't transform after photoirradiation over the same time, while, performing the reaction without the use of the solar simulator, no interaction between PS and indoles was observed.

As a representative example, the effect of the CIs on the oxidation of DHI (1:1 mol/mol) photoinduced by RF was then evaluated. Figure 6.10 reports the absorbance of the mixtures at 600 nm, chosen as the analytical wavelength to detect melanin formation avoiding the interference of CIs absorption. However, the presence of CIs led only to a slight though non-statistically significant decrease of melanin formation.

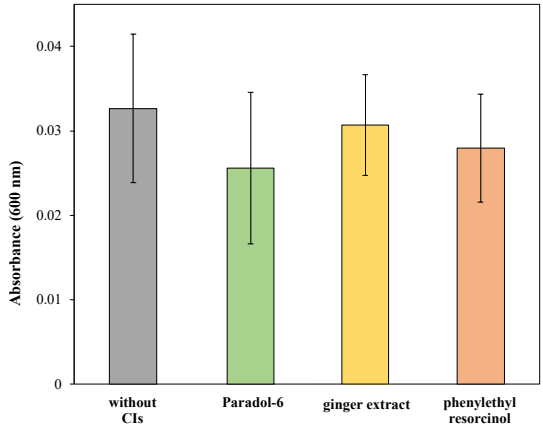

Figure 6.10. Absorbance at 600 nm of DHI (50 mM) irradiated mixture containing RF (1 mM) in the presence or absence of CIs after 1 h. Mean ± SD values of three experiments are reported.

To obtain more information about DHI or DHICA decay during the photoinduced oxidation, the HPLC analysis was performed. As shown in Figure 6.11_a, the consumption of DHI, equal to ca. 80% after 1 h in the presence of PS only, was significantly reduced in the presence of equimolar amounts of CIs. In particular, best results were obtained with phenylethyl resorcinol, which reduced the consumption of the indole to ca. 60% after 1 h. Analogous results were obtained carrying out the photooxidation of DHICA (Figure 6.11_b). In this case, paradol-6 and phenylethyl resorcinol led to an approximately 50% consumption of the indole after 1 h.

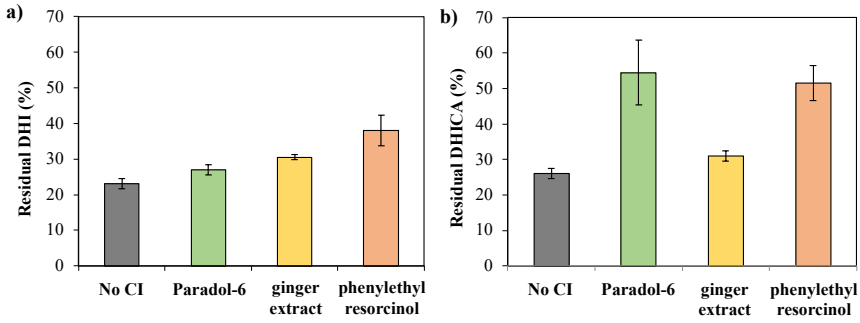

Figure 6.11. Residual concentration (%) of a) DHI and b) DHICA after 1 h photoirradiation in the presence of RF (1 mM) and in the presence or absence of CIs. Mean ± SD values of three experiments are reported.

For comparison, the same experiments were also run using pPIX as PS, instead of RF. However, no ameliorative effects were observed in the presence of CIs, while even higher indole consumption was observed with phenylethyl resorcinol. On this basis, it was possible to conclude that CIs could only scavenge the species generated by RF (that is superoxide and hydrogen peroxide), but not the singlet oxygen generated by pPIX.

In order to validate this theory, the photoinduced oxidation of DHI and DHICA was subsequentially carried out in the presence of 2-benzylaminobenzoic acid as CI (1:1 mol/mol) over 1 h reaction time. This compound is indeed known to act as a selective scavenger of singlet oxygen.[357,358]

As expected, using pPIX the 2-benzylaminobenzoic acid significantly reduced the indoles decay (Figure 6.12), protecting them from photooxidation, while in the RF-sensitized irradiation an equal or even higher consumption of the indoles was observed (Figure 6.13).

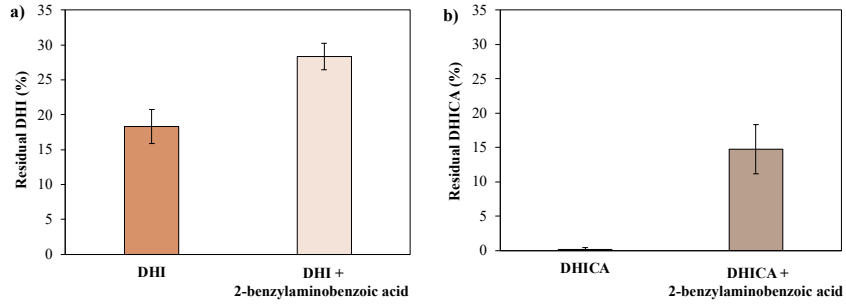

Figure 6.12. Residual concentration (%) of a) DHI and b) DHICA after 1 h photooxidation in the presence of pPIX (1 mM) and in the presence or absence of 2-benzylaminobenzoic acid. Mean ± SD values of three experiments are reported.

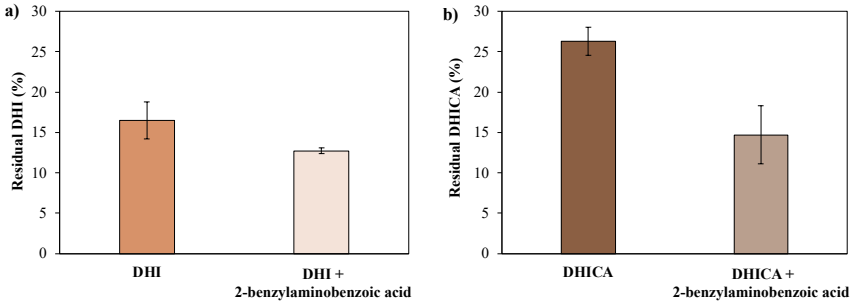

Figure 6.13. Residual concentration (%) of a) DHI and b) DHICA after 1 h photooxidation in the presence of RF (1 mM) and in the presence or absence of 2-benzylaminobenzoic acid. Mean ± SD values of three experiments are reported.

6.2.3 Evaluation of the effects of CIs on photoinduced lipid peroxidation

Further experiments were directed to obtain information about the photoprotective role of the CIs against the damage induces by solar light in an accessible model of lipid peroxidation, that is soybean phosphatidylcholine liposomes at high content (ca. 70%)[359] of polyunsaturated fatty acids (PUFA).

In this specific case, the combination with a photosensitizer was necessary, since PUFA don't absorb the radiation in the emission region of solar simulator. Moreover, considering that the photosensitized oxidation can take place through both type I and type II mechanism (*i.e.* generation of radicals via electron transfer or hydrogen abstraction and energy transfer from the triplet state of the photosensitizer to the molecular oxygen to form $^1O_2$,[356,360] respectively), RF was chosen as type I/II PS.

The lipid peroxidation of PUFA lead to the development of primary oxidation products, namely, conjugated dienes (conjugated hydroperoxides), and trienes (carbonyls conjugated to dienes), absorbing at 234 and 270 nm, respectively. However, considering that RF absorb at 270 nm, lipid peroxidation of PUFA can be followed by monitoring the formation of dienes only.

First experiments were directed to the optimization of the reaction conditions in terms of time and PS concentration. The best results were obtained after 15 min of exposure to the radiation. In fact, by prolonging this time the concentration of dienes decreased due to the formation of secondary products from further reactions, as reported in several studies.[361,362] Concerning PS concentration, RF at 20 mM led to a significant dienes' formation over the selected exposure time.

For comparison, subsequent experiments were also carried out using pPIX and Rose Bengal (RB), that is pure type II photosensitizers.[363] Analogously to RF, RB proved able to induce an appreciable formation of dienes at 20 mM over 15 min, while no appreciable peroxidation of linoleic acid was observed with pPIX, even at higher concentration.

Finally, control experiments were carried out without the use of the solar simulator. In this case generation of conjugated dienes were not observed.

The above reported optimized reaction conditions were subsequentially used to evaluate the effect of the selected CIs on the photoinduced oxidation of the main PUFA, *i.e.* linoleic acid, a readily available substrate. The data in Figure 6.14 and 6.15 are reported as variation of absorbance at 234 nm (ΔA(%)), with respect to the control, corresponding to the 100% of lipid peroxidation obtained in the absence of CIs. Moreover, the contributions of CIs and PS at 234 nm were introduced as correction.

In the RF-sensitized reaction (Figure 6.14), paradol-6 and ginger extract gave good results halving the amount of generated dienes, while, in the RB-sensitized reaction (Figure 6.15), paradol-6 and phenylethyl resorcinol performed better than gingerol extract, leading to up a 70% decrease of dienes generation in the case of paradol-6. For completeness of information, dose–response curves were also recorded, confirming the previous results.

In further experiments, the effect of DHI and DHICA melanins on the photoinduced oxidation of linoleic acid was evaluated. DHI and DHICA melanins, reported as good models of natural pigments[112,246], were obtained through enzymatic oxidation using a procedure already reported in literature.[115]

In order to limit the absorption contribution at 234 nm, 0.0125 mg/mL of DHICA melanin and 0.05 mg/mL of DHI melanin were used. Interestingly, as observed in Figure 6.14 and 6.15, the combination between melanins and CIs led to a reduction of lipid peroxidation to varying degrees. As control, an increase of lipid peroxidation caused by DHI/DHICA melanin was observed carrying out the photoinduced reactions in the absence of CIs.

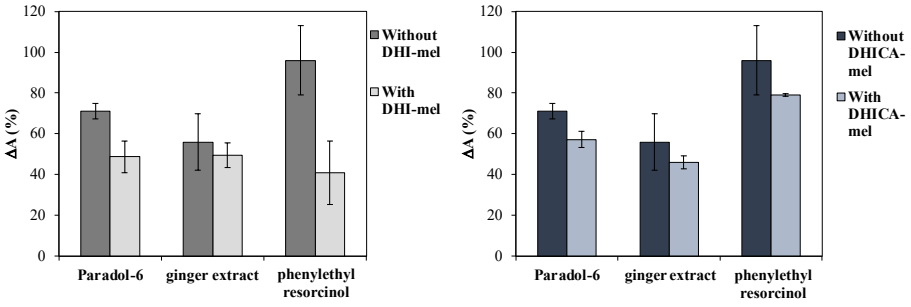

Figure 6.14. Changes of the absorbance (ΔA(%)) at 234 nm of 2.5 mM linoleic acid oxidation mixture containing 20 mM RF, 20 mM CIs and 0.05 mg/mL DHI melanin or 0.0125 mg/mL DHICA melanin. Mean ± SD values of three experiments are reported.

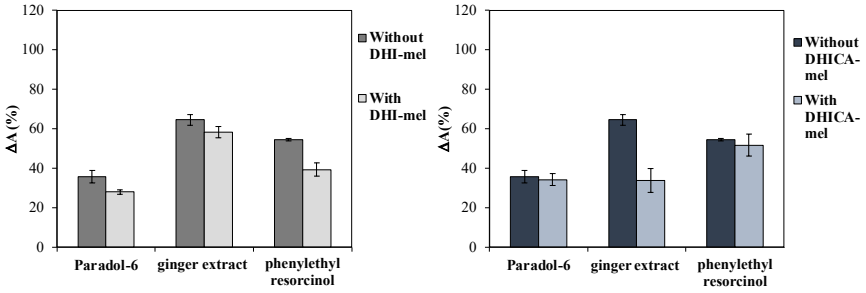

Figure 6.15. Changes of the absorbance (ΔA(%)) at 234 nm of 2.5 mM linoleic acid oxidation mixture containing 20 mM B, 20 mM CIs and 0.05 mg/mL DHI melanin or 0.0125 mg/mL DHICA melanin. Mean ± SD values of three experiments are reported.

A more complex model was subsequently used to investigate the photoinduced lipid oxidative damage. In particular, liposomes of phosphatidylcholine from soybean (SoyPC) were chosen. Indeed, phosphatidylcholine is the most abundant phospholipid in eukaryotic cellular membranes, besides being characterized by a high content of PUFAs.

Using RF as photosensitiser, no lipid peroxidation was induced by photoirradiation under the solar simulator, even using high concentrations of PS or long exposure times, likely because of the reported capability of liposomes to stabilize RF.[364] On the other hand, RB led to a considerable peroxidation of the substrate, which was not inhibited by the tested CIs. So, considering again that RF is a type I/II PS, while RB can only act through the generation of singlet oxygen, it can be assumed that paradol-6 and ginger extract can only control the formation and/or scavenge radical oxygen-derived species. This hypothesis was subsequentially validates evaluating the effect of 2-aminobenylbenzoic acid, similarly to what was previously done. The compounds proved able to inhibit liposome peroxidation by ca. 20%. A synergic effect was observed using the CIs in combination with DHI melanin, tested as a representative example, whereas melanin alone was ineffective (Figure 6.16).

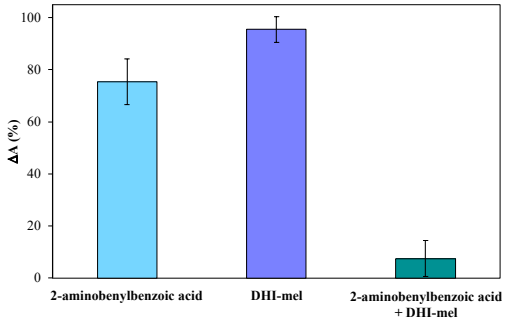

Figure 6.16. Changes of the absorbance (ΔA(%)) at 234 nm of 250 μM liposome solutions containing in the presence of 20 mM RB, 20 mM 2-aminobenylbenzoic acid, and 0.05 mg/mL DHI melanin. Mean ± SD values of three experiments are reported.

6.2.4 Evaluation of the effects of CIs effect and melanins on UV-induced damages on a DNA model

In order to evaluate the potential protective role of CIs against UV-induced damages in DNA, the pyrimidine thymine base was chosen as model system. Indeed, it is one of the nitrogenous bases most sensitive to UV-induced damage that can lead to different photoproducts including cyclopyrimidine dimers, which can in turn induce cells death or be the origin of sequential mutations.[365]

The formation of these products in DNA can be easily mimicked in the laboratory by following the formation of thymine-thymine dimers or determining their levels in irradiated DNA hydrolysate by HPLC.

Modifying a procedure reported in literature,[366] a standard solution of thymine dimers was prepared using a 2 mM ethanolic solution of thymine irradiated at 254 nm for 10 min. The HPLC profile of the reaction mixture (Figure 6.17) showed the presence of thymine eluted at 15 min, together with two products eluted at 10 and 14 min identified as thymine dimers by LC-MS analysis ($[M+H]^+$ at *m/z* 253).

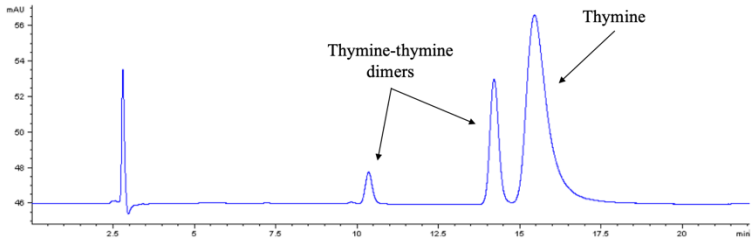

Figure 6.17. HPLC profile of an ethanolic thymine solution irradiated at 254 nm for 10 min.

Carrying out the irradiation at 254 nm in air over 3 h, a consumption of thymine of ca. 50% was observed.

Then, the irradiation of thymine under these conditions was conducted in the presence of CIs. However, HPLC analysis allowed to monitor only the consumption of thymine, because CIs overlapped with thymine dimers in the elutographic conditions developed. As shown in Figure 6.18, all the CIs were capable of almost completely inhibit thymine photodimerization. The observed trend was also confirmed by dose-response curves.

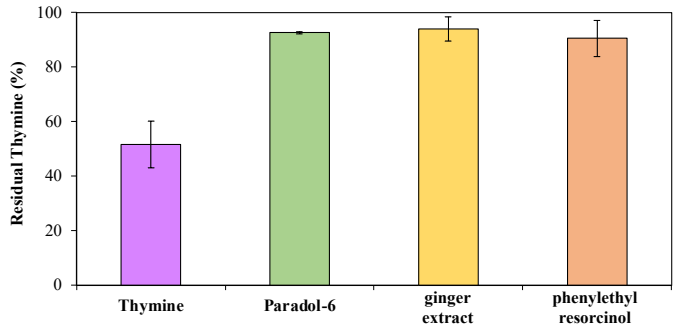

Figure 6.18. Residual thymine expressed as percentage with respect to a non-photoexposed thymine solution (2 mM) (CTRL) photoirradiated at 254 nm for 3 h in the presence or absence of CIs (50 mM). Mean ± SD values from three experiments are reported.

Subsequently, the effect of DHI and DHICA melanins was evaluated.

When the thymine solution was irradiated in the presence of DHI melanin only (0.05 mg/mL), a 73% of residual thymine was observed, comparable to the result obtained using DHICA melanin (0.004 mg/mL) (72%), and only a small synergic effect was observed combining melanins and CIs.

Finally, in other preliminary experiments, a previously reported methodology was adapted in order to assess the damage induced by UV in a DNA[366] sample, and thymine, derived from hydrolysis of UV-irradiated DNA, was quantified

by HPLC in comparison to a not photoexposed DNA sample. The hydrolysis conditions were optimized to get reproducibility in thymine level determinations, while chromatographic conditions were optimized to avoid that other products derived from DNA hydrolysis could interfere with thymine detection. In agreement with the previous data on free thymine, CIs included in the photoirradiation mixture, particularly paradol-6 and phenylethyl resorcinol, proved to be able to slightly protect the substrate (Figure 6.19).

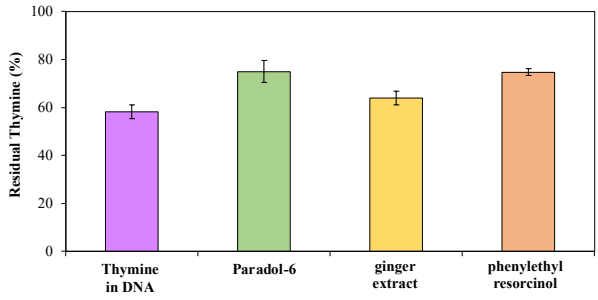

Figure 6.19. Residual thymine in DNA expressed as percentage with respect to a non-photoexposed solution (CTRL) determined in a DNA solution photoirradiated at 254 nm for 3 h in the presence or absence of CIs (50 mM). Mean ± SD values from three experiments are reported.

6.2.5 Conclusions

Selected CIs characterized by the presence of a phenol moiety were tested for the prevention of skin hyperpigmentation. In particular, gingerol and resorcinol-based CIs proved to be effective inhibitors of DHI and DHICA photooxidation, used as *in vitro* model of IPD, likely due to their ability to scavenge hydrogen peroxide and superoxide. Moreover, using model systems of lipid peroxidation and DNA damage, CIs also resulted to be able to exert a photoprotective role against the damages induced by solar light. In some

cases, an enhanced effect was observed combining CIs with DHI or DHICA melanins.

Although preliminary, these results open new perspectives in the design of skin care formulations for ameliorating skin spots and contrasting ageing processes including those associated to sun exposure.

6.2.6 Experimental section

Materials and methods. DHI, DHICA, DHI melanin and DHICA melanin were prepared using previously developed protocols.[115] CIs (paradol-6, ginger extract, phenylethyl resorcinol and 2-benzylaminobenzoic acid) were provided by Symrise AG (Holzminden, Germany). Sodium bisulphite, tris(hydroxymethyl)aminomethane (Tris) and ethylenediaminetetraacetic acid (EDTA) were purchased by Sigma Aldrich. Sodium dodecyl sulphate (SDS), linoleic acid, liposomes of phosphatidylcholine from soybean (containing 13% palmitic (C16:0), 4% stearic (C18:0), 10% oleic (C18:1), 64% linoleic (C18:2), and 6% linolenic (C18:3)), thymine, calf thymus DNA, riboflavin and protoporphyrin IX were purchased from Merck and used as obtained.

Photoirradiation was carried out using a solar simulator (Thermo Oriel66902) at 60 watts or a multirays "merry-go-round" photoreactor (Helios Italquartz, Cambiago, Italy) equipped with lamps at 254 nm.

UV-Vis spectra were recorded on V-730 UV-visible spectrophotometer.

HPLC analyses were performed on an instrument equipped with an Agilent G1314A UV-Vis detector, using a Phenomenex Sphereclone C18 column (250 × 4.60 mm, 5 μm) at a flow rate of 1.0 mL/min; the isocratic elution was as follows:

- DHI and DHICA analysis: 1% formic acid (solvent A)/acetonitrile (solvent B) 75:25 v/v; the detection wavelength was set at 280 nm;

- thymine and thymine dimers analysis: 10 mM PB (pH 6.8); the detection wavelength was set at 220 nm.

LC-MS analysis were run on an Agilent LC-MS ESI-TOF 1260/6230DA instrument operating in positive and negative ionization mode in the following conditions: nebulizer pressure 35 psig; drying gas (nitrogen) 5 L/min, 325 ◦C; capillary voltage 3500 V; fragmentor voltage 175 V. A Eclipse Plus C18 column (150 × 4.6 mm, 5 μm) at a flow rate of 0.4 mL/min was used, using the eluant 2.

Photoinduced oxidation of DHI and DHICA. DHI or DHICA solution were prepared in 0.1 M phosphate buffer at pH 7.0 (50 mM) in a Petri dish covered with a quartz slide to avoid evaporation of the solvent, photoirradiated using a solar simulator and periodically analyzed by UV-vis spectrophotometry or HPLC without further dilution or work up. The photosensitizer (RF or pPIX) was added to the solution of the indoles at 1 mM final concentration. When required, paradol-6, ginger extract, phenylethyl resorcinol or 2-benzylaminobenzoic were added to the mixture (50 mM). Control experiments were run under the same conditions using only PS or the indole.

Photooxidation of linoleic acid. A solution of linoleic acid at 2.5 mM concentration was prepared using 0.1 M phosphate buffer at pH 7.0 and 0.1 M SDS. The obtained mixture, in the presence of the appropriate RF or RB (20 mM), was then put in a Petri dish covered with a quartz slide to avoid evaporation of the solvent and exposed to the solar simulator radiation. The mixture was periodically analyzed by UV-vis spectrophotometry without further dilution or work-up to improve the reproducibility of the experiments. In further experiments, CIs (20 mM), DHI melanin (0.05 mg/mL) or DHICA melanin (0.0125 mg/mL) were also included. Melanins were added as a suspension in water.[367]

Photooxidation of soybean phosphatidylcholine liposomes. A suspension of soybean phosphatidylcholine liposomes (250 mM) in 0.1 M phosphate buffer at pH 7.0 was prepared. The obtained mixture, in the presence of the appropriate photosensitizer (RF, pPIX or RB) at 20 mM and with or without the CIs (20 mM), was then put in a Petri dish covered with a quartz slide to avoid evaporation of the solvent and exposed to the solar simulator radiation. The mixture was periodically analyzed by UV-Vis spectrophotometry without further dilution or work-up to improve the reproducibility of the experiments. In other experiments, DHI melanin (0.05 mg/mL) was also included, as representative example, added as a suspension in water.[367]

Photoinduced decay of free or DNA thymine. A 2 mM thymine solution was prepared using 0.1 M phosphate buffer at pH 7.0. The obtained mixture, in the absence or presence of CIs (50 mM), was then put in a Petri dish covered with a quartz slide to avoid evaporation of the solvent and exposed to a multiray "merry-go-round" photoreactor. Also argon atmosphere or the use of sodium bisulphite as reducing agent were tested. The mixture was periodically analyzed by UV-Vis spectrophotometry after dilution to 80 mM concentration. In further experiments, DHI melanin (0.05 mg/mL) or DHICA melanin (0.0125 mg/mL) were also included as a suspension in water.[367]

Photoinduced DNA damage. A DNA solution was prepared combining 25 mg of calf thymus DNA in 4 mM Tris–HCl buffer solution (pH 7.4) and 0.4 mM EDTA and stirred for 24 h. In order to reduce shearing of the DNA, no sonication or stirring was used (in agreement with the manufacturer instructions). 500 mL of the prepared solution was then put in a Petri dish, in the absence or presence of CIs (50 mM), covered with a quartz slide to avoid evaporation of the solvent and exposed to a multiray "merry-go-round" photoreactor for 3 h. 30 mL of the irradiated solution were mixed with 1 mL trifluoracetic acid in a glass vial under argon atmosphere, stirred at 160 °C for

1 h and finally cooled and dried under vacuum. The obtained residue was dissolved in water (200 mL) and then analysed by HPLC.

List of abbreviations

ABS Aqueous Biphasic System

ABTS 2,2-Azino-bis-(3-ethyl- BenzThiazoline-6-Sulphonic acid)

AgNPs AgNanoParticles

CA Caffeic Acid

CAME Caffeic Acid Methyl Ester

CAN Cerium(IV) Ammonium Nitrate

CFU Colony-Forming Unit

CGA Chlorogenic Acid

CHT Chitosan

CIs Cosmetic Ingredients

CM Conventional Maceration

CNCs Cellulose Nanocrystals

CS Chestnut Shells

CSL Chestnut Shells Lignin

CT Condensed Tannins

CTC Condensed Tannins Content

CTRL Control

CUPRAC CUPric ion Reducing Antioxidant Capacity

DES Deep Eutectic Solvent

DHI 5,6-dihydroxyindole

DHICA 5,6-dihydroxyindole-2-carboxylic acid

DMSO dimethyl sulphoxide

DPPH 2,2-diphenyl-1-picryl-hydrazyl

EB EthylBenzene

EDTA Ethylenediaminetetraacetic acid

EPR Electron paramagnetic resonance

Eq Equivalent

Eqs Equivalents

ESI$^+$/MS Electrospray Ionisation Mass Spectrometry

FRAP Ferric Reducing/Antioxidant Power

GA Gallic Acid

GC Gas Chromatography

H_2O_2 Hydrogen Peroxide

HaCat Human Keratinocytes

HBA Hydrogen Bond Acceptor

HBD Hydrogen Bond Donor

HDF Human Dermal Fibroblasts

HFP 1,1,1,3,3,3-HexaFluoro-2-Propanol

HMDA Hexamethylenediamine

hMSCs human Mesenchymal Stem Cells

HPLC High Pressure Liquid Chromatography

HRP Horseradish peroxidase

HT Hydrolyzable Tannins

ICP-MS Inductively coupled plasma mass spectrometry

ILs Ionic Liquids

IPD Immediate Pigment Darkening

L-DOPA 3,4-dihydroxy-L-phenylalanine

LA Lipoic Acid

LC-MS Liquid Chromatography-Mass Spectrometry

LCA Life Cycle Assessment

LP Lower salt-Phase

MAE Microwave Assisted Extraction

MALDI Maldi Assisted Laser Desorption Ionization

MeDHICA Methyl ester of 5,6-dihydroxyindole-2-carboxylic acid

MTT 3-(4,5-dimethyl-2-thiazolyl)-2,5-diphenyl-2H-tetrazolium bromide

NMR Nuclear Magnetic Resonance

OPA o-phthalaldehyde

PA PhenylAcetylene

PB Phosphate Buffer

PDA PolyDopAmine

PDCA Pyrrole-2,3-DiCarboxylic Acid

PDLLA Poly(D,L-lactic) Acid

PN Pine Needles

Poly Polystyrene

PolyCAME Poly(caffeic acid methyl ester)

PPG400 PolyPropylene Glycol 400

pPIX Protoporphyrin IX

PPO PolyPhenol Oxidases

PPS Pomegranate Peels and Seeds

PS PhotoSensitizers

PTCA Pyrrole-2,3-TriCarboxylic Acid

PTeCA Pyrrole-2,3-TetraCarboxylic Acid

PUF PolyUrethane Foam

PUFA PolyUnsaturated Fatty Acids

RB Rose Bengal

RF Riboflavin

RFU Relative Fluorescence Units

ROS Reactive Oxygen Species

Rt Retention Time

SCSs Structured Catalytic Supports

SDS Sodium Dodecyl Sulphate

SEM Scanning Electron Microscopy

SPI Soy Proteins Isolate

ST STyrene

TAN/C Chestnut TANnins

TAN/G Gall TANnins

TAN/Q Quebracho TANnins

TAN/T Tara TANnins

TAT Triazatruxene derivatives

TBARS ThioBarbituric Acid Reactive Substances

TEG Thromboelastography

TEM Transmission Electron Microscopy

TLC Thin layer chromatography

TPC Total Phenolic Content

TPTZ 2,4,6-tris(2-pyridyl)-s-triazine

Tris Tris (hydroxymethyl) aminomethane

Trolox (±)-6-hydroxy-2,5,7,8-tetramethylchromane-2-carboxylic acid

UAE Ultrasound Assisted Extraction

UP Upper polymer-Phase

UV Ultraviolet

Vis Visible

WPI Whey Proteins Isolate

WVP Water Vapour Permeability

XPS X-ray Photoelectron Spectroscopy

XRD X-Ray Diffraction

References

(1) Pott, D. M.; Osorio, S.; Vallarino, J. G. From Central to Specialized Metabolism: An Overview of Some Secondary Compounds Derived From the Primary Metabolism for Their Role in Conferring Nutritional and Organoleptic Characteristics to Fruit. *Front. Plant. Sci.* **2019**, *10*. doi: 10.3389/fpls.2019.00835.

(2) Cheynier, V. Phenolic Compounds: From Plants to Foods. *Phytochem. Rev.* **2012**, *11* (2–3), 153–177. doi:10.1007/s11101-012-9242-8.

(3) Koroleva, O.; Torkova, A.; Nikolaev, I.; Khrameeva, E.; Fedorova, T.; Tsentalovich, M.; Amarowicz, R. Evaluation of the Antiradical Properties of Phenolic Acids. *Int. J. Mol. Sci.* **2014**, *15* (9), 16351–16380. doi:10.3390/ijms150916351.

(4) Birben, E.; Sahiner, U. M.; Sackesen, C.; Erzurum, S.; Kalayci, O. Oxidative Stress and Antioxidant Defense. *World Allergy Organization J.* **2012**, *5* (1), 9–19. doi: 10.1097/WOX.0b013e3182439613.

(5) Lushchak, V. I. Free Radicals, Reactive Oxygen Species, Oxidative Stress and Its Classification. *Chem. Biol. Interact.* **2014**, *224*, 164–175. doi: 10.1016/j.cbi.2014.10.016.

(6) Martinez-Gomez, A.; Caballero, I.; Blanco, C. A. Phenols and Melanoidins as Natural Antioxidants in Beer. Structure, Reactivity and Antioxidant Activity. *Biomolecules* **2020**, *10* (3), 400. doi: 10.3390/biom10030400.

(7) Bartosz, G. Reactive Oxygen Species: Destroyers or Messengers? *Biochem. Pharmacol.* **2009**, *77* (8), 1303–1315. doi: 10.1016/j.bcp.2008.11.009.

(8) Kaur, R.; Kaur, J.; Mahajan, J.; Kumar, R.; Arora, S. Oxidative Stress-Implications, Source and Its Prevention. *Environ. Sci. Pollut. Res. Int.* **2014**, *21* (3), 1599–1613. doi: 10.1007/s11356-013-2251-3.

(9) Liguori, I.; Russo, G.; Curcio, F.; Bulli, G.; Aran, L.; Della-Morte, D.; Gargiulo, G.; Testa, G.; Cacciatore, F.; Bonaduce, D.; Abete, P. Oxidative Stress, Aging, and Diseases. *Clin. Interv. Aging.* **2018**, *Volume 13*, 757–772. doi: 10.2147/CIA.S158513.

(10) Amorati, R.; Valgimigli, L. Advantages and Limitations of Common Testing Methods for Antioxidants. *Free Radic. Res.* **2015**, *49* (5), 633–649. doi: 10.3109/10715762.2014.996146.

(11) Kiokias, S.; Proestos, C.; Oreopoulou, V. Phenolic Acids of Plant Origin—A Review on Their Antioxidant Activity In Vitro (O/W Emulsion Systems) Along with Their in Vivo Health Biochemical Properties. *Foods.* **2020**, *9* (4), 534. doi: 10.3390/foods9040534.

(12) Oluwole, O.; Fernando, W. B.; Lumanlan, J.; Ademuyiwa, O.; Jayasena, V. Role of Phenolic Acid, Tannins, Stilbenes, Lignans and Flavonoids in Human Health – a Review. *Int. J. Food Sci. Technol.* **2022**, *57* (10), 6326–6335. doi: 10.1111/ijfs.15936.

(13) Balasundram, N.; Sundram, K.; Samman, S. Phenolic Compounds in Plants and Agri-Industrial by-Products: Antioxidant Activity, Occurrence, and Potential Uses. *Food Chem.* **2006**, *99* (1), 191–203. doi: 10.1016/j.foodchem.2005.07.042.

(14) Shahidi, F.; Ambigaipalan, P. Phenolics and Polyphenolics in Foods, Beverages and Spices: Antioxidant Activity and Health Effects – A Review. *J. Funct. Foods.* **2015**, *18*, 820–897. doi: 10.1016/j.jff.2015.06.018.

(15) Ha, L. T. N. Phenolic compounds and health benefites. *Vietnam J. Agri. Sci.* **2016**, *14*, 1107–1118.

(16) Magalhães, M.; Manadas, B.; Efferth, T.; Cabral, C. Chemoprevention and Therapeutic Role of Essential Oils and Phenolic Compounds: Modeling Tumor Microenvironment in Glioblastoma. *Pharmacol. Res.* **2021**, *169*, 105638. doi: 10.1016/j.phrs.2021.105638.
(17) Huang, M.-T.; Ferraro, T. Phenolic Compounds in Food and Cancer Prevention. In *Phenolic Compounds in Food and Their Effects on Health II*; ACS Symposium Series. **1992**, 8–34. doi: 10.1021/bk-1992-0507.ch002.
(18) Vinayagam, R.; Jayachandran, M.; Xu, B. Antidiabetic Effects of Simple Phenolic Acids: A Comprehensive Review. *Phytother. Res.* **2016**, *30* (2), 184–199. doi: 10.1002/ptr.5528.
(19) Ofosu, F. K.; Daliri, E. B.-M.; Elahi, F.; Chelliah, R.; Lee, B.-H.; Oh, D.-H. New Insights on the Use of Polyphenols as Natural Preservatives and Their Emerging Safety Concerns. *Front. Sustain. Food Syst.* **2020**, *4*. doi: 10.3389/fsufs.2020.525810.
(20) Martillanes, S.; Rocha-Pimienta, J.; Cabrera-Bañegil, M.; Martín-Vertedor, D.; Delgado-Adámez, J. Application of Phenolic Compounds for Food Preservation: Food Additive and Active Packaging. In *Phenolic Compounds - Biological Activity*; InTech, **2017**. doi: 10.5772/66885.
(21) Bouarab Chibane, L.; Degraeve, P.; Ferhout, H.; Bouajila, J.; Oulahal, N. Plant Antimicrobial Polyphenols as Potential Natural Food Preservatives. *J. Sci. Food Agric.* **2019**, *99* (4), 1457–1474. doi: 10.1002/jsfa.9357.
(22) Panzella, L.; Napolitano, A. Natural Phenol Polymers: Recent Advances in Food and Health Applications. *Antioxidants.* **2017**, *6* (2), 30. doi: 10.3390/antiox6020030.
(23) Panzella, L.; Napolitano, A. Condensed Tannins, a Viable Solution To Meet the Need for Sustainable and Effective Multifunctionality in Food Packaging: Structure, Sources, and Properties. *J. Agric. Food Chem.* **2022**, *70* (3), 751–758. doi: 10.1021/acs.jafc.1c07229.
(24) de Lima Cherubim, D. J.; Buzanello Martins, C. V.; Oliveira Fariña, L.; da Silva de Lucca, R. A. Polyphenols as Natural Antioxidants in Cosmetics Applications. *J. Cosmet. Dermatol.* **2020**, *19* (1), 33–37. doi: 10.1111/jocd.13093.
(25) Panzella, L.; Napolitano, A. Natural and Bioinspired Phenolic Compounds as Tyrosinase Inhibitors for the Treatment of Skin Hyperpigmentation: Recent Advances. *Cosmetics.* **2019**, *6* (4), 57. doi: 10.3390/cosmetics6040057.
(26) Saiz-Poseu, J.; Sedõ, J.; García, B.; Benaiges, C.; Parella, T.; Alibés, R.; Hernando, J.; Busqué, F.; Ruiz-Molina, D. Versatile Nanostructured Materials via Direct Reaction of Functionalized Catechols. *Adv. Mater.s* **2013**, *25* (14), 2066–2070. doi: 10.1002/adma.201204383.
(27) Guo, J.; Suma, T.; Richardson, J. J.; Ejima, H. Modular Assembly of Biomaterials Using Polyphenols as Building Blocks. *ACS Biomater. Sci. Eng.* **2019**, *5* (11), 5578–5596. doi: 10.1021/acsbiomaterials.8b01507.
(28) Rahim, Md. A.; Kristufek, S. L.; Pan, S.; Richardson, J. J.; Caruso, F. Phenolic Building Blocks for the Assembly of Functional Materials. *Angew. Chem., Int. Ed. Engl.* **2019**, *58* (7), 1904–1927. doi: 10.1002/anie.201807804.
(29) Wu, D.; Zhou, J.; Creyer, M. N.; Yim, W.; Chen, Z.; Messersmith, P. B.; Jokerst, J. V. Phenolic-Enabled Nanotechnology: Versatile Particle Engineering for Biomedicine. *Chem. Soc. Rev.* **2021**, *50* (7), 4432–4483. doi: 10.1039/D0CS00908C.
(30) Simon, J. D.; Peles, D. N. The Red and the Black. *Acc. Chem. Res.* **2010**, *43* (11), 1452–1460. doi: 10.1021/ar100079y.
(31) Ito, S.; Wakamatsu, K.; d'ischia, M.; Napolitano, A.; Pezzella, A. Structure of Melanins. In *Melanins and Melanosomes*; Wiley. **2011**, 167–185. doi: 10.1002/9783527636150.ch6.

(32) Borovanský, J.; Riley, P. A. Physiological and Pathological Functions of Melanosomes. In *Melanins and Melanosomes*; Wiley. **2011**, 343–381. doi: 10.1002/9783527636150.ch12.
(33) Cichorek, M.; Wachulska, M.; Stasiewicz, A.; Tymińska, A. Skin Melanocytes: Biology and Development. *Postepy. Dermatol. Alergol.* **2013**, *30* (1), 30–41. doi: 10.5114/pdia.2013.33376.
(34) Moreiras, H.; Seabra, M. C.; Barral, D. C. Melanin Transfer in the Epidermis: The Pursuit of Skin Pigmentation Control Mechanisms. *Int. J. Mol. Sci.* **2021**, *22* (9), 4466. doi: 10.3390/ijms22094466.
(35) Donato, P. Di; Napolitano, A. 1,4-Benzothiazines as Key Intermediates in the Biosynthesis of Red Hair Pigment Pheomelanins. *Pigment. Cell. Res.* **2003**, *16* (5), 532–539. doi: 10.1034/j.1600-0749.2003.00085.x.
(36) Panzella, L.; Napolitano, A.; d'Ischia, M. Is DHICA the Key to Dopachrome Tautomerase and Melanocyte Functions? *Pigment Cell Melanoma Res.* **2011**, *24* (1), 248–249. doi: 10.1111/j.1755-148X.2010.00771.x.
(37) Palumbo, A.; d'Ischia, M.; Misuraca, G.; Prota, G.; Schultz, T. M. Structural Modifications in Biosynthetic Melanins Induced by Metal Ions. *Biochimica et Biophysica Acta (BBA) - General Subjects* **1988**, *964* (2), 193–199. doi: 10.1016/0304-4165(88)90166-3.
(38) Ito, S.; Wakamatsu, K. Chemistry of Mixed Melanogenesis—Pivotal Roles of Dopaquinone †. *Photochem. Photobiol.* **2008**, *84* (3), 582–592. doi: 10.1111/j.1751-1097.2007.00238.x.
(39) Meredith, P.; Sarna, T. The Physical and Chemical Properties of Eumelanin. *Pigment Cell Res.* **2006**, *19* (6), 572–594. doi: 10.1111/j.1600-0749.2006.00345.x.
(40) Cavallini, C.; Vitiello, G.; Adinolfi, B.; Silvestri, B.; Armanetti, P.; Manini, P.; Pezzella, A.; D'ischia, M.; Luciani, G.; Menichetti, L. Melanin and Melanin-like Hybrid Materials in Regenerative Medicine. *Nanomaterials.* **2020**, *10* (8), 1–32. doi: 10.3390/nano10081518.
(41) d'Ischia, M.; Wakamatsu, K.; Cicoira, F.; Di Mauro, E.; Garcia-Borron, J. C.; Commo, S.; Galván, I.; Ghanem, G.; Kenzo, K.; Meredith, P.; Pezzella, A.; Santato, C.; Sarna, T.; Simon, J. D.; Zecca, L.; Zucca, F. A.; Napolitano, A.; Ito, S. Melanins and Melanogenesis: From Pigment Cells to Human Health and Technological Applications. *Pigment Cell Melanoma Res.* **2015**, *28* (5), 520–544. doi: 10.1111/pcmr.12393.
(42) Panzella, L.; Melone, L.; Pezzella, A.; Rossi, B.; Pastori, N.; Perfetti, M.; D'Errico, G.; Punta, C.; D'Ischia, M. Surface-Functionalization of Nanostructured Cellulose Aerogels by Solid State Eumelanin Coating. *Biomacromolecules.* **2016**, *17* (2), 564–571. doi: 10.1021/acs.biomac.5b01497.
(43) Kleinert, M.; Barth, T. Phenols from Lignin. *Chem. Eng. Technol.* **2008**, *31* (5), 736–745. doi: 10.1002/ceat.200800073.
(44) Boerjan, W.; Ralph, J.; Baucher, M. Lignin Biosynthesis. *Annu. Rev. Plant Biol.* **2003**, *54* (1), 519–546. doi: 10.1146/annurev.arplant.54.031902.134938.
(45) Zevallos Torres, L. A.; Lorenci Woiciechowski, A.; de Andrade Tanobe, V. O.; Karp, S. G.; Guimarães Lorenci, L. C.; Faulds, C.; Soccol, C. R. Lignin as a Potential Source of High-Added Value Compounds: A Review. *J. Clean. Prod.* **2020**, *263*, 121499. doi: 10.1016/j.jclepro.2020.121499.
(46) Lourenço, A.; Pereira, H. Compositional Variability of Lignin in Biomass. In *Lignin - Trends and Applications*. InTech, **2018**. doi: 10.5772/intechopen.71208.
(47) Tribot, A.; Amer, G.; Abdou Alio, M.; de Baynast, H.; Delattre, C.; Pons, A.; Mathias, J.-D.; Callois, J.-M.; Vial, C.; Michaud, P.; Dussap, C.-G. Wood-Lignin: Supply, Extraction Processes and Use as Bio-Based Material. *Eur. Polym. J.* **2019**, *112*, 228–240. doi: 10.1016/j.eurpolymj.2019.01.007.

(48) Liu, Q.; Luo, L.; Zheng, L. Lignins: Biosynthesis and Biological Functions in Plants. *Int. J. Mol. Sci.* **2018**, *19* (2), 335. doi: 10.3390/ijms19020335.
(49) Baurhoo, B.; Ruiz-Feria, C. A.; Zhao, X. Purified Lignin: Nutritional and Health Impacts on Farm Animals—A Review. *Anim. Feed Sci. Technol.* **2008**, *144* (3–4), 175–184. doi: 10.1016/j.anifeedsci.2007.10.016.
(50) Spiridon, I. Extraction of Lignin and Therapeutic Applications of Lignin-Derived Compounds. A Review. *Environ. Chem. Lett.* **2020**, *18* (3), 771–785. doi: 10.1007/s10311-020-00981-3.
(51) Iravani, S.; Varma, R. S. Greener Synthesis of Lignin Nanoparticles and Their Applications. *Green Chem.* **2020**, *22* (3), 612–636. doi: 10.1039/C9GC02835H.
(52) Lizundia, E.; Sipponen, M. H.; Greca, L. G.; Balakshin, M.; Tardy, B. L.; Rojas, O. J.; Puglia, D. Multifunctional Lignin-Based Nanocomposites and Nanohybrids. *Green Chem.* **2021**, *23* (18), 6698–6760. doi: 10.1039/D1GC01684A.
(53) Zhou, S.-J.; Wang, H.-M.; Xiong, S.-J.; Sun, J.-M.; Wang, Y.-Y.; Yu, S.; Sun, Z.; Wen, J.-L.; Yuan, T.-Q. Technical Lignin Valorization in Biodegradable Polyester-Based Plastics (BPPs). *ACS Sustain. Chem. Eng.* **2021**, *9* (36), 12017–12042. doi: 10.1021/acssuschemeng.1c03705.
(54) Wang, H.-M.; Yuan, T.-Q.; Song, G.-Y.; Sun, R.-C. Advanced and Versatile Lignin-Derived Biodegradable Composite Film Materials toward a Sustainable World. *Green Chem.* **2021**, *23* (11), 3790–3817. doi: 10.1039/D1GC00790D.
(55) Liao, J. J.; Latif, N. H. A.; Trache, D.; Brosse, N.; Hussin, M. H. Current Advancement on the Isolation, Characterization and Application of Lignin. *Int. J. Biol. Macromol.* **2020**, *162*, 985–1024. doi: 10.1016/j.ijbiomac.2020.06.168.
(56) Liu, R.; Dai, L.; Xu, C.; Wang, K.; Zheng, C.; Si, C. Lignin-Based Micro- and Nanomaterials and Their Composites in Biomedical Applications. *ChemSusChem.* **2020**, *13* (17), 4266–4283. doi: 10.1002/cssc.202000783.
(57) Tang, Q.; Qian, Y.; Yang, D.; Qiu, X.; Qin, Y.; Zhou, M. Lignin-Based Nanoparticles: A Review on Their Preparations and Applications. *Polymers (Basel).* **2020**, *12* (11), 2471. doi: 10.3390/polym12112471.
(58) Koleckar, V.; Kubikova, K.; Rehakova, Z.; Kuca, K.; Jun, D.; Jahodar, L.; Opletal, L. Condensed and Hydrolysable Tannins as Antioxidants Influencing the Health. *Mini-Rev. Med. Chem.* **2008**, *8* (5), 436–447. doi: 10.2174/138955708784223486.
(59) Unusan, N. Proanthocyanidins in Grape Seeds: An Updated Review of Their Health Benefits and Potential Uses in the Food Industry. *J. Funct. Foods.* **2020**, *67*, 103861. doi: 10.1016/j.jff.2020.103861.
(60) Reid, D. G.; Bonnet, S. L.; Kemp, G.; van der Westhuizen, J. H. Analysis of Commercial Proanthocyanidins. Part 4: Solid State 13C NMR as a Tool for in Situ Analysis of Proanthocyanidin Tannins, in Heartwood and Bark of Quebracho and Acacia, and Related Species. *Phytochem.* **2013**, *94*, 243–248. doi: 10.1016/j.phytochem.2013.06.007.
(61) Haslam, E.; Cai, Y. Plant Polyphenols (Vegetable Tannins): Gallic Acid Metabolism. *Nat. Prod. Rep.* **1994**, *11*, 41. doi: 10.1039/np9941100041.
(62) Peng, S.; Scalbert, A.; Monties, B. Insoluble Ellagitannins in Castanea Sativa and Quercus Petraea Woods. *Phytochemistry* **1991**, *30* (3), 775–778. doi: 10.1016/0031-9422(91)85250-4.
(63) Comandini, P.; Lerma-García, M. J.; Simó-Alfonso, E. F.; Toschi, T. G. Tannin Analysis of Chestnut Bark Samples (Castanea Sativa Mill.) by HPLC-DAD–MS. *Food Chem.* **2014**, *157*, 290–295. doi: 10.1016/j.foodchem.2014.02.003.
(64) Pizzi, A. Tannins: Prospectives and Actual Industrial Applications. *Biomolecules.* **2019**, *9* (8), 344. doi: 10.3390/biom9080344.
(65) Porter, L. J. Tannins. *Methods in Plant Biochem.* **1989**, *1*, 389–419. doi : 10.1016/B978-0-12-461011-8.50017-2.

(66) Buzzini, P.; Arapitsas, P.; Goretti, M.; Branda, E.; Turchetti, B.; Pinelli, P.; Ieri, F.; Romani, A. Antimicrobial and Antiviral Activity of Hydrolysable Tannins. *Mini-Rev. Med. Chem.* **2008**, *8* (12), 1179–1187. doi: 10.2174/138955708786140990.

(67) Hussain, G.; Huang, J.; Rasul, A.; Anwar, H.; Imran, A.; Maqbool, J.; Razzaq, A.; Aziz, N.; Makhdoom, E. ul H.; Konuk, M.; Sun, T. Putative Roles of Plant-Derived Tannins in Neurodegenerative and Neuropsychiatry Disorders: An Updated Review. *Molecules.* **2019**, *24* (12), 2213. doi: 10.3390/molecules24122213.

(68) Gauden, M.; Pezzella, A.; Panzella, L.; Neves-Petersen, M. T.; Skovsen, E.; Petersen, S. B.; Mullen, K. M.; Napolitano, A.; D'Ischia, M.; Sundström, V. Role of Solvent, PH, and Molecular Size in Excited-State Deactivation of Key Eumelanin Building Blocks: Implications for Melanin Pigment Photostability. *J. Am. Chem. Soc.* **2008**, *130* (50), 17038–17043. doi: 10.1021/ja806345q.

(69) Bernardus Mostert, A.; Davy, K. J. P.; Ruggles, J. L.; Powell, B. J.; Gentle, I. R.; Meredith, P. Gaseous Adsorption in Melanins: Hydrophilic Biomacromolecules with High Electrical Conductivities. *Langmuir.* **2010**, *26* (1), 412–416. doi: 10.1021/la901290f.

(70) Dias, R.; Perez-Gregorio, R.; Mateus, N.; De Freitas, V. The Interaction between Tannins and Gliadin Derived Peptides in a Celiac Disease Perspective. *RSC Adv.* **2015**, *5* (41), 32151–32158. doi: 10.1039/C5RA02968F.

(71) Shirmohammadli, Y.; Efhamisisi, D.; Pizzi, A. Tannins as a Sustainable Raw Material for Green Chemistry: A Review. *Ind. Crops. Prod.* **2018**, *126*, 316–332. doi: 10.1016/j.indcrop.2018.10.034.

(72) Pizzi, A. Tannins: Prospectives and Actual Industrial Applications. *Biomolecules.* **2019**, *9* (8), 344. doi: 10.3390/biom9080344.

(73) Matamala, G.; Smeltzer, W.; Droguett, G. Comparison of Steel Anticorrosive Protection Formulated with Natural Tannins Extracted from Acacia and from Pine Bark. *Corros. Sci.* **2000**, *42* (8), 1351–1362. doi: 10.1016/S0010-938X(99)00137-7.

(74) Noor Idora, M. S.; Quen, L. K.; Kang, H. S. Effect of Tannin from Rhizophora Apiculate as Corrosion Inhibitor for Epoxy Paint on Mild Steel. *J. Phys. Conf. Ser.* **2017**, *890* (1), 012062. doi: 10.1088/1742-6596/890/1/012062.

(75) Hadzich, A.; Flores, S.; Caprari, J.; Romagnoli, R. Study of Zinc Tannates Prepared with Tara Powder (Caesalpinia Spinosa) as Anticorrosive Pigments in Alkyd Paints and Wash Primer Formulations. *Prog. Org. Coat.* **2018**, *117*, 35–46. doi: 10.1016/j.porgcoat.2017.12.019.

(76) Pérez, M.; Blustein, G.; García, M.; Del Amo, B.; Stupak, M. Cupric Tannate: A Low Copper Content Antifouling Pigment. *Prog. Org. Coat.* **2006**, *55* (4), 311–315. doi: 10.1016/j.porgcoat.2005.11.014.

(77) Koopmann, A.-K.; Schuster, C.; Torres-Rodríguez, J.; Kain, S.; Pertl-Obermeyer, H.; Petutschnigg, A.; Hüsing, N. Tannin-Based Hybrid Materials and Their Applications: A Review. *Molecules.* **2020**, *25* (21), 4910. doi: 10.3390/molecules25214910.

(78) Fermoso, F. G.; Serrano, A.; Alonso-Fariñas, B.; Fernández-Bolaños, J.; Borja, R.; Rodríguez-Gutiérrez, G. Valuable Compound Extraction, Anaerobic Digestion, and Composting: A Leading Biorefinery Approach for Agricultural Wastes. *J. Agric. Food Chem.* **2018**, *66* (32), 8451–8468. doi: 10.1021/acs.jafc.8b02667.

(79) Zuin, V. G.; Ramin, L. Z. Green and Sustainable Separation of Natural Products from Agro-Industrial Waste: Challenges, Potentialities, and Perspectives on Emerging Approaches. *Top. Curr. Chem.* **2018**, *376* (1), 3. doi: 10.1007/s41061-017-0182-z.

(80) Xia, H.; Houghton, J. A.; Clark, J. H.; Matharu, A. S. Potential Utilization of Unavoidable Food Supply Chain Wastes–Valorization of Pea Vine Wastes. *ACS Sustain. Chem. Eng.* **2016**, *4* (11), 6002–6009. doi: 10.1021/acssuschemeng.6b01297.

(81) Macias-Corral, M.; Samani, Z.; Hanson, A.; Smith, G.; Funk, P.; Yu, H.; Longworth, J. Anaerobic Digestion of Municipal Solid Waste and Agricultural Waste and the Effect of Co-Digestion with Dairy Cow Manure. *Bioresour. Technol.* **2008**, *99* (17), 8288–8293. doi: 10.1016/j.biortech.2008.03.057.
(82) Fierascu, R. C.; Sieniawska, E.; Ortan, A.; Fierascu, I.; Xiao, J. Fruits By-Products – A Source of Valuable Active Principles. A Short Review. *Front. Bioeng. Biotechnol.* **2020**, *8*. doi: 10.3389/fbioe.2020.00319.
(83) Stalikas, C. D. Extraction, Separation, and Detection Methods for Phenolic Acids and Flavonoids. *J. Sep. Sci.* **2007**, *30* (18), 3268–3295. doi: 10.1002/jssc.200700261.
(84) Ikeda, M. Public Health Problems of Organic Solvents. *Toxicol. Lett.* **1992**, *64–65*, 191–201. doi: 10.1016/0378-4274(92)90189-Q.
(85) Talmaciu, A. I.; Volf, I.; Popa, V. I. A Comparative Analysis of the 'Green' Techniques Applied for Polyphenols Extraction from Bioresources. *Chem. Biodivers.* **2015**, *12* (11), 1635–1651. doi: 10.1002/cbdv.201400415.
(86) Garcia-Salas, P.; Morales-Soto, A.; Segura-Carretero, A.; Fernández-Gutiérrez, A. Phenolic-Compound-Extraction Systems for Fruit and Vegetable Samples. *Molecules.* **2010**, *15* (12), 8813–8826. doi: 10.3390/molecules15128813.
(87) Tiwari, B. K. Ultrasound: A Clean, Green Extraction Technology. *TrAC Trends Anal. Chem.* **2015**, *71*, 100–109. doi: 10.1016/j.trac.2015.04.013.
(88) Paiva, A.; Craveiro, R.; Aroso, I.; Martins, M.; Reis, R. L.; Duarte, A. R. C. Natural Deep Eutectic Solvents – Solvents for the 21st Century. *ACS Sustain. Chem. Eng.* **2014**, *2* (5), 1063–1071. doi: 10.1021/sc500096j.
(89) Ruesgas-Ramón, M.; Figueroa-Espinoza, M. C.; Durand, E. Application of Deep Eutectic Solvents (DES) for Phenolic Compounds Extraction: Overview, Challenges, and Opportunities. *J. Agric. Food. Chem.* **2017**, *65* (18), 3591–3601. doi: 10.1021/acs.jafc.7b01054.
(90) Abbott, A. P.; Capper, G.; Davies, D. L.; Rasheed, R. K.; Tambyrajah, V. Novel Solvent Properties of Choline Chloride/Urea Mixtures. *Chem. Commun.* **2003**, *9*, 70–71. doi: 10.1039/b210714g.
(91) Radošević, K.; Cvjetko Bubalo, M.; Gaurina Srček, V.; Grgas, D.; Landeka Dragičević, T.; Radojčić Redovniković, I. Evaluation of Toxicity and Biodegradability of Choline Chloride Based Deep Eutectic Solvents. *Ecotoxicol. Environ. Saf.* **2015**, *112*, 46–53. doi: 10.1016/j.ecoenv.2014.09.034.
(92) Zhang, Q.; De Oliveira Vigier, K.; Royer, S.; Jérôme, F. Deep Eutectic Solvents: Syntheses, Properties and Applications. *Chem. Soc. Rev.* **2012**, *41* (21), 7108. doi: 10.1039/c2cs35178a.
(93) Francisco, M.; van den Bruinhorst, A.; Kroon, M. C. Low-Transition-Temperature Mixtures (LTTMs): A New Generation of Designer Solvents. *Angew. Chem., Int. Ed. Engl.* **2013**, *52* (11), 3074–3085. doi: 10.1002/anie.201207548.
(94) Abbott, A. P.; Barron, J. C.; Ryder, K. S.; Wilson, D. Eutectic-Based Ionic Liquids with Metal-Containing Anions and Cations. *Chem. – A Eur. J.* **2007**, *13* (22), 6495–6501. doi: 10.1002/chem.200601738.
(95) Tang, B.; Zhang, H.; Row, K. H. Application of Deep Eutectic Solvents in the Extraction and Separation of Target Compounds from Various Samples. *J Sep Sci* **2015**, *38* (6), 1053–1064. doi: 10.1002/jssc.201401347.
(96) Antenucci, S.; Panzella, L.; Farina, H.; Ortenzi, M. A.; Caneva, E.; Martinotti, S.; Ranzato, E.; Burlando, B.; d'Ischia, M.; Napolitano, A.; Verotta, L. Powering Tyrosol Antioxidant Capacity and Osteogenic Activity by Biocatalytic Polymerization. *RSC Adv.* **2016**, *6* (4), 2993–3002. doi: 10.1039/C5RA23004G.
(97) Monti, D.; Ottolina, G.; Carrea, G.; Riva, S. Redox Reactions Catalyzed by Isolated Enzymes. *Chem. Rev.* **2011**, *111* (7), 4111–4140. doi: 10.1021/cr100334x.

(98) Daquino, C.; Rescifina, A.; Spatafora, C.; Tringali, C. Biomimetic Synthesis of Natural and "Unnatural" Lignans by Oxidative Coupling of Caffeic Esters. *European J. Org. Chem.* **2009**, *2009* (36), 6289–6300. doi: 10.1002/ejoc.200900804.

(99) Saliu, F.; Tolppa, E.-L.; Zoia, L.; Orlandi, M. Horseradish Peroxidase Catalyzed Oxidative Cross-Coupling Reactions: The Synthesis of 'Unnatural' Dihydrobenzofuran Lignans. *Tetrahedron Lett.* **2011**, *52* (30), 3856–3860. doi: 10.1016/j.tetlet.2011.05.072.

(100) Ambrogi, V.; Panzella, L.; Persico, P.; Cerruti, P.; Lonz, C. A.; Carfagna, C.; Verotta, L.; Caneva, E.; Napolitano, A.; d'Ischia, M. An Antioxidant Bioinspired Phenolic Polymer for Efficient Stabilization of Polyethylene. *Biomacromolecules.* **2014**, *15* (1), 302–310. doi: 10.1021/bm4015478.

(101) Henry, B. L.; Monien, B. H.; Bock, P. E.; Desai, U. R. A Novel Allosteric Pathway of Thrombin Inhibition. *J. Biol. Chem.* **2007**, *282* (44), 31891–31899. doi: 10.1074/jbc.M704257200.

(102) Thi, T. H.; Matsusaki, M.; Shi, D.; Kaneko, T.; Akashi, M. Synthesis and Properties of Coumaric Acid Derivative Homo-Polymers. *J. Biomater. Sci. Polym. Ed.* **2008**, *19* (1), 75–85. doi: 10.1163/156856208783227668.

(103) Vlachogianni, I. C.; Fragopoulou, E.; Kostakis, I. K.; Antonopoulou, S. In Vitro Assessment of Antioxidant Activity of Tyrosol, Resveratrol and Their Acetylated Derivatives. *Food Chem.* **2015**, *177*, 165–173. doi: 10.1016/j.foodchem.2014.12.092.

(104) Freeman, B. A.; Baker, P. R. S.; Schopfer, F. J.; Woodcock, S. R.; Napolitano, A.; d'Ischia, M. Nitro-Fatty Acid Formation and Signaling. *J. Biol. Chem.* **2008**, *283* (23), 15515–15519. doi: 10.1074/jbc.R800004200.

(105) Fragopoulou, E.; Nomikos, T.; Karantonis, H. C.; Apostolakis, C.; Pliakis, E.; Samiotaki, M.; Panayotou, G.; Antonopoulou, S. Biological Activity of Acetylated Phenolic Compounds. *J. Agric. Food Chem.* **2007**, *55* (1), 80–89. doi: 10.1021/jf0627221.

(106) Je, I.-G.; Kim, D.-S.; Kim, S.-W.; Lee, S.; Lee, H.-S.; Park, E. K.; Khang, D.; Kim, S.-H. Tyrosol Suppresses Allergic Inflammation by Inhibiting the Activation of Phosphoinositide 3-Kinase in Mast Cells. *PLoS One.* **2015**, *10* (6), e0129829. doi: 10.1371/journal.pone.0129829.

(107) Alfieri, M. L.; Panzella, L.; Duarte, B.; Gonçalves-Monteiro, S.; Marques, F.; Morato, M.; Correia-da-Silva, M.; Verotta, L.; Napolitano, A. Sulfated Oligomers of Tyrosol: Toward a New Class of Bioinspired Nonsaccharidic Anticoagulants. *Biomacromolecules.* **2021**, *22* (2), 399–409. doi: 10.1021/acs.biomac.0c01254.

(108) Borovanský, J.; Riley, P. A. Physiological and Pathological Functions of Melanosomes. In *Melanins and Melanosomes*; Wiley, **2011**, 343–381. doi: 10.1002/9783527636150.ch12.

(109) d'Ischia, M.; Napolitano, A.; Pezzella, A.; Meredith, P.; Buehler, M. Melanin Biopolymers: Tailoring Chemical Complexity for Materials Design. *Angew. Chem., Int. Ed. Engl.* **2020**, *59* (28), 11196–11205. doi: 10.1002/anie.201914276.

(110) Panzella, L.; Gentile, G.; D'Errico, G.; Della Vecchia, N. F.; Errico, M. E.; Napolitano, A.; Carfagna, C.; d'Ischia, M. Atypical Structural and π-Electron Features of a Melanin Polymer That Lead to Superior Free-Radical-Scavenging Properties. *Angew. Chem., Int. Ed. Engl.* **2013**, *52* (48), 12684–12687. doi: 10.1002/anie.201305747.

(111) Micillo, R.; Iacomino, M.; Perfetti, M.; Panzella, L.; Koike, K.; D'Errico, G.; d'Ischia, M.; Napolitano, A. Unexpected Impact of Esterification on the Antioxidant Activity and (Photo)Stability of a Eumelanin from 5,6-dihydroxyindole-2-carboxylic Acid. *Pigment Cell Melanoma Res.* **2018**, *31* (4), 475–483. doi: 10.1111/pcmr.12689.

(112) Micillo, R.; Panzella, L.; Koike, K.; Monfrecola, G.; Napolitano, A.; D'Ischia, M. "Fifty Shades" of Black and Red or How Carboxyl Groups Fine Tune Eumelanin and Pheomelanin Properties. *Int. J. Mol. Sci.* **2016**, *17* (5), 746. doi: 10.3390/ijms17050746.
(113) Simon, J. D.; Peles, D. N. The Red and the Black. *Acc. Chem. Res.* **2010**, *43* (11), 1452–1460. doi: 10.1021/ar100079y.
(114) Ito, S.; Wakamatsu, K.; d'ischia, M.; Napolitano, A.; Pezzella, A. Structure of Melanins. In *Melanins and Melanosomes*; Wiley, **2011**, 167–185. doi: 10.1002/9783527636150.ch6.
(115) d'Ischia, M.; Wakamatsu, K.; Napolitano, A.; Briganti, S.; Garcia-Borron, J.; Kovacs, D.; Meredith, P.; Pezzella, A.; Picardo, M.; Sarna, T.; Simon, J. D.; Ito, S. Melanins and Melanogenesis: Methods, Standards, Protocols. *Pigment Cell Melanoma Res.* **2013**, *26* (5), 616–633. doi: 10.1111/pcmr.12121.
(116) Cao, W.; Zhou, X.; McCallum, N. C.; Hu, Z.; Ni, Q. Z.; Kapoor, U.; Heil, C. M.; Cay, K. S.; Zand, T.; Mantanona, A. J.; Jayaraman, A.; Dhinojwala, A.; Deheyn, D. D.; Shawkey, M. D.; Burkart, M. D.; Rinehart, J. D.; Gianneschi, N. C. Unraveling the Structure and Function of Melanin through Synthesis. *J. Am. Chem. Soc.* **2021**, *143* (7), 2622–2637. doi: 10.1021/jacs.0c12322.
(117) Arzillo, M.; Mangiapia, G.; Pezzella, A.; Heenan, R. K.; Radulescu, A.; Paduano, L.; d'Ischia, M. Eumelanin Buildup on the Nanoscale: Aggregate Growth/Assembly and Visible Absorption Development in Biomimetic 5,6-Dihydroxyindole Polymerization. *Biomacromolecules.* **2012**, *13* (8), 2379–2390. doi:.1021/bm3006159.
(118) Simon, J. D.; Peles, D.; Wakamatsu, K.; Ito, S. Current Challenges in Understanding Melanogenesis: Bridging Chemistry, Biological Control, Morphology, and Function. *Pigment Cell Melanoma Res.* **2009**, *22* (5), 563–579. doi: 10.1111/j.1755-148X.2009.00610.x.
(119) d'Ischia, M.; Napolitano, A.; Pezzella, A.; Meredith, P.; Buehler, M. Melanin Biopolymers: Tailoring Chemical Complexity for Materials Design. *Angew. Chem., Int. Ed. Engl.* **2020**, *59*, 11196–11205. doi: 10.1002/anie.201914276.
(120) d'Ischia, M.; Napolitano, A.; Ball, V.; Chen, C.-T.; Buehler, M. J. Polydopamine and Eumelanin: From Structure–Property Relationships to a Unified Tailoring Strategy. *Acc. Chem. Res.* **2014**, *47* (12), 3541–3550. doi: 10.1021/ar500273y.
(121) Prampolini, G.; Cacelli, I.; Ferretti, A. Intermolecular Interactions in Eumelanins: A Computational Bottom-up Approach. I. Small Building Blocks. *RSC Adv.* **2015**, *5* (48), 38513–38526. doi: 10.1039/C5RA03773E.
(122) d'Ischia, M.; Napolitano, A.; Tsiakas, K.; Prota, G. New Intermediates in the Oxidative Polymerisation of 5,6-Dihydroxyindole to Melanin Promoted by the Peroxidase/H2O2 System. *Tetrahedron.* **1990**, *46* (16), 5789–5796. doi: 10.1016/S0040-4020(01)87775-9.
(123) d'Ischia, M.; Napolitano, A.; Pezzella, A. 5,6-Dihydroxyindole Chemistry: Unexplored Opportunities beyond Eumelanin. *Eur. J. Org. Chem.* **2011**, *2011*, 5501–5516. doi: 10.1002/ejoc.201100796.
(124) Napolitano, A.; Corradini, M. G.; Prota, G. A Reinvestigation of the Structure of Melanochrome. *Tetrahedron Lett.* **1985**, *26* (23), 2805–2808. doi: 10.1016/S0040-4039(00)94917-7.
(125) Panzella, L.; Pezzella, A.; Napolitano, A.; d'Ischia, M. The First 5,6-Dihydroxyindole Tetramer by Oxidation of 5,5',6,6'-Tetrahydroxy- 2,4'-Biindolyl and an Unexpected Issue of Positional Reactivity En Route to Eumelanin-Related Polymers. *Org. Lett.* **2007**, *9* (7), 1411–1414. doi: 10.1021/ol070268w.
(126) James, S. L.; Adams, C. J.; Bolm, C.; Braga, D.; Collier, P.; Friščić, T.; Grepioni, F.; Harris, K. D. M.; Hyett, G.; Jones, W.; Krebs, A.; Mack, J.; Maini, L.; Orpen, A. G.;

Parkin, I. P.; Shearouse, W. C.; Steed, J. W.; Waddell, D. C. Mechanochemistry: Opportunities for New and Cleaner Synthesis. *Chem. Soc. Rev.* **2012**, *41* (1), 413–447. doi: 10.1039/C1CS15171A.

(127) Wang, G.-W. Mechanochemical Organic Synthesis. *Chem. Soc. Rev.* **2013**, *42* (18), 7668. doi: 10.1039/c3cs35526h.

(128) Howard, J. L.; Cao, Q.; Browne, D. L. Mechanochemistry as an Emerging Tool for Molecular Synthesis: What Can It Offer? *Chem. Sci.* **2018**, *9* (12), 3080–3094. doi: 10.1039/C7SC05371A.

(129) Cao, Q.; Howard, J. L.; Crawford, D. E.; James, S. L.; Browne, D. L. Translating Solid State Organic Synthesis from a Mixer Mill to a Continuous Twin Screw Extruder. *Green Chem.* **2018**, *20* (19), 4443–4447. doi: 10.1039/C8GC02036A.

(130) Juaristi, E.; Avila-Ortiz, C. G. Salient Achievements in Synthetic Organic Chemistry Enabled by Mechanochemical Activation. *Synthesis.* **2023**, *55* (16), 2439–2459. doi: 10.1055/a-2085-3410.

(131) Margetić, D. A Synopsis of Ball Milling Organic Synthesis in the Last 25 Years. *Curr. Org. Chem.* **2023**, *27* (7), 580–584. doi: 10.2174/1385272827666230407082210.

(132) Hernández, J. G.; Bolm, C. Altering Product Selectivity by Mechanochemistry. *J. Org. Chem.* **2017**, *82* (8), 4007–4019. doi: 10.1021/acs.joc.6b02887.

(133) Manini, P.; d'Ischia, M.; Milosa, M.; Prota, G. Acid-Promoted Competing Pathways in the Oxidative Polymerization of 5,6-Dihydroxyindoles and Related Compounds: Straightforward Cyclotrimerization Routes to Diindolocarbazole Derivatives. *J. Org. Chem.* **1998**, *63* (20), 7002–7008. doi: 10.1021/jo980875k.

(134) Pezzella, A.; Napolitano, A.; d'Ischia, M.; Prota, G. Oxidative Polymerisation of 5,6-Dihydroxyindole-2-Carboxylic Acid to Melanin: A New Insight. *Tetrahedron.* **1996**, *52* (23), 7913–7920. doi: 10.1016/0040-4020(96)00362-6.

(135) Pezzella, A.; Panzella, L.; Crescenzi, O.; Napolitano, A.; Navaratman, S.; Edge, R.; Land, E. J.; Barone, V.; d'Ischia, M. Short-Lived Quinonoid Species from 5,6-Dihydroxyindole Dimers En Route to Eumelanin Polymers: Integrated Chemical, Pulse Radiolytic, and Quantum Mechanical Investigation. *J. Am. Chem. Soc.* **2006**, *128* (48), 15490–15498. doi: 10.1021/ja0650246.

(136) Damm, C.; Peukert, W. Mechano-Chemical Radical Formation and Polymerization Initiation during Wet Grinding of Alumina. *J. Colloid. Interface Sci.* **2011**, *363* (1), 386–392. doi: 10.1016/j.jcis.2011.07.020.

(137) Ito, S.; Wakamatsu, K.; Glass, K.; Simon, J. D. High-Performance Liquid Chromatography Estimation of Cross-Linking of Dihydroxyindole Moiety in Eumelanin. *Anal. Biochem.* **2013**, *434* (2), 221–225. doi: 10.1016/j.ab.2012.12.005.

(138) Panzella, L.; Manini, P.; Monfrecola, G.; D'Ischia, M.; Napolitano, A. An Easy-to-run Method for Routine Analysis of Eumelanin and Pheomelanin in Pigmented Tissues. *Pigment Cell Res.* **2007**, *20* (2), 128–133. doi: 10.1111/j.1600-0749.2006.00359.x.

(139) Napolitano, A.; Vincensi, M. R.; Di Donato, P.; Prota, G.; Monfrecola, G. Microanalysis of Melanins in Mammalian Hair by Alkaline Hydrogen Peroxide Degradation: Identification of a New Structural Marker of Pheomelanins. *J. Invest. Dermatol.* **2000**, *114* (6), 1141–1147. doi: 10.1046/j.1523-1747.2000.00977.x.

(140) Napolitano, A.; Pezzella, A.; d'Ischia, M.; Prota, G. New Pyrrole Acids by Oxidative Degradation of Eumelanins with Hydrogen Peroxide. Further Hints to the Mechanism of Pigment Breakdown. *Tetrahedron.* **1996**, *52* (26), 8775–8780. doi: 10.1016/0040-4020(96)00418-8.

(141) della Vecchia, N. F.; Cerruti, P.; Gentile, G.; Errico, M. E.; Ambrogi, V.; D'Errico, G.; Longobardi, S.; Napolitano, A.; Paduano, L.; Carfagna, C.; d'Ischia, M. Artificial Biomelanin: Highly Light-Absorbing Nano-Sized Eumelanin by Biomimetic

Synthesis in Chicken Egg White. *Biomacromolecules.* **2014**, *15* (10), 3811–3816. doi: 10.1021/bm501139h.
(142) Pezzella, A.; Iadonisi, A.; Valerio, S.; Panzella, L.; Napolitano, A.; Adinolfi, M.; d'Ischia, M. Disentangling Eumelanin "Black Chromophore": Visible Absorption Changes As Signatures of Oxidation State- and Aggregation-Dependent Dynamic Interactions in a Model Water-Soluble 5,6-Dihydroxyindole Polymer. *J. Am. Chem. Soc.* **2009**, *131* (42), 15270–15275. doi: 10.1021/ja905162s.
(143) Micillo, R.; Panzella, L.; Iacomino, M.; Prampolini, G.; Cacelli, I.; Ferretti, A.; Crescenzi, O.; Koike, K.; Napolitano, A.; d'Ischia, M. Eumelanin Broadband Absorption Develops from Aggregation-Modulated Chromophore Interactions under Structural and Redox Control. *Sci. Rep.* **2017**, *7* (1), 41532. doi: 10.1038/srep41532.
(144) Adamo, C.; Scuseria, G. E.; Barone, V. Accurate Excitation Energies from Time-Dependent Density Functional Theory: Assessing the PBE0 Model. *J. Chem. Phys.* **1999**, *111* (7), 2889–2899. doi: 10.1063/1.479571.
(145) Scalmani, G.; Frisch, M. J.; Mennucci, B.; Tomasi, J.; Cammi, R.; Barone, V. Geometries and Properties of Excited States in the Gas Phase and in Solution: Theory and Application of a Time-Dependent Density Functional Theory Polarizable Continuum Model. *J. Chem. Phys.* **2006**, *124* (9). doi: 10.1063/1.2173258.
(146) Chai, J.-D.; Head-Gordon, M. Long-Range Corrected Hybrid Density Functionals with Damped Atom–Atom Dispersion Corrections. *Phys. Chem. Chem. Phys.* **2008**, *10* (44), 6615. doi: 10.1039/b810189b.
(147) Yanai, T.; Tew, D. P.; Handy, N. C. A New Hybrid Exchange–Correlation Functional Using the Coulomb-Attenuating Method (CAM-B3LYP). *Chem. Phys. Lett.* **2004**, *393* (1–3), 51–57. doi: 10.1016/j.cplett.2004.06.011.
(148) Atilano-Camino, M. M.; Álvarez-Valencia, L. H.; García-González, A.; García-Reyes, R. B. Improving Laccase Production from Trametes Versicolor Using Lignocellulosic Residues as Cosubstrates and Evaluation of Enzymes for Blue Wastewater Biodegradation. *J. Environ. Manage.* **2020**, *275*, 111231. doi: 10.1016/j.jenvman.2020.111231.
(149) Shakerian, F.; Zhao, J.; Li, S.-P. Recent Development in the Application of Immobilized Oxidative Enzymes for Bioremediation of Hazardous Micropollutants – A Review. *Chemosphere.* **2020**, *239*, 124716. doi: 10.1016/j.chemosphere.2019.124716.
(150) Attia, E. Z.; Farouk, H. M.; Abdelmohsen, U. R.; El-Katatny, M. H. Antimicrobial and Extracellular Oxidative Enzyme Activities of Endophytic Fungi Isolated from Alfalfa (Medicago Sativa) Assisted by Metabolic Profiling. *South African Journal of Botany.* **2020**, *134*, 156–162. doi: 10.1016/j.sajb.2019.12.003.
(151) Brown, M. A.; Zhao, Z.; Grant Mauk, A. Expression and Characterization of a Recombinant Multi-Copper Oxidase: Laccase IV from Trametes Versicolor. *Inorganica Chim. Acta.* **2002**, *331* (1), 232–238. doi: 10.1016/S0020-1693(01)00814-3.
(152) Tuomela, M.; Hatakka, A. Oxidative Fungal Enzymes for Bioremediation. In *Comprehensive Biotechnology*; Elsevier, **2011**, *6*, 183–196. doi: 10.1016/B978-0-08-088504-9.00370-6.
(153) Shiraishi, T.; Sannami, Y.; Kamitakahara, H.; Takano, T. Comparison of a Series of Laccase Mediators in the Electro-Oxidation Reactions of Non-Phenolic Lignin Model Compounds. *Electrochim. Acta.* **2013**, *106*, 440–446. doi: 10.1016/j.electacta.2013.05.112.
(154) Debnath, R.; Saha, T. An Insight into the Production Strategies and Applications of the Ligninolytic Enzyme Laccase from Bacteria and Fungi. *Biocatal. Agri.c Biotechnol.* **2020**, *26*, 101645. doi: 10.1016/j.bcab.2020.101645.

(155) Fernández-Fernández, M.; Sanromán, M. Á.; Moldes, D. Recent Developments and Applications of Immobilized Laccase. *Biotechnol. Adv.* **2013**, *31* (8), 1808–1825. doi: 10.1016/j.biotechadv.2012.02.013.
(156) Rodríguez Couto, S.; Toca Herrera, J. L. Industrial and Biotechnological Applications of Laccases: A Review. *Biotechnol. Adv.* **2006**, *24* (5), 500–513. doi: 10.1016/j.biotechadv.2006.04.003.
(157) Pinto, P. A.; Fraga, I.; Bezerra, R. M. F.; Dias, A. A. Phenolic and Non-Phenolic Substrates Oxidation by Laccase at Variable Oxygen Concentrations: Selection of Bisubstrate Kinetic Models from Polarographic Data. *Biochem Eng J* **2020**, *153*, 107423. doi: 10.1016/j.bej.2019.107423.
(158) Dwivedi, U. N.; Singh, P.; Pandey, V. P.; Kumar, A. Structure–Function Relationship among Bacterial, Fungal and Plant Laccases. *J. Mol. Catal. B. Enzym.* **2011**, *68* (2), 117–128. doi: 10.1016/j.molcatb.2010.11.002.
(159) Xu, F. Effects of Redox Potential and Hydroxide Inhibition on the PH Activity Profile of Fungal Laccases. *J. Biol. Chem.* **1997**, *272* (2), 924–928. doi: 10.1074/jbc.272.2.924.
(160) Baldrian, P. Fungal Laccases – Occurrence and Properties. *FEMS Microbiol. Rev.* **2006**, *30* (2), 215–242. doi: 10.1111/j.1574-4976.2005.00010.x.
(161) d'Ischia, M.; Napolitano, A.; Prota, G. Peroxidase as an Alternative to Tyrosinase in the Oxidative Polymerization of 5,6-Dihydroxyindoles to Melanin(s). *Biochim. Biophys. Acta, Gen. Subj.* **1991**, *1073* (2), 423–430. doi: 10.1016/0304-4165(91)90152-7.
(162) Itoh, T.; Takagi, Y. Laccase-Catalyzed Reactions in Ionic Liquids for Green Sustainable Chemistry. *ACS Sustain. Chem. Eng.* **2021**, *9* (4), 1443–1458. doi: 10.1021/acssuschemeng.0c07097.
(163) Varriale, S.; Delorme, A. E.; Andanson, J.-M.; Devemy, J.; Malfreyt, P.; Verney, V.; Pezzella, C. Enhancing the Thermostability of Engineered Laccases in Aqueous Betaine-Based Natural Deep Eutectic Solvents. *ACS Sustain. Chem. Eng.* **2022**, *10* (1), 572–581. doi: 10.1021/acssuschemeng.1c07104.
(164) Goldfeder, M.; Fishman, A. Modulating Enzyme Activity Using Ionic Liquids or Surfactants. *Appl. Microbiol. Biotechnol.* **2014**, *98* (2), 545–554. doi: 10.1007/s00253-013-5395-7.
(165) Capela, E. V.; Valente, A. I.; Nunes, J. C. F.; Magalhães, F. F.; Rodríguez, O.; Soto, A.; Freire, M. G.; Tavares, A. P. M. Insights on the Laccase Extraction and Activity in Ionic-Liquid-Based Aqueous Biphasic Systems. *Sep. Purif. Technol.* **2020**, *248*, 117052. doi: 10.1016/j.seppur.2020.117052.
(166) Pezzella, A.; Vogna, D.; Prota, G. Synthesis of Optically Active Tetrameric Melanin Intermediates by Oxidation of the Melanogenic Precursor 5,6-Dihydroxyindole-2-Carboxylic Acid under Biomimetic Conditions. *Tetrahedron Asymmetry.* **2003**, *14* (9), 1133–1140. doi: 10.1016/S0957-4166(03)00156-3.
(167) Ferreira, A. M.; Passos, H.; Okafuji, A.; Tavares, A. P. M.; Ohno, H.; Freire, M. G.; Coutinho, J. A. P. An Integrated Process for Enzymatic Catalysis Allowing Product Recovery and Enzyme Reuse by Applying Thermoreversible Aqueous Biphasic Systems. *Green Chem.* **2018**, *20* (6), 1218–1223. doi: 10.1039/C7GC03880A.
(168) Zhang, H.; Lu, M.; Jiang, H.; Wu, Z.-Y.; Zhou, D.-D.; Li, D.-Q.; Yang, F.-Q. Tyrosinase-Mediated Dopamine Polymerization Modified Magnetic Alginate Beads for Dual-Enzymes Encapsulation: Preparation, Performance and Application. *Colloids Surf. B Biointerfaces.* **2020**, *188*, 110800. doi: 10.1016/j.colsurfb.2020.110800.
(169) Ferreira, A. M.; Valente, A. I.; Castro, L. S.; Coutinho, J. A. P.; Freire, M. G.; Tavares, A. P. M. Sustainable Liquid Supports for Laccase Immobilization and

Reuse: Degradation of Dyes in Aqueous Biphasic Systems. *Biotechno.l Bioeng.* **2021**, *118* (7), 2514–2523. doi: 10.1002/bit.27764.

(170) Muñiz-Mouro, A.; Ferreira, A. M.; Coutinho, J. A. P.; Freire, M. G.; Tavares, A. P. M.; Gullón, P.; González-García, S.; Eibes, G. Integrated Biocatalytic Platform Based on Aqueous Biphasic Systems for the Sustainable Oligomerization of Rutin. *ACS Sustain. Chem. Eng.* **2021**, *9* (29), 9941–9950. doi: 10.1021/acssuschemeng.1c03399.

(171) Dinis, T. B. V.; Passos, H.; Lima, D. L. D.; Sousa, A. C. A.; Coutinho, J. A. P.; Esteves, V. I.; Freire, M. G. Simultaneous Extraction and Concentration of Water Pollution Tracers Using Ionic-Liquid-Based Systems. *J. Chromatogr. A.* **2018**, *1559*, 69–77. doi: 10.1016/j.chroma.2017.07.084.

(172) Freire, M. G.; Cláudio, A. F. M.; Araújo, J. M. M.; Coutinho, J. A. P.; Marrucho, I. M.; Lopes, J. N. C.; Rebelo, L. P. N. Aqueous Biphasic Systems: A Boost Brought about by Using Ionic Liquids. *Chem. Soc. Rev.* **2012**, *41* (14), 4966. doi: 10.1039/c2cs35151j.

(173) Magalhães, F. F.; Pereira, A. F.; Freire, M. G.; Tavares, A. P. M. New Liquid Supports in the Development of Integrated Platforms for the Reuse of Oxidative Enzymes and Polydopamine Production. *Front. Bioeng. Biotechnol.* **2022**, *10*. doi: 10.3389/fbioe.2022.1037322.

(174) Pamidipati, S.; Ahmed, A. A First Report on Competitive Inhibition of Laccase Enzyme by Lignin Degradation Intermediates. *Folia Microbiol.* **2020**, *65* (2), 431–437. doi: 10.1007/s12223-019-00765-5.

(175) Goupy, P.; Dufour, C.; Loonis, M.; Dangles, O. Quantitative Kinetic Analysis of Hydrogen Transfer Reactions from Dietary Polyphenols to the DPPH Radical. *J. Agric. Food Chem.* **2003**, *51* (3), 615–622. doi: 10.1021/jf025938l.

(176) Gökmen, V.; Serpen, A.; Fogliano, V. Direct Measurement of the Total Antioxidant Capacity of Foods: The 'QUENCHER' Approach. *Trends Food Sci. Technol.* **2009**, *20* (6–7), 278–288. doi: 10.1016/j.tifs.2009.03.010.

(177) Benzie, I. F. F.; Strain, J. J. The Ferric Reducing Ability of Plasma (FRAP) as a Measure of "Antioxidant Power": The FRAP Assay. *Anal. Biochem.* **1996**, *239* (1), 70–76. doi: 10.1006/abio.1996.0292.

(178) Moccia, F.; Agustin-Salazar, S.; Verotta, L.; Caneva, E.; Giovando, S.; D'Errico, G.; Panzella, L.; D'Ischia, M.; Napolitano, A. Antioxidant Properties of Agri-Food Byproducts | and Specific Boosting Effects of Hydrolytic Treatments. *Antioxidants.* **2020**, *9* (5). doi: 10.3390/antiox9050438.

(179) Han, H.; Lee, K. Systematic Approach to Mimic Phenolic Natural Polymers for Biofabrication. *Polymers.* **2022**, *14* (7), 1282. doi: 10.3390/polym14071282.

(180) Rawal, S.; Patel, M. M. Threatening Cancer with Nanoparticle Aided Combination Oncotherapy. *J. Control. Release.* **2019**, *301*, 76–109. doi: 10.1016/j.jconrel.2019.03.015.

(181) Ghaffarlou, M.; Sütekin, S. D.; Hammamchi, H.; İlk, S.; Güven, O.; Barsbay, M. Poly(Acrylic Acid)- *b* -Poly(Vinylamine) Copolymer: Decoration with Silver Nanoparticles, Antibacterial Properties, Quorum Sensing Activity, and Cytotoxicity on Breast Cancer and Fibroblast Cell Lines. *ACS Appl Polym. Mater.* **2022**, *4* (10), 7268–7281. doi: 10.1021/acsapm.2c00906.

(182) Rahman, L.; Sarwar, Y.; Khaliq, S.; Inayatullah; Abbas, W.; Mobeen, A.; Ullah, A.; Hussain, S. Z.; Khan, W. S.; Kyriazi, M.-E.; Hussain, I.; Kanaras, A. G.; Rehman, A. Surfactin-Conjugated Silver Nanoparticles as an Antibacterial and Antibiofilm Agent against *Pseudomonas Aeruginosa*. *ACS Appl. Mater. Interfaces.* **2023**, *15* (37), 43321–43331. doi: 10.1021/acsami.3c07071.

(183) Argenziano, R.; Moccia, F.; Esposito, R.; D'Errico, G.; Panzella, L.; Napolitano, A. Recovery of Lignins with Potent Antioxidant Properties from Shells of Edible Nuts

by a Green Ball Milling/Deep Eutectic Solvent (DES)-Based Protocol. *Antioxidant.s* **2022**, *11* (10), 1860. doi: 10.3390/antiox11101860.
(184) Moccia, F.; Gallucci, N.; Giovando, S.; Zuorro, A.; Lavecchia, R.; D'Errico, G.; Panzella, L.; Napolitano, A. A Tunable Deep Eutectic Solvent-Based Processing for Valorization of Chestnut Wood Fiber as a Source of Ellagic Acid and Lignin. *J Environ Chem Eng* **2022**, *10* (3), 107773. doi: 10.1016/j.jece.2022.107773.
(185) Guo, X.; Junna, X.; Wolcott, M. P.; Zhang, J. Mechanochemical Oleation of Lignin Through Ball Milling and Properties of Its Blends with PLA. *ChemistrySelect.* **2016**, *1* (13), 3449–3454. doi: 10.1002/slct.201600633.
(186) Zinovyev, G.; Sumerskii, I.; Rosenau, T.; Balakshin, M.; Potthast, A. Ball Milling's Effect on Pine Milled Wood Lignin's Structure and Molar Mass. *Molecules.* **2018**, *23* (9), 2223. doi: 10.3390/molecules23092223.
(187) Dabral, S.; Wotruba, H.; Hernández, J. G.; Bolm, C. Mechanochemical Oxidation and Cleavage of Lignin β-O-4 Model Compounds and Lignin. *ACS Sustain. Chem. Eng.* **2018**, *6* (3), 3242–3254. doi: 10.1021/acssuschemeng.7b03418.
(188) Yang, G.; An, X.; Yang, S. The Effect of Ball Milling Time on the Isolation of Lignin in the Cell Wall of Different Biomass. *Front. Bioeng. Biotechnol.* **2021**, *9*. doi: 10.3389/fbioe.2021.807625.
(189) Liu, J.; Li, X.; Row, K. H. Development of Deep Eutectic Solvents for Sustainable Chemistry. *J. Mol. Liq.* **2022**, *362*, 119654. doi: 10.1016/j.molliq.2022.119654.
(190) Ling, J. K. U.; Hadinoto, K. Deep Eutectic Solvent as Green Solvent in Extraction of Biological Macromolecules: A Review. *Int. J. Mol. Sci.* **2022**, *23* (6), 3381. doi: 10.3390/ijms23063381.
(191) Ijardar, S. P.; Singh, V.; Gardas, R. L. Revisiting the Physicochemical Properties and Applications of Deep Eutectic Solvents. *Molecules.* **2022**, *27* (4), 1368. doi: 10.3390/molecules27041368.
(192) Chen, Z.; Ragauskas, A.; Wan, C. Lignin Extraction and Upgrading Using Deep Eutectic Solvents. *Ind. Crops. Prod.* **2020**, *147*, 112241. doi: 10.1016/j.indcrop.2020.112241.
(193) Dheyab, A. S.; Abu Bakar, M. F.; AlOmar, M.; Sabran, S. F.; Muhamad Hanafi, A. F.; Mohamad, A. Deep Eutectic Solvents (DESs) as Green Extraction Media of Beneficial Bioactive Phytochemicals. *Separations.* **2021**, *8* (10), 176. doi: 10.3390/separations8100176.
(194) Sogut, E.; Seydim, A. C. Utilization of Chestnut Shell Lignin in Alginate Films. *J. Sci. Food Agric.* **2023**, *103* (3), 1049–1058. doi: 10.1002/jsfa.11785.
(195) Hernández, J. G.; Friščić, T. Metal-Catalyzed Organic Reactions Using Mechanochemistry. *Tetrahedron Lett.* **2015**, *56* (29), 4253–4265. doi: 10.1016/j.tetlet.2015.03.135.
(196) Šepelák, V.; Düvel, A.; Wilkening, M.; Becker, K.-D.; Heitjans, P. Mechanochemical Reactions and Syntheses of Oxides. *Chem. Soc. Rev.* **2013**, *42* (18), 7507. doi: 10.1039/c2cs35462d.
(197) Rightmire, N. R.; Hanusa, T. P. Advances in Organometallic Synthesis with Mechanochemical Methods. *Dalton Transactions.* **2016**, *45* (6), 2352–2362. doi: 10.1039/C5DT03866A.
(198) Jones, W.; Eddleston, M. D. Introductory Lecture: Mechanochemistry, a Versatile Synthesis Strategy for New Materials. *Faraday Discuss.* **2014**, *170*, 9–34. doi: 10.1039/C4FD00162A.
(199) Stolle, A.; Szuppa, T.; Leonhardt, S. E. S.; Ondruschka, B. Ball Milling in Organic Synthesis: Solutions and Challenges. *Chem. Soc. Rev.* **2011**, *40* (5), 2317. doi: 10.1039/c0cs00195c.
(200) Argenziano, R.; Agustin-Salazar, S.; Panaro, A.; Calarco, A.; Di Salle, A.; Aprea, P.; Cerruti, P.; Panzella, L.; Napolitano, A. Combining the Potent Reducing Properties

of Pecan Nutshell with a Solvent-Free Mechanochemical Approach for Synthesizing High Ag0 Content-Silver Nanoparticles: An Eco-Friendly Route to an Efficient Multifunctional Photocatalytic, Antibacterial, and Antioxidant Material. *Nanomaterials.* **2023**, *13* (5), 821. doi: 10.3390/nano13050821.

(201) Xu, T.; Yang, H.; Yang, D.; Yu, Z.-Z. Polylactic Acid Nanofiber Scaffold Decorated with Chitosan Islandlike Topography for Bone Tissue Engineering. *ACS Appl. Mater. Interfaces.* **2017**, *9* (25), 21094–21104. doi: 10.1021/acsami.7b01176.

(202) Ciarfaglia, N.; Pepe, A.; Piccirillo, G.; Laezza, A.; Daum, R.; Schenke-Layland, K.; Bochicchio, B. Nanocellulose and Elastin Act as Plasticizers of Electrospun Bioinspired Scaffolds. *ACS Appl. Polym. Mater.* **2020**, *2* (11), 4836–4847. doi: 10.1021/acsapm.0c00790.

(203) Harrison, J. J.; Stremick, C. A.; Turner, R. J.; Allan, N. D.; Olson, M. E.; Ceri, H. Microtiter Susceptibility Testing of Microbes Growing on Peg Lids: A Miniaturized Biofilm Model for High-Throughput Screening. *Nat. Protoc.* **2010**, *5* (7), 1236–1254. doi: 10.1038/nprot.2010.71.

(204) Sabaté Brescó, M.; Harris, L. G.; Thompson, K.; Stanic, B.; Morgenstern, M.; O'Mahony, L.; Richards, R. G.; Moriarty, T. F. Pathogenic Mechanisms and Host Interactions in Staphylococcus Epidermidis Device-Related Infection. *Front. Microbiol.* **2017**, *8* (AUG). doi: 10.3389/fmicb.2017.01401.

(205) Coli, P.; Jemt, T. Are Marginal Bone Level Changes around Dental Implants Due to Infection? *Clin. Implant Dent. Relat. Res.* **2021**, *23* (2), 170–177. doi: 10.1111/cid.12971.

(206) Fabre, V.; Amoah, J.; Cosgrove, S. E.; Tamma, P. D. Antibiotic Therapy for Pseudomonas Aeruginosa Bloodstream Infections: How Long Is Long Enough? *Clinical Infectious Diseases* **2019**, *69* (11), 2011–2014. doi: 10.1093/cid/ciz223.

(207) Sorrentino, R.; Cochis, A.; Azzimonti, B.; Caravaca, C.; Chevalier, J.; Kuntz, M.; Porporati, A. A.; Streicher, R. M.; Rimondini, L. Reduced Bacterial Adhesion on Ceramics Used for Arthroplasty Applications. *J. Eur. Ceram. Soc.* **2018**, *38* (3), 963–970. doi: 10.1016/j.jeurceramsoc.2017.10.008.

(208) Cochis, A.; Barberi, J.; Ferraris, S.; Miola, M.; Rimondini, L.; Vernè, E.; Yamaguchi, S.; Spriano, S. Competitive Surface Colonization of Antibacterial and Bioactive Materials Doped with Strontium and/or Silver Ions. *Nanomaterials.* **2020**, *10* (1), 120. doi: 10.3390/nano10010120.

(209) Gamna, F.; Cochis, A.; Mojsoska, B.; Kumar, A.; Rimondini, L.; Spriano, S. Nano-Topography and Functionalization with the Synthetic Peptoid GN2-Npm9 as a Strategy for Antibacterial and Biocompatible Titanium Implants. *Heliyon.* **2024**, *10* (2), e24246. doi: 10.1016/j.heliyon.2024.e24246.

(210) Gristina, A. G. Biomaterial-Centered Infection: Microbial Adhesion Versus Tissue Integration. *Clin. Orthop. Relat. Res.* **1987**, *237* (4822), 1588–1595. doi: 10.1126/science.3629258.

(211) Eijkel, B. I. M.; Apachitei, I.; Fratila-Apachitei, L. E.; Zadpoor, A. A. In Vitro Co-Culture Models for the Assessment of Orthopedic Antibacterial Biomaterials. *Front. Bioeng. Biotechnol.* **2024**, *12*. doi: 10.3389/fbioe.2024.1332771.

(212) Mezey, É.; Nemeth, K. Mesenchymal Stem Cells and Infectious Diseases: Smarter than Drugs. *Immunol. Lett.* **2015**, *168* (2), 208–214. doi: 10.1016/j.imlet.2015.05.020.

(213) Li, J.; Tian, X.; Hua, T.; Fu, J.; Koo, M.; Chan, W.; Poon, T. Chitosan Natural Polymer Material for Improving Antibacterial Properties of Textiles. *ACS Appl. Bio. Mater.* **2021**, *4* (5), 4014–4038. doi: 10.1021/acsabm.1c00078.

(214) Chipera, S. J.; Bish, D. L. Fitting Full X-Ray Diffraction Patterns for Quantitative Analysis: A Method for Readily Quantifying Crystalline and Disordered Phases. *Adv. Mater. Phys. Chem.* **2013**, *03* (01), 47–53. doi: 10.4236/ampc.2013.31A007.

(215) Toby, B. H.; Von Dreele, R. B. *GSAS-II* : The Genesis of a Modern Open-Source All Purpose Crystallography Software Package. *J. Appl. Crystallogr.* **2013**, *46* (2), 544–549. doi: 10.1107/S0021889813003531.
(216) Panzella, L.; Cerruti, P.; Aprea, P.; Paolillo, R.; Pellegrino, G.; Moccia, F.; Condorelli, G. G.; Vollaro, A.; Ambrogi, V.; Catania, M. R.; d'Ischia, M.; Napolitano, A. Silver Nanoparticles on Hydrolyzed Spent Coffee Grounds (HSCG) for Green Antibacterial Devices. *J. Clean. Prod.* **2020**, *268*, 122352. doi: 10.1016/j.jclepro.2020.122352.
(217) Seifzadeh, N.; Ali Sahari, M.; Barzegar, M.; Ahmadi Gavlighi, H.; Calani, L.; Del Rio, D.; Galaverna, G. Evaluation of Polyphenolic Compounds in Membrane Concentrated Pistachio Hull Extract. *Food Chem.* **2019**, *277*, 398–406. doi: 10.1016/j.foodchem.2018.10.001.
(218) Apak, R.; Güçlü, K.; Özyürek, M.; Karademi˙r, S. E.; Altun, M. Total Antioxidant Capacity Assay of Human Serum Using Copper(II)-Neocuproine as Chromogenic Oxidant: The CUPRAC Method. *Free Radic. Res.* **2005**, *39* (9), 949–961. doi: 10.1080/10715760500210145.
(219) Cochis, A.; Azzimonti, B.; Della Valle, C.; De Giglio, E.; Bloise, N.; Visai, L.; Cometa, S.; Rimondini, L.; Chiesa, R. The Effect of Silver or Gallium Doped Titanium against the Multidrug Resistant Acinetobacter Baumannii. *Biomaterials.* **2016**, *80*, 80–95. doi: 10.1016/j.biomaterials.2015.11.042.
(220) Cui, S.; Xie, Y.; Wei, X.; Zhang, K.; Chen, X. Exploration of the Chemical Linkages between Lignin and Cellulose in Poplar Wood with 13C and Deuterium Dual Isotope Tracer. *Ind. Crops. Prod.* **2022**, *187*, 115452. doi: 10.1016/j.indcrop.2022.115452.
(221) Yang, W.; Wang, X.; Jiao, L.; Bian, H.; Qiao, Y.; Dai, H. Synthetic Polymers Based on Lignin-Derived Aromatic Monomers for High-Performance Energy-Storage Materials. *J. Mater. Chem. A Mater.* **2020**, *8* (45), 24065–24074. doi: 10.1039/D0TA08635E.
(222) Beckers, S. J.; Fischer, J.; Wurm, F. R. Synthetic Lignin-like and Degradable Nanocarriers. *Polym. Chem.* **2021**, *12* (32), 4661–4667. doi: 10.1039/D1PY00818H.
(223) Stafford, H. A. Differences Between Lignin-like Polymers Formed by Peroxidation of Eugenol and Ferulic Acid in Leaf Sections of Phleum. *Plant. Physiol.* **1960**, *35* (1), 108–114. doi: 10.1104/pp.35.1.108.
(224) Fournand, D. Initial Steps of the Peroxidase-Catalyzed Polymerization of Coniferyl Alcohol and/or Sinapyl Aldehyde Capillary Zone Electrophoresis Study of PH Effect. *Phytochemistry.* **2003**, *62* (2), 139–146. doi: 10.1016/S0031-9422(02)00573-3.
(225) Reale, S.; Attanasio, F.; Spreti, N.; De Angelis, F. Lignin Chemistry: Biosynthetic Study and Structural Characterisation of Coniferyl Alcohol Oligomers Formed In Vitro in a Micellar Environment. *Chem. Eur. J.* **2010**, *16* (20), 6077–6087. doi: 10.1002/chem.200903302.
(226) Kleine, T.; Buendia, J.; Bolm, C. Mechanochemical Degradation of Lignin and Wood by Solvent-Free Grinding in a Reactive Medium. *Green Chem.* **2013**, *15* (1), 160–166. doi: 10.1039/C2GC36456E.
(227) Dwivedi, R. K.; Singh, R. P.; Bhattacharya, T. K. Studies on Bio-Pretreatment of Pine Needles for Sustainable Energy Thereby Preventing Wild Forest Fires. *Curr. Sci.* **2016**, *111* (2), 388. doi: 10.18520/cs/v111/i2/388-394.
(228) Bhattacharya, R.; Arora, S.; Ghosh, S. Utilization of Waste Pine Needles for the Production of Cellulolytic Enzymes in a Solid State Fermentation Bioreactor and High Calorific Value Fuel Pellets from Fermented Residue: Towards a Biorefinery Approach. *Renew. Energy.* **2022**, *195*, 1064–1076. doi: 10.1016/j.renene.2022.06.067.

(229) Mazza, G.; Manetti, M. C. Growth Rate and Climate Responses of Pinus Pinea L. in Italian Coastal Stands over the Last Century. *Clim. Change.* **2013**, *121* (4), 713–725. doi: 10.1007/s10584-013-0933-y.
(230) Oreopoulou, A.; Tsimogiannis, D.; Oreopoulou, V. Extraction of Polyphenols From Aromatic and Medicinal Plants: An Overview of the Methods and the Effect of Extraction Parameters. In *Polyphenols in Plants*; Elsevier, **2019**, 243–259. doi: 10.1016/B978-0-12-813768-0.00025-6.
(231) Sridhar, A.; Ponnuchamy, M.; Kumar, P. S.; Kapoor, A.; Vo, D.-V. N.; Prabhakar, S. Techniques and Modeling of Polyphenol Extraction from Food: A Review. *Environ. Chem. Lett.* **2021**, *19* (4), 3409–3443. doi: 10.1007/s10311-021-01217-8.
(232) Ameer, K.; Shahbaz, H. M.; Kwon, J. Green Extraction Methods for Polyphenols from Plant Matrices and Their Byproducts: A Review. *Compr. Rev. Food Sci. Food Saf.* **2017**, *16* (2), 295–315. doi: 10.1111/1541-4337.12253.
(233) de Hoyos-Martínez, P. L.; Merle, J.; Labidi, J.; Charrier – El Bouhtoury, F. Tannins Extraction: A Key Point for Their Valorization and Cleaner Production. *J. Clean. Prod.* **2019**, *206*, 1138–1155. doi: 10.1016/j.jclepro.2018.09.243.
(234) Panzella, L.; Moccia, F.; Nasti, R.; Marzorati, S.; Verotta, L.; Napolitano, A. Bioactive Phenolic Compounds From Agri-Food Wastes: An Update on Green and Sustainable Extraction Methodologies. *Front. Nutr.* **2020**, *7*. doi: 10.3389/fnut.2020.00060.
(235) Vilaplana, F.; Ventura, S. P. M.; Sudarsanam, P.; Abdoulmoumine, N.; Carrier, D. J. Effective Assessment Practices for Using Sustainability Metrics: Biomass Processing. *ACS Sustain. Chem. Eng.* **2021**, *9* (44), 14654–14656. doi: 10.1021/acssuschemeng.1c07180.
(236) Aspé, E.; Fernández, K. The Effect of Different Extraction Techniques on Extraction Yield, Total Phenolic, and Anti-Radical Capacity of Extracts from Pinus Radiata Bark. *Ind. Crops. Prod.* **2011**, *34* (1), 838–844. doi: 10.1016/j.indcrop.2011.02.002.
(237) Liazid, A.; Schwarz, M.; Varela, R. M.; Palma, M.; Guillén, D. A.; Brigui, J.; Macías, F. A.; Barroso, C. G. Evaluation of Various Extraction Techniques for Obtaining Bioactive Extracts from Pine Seeds. *Food Bioprod. Process.* **2010**, *88* (2–3), 247–252. doi: 10.1016/j.fbp.2009.11.004.
(238) González-González, G. M.; Palomo-Ligas, L.; Nery-Flores, S. D.; Ascacio-Valdés, J. A.; Sáenz-Galindo, A.; Flores-Gallegos, A. C.; Zakaria, Z. A.; Aguilar, C. N.; Rodríguez-Herrera, R. Coffee Pulp as a Source for Polyphenols Extraction Using Ultrasound, Microwave, and Green Solvents. *Environ. Qual. Manage.* **2022**, *32* (1), 451–461. doi: 10.1002/tqem.21903.
(239) Salzano de Luna, M.; Vetrone, G.; Viggiano, S.; Panzella, L.; Marotta, A.; Filippone, G.; Ambrogi, V. Pine Needles as a Biomass Resource for Phenolic Compounds: Trade-Off between Efficiency and Sustainability of the Extraction Methods by Life Cycle Assessment. *ACS Sustain. Chem. Eng.* **2023**, *11* (12), 4670–4677. doi: 10.1021/acssuschemeng.2c06698.
(240) Paniwnyk, L.; Beaufoy, E.; Lorimer, J. P.; Mason, T. J. The Extraction of Rutin from Flower Buds of Sophora Japonica. *Ultrason. Sonochem.* **2001**, *8* (3), 299–301. doi: 10.1016/S1350-4177(00)00075-4.
(241) Song, J.; Chen, S.; Zhao, X.; Cheng, J.; Ma, Y.; Ren, S.; Li, S. Simple, Green, Ultrasound-Assisted Preparation of Novel Core–Shell Microcapsules from Octyl Methoxycinnamate and Oligomeric Proanthocyanidins for UV-Stable Sunscreen. *RSC Adv.* **2021**, *11* (11), 6374–6382. doi: 10.1039/D0RA09116B.
(242) Jiang, X.; Liu, Y.; Wu, Y.; Tan, H.; Meng, F.; Wang, Y. sheng; Li, M.; Zhao, L.; Liu, L.; Qian, Y.; Gao, L.; Xia, T. Analysis of Accumulation Patterns and Preliminary Study on the Condensation Mechanism of Proanthocyanidins in the Tea Plant [Camellia Sinensis]. *Sci. Rep.* **2015**, *5* (1), 8742. doi: 10.1038/srep08742.

(243) Bährle, C.; Nick, T. U.; Bennati, M.; Jeschke, G.; Vogel, F. High-Field Electron Paramagnetic Resonance and Density Functional Theory Study of Stable Organic Radicals in Lignin: Influence of the Extraction Process, Botanical Origin, and Protonation Reactions on the Radical g Tensor. *J. Phys. Chem. A.* **2015**, *119* (24), 6475–6482. doi: 10.1021/acs.jpca.5b02200.

(244) Panzella, L.; D'Errico, G.; Vitiello, G.; Perfetti, M.; Alfieri, M. L.; Napolitano, A.; D'Ischia, M. Disentangling Structure-Dependent Antioxidant Mechanisms in Phenolic Polymers by Multiparametric EPR Analysis. *Chem. Commun.* **2018**, *54* (68), 9426–9429. doi: 10.1039/c8cc05989f.

(245) Moccia, F.; Agustin-Salazar, S.; Berg, A.-L.; Setaro, B.; Micillo, R.; Pizzo, E.; Weber, F.; Gamez-Meza, N.; Schieber, A.; Cerruti, P.; Panzella, L.; Napolitano, A. Pecan (*Carya Illinoinensis* (Wagenh.) K. Koch) Nut Shell as an Accessible Polyphenol Source for Active Packaging and Food Colorant Stabilization. *ACS Sustain. Chem. Eng.* **2020**, *8* (17), 6700–6712. doi: 10.1021/acssuschemeng.0c00356.

(246) Panzella, L.; Gentile, G.; D'Errico, G.; Della Vecchia, N. F.; Errico, M. E.; Napolitano, A.; Carfagna, C.; d'Ischia, M. Atypical Structural and Π-Electron Features of a Melanin Polymer That Lead to Superior Free-Radical-Scavenging Properties. *Angew. Chem., Int. Ed. Engl.* **2013**, *52* (48), 12684–12687. doi: 10.1002/anie.201305747.

(247) Kanerva, S.; Kitunen, V.; Kiikkilä, O.; Loponen, J.; Smolander, A. Response of Soil C and N Transformations to Tannin Fractions Originating from Scots Pine and Norway Spruce Needles. *Soil Biol. Biochem.* **2006**, *38* (6), 1364–1374. doi: 10.1016/j.soilbio.2005.10.013.

(248) Szwajkowska-Michałek, L.; Przybylska-Balcerek, A.; Rogoziński, T.; Stuper-Szablewska, K. Phenolic Compounds in Trees and Shrubs of Central Europe. *Appl. Sci.* **2020**, *10* (19), 6907. doi: 10.3390/app10196907.

(249) Hlushko, H.; Cubides, Y.; Hlushko, R.; Kelly, T. M.; Castaneda, H.; Sukhishvili, S. A. Hydrophobic Antioxidant Polymers for Corrosion Protection of an Aluminum Alloy. *ACS Sustain. Chem. Eng.* **2018**, *6* (11), 14302–14313. doi: 10.1021/acssuschemeng.8b02966.

(250) Rosliza, R.; Wan Nik, W. B. Improvement of Corrosion Resistance of AA6061 Alloy by Tapioca Starch in Seawater. *Curr. Appl. Phys.* **2010**, *10* (1), 221–229. doi: 10.1016/j.cap.2009.05.027.

(251) Xhanari, K.; Finšgar, M. Organic Corrosion Inhibitors for Aluminum and Its Alloys in Chloride and Alkaline Solutions: A Review. *Arab. J. Chem.* **2019**, *12* (8), 4646–4663. doi: 10.1016/j.arabjc.2016.08.009.

(252) Natishan, P. M.; O'Grady, W. E. Chloride Ion Interactions with Oxide-Covered Aluminum Leading to Pitting Corrosion: A Review. *J. Electrochem. Soc.* **2014**, *161* (9), C421–C432. doi: 10.1149/2.1011409jes.

(253) Gerengi, H. Anticorrosive Properties of Date Palm (*Phoenix Dactylifera* L.) Fruit Juice on 7075 Type Aluminum Alloy in 3.5% NaCl Solution. *Ind. Eng. Chem. Res.* **2012**, *51* (39), 12835–12843. doi: 10.1021/ie301771u.

(254) Guedes, D.; Martins, G. R.; Jaramillo, L. Y. A.; Simas Bernardes Dias, D.; da Silva, A. J. R.; Lutterbach, M. T. S.; Reznik, L. Y.; Sérvulo, E. F. C.; Alviano, C. S.; Alviano, D. S. Proanthocyanidins with Corrosion Inhibition Activity for AISI 1020 Carbon Steel under Neutral PH Conditions of Coconut (*Cocos Nucifera* L.) Husk Fibers. *ACS Omega.* **2021**, *6* (10), 6893–6901. doi: 10.1021/acsomega.0c06104.

(255) Muñoz-García, A. B.; Sannino, F.; Vitiello, G.; Pirozzi, D.; Minieri, L.; Aronne, A.; Pernice, P.; Pavone, M.; D'Errico, G. Origin and Electronic Features of Reactive Oxygen Species at Hybrid Zirconia-Acetylacetonate Interfaces. *ACS Appl. Mater. Interfaces* **2015**, *7* (39), 21662–21667. doi: 10.1021/acsami.5b06988.

(256) Herald, T. J.; Gadgil, P.; Perumal, R.; Bean, S. R.; Wilson, J. D. High-Throughput Micro-Plate HCl-Vanillin Assay for Screening Tannin Content in Sorghum Grain. *J. Sci. Food Agric.* **2014**, *94* (10), 2133–2136. doi: 10.1002/jsfa.6538.
(257) Panzella, L.; Eidenberger, T.; Napolitano, A.; d'Ischia, M. Black Sesame Pigment: DPPH Assay-Guided Purification, Antioxidant/Antinitrosating Properties, and Identification of a Degradative Structural Marker. *J. Agric. Food Chem.* **2012**, *60* (36), 8895–8901. doi: 10.1021/jf2053096.
(258) Panzella, L. Natural Phenolic Compounds for Health, Food and Cosmetic Applications. *Antioxidants.* **2020**, *9* (5), 427. doi: 10.3390/antiox9050427.
(259) Greco, G.; Wakamatsu, K.; Panzella, L.; Ito, S.; Napolitano, A.; D'Ischia, M. Isomeric Cysteinyldopas Provide a (Photo)Degradable Bulk Component and a Robust Structural Element in Red Human Hair Pheomelanin. *Pigm. Cell Melanoma Res.* **2009**, *22* (3), 319–327. doi: 10.1111/j.1755-148X.2009.00561.x.
(260) Panzella, L.; Eidenberger, T.; Napolitano, A. Anti-Amyloid Aggregation Activity of Black Sesame Pigment: Toward a Novel Alzheimer's Disease Preventive Agent. *Molecules.* **2018**, *23* (3), 676. doi: 10.3390/molecules23030676.
(261) Peng, H.; Zhang, X.; Papaefthimiou, V.; Pham-Huu, C.; Ritleng, V. Pd-Functionalized Polydopamine-Coated Polyurethane Foam: A Readily Prepared and Highly Reusable Structured Catalyst for Selective Alkyne Semi-Hydrogenation and Suzuki Coupling under Air. *Green Chem.* **2023**, *25* (1), 264–279. doi: 10.1039/D2GC03283J.
(262) Richardson, J. T.; Peng, Y.; Remue, D. Properties of Ceramic Foam Catalyst Supports: Pressure Drop. *Appl. Catal. A Gen.* **2000**, *204* (1), 19–32. doi: 10.1016/S0926-860X(00)00508-1.
(263) Domínguez-Domínguez, S.; Berenguer-Murcia, Á.; Pradhan, B. K.; Linares-Solano, Á.; Cazorla-Amorós, D. Semihydrogenation of Phenylacetylene Catalyzed by Palladium Nanoparticles Supported on Carbon Materials. *J. Phys. Chem. C.* **2008**, *112* (10), 3827–3834. doi: 10.1021/jp710693u.
(264) Zhang, Y.; Li, W.; Li, J.; Li, F.; Xue, W.; Zhao, X.; Wang, Y. Synthesis of *p* -Aminophenol by Transfer Hydrogenation of Nitrobenzene with Formic Acid as a Hydrogen Source. *New J. Chem.* **2024**, *48* (2), 664–673. doi: 10.1039/D3NJ04360F.
(265) Sheng, Y.; Liu, Y.; Yin, Y.; Zou, X.; Ren, J.; Wu, B.; Wang, X.; Lu, X. Rh Promotional Effects on Pt–Rh Alloy Catalysts for Chemoselective Hydrogenation of Nitrobenzene to p-Aminophenol. *Chem. Eng. J.* **2023**, *452*, 139448. doi: 10.1016/j.cej.2022.139448.
(266) Biffis, A.; Centomo, P.; Del Zotto, A.; Zecca, M. Pd Metal Catalysts for Cross-Couplings and Related Reactions in the 21st Century: A Critical Review. *Chem. Rev.* **2018**, *118*, 2249–2295. doi: 10.1021/acs.chemrev.7b00443.
(267) Leo, A.; Hansch, C.; Elkins, D. Partition Coefficients and Their Uses. *Chem. Rev.* **1971**, *71* (6), 525–616. doi: 10.1021/cr60274a001.
(268) Niki, E. Assessment of Antioxidant Capacity in Vitro and in Vivo. *Free Radic. Biol. Med.* **2010**, *49* (4), 503–515. doi: 10.1016/j.freeradbiomed.2010.04.016.
(269) Wlaschek, M.; Tantcheva-Poór, I.; Naderi, L.; Ma, W.; Schneider, L. A.; Razi-Wolf, Z.; Schüller, J.; Scharffetter-Kochanek, K. Solar UV Irradiation and Dermal Photoaging. *J. Photochem. Photobiol. B.* **2001**, *63* (1–3), 41–51. doi: 10.1016/S1011-1344(01)00201-9.
(270) Kurisawa, M.; Chung, J. E.; Kim, Y. J.; Uyama, H.; Kobayashi, S. Amplification of Antioxidant Activity and Xanthine Oxidase Inhibition of Catechin by Enzymatic Polymerization. *Biomacromolecules.* **2003**, *4* (3), 469–471. doi: 10.1021/bm034012z.
(271) Amorati, R.; Fumo, M. G.; Menichetti, S.; Mugnaini, V.; Pedulli, G. F. Electronic and Hydrogen Bonding Effects on the Chain-Breaking Activity of Sulfur-Containing

Phenolic Antioxidants. *J. Org. Chem.* **2006**, *71* (17), 6325–6332. doi: 10.1021/jo060281e.
(272) Alfieri, M. L.; Panzella, L.; Amorati, R.; Cariola, A.; Valgimigli, L.; Napolitano, A. Role of Sulphur and Heavier Chalcogens on the Antioxidant Power and Bioactivity of Natural Phenolic Compounds. *Biomolecules.* **2022**, *12* (1), 90. doi: 10.3390/biom12010090.
(273) Kumar, S.; Johansson, H.; Engman, L.; Valgimigli, L.; Amorati, R.; Fumo, M. G.; Pedulli, G. F. Regenerable Chain-Breaking 2,3-Dihydrobenzo[*b*]Selenophene-5-Ol Antioxidants. *J. Org. Chem.* **2007**, *72* (7), 2583–2595. doi: 10.1021/jo0700023.
(274) Nair, V.; Augustine, A.; George, T. G. A Facile CAN-Mediated Synthesis of Selenocyanates from Arylalkenes and Heteroarenes. *Eur. J. Org. Chem.* **2002**, No. 14, 2363–2366. doi: 10.1002/1099-0690(200207)2002:14<2363::AID-EJOC2363>3.0.CO;2-7.
(275) Bhabak, K. P.; Mugesh, G. Functional Mimics of Glutathione Peroxidase: Bioinspired Synthetic Antioxidants. *Acc. Chem. Res.* **2010**, *43* (11), 1408–1419. doi: 10.1021/ar100059g.
(276) Plano, D.; Baquedano, Y.; Moreno-Mateos, D.; Font, M.; Jiménez-Ruiz, A.; Palop, J. A.; Sanmartín, C. Selenocyanates and Diselenides: A New Class of Potent Antileishmanial Agents. *Eur. J. Med. Chem.* **2011**, *46* (8), 3315–3323. doi: 10.1016/j.ejmech.2011.04.054.
(277) Krief, A.; Delmotte, C.; Dumont, W. Chemoselective Reduction of Organoselenocyanates to Diselenides and Selenolates. *Tetrahedron.* **1997**, *53* (36), 12147–12158. doi: 10.1016/S0040-4020(97)00548-6.
(278) Mourtzinos, I.; Goula, A. Polyphenols in Agricultural Byproducts and Food Waste. In *Polyphenols in Plants*; Elsevier, **2019**, pp 23–44. doi: 10.1016/B978-0-12-813768-0.00002-5.
(279) Marra, F.; Petrovicova, B.; Canino, F.; Maffia, A.; Mallamaci, C.; Muscolo, A. Pomegranate Wastes Are Rich in Bioactive Compounds with Potential Benefit on Human Health. *Molecules.* **2022**, *27* (17), 5555. doi: 10.3390/molecules27175555.
(280) Das, A. K.; Nanda, P. K.; Chowdhury, N. R.; Dandapat, P.; Gagaoua, M.; Chauhan, P.; Pateiro, M.; Lorenzo, J. M. Application of Pomegranate By-Products in Muscle Foods: Oxidative Indices, Colour Stability, Shelf Life and Health Benefits. *Molecules.* **2021**, *26* (2), 467. doi: 10.3390/molecules26020467.
(281) Sweidan, N.; Abu Rayyan, W.; Mahmoud, I.; Ali, L. Phytochemical Analysis, Antioxidant, and Antimicrobial Activities of Jordanian Pomegranate Peels. *PLoS One.* **2023**, *18* (11), e0295129. doi: 10.1371/journal.pone.0295129.
(282) Rosas-Burgos, E. C.; Burgos-Hernández, A.; Noguera-Artiaga, L.; Kačániová, M.; Hernández-García, F.; Cárdenas-López, J. L.; Carbonell-Barrachina, Á. A. Antimicrobial Activity of Pomegranate Peel Extracts as Affected by Cultivar. *J. Sci. Food Agric.* **2017**, *97* (3), 802–810. doi: 10.1002/jsfa.7799.
(283) Chen, J.; Liao, C.; Ouyang, X.; Kahramanoğlu, I.; Gan, Y.; Li, M. Antimicrobial Activity of Pomegranate Peel and Its Applications on Food Preservation. *J. Food Qual.* **2020**, *2020*, 1–8. doi: 10.1155/2020/8850339.
(284) Kanatt, S. R.; Chander, R.; Sharma, A. Antioxidant and Antimicrobial Activity of Pomegranate Peel Extract Improves the Shelf Life of Chicken Products. *Int. J. Food Sci. Technol.* **2010**, *45* (2), 216–222. doi: 10.1111/j.1365-2621.2009.02124.x.
(285) Dimitrijevic, J.; Tomovic, M.; Bradic, J.; Petrovic, A.; Jakovljevic, V.; Andjic, M.; Živković, J.; Milošević, S. Đ.; Simanic, I.; Dragicevic, N. Punica Granatum L. (Pomegranate) Extracts and Their Effects on Healthy and Diseased Skin. *Pharmaceutics.* **2024**, *16* (4), 458. doi: 10.3390/pharmaceutics16040458.
(286) Cruz, V.; Rojas, R.; Saucedo-Pompa, S.; Martínez, D. G.; Aguilera-Carbó, A. F.; Alvarez, O. B.; Rodríguez, R.; Ruiz, J.; Aguilar, C. N. Improvement of Shelf Life

and Sensory Quality of Pears Using a Specialized Edible Coating. *J. Chem.* **2015**, *2015*, 1–7. doi: 10.1155/2015/138707.

(287) Schmid, M.; Müller, K. Whey Protein-Based Packaging Films and Coatings. In *Whey Proteins*; Elsevier, **2019**, 407–437. doi: 10.1016/B978-0-12-812124-5.00012-6.

(288) Kumar, N.; Daniloski, D.; Pratibha; Neeraj; D'Cunha, N. M.; Naumovski, N.; Petkoska, A. T. Pomegranate Peel Extract – A Natural Bioactive Addition to Novel Active Edible Packaging. *Food Res. Int.* **2022**, *156*, 111378. doi: 10.1016/j.foodres.2022.111378.

(289) García-Villalba, R.; Espín, J. C.; Aaby, K.; Alasalvar, C.; Heinonen, M.; Jacobs, G.; Voorspoels, S.; Koivumäki, T.; Kroon, P. A.; Pelvan, E.; Saha, S.; Tomás-Barberán, F. A. Validated Method for the Characterization and Quantification of Extractable and Nonextractable Ellagitannins after Acid Hydrolysis in Pomegranate Fruits, Juices, and Extracts. *J. Agric. Food Chem.* **2015**, *63* (29), 6555–6566. doi: 10.1021/acs.jafc.5b02062.

(290) Malviya, S.; Arvind; Jha, A.; Hettiarachchy, N. Antioxidant and Antibacterial Potential of Pomegranate Peel Extracts. *J. Food Sci. Technol.* **2014**, *51* (12), 4132–4137. doi: 10.1007/s13197-013-0956-4.

(291) Sadh, P. K.; Kumar, S.; Chawla, P.; Duhan, J. S. Fermentation: A Boon for Production of Bioactive Compounds by Processing of Food Industries Wastes (By-Products). *Molecules.* **2018**, *23* (10), 2560. doi: 10.3390/molecules23102560.

(292) Walker, M.; Phillips, C. A. *Alicyclobacillus Acidoterrestris*: An Increasing Threat to the Fruit Juice Industry? *Int. J. Food Sci. Technol.* **2008**, *43* (2), 250–260. doi: 10.1111/j.1365-2621.2006.01427.x.

(293) Arciello, A.; Panzella, L.; Dell'Olmo, E.; Abdalrazeq, M.; Moccia, F.; Gaglione, R.; Agustin-Salazar, S.; Napolitano, A.; Mariniello, L.; Giosafatto, C. V. L. Development and Characterization of Antimicrobial and Antioxidant Whey Protein-Based Films Functionalized with Pecan (Carya Illinoinensis) Nut Shell Extract. *Food Packag. Shelf Life.* **2021**, *29*, 100710. doi: 10.1016/j.fpsl.2021.100710.

(294) Alvarez-Perez, O. B.; Ventura-Sobrevilla, J. M.; Torres-León, C.; Rojas-Molina, R.; Rodríguez-Herrera, R.; Aguilar-González, M. A.; Aguilar, C. N. Development and Characterization of Whey Protein Films Incorporated with Tarbush Polyphenols and Candelilla Wax. *Food Biosci.* **2022**, *45*, 101505. doi: 10.1016/j.fbio.2021.101505.

(295) Kandasamy, S.; Yoo, J.; Yun, J.; Kang, H.-B.; Seol, K.-H.; Kim, H.-W.; Ham, J.-S. Application of Whey Protein-Based Edible Films and Coatings in Food Industries: An Updated Overview. *Coatings.* **2021**, *11* (9), 1056. doi: 10.3390/coatings11091056.

(296) Saravani, M.; Ehsani, A.; Aliakbarlu, J.; Ghasempour, Z. Gouda Cheese Spoilage Prevention: Biodegradable Coating Induced by *Bunium Persicum* Essential Oil and Lactoperoxidase System. *Food Sci. Nutr.* **2019**, *7* (3), 959–968. doi: 10.1002/fsn3.888.

(297) Papastergiadis, A.; Mubiru, E.; Van Langenhove, H.; De Meulenaer, B. Malondialdehyde Measurement in Oxidized Foods: Evaluation of the Spectrophotometric Thiobarbituric Acid Reactive Substances (TBARS) Test in Various Foods. *J. Agric. Food. Chem.* **2012**, *60* (38), 9589–9594. doi: 10.1021/jf302451c.

(298) Pathare, P. B.; Opara, U. L.; Al-Said, F. A.-J. Colour Measurement and Analysis in Fresh and Processed Foods: A Review. *Food Bioproc. Tech.* **2013**, *6* (1), 36–60. doi: 10.1007/s11947-012-0867-9.

(299) Oakes, K. D.; Van Der Kraak, G. J. Utility of the TBARS Assay in Detecting Oxidative Stress in White Sucker (Catostomus Commersoni) Populations Exposed to

Pulp Mill Effluent. *Aquatic. Toxicology.* **2003**, *63* (4), 447–463. doi: 10.1016/S0166-445X(02)00204-7.
(300) Guo, Q.; Chen, J.; Wang, J.; Zeng, H.; Yu, J. Recent Progress in Synthesis and Application of Mussel-Inspired Adhesives. *Nanoscale.* **2020**, *12* (3), 1307–1324. doi: 10.1039/C9NR09780E.
(301) Suárez-García, S.; Sedó, J.; Saiz-Poseu, J.; Ruiz-Molina, D. Copolymerization of a Catechol and a Diamine as a Versatile Polydopamine-Like Platform for Surface Functionalization: The Case of a Hydrophobic Coating. *Biomimetics.* **2017**, *2* (4), 22. doi: 10.3390/biomimetics2040022.
(302) Saiz-Poseu, J.; Mancebo-Aracil, J.; Nador, F.; Busqué, F.; Ruiz-Molina, D. The Chemistry behind Catechol-Based Adhesion. *Angew. Chem., Int. Ed. Engl.* **2019**, *58* (3), 696–714. doi: 10.1002/anie.201801063.
(303) Yu, W.; Cui, Y.; Han, M.; Jia, P.; Zhao, Y.; Zhang, M.; Sun, Y.; Nian, R. Mussel-Inspired Chemistry in Producing Mechanically Robust and Bioactive Hydrogels as Skin Dressings. *Mater. Today Chem.* **2023**, *27*, 101272. doi: 10.1016/j.mtchem.2022.101272.
(304) Deng, X.; Huang, B.; Wang, Q.; Wu, W.; Coates, P.; Sefat, F.; Lu, C.; Zhang, W.; Zhang, X. A Mussel-Inspired Antibacterial Hydrogel with High Cell Affinity, Toughness, Self-Healing, and Recycling Properties for Wound Healing. *ACS Sustain. Chem. Eng.* **2021**, *9* (8), 3070–3082. doi: 10.1021/acssuschemeng.0c06672.
(305) Guo, J.; Sun, W.; Kim, J. P.; Lu, X.; Li, Q.; Lin, M.; Mrowczynski, O.; Rizk, E. B.; Cheng, J.; Qian, G.; Yang, J. Development of Tannin-Inspired Antimicrobial Bioadhesives. *Acta Biomater.* **2018**, *72*, 35–44. doi: 10.1016/j.actbio.2018.03.008.
(306) Gan, D.; Xing, W.; Jiang, L.; Fang, J.; Zhao, C.; Ren, F.; Fang, L.; Wang, K.; Lu, X. Plant-Inspired Adhesive and Tough Hydrogel Based on Ag-Lignin Nanoparticles-Triggered Dynamic Redox Catechol Chemistry. *Nat. Commun.* **2019**, *10* (1), 1487. doi: 10.1038/s41467-019-09351-2.
(307) Cholewinski, A.; Yang, F. (Kuo); Zhao, B. Algae–Mussel-Inspired Hydrogel Composite Glue for Underwater Bonding. *Mater. Horiz.* **2019**, *6* (2), 285–293. doi: 10.1039/C8MH01421C.
(308) Mortier, C.; Costa, D. C. S.; Oliveira, M. B.; Haugen, H. J.; Lyngstadaas, S. P.; Blaker, J. J.; Mano, J. F. Advanced Hydrogels Based on Natural Macromolecules: Chemical Routes to Achieve Mechanical Versatility. *Mater. Today Chem.* **2022**, *26*, 101222. doi: 10.1016/j.mtchem.2022.101222.
(309) Friedman, M.; Brandon, D. L. Nutritional and Health Benefits of Soy Proteins. *J. Agric. Food Chem.* **2001**, *49* (3), 1069–1086. doi: 10.1021/jf0009246.
(310) Lamaming, S. Z.; Lamaming, J.; Rawi, N. F. M.; Hashim, R.; Kassim, M. H. M.; Hussin, M. H.; Bustami, Y.; Sulaiman, O.; Amini, M. H. M.; Hiziroglu, S. Improvements and Limitation of Soy Protein-based Adhesive: A Review. *Polym. Eng. Sci.* **2021**, *61* (10), 2393–2405. doi: 10.1002/pen.25782.
(311) Liu, J.; Li, Z.; Lin, Q.; Jiang, X.; Yao, J.; Yang, Y.; Shao, Z.; Chen, X. A Robust, Resilient, and Multi-Functional Soy Protein-Based Hydrogel. *ACS Sustain. Chem. Eng.* **2018**, *6* (11), 13730–13738. doi: 10.1021/acssuschemeng.8b01450.
(312) Luo, Y.; Wang, Y.; Xia, C.; Ahmad, A.; Yang, R.; Li, X.; Shi, S. Q.; Li, J.; Guo, M.; Nadda, A. K.; Ahamad, T.; Le, Q. Van. Eco-Friendly Soy Protein Isolate-Based Films Strengthened by Water-Soluble Glycerin Epoxy Resin. *Prog. Org. Coat.* **2022**, *162*, 106566. doi: 10.1016/j.porgcoat.2021.106566.
(313) Pang, H.; Ma, C.; Zhang, S. Conversion of Soybean Oil Extraction Wastes into High-Performance Wood Adhesives Based on Mussel-Inspired Cation-π Interactions. *Int. J. Biol. Macromol.* **2022**, *209*, 83–92. doi: 10.1016/j.ijbiomac.2022.03.152.
(314) Wang, Z.; Kang, H.; Liu, H.; Zhang, S.; Xia, C.; Wang, Z.; Li, J. Dual-Network Nanocross-Linking Strategy to Improve Bulk Mechanical and Water-Resistant

Adhesion Properties of Biobased Wood Adhesives. *ACS Sustain. Chem. Eng.* **2020**, *8* (44), 16430–16440. doi: 10.1021/acssuschemeng.0c04913.
(315) Kang, H.; Wang, Z.; Zhang, W.; Li, J.; Zhang, S. Physico-Chemical Properties Improvement of Soy Protein Isolate Films through Caffeic Acid Incorporation and Tri-Functional Aziridine Hybridization. *Food Hydrocoll.* **2016**, *61*, 923–932. doi: 10.1016/j.foodhyd.2016.07.009.
(316) Li, Y.; Huang, X.; Xu, Y.; Ma, C.; Cai, L.; Zhang, J.; Luo, J.; Li, J.; Li, J.; Shi, S. Q.; Gao, Q. A Bio-Inspired Multifunctional Soy Protein-Based Material: From Strong Underwater Adhesion to 3D Printing. *Chem. Eng. J.* **2022**, *430*, 133017. doi: 10.1016/j.cej.2021.133017.
(317) Wang, Z.; Kang, H.; Zhang, W.; Zhang, S.; Li, J. Improvement of Interfacial Adhesion by Bio-Inspired Catechol-Functionalized Soy Protein with Versatile Reactivity: Preparation of Fully Utilizable Soy-Based Film. *Polymers.* **2017**, *9* (3), 95. doi: 10.3390/polym9030095.
(318) Wang, L.; Liu, J.; Zhang, W.; Zhang, D.; Li, J.; Zhang, S. Biomimetic Soy Protein-based Exterior-use Films with Excellent UV-blocking Performance from Catechol Derivative *Acacia Mangium* Tannin. *J. Appl. Polym. Sci.* **2021**, *138* (15). doi: 10.1002/app.50185.
(319) Podlena, M.; Böhm, M.; Saloni, D.; Velarde, G.; Salas, C. Tuning the Adhesive Properties of Soy Protein Wood Adhesives with Different Coadjutant Polymers, Nanocellulose and Lignin. *Polymers.* **2021**, *13* (12), 1972. doi: 10.3390/polym13121972.
(320) Huang, W.; Sun, X. Adhesive Properties of Soy Proteins Modified by Urea and Guanidine Hydrochloride. *J. Am. Oil Chem. Soc.* **2000**, *77* (1), 101–104. doi: 10.1007/s11746-000-0016-6.
(321) Iacomino, M.; Weber, F.; Gleichenhagen, M.; Pistorio, V.; Panzella, L.; Pizzo, E.; Schieber, A.; d'Ischia, M.; Napolitano, A. Stable Benzacridine Pigments by Oxidative Coupling of Chlorogenic Acid with Amino Acids and Proteins: Toward Natural Product-Based Green Food Coloring. *J. Agric. Food Chem.* **2017**, *65* (31), 6519–6528. doi: 10.1021/acs.jafc.7b00999.
(322) Zhou, S.-D.; Huang, L.; Meng, L.; Lin, Y.-F.; Xu, X.; Dong, M.-S. Soy Protein Isolate -(-)-Epigallocatechin Gallate Conjugate: Covalent Binding Sites Identification and IgE Binding Ability Evaluation. *Food Chem.* **2020**, *333*, 127400. doi: 10.1016/j.foodchem.2020.127400.
(323) Ghahri, S.; Chen, X.; Pizzi, A.; Hajihassani, R.; Papadopoulos, A. N. Natural Tannins as New Cross-Linking Materials for Soy-Based Adhesives. *Polymers.* **2021**, *13* (4), 595. doi: 10.3390/polym13040595.
(324) Boatright, W. L.; Jahan, M. S.; Walters, B. M.; Miller, A. F.; Cui, D.; Hustedt, E. J.; Lei, Q. Carbon-Centered Radicals in Isolated Soy Proteins. *J. Food Sci.* **2008**, *73* (3). doi: 10.1111/j.1750-3841.2008.00693.x.
(325) Boatright, W. L.; Lei, Q.; Shah Jahan, M. Effect of Storage Conditions on Carbon-Centered Radicals in Soy Protein Products. *J. Agric. Food Chem.* **2009**, *57* (17), 7969–7973. doi: 10.1021/jf900087v.
(326) Liu, J.; Yong, H.; Yao, X.; Hu, H.; Yun, D.; Xiao, L. Recent Advances in Phenolic–Protein Conjugates: Synthesis, Characterization, Biological Activities and Potential Applications. *RSC Adv.* **2019**, *9* (61), 35825–35840. doi: 10.1039/C9RA07808H.
(327) Wang, Z.-Q.; Song, Q.-Y.; Su, J.-C.; Tang, W.; Song, J.-G.; Huang, X.-J.; An, J.; Li, Y.-L.; Ye, W.-C.; Wang, Y. Caffeic Acid Oligomers from Mesona Chinensis and Their In Vitro Antiviral Activities. *Fitoterapia.* **2020**, *144*, 104603. doi: 10.1016/j.fitote.2020.104603.

(328) Villiou, M.; Paez, J. I.; del Campo, A. Photodegradable Hydrogels for Cell Encapsulation and Tissue Adhesion. *ACS Appl. Mater. Interfaces.* **2020**, *12* (34), 37862–37872. doi: 10.1021/acsami.0c08568.
(329) van Meerloo, J.; Kaspers, G. J. L.; Cloos, J. Cell Sensitivity Assays: The MTT Assay; **2011**, 237–245. doi: 10.1007/978-1-61779-080-5_20.
(330) Gaglione, R.; Dell'Olmo, E.; Bosso, A.; Chino, M.; Pane, K.; Ascione, F.; Itri, F.; Caserta, S.; Amoresano, A.; Lombardi, A.; Haagsman, H. P.; Piccoli, R.; Pizzo, E.; Veldhuizen, E. J. A.; Notomista, E.; Arciello, A. Novel Human Bioactive Peptides Identified in Apolipoprotein B: Evaluation of Their Therapeutic Potential. *Biochem. Pharmacol.* **2017**, *130*, 34–50. doi: 10.1016/j.bcp.2017.01.009.
(331) Hearing, V. J.; Tsukamoto, K. Enzymatic Control of Pigmentation in Mammals. *FASEB J.* **1991**, *5* (14), 2902–2909. doi: 10.1096/fasebj.5.14.1752358.
(332) Pillaiyar, T.; Manickam, M.; Namasivayam, V. Skin Whitening Agents: Medicinal Chemistry Perspective of Tyrosinase Inhibitors. *J. Enzyme Inhib. Med. Chem.* **2017**, *32* (1), 403–425. doi: 10.1080/14756366.2016.1256882.
(333) Solano, F. On the Metal Cofactor in the Tyrosinase Family. *Int. J. Mol. Sci.* **2018**, *19* (2), 633. doi: 10.3390/ijms19020633.
(334) Land, E. J.; Ramsden, C. A.; Riley, P. A. Tyrosinase Autoactivation and the Chemistry of *Ortho* -Quinone Amines. *Acc. Chem. Res.* **2003**, *36* (5), 300–308. doi: 10.1021/ar020062p.
(335) Riley, P. A. Tyrosinase Kinetics: A Semi-Quantitative Model of the Mechanism of Oxidation of Monohydric and Dihydric Phenolic Substrates. *J. Theor. Biol.* **2000**, *203* (1), 1–12. doi: 10.1006/jtbi.1999.1061.
(336) Davis, E. C.; Callender, V. D. Postinflammatory Hyperpigmentation A Review of the Epidemiology, Clinical Features, and Treatment Options in Skin of Color. *J. Clin. Aesthet. Dermatol.* **2010**, *3*, 20–31.
(337) Yamaguchi, Y.; Hearing, V. J. Melanocytes and Their Diseases. *Cold Spring Harb. Perspect. Med.* **2014**, *4* (5). doi: 10.1101/cshperspect.a017046.
(338) Virador, V.; Matsunaga, N.; Matsunaga, J.; Valencia, J.; Oldham, R. J.; Kameyama, K.; Peck, G. L.; Ferrans, V. J.; Vieira, W. D.; Abdel-Malek, Z. A.; Hearing, V. J. Production of Melanocyte-Specific Antibodies to Human Melanosomal Proteins: Expression Patterns in Normal Human Skin and in Cutaneous Pigmented Lesions. *Pigment Cell Res.* **2001**, *14* (4), 289–297. doi: 10.1034/j.1600-0749.2001.140410.x.
(339) Tilley, A.; McHenry, M. P.; McHenry, J. A.; Solah, V.; Bayliss, K. Enzymatic Browning: The Role of Substrates in Polyphenol Oxidase Mediated Browning. *Curr. Res. Food Sci.* **2023**, *7*, 100623. doi: 10.1016/j.crfs.2023.100623.
(340) Moon, K. M.; Kwon, E.-B.; Lee, B.; Kim, C. Y. Recent Trends in Controlling the Enzymatic Browning of Fruit and Vegetable Products. *Molecules.* **2020**, *25* (12), 2754. doi: 10.3390/molecules25122754.
(341) Mann, T.; Gerwat, W.; Batzer, J.; Eggers, K.; Scherner, C.; Wenck, H.; Stäb, F.; Hearing, V. J.; Röhm, K.-H.; Kolbe, L. Inhibition of Human Tyrosinase Requires Molecular Motifs Distinctively Different from Mushroom Tyrosinase. *J. Invest. Derm.* **2018**, *138* (7), 1601–1608. doi: 10.1016/j.jid.2018.01.019.
(342) Bang, E.; Noh, S.-G.; Ha, S.; Jung, H. J.; Kim, D. H.; Lee, A. K.; Hyun, M. K.; Kang, D.; Lee, S.; Park, C.; Moon, H. R.; Chung, H. Y. Evaluation of the Novel Synthetic Tyrosinase Inhibitor (Z)-3-(3-Bromo-4-Hydroxybenzylidene)Thiochroman-4-One (MHY1498) In Vitro and In Silico. *Molecules.* **2018**, *23* (12), 3307. doi: 10.3390/molecules23123307.
(343) Briganti, S.; Camera, E.; Picardo, M. Chemical and Instrumental Approaches to Treat Hyperpigmentation. *Pigment Cell Res.* **2003**, *16* (2), 101–110. doi: 10.1034/j.1600-0749.2003.00029.x.

(344) Takeuchi, S.; Zhang, W.; Wakamatsu, K.; Ito, S.; Hearing, V. J.; Kraemer, K. H.; Brash, D. E. Melanin Acts as a Potent UVB Photosensitizer to Cause an Atypical Mode of Cell Death in Murine Skin. *Proc. Nat. Acad. Sci.* **2004**, *101* (42), 15076–15081. doi: 10.1073/pnas.0403994101.

(345) Chiarelli-Neto, O.; Ferreira, A. S.; Martins, W. K.; Pavani, C.; Severino, D.; Faião-Flores, F.; Maria-Engler, S. S.; Aliprandini, E.; Martinez, G. R.; Di Mascio, P.; Medeiros, M. H. G.; Baptista, M. S. Melanin Photosensitization and the Effect of Visible Light on Epithelial Cells. *PLoS One.* **2014**, *9* (11), e113266. doi: 10.1371/journal.pone.0113266.

(346) Vile, G. F.; Tyrrell, R. M. Uva Radiation-Induced Oxidative Damage to Lipids and Proteins in Vitro and in Human Skin Fibroblasts Is Dependent on Iron and Singlet Oxygen. *Free Radic. Biol. Med.* **1995**, *18* (4), 721–730. doi: 10.1016/0891-5849(94)00192-M.

(347) Berneburg, M.; Grether-Beck, S.; Kürten, V.; Ruzicka, T.; Briviba, K.; Sies, H.; Krutmann, J. Singlet Oxygen Mediates the UVA-Induced Generation of the Photoaging-Associated Mitochondrial Common Deletion. *J. Biol. Chem.* **1999**, *274* (22), 15345–15349. doi: 10.1074/jbc.274.22.15345.

(348) Szewczyk, G.; Zadlo, A.; Sarna, M.; Ito, S.; Wakamatsu, K.; Sarna, T. Aerobic Photoreactivity of Synthetic Eumelanins and Pheomelanins: Generation of Singlet Oxygen and Superoxide Anion. *Pigment Cell Melanoma Res.* **2016**, *29* (6), 669–678. doi: 10.1111/pcmr.12514.

(349) Funasaka, Y.; Komoto, M.; Ichihashi, M. Depigmenting Effect of A-Tocopheryl Ferulate on Normal Human Melanocytes. *Pigment Cell Res.* **2000**, *13*, 170–174. doi: 10.1111/j.0893-5785.2000.130830.x.

(350) Hanson, K. M.; Gratton, E.; Bardeen, C. J. Sunscreen Enhancement of UV-Induced Reactive Oxygen Species in the Skin. *Free Radic. Biol. Med.* **2006**, *41* (8), 1205–1212. doi: 10.1016/j.freeradbiomed.2006.06.011.

(351) Hönigsmann, H.; Schuler, G.; Aberer, W.; Romani, N.; Wolff, K. Immediate Pigment Darkening Phenomenon. A Reevaluation of Its Mechanisms. *J. Invest. Dermatol.* **1986**, *87* (5), 648–652. doi: 10.1111/1523-1747.ep12456326.

(352) Mahmoud, B. H.; Ruvolo, E.; Hexsel, C. L.; Liu, Y.; Owen, M. R.; Kollias, N.; Lim, H. W.; Hamzavi, I. H. Impact of Long-Wavelength UVA and Visible Light on Melanocompetent Skin. *J. Invest. Dermatol.* **2010**, *130* (8), 2092–2097. doi: 10.1038/jid.2010.95.

(353) Mao, Q.-Q.; Xu, X.-Y.; Cao, S.-Y.; Gan, R.-Y.; Corke, H.; Beta, T.; Li, H.-B. Bioactive Compounds and Bioactivities of Ginger (Zingiber Officinale Roscoe). *Foods.* **2019**, *8* (6), 185. doi: 10.3390/foods8060185.

(354) Kolbe, L.; Mann, T.; Gerwat, W.; Batzer, J.; Ahlheit, S.; Scherner, C.; Wenck, H.; Stäb, F. 4-n-butylresorcinol, a Highly Effective Tyrosinase Inhibitor for the Topical Treatment of Hyperpigmentation. *J. Eur. Acad. Dermatol. Venereol.* **2013**, *27* (s1), 19–23. doi: 10.1111/jdv.12051.

(355) Kang, M.; Park, S.-H.; Park, S. J.; Oh, S. W.; Yoo, J. A.; Kwon, K.; Kim, J.; Yu, E.; Cho, J. Y.; Lee, J. P44/42 MAPK Signaling Is a Prime Target Activated by Phenylethyl Resorcinol in Its Anti-Melanogenic Action. *Phytomedicine.* **2019**, *58*, 152877. doi: 10.1016/j.phymed.2019.152877.

(356) Wondrak, G. T.; Jacobson, M. K.; Jacobson, E. L. Endogenous UVA-Photosensitizers: Mediators of Skin Photodamage and Novel Targets for Skin Photoprotection. *Photochem. Photobiol. Sci.* **2006**, *5* (2), 215–237. doi: 10.1039/b504573h.

(357) Allen, J. M.; Engenolf, S.; Allen, S. K. Rapid Reaction of Singlet Molecular Oxygen (1O2) with p-Aminobenzoic Acid (PABA) in Aqueous Solution. *Biochem. Biophys. Res. Commun.* **1995**, *212* (3), 1145–1151. doi: 10.1006/bbrc.1995.2088.

(358) Hu, M.-L.; Chen, Y.-K.; Chen, L.-C.; Sano, M. Para-Aminobenzoic Acid Scavenges Reactive Oxygen Species and Protects DNA against UV and Free Radical Damage. *J. Nutr. Biochem.* **1995**, *6* (9), 504–508. doi: 10.1016/0955-2863(95)00082-B.

(359) Thomas, A. H.; Catalá, Á.; Vignoni, M. Soybean Phosphatidylcholine Liposomes as Model Membranes to Study Lipid Peroxidation Photoinduced by Pterin. *Biochim. Biophys. Acta-Biomembr.* **2016**, *1858* (1), 139–145. doi: 10.1016/j.bbamem.2015.11.002.

(360) Boscá, F.; Miranda, M. A.; Morera, I. M.; Samadi, A. Involvement of Type I and Type II Mechanisms in the Linoleic Acid Peroxidation Photosensitized by Tiaprofenic Acid. *J. Photochem. Photobio.l B* **2000**, *58* (1), 1–5. doi: 10.1016/S1011-1344(00)00102-0.

(361) Domingues, M. R. M.; Simões, C.; da Costa, J. P.; Reis, A.; Domingues, P. Identification of 1-palmitoyl-2-linoleoyl-phosphatidylethanolamine Modifications under Oxidative Stress Conditions by LC-MS/MS. *Biomed. Chromatogr.* **2009**, *23* (6), 588–601. doi: 10.1002/bmc.1157.

(362) Gruber, F.; Bicker, W.; Oskolkova, O. V.; Tschachler, E.; Bochkov, V. N. A Simplified Procedure for Semi-Targeted Lipidomic Analysis of Oxidized Phosphatidylcholines Induced by UVA Irradiation. *J. Lipid. Res.* **2012**, *53* (6), 1232–1242. doi: 10.1194/jlr.D025270.

(363) Fischer, B. B.; Krieger-Liszkay, A.; Eggen, R. I. L. Photosensitizers Neutral Red (Type I) and Rose Bengal (Type II) Cause Light-Dependent Toxicity in *Chlamydomonas Reinhardtii* and Induce the *Gpxh* Gene via Increased Singlet Oxygen Formation. *Environ. Sci. Technol.* **2004**, *38* (23), 6307–6313. doi: 10.1021/es049673y.

(364) Ahmad, I.; Arsalan, A.; Ali, S. A.; Sheraz, M. A.; Ahmed, S.; Anwar, Z.; Munir, I.; Shah, M. R. Formulation and Stabilization of Riboflavin in Liposomal Preparations. *J. Photochem. Photobiol. B.* **2015**, *153*, 358–366. doi: 10.1016/j.jphotobiol.2015.10.017.

(365) Douki, T.; von Koschembahr, A.; Cadet, J. Insight in DNA Repair of UV-induced Pyrimidine Dimers by Chromatographic Methods. *Photochem. Photobiol.* **2017**, *93* (1), 207–215. doi: 10.1111/php.12685.

(366) Zhang, L.; Hu, Y. Determination of Laser-Induced Thymine–Thymine Dimer in DNA by LC. *J. Pharm. Biomed. Anal.* **2002**, *29* (1–2), 95–102. doi: 10.1016/S0731-7085(02)00030-4.

(367) Liberti, D.; Alfieri, M. L.; Monti, D. M.; Panzella, L.; Napolitano, A. A Melanin-Related Phenolic Polymer with Potent Photoprotective and Antioxidant Activities for Dermo-Cosmetic Applications. *Antioxidants.* **2020**, *9* (4), 270. doi: 10.3390/antiox9040270.